Cartographie et fonctions des fragments issus du facteur de guidage axonal Slit

Thibault Gardette

N° d'ordre NNT : **2020LYSE1093**

THESE de DOCTORAT DE L'UNIVERSITE DE LYON
opérée au sein de
l'Université Claude Bernard Lyon 1

Ecole Doctorale N° 340
Biologie Moléculaire, Intégrative et Cellulaire

Spécialité de doctorat : Sciences Biologiques
Discipline : Neurodéveloppement

Soutenue publiquement le 08/04/2020, par :
Thibault Gardette

Cartographie et fonctions des fragments issus du facteur de guidage axonal Slit

---

Devant le jury composé de :

DURAND Bénédicte, PR Université Claude Bernard Lyon1 – Présidente du jury

DUBAND Jean-Loup, DR Université Paris Est Créteil – Rapporteur
DUSART Isabelle, DR Sorbonne Université – Rapporteure
NAWABI Homaira, CR Université Grenoble Alpes - Examinatrice
RAINETEAU Olivier, DR Université Claude Bernard Lyon1 – Examinateur

TAUSZIG-DELAMASURE Servane, DR Université Claude Bernard Lyon1 – Directrice de thèse
CASTELLANI Valérie, DR Université Claude Bernard Lyon1 – Invitée

Remerciements

Je tiens à remercier mes deux rapporteurs, Jean-Loup Duband et Isabelle Dusart, pour avoir pris le temps (en pleine pandémie) d'évaluer mes travaux de thèse. Je remercie également Bénédicte Durand, Homaira Nawabi et Olivier Raineteau pour avoir accepté de participer à mon jury de thèse.

Je remercie Samir Merabet et Homaira Nawabi (oui, deux fois) qui, lors de mes comités de suivi de thèse, m'ont prodigué conseils et encouragements. Je remercie également Samir Merabet (deux fois aussi, je suis généreux) et Jonathan Reboulet pour l'aide au développement de la BiFC.

Je remercie Servane Tauszig-Delamasure, elle dira à qui veut l'entendre qu'elle n'est pas patiente. Après 4 années à travailler avec elle, je sais que c'est faux. Je te remercie donc pour ta patience, face aux difficultés du projet, mais aussi pour ton empathie, pour ton écoute, pour tes conseils et tes enseignements. Je n'aurais sûrement pas fini cette thèse sous la direction d'une autre personne. Je réalise qu'il est rare de rencontrer des gens comme toi, merci pour tout ce que j'ai cité et encore plus.

Je remercie également Valérie Castellani pour son aide, pour son incroyable esprit difficile à suivre. Merci à toi de m'avoir offert l'opportunité de réaliser ma thèse ici. Cette chance m'aura permis de grandir scientifiquement, mais aussi humainement. Et ça grâce à toi et à toute l'équipe que j'aurais pu ne jamais rencontrer.

On en vient donc à l'équipe que je remercie chaudement. Votre soutien et votre bonne humeur, nos discussions et nos rires ont fait de cette thèse un moment des plus agréables, même dans ses moments les plus désagréables. Je tiens particulièrement à ne pas te remercier Céline, car les longues séances de pose de DiI sont ta faute, mais je tiens à te remercier d'avoir pris tellement de temps à m'enseigner le geste et le regard. Je tiens à remercier Aurora, qui m'a formé à la dissection et au rhum arrangé. Merci Mumu, pour tes connaissances infinies sur le clonage, pour ton aide de tous les jours, mais surtout pour ton humour beauf qui ne fait rire que nous. Merci KK, je t'ai refilé la patate chaude des WB, tu m'as refilé ta bonne humeur qui égaye mes semaines, tes photos de montagne qui égayent mes week-ends, et tes recettes qui égayent mes plats – je crois que tu t'es fait un peu roulée. Merci Hug Duc Le Duc, tu m'as soutenu (parfois sans le vouloir ou le savoir), tu m'as poussé dans mes réflexions, on a progressé ensemble sur la révolution… Je pourrai continuer longtemps mais je garde le reste pour le tome 2 de notre relation. Merci Jul pour ton savoir : sur mon sujet, sur la microscopie, sur tout. Merci pour nos discussions jusqu'à pas d'heure qui m'empêche de faire les courses mais qui me nourrissent intellectuellement. Merci Clélia pour ta gentillesse et ta bienveillance, et surtout pour tes petites phrases cinglantes (in)volontaires, on commence à se connaître depuis longtemps, mais il est toujours aussi agréable de passer du temps ensemble.

Merci à Denis, Bruno, Elisabeth, Christel et Camilla du CIQLE pour votre pédagogie. Tous nos travaux n'apparaissent pas dans cette thèse, mais merci de m'avoir donné l'opportunité de les réaliser.

Merci à Alexandra, Lisa-Marie du SCAR, et Jean-Michel, Aurélie et Maxime d'ALECS. Mes demandes étaient souvent changeantes et à la dernière minute, mais vous avez toujours su travailler avec moi.

Merci à Nini qui m'a débloqué un mois de clonages infructueux en une question. Merci à tous mes amis de m'avoir soutenu (parfois presque littéralement) au cours de cette thèse. Merci aux copains du CRCL, merci aux copains de la fac, merci à Bouboule/Meurion/Emmy/Litchi. Merci à Alice de m'avoir

supporté (dans plusieurs sens du terme) à travers cette période difficile. Merci à ma deuxième famille, celle de la cour carrée, malgré mon absence grandissante au cours de cette thèse rien n'a changé. Merci surtout à ma première famille, celle du sang, vous ne m'avez jamais reproché mes absences (physiques ou mentales) et avez tout fait pour que je sois heureux, j'espère pouvoir vous rendre ce que vous m'avez offert. Merci surtout à mes parents, votre gentillesse, votre abnégation, votre intelligence ont toujours été un modèle pour moi. J'espère que vous êtes aussi fier de votre fils que je suis fier de mes parents.

J'ai hâte de tous vous retrouver.

Résumé en français

Cartographie et fonctions des fragments issus du facteur de guidage axonal Slit

Au cours du développement embryonnaire, les neurones étendent leur axone à travers l'organisme pour connecter leur cible finale. Cette navigation axonale est finement contrôlée par de multiples signaux permettant une trajectoire stéréotypée, et présente différentes étapes. Chez les bilatériens, un niveau de complexité supplémentaire apparaît avec les commissures. Ces dernières sont composées d'axones traversant la ligne médiane, permettant ainsi d'interconnecter les deux moitiés du système nerveux central (SNC). Leur formation est essentielle pour l'intégration et la coordination des commandes motrices, des modalités sensorielles, mais également pour le traitement des informations cérébrales.

Au sein de la moelle épinière, différentes sources de signaux attractifs et répulsifs vont guider les axones commissuraux jusqu'à la plaque du plancher (PP) où ils traversent la ligne médiane. Si la PP est une source d'attractants, elle a la particularité d'exprimer également des répulsifs sans que cela n'empêche les axones commissuraux de la traverser. Ces derniers naviguent au niveau des prolongements basaux des cellules gliales de la PP, et vont alors être sensibilisés aux signaux répulsifs. Ce mécanisme permet aux axones d'être expulsés de la PP, puis de la longer sans jamais la retraverser afin d'atteindre leur cible finale. Différentes signalisations répulsives sont impliquées dans la traversée de la PP, les principales étant : SlitN *via* les récepteurs Roundabout1 et 2 (Robo1 et 2) ; SlitC *via* le récepteur PlexinA1 (PlxnA1) ; Semaphorin3B (Sema3B) *via* le complexe PlxnA1-Neuropilin2 (Nrp2). Des études de trajectoires axonales dans la PP – chez différents mutants dans lesquels ces ligands, ou récepteurs, sont invalidés – suggèrent que les signalisations répulsives contrôlent la traversée *via* différents mécanismes. Cependant, le lien entre ces mécanismes et ces signalisations restent encore mal connu. Cela s'explique entre autres par la difficulté d'isoler chaque signalisation. En effet, côté récepteurs, l'invalidation de PlxnA1 va affecter à la fois les signalisations SlitC et Sema3B. Côté ligands, SlitN et SlitC étant des fragments issus du clivage de la protéine Slit, l'invalidation de cette dernière va affecter les signalisations médiées par Robo1-2 et PlxnA1.

Ma thèse a porté sur l'étude d'une lignée murine mutante développée suite à de précédents travaux, réalisés dans notre équipe, montrant que la mutation PlxnA1^{Y1815F} abroge spécifiquement la signalisation SlitC/PlxnA1 *in vitro*. Nous avons pu observer des défauts de trajectoire, au sein de la PP, caractéristiques de cette signalisation. Ainsi, nous pouvons supposer que la signalisation SlitC/PlxnA1 va spécifiquement contraindre les axones dans une trajectoire rectiligne et les empêcher de faire demi-tour. Afin de comprendre l'émergence de spécificités fonctionnelles, j'ai suivi l'hypothèse d'une

différence dans la présentation des ligands. Dans ce but, j'ai développé divers outils, le principal permettant de suivre les fragments issus du clivage de Slit2 *in vivo*. J'ai ainsi pu montrer que SlitN et SlitC sont présentés aux axones de manière similaire, révélant que les spécificités fonctionnelles ne semblent pas liées à la présentation des ligands. De plus, cet outil m'a permis de montrer que les signaux Slit diffusent moins dans le compartiment basal de la PP en absence de clivage. Ce résultat révèle l'importance du clivage de Slit pour obtenir une présentation correcte des signaux.

En parallèle, j'ai cherché à améliorer notre compréhension de la traversée en m'intéressant à l'environnement physique que constitue la PP. Pour cela, j'ai imagé des cellules gliales individuelles et des axones uniques au sein d'une PP marquée. Des reconstructions 3D de ces images m'ont permis de révéler l'étonnante complexité morphologique des cellules de la PP, mais également le contact étroit entre les axones et les prolongements basaux des cellules gliales. Cette information est indispensable à notre compréhension de la traversée pour plusieurs raisons : 1) les contraintes mécaniques peuvent en partie forcer une trajectoire axonale rectiligne ; 2) un environnement encombré va influencer la diffusion des ligands ; 3) le contact étroit entre axone et cellule de la PP va permettre des signalisations de membrane à membrane et une concentration forte des signaux.

English summary

Cartography and functions of the fragments from Slit axon guidance cue

During embryonic development, neurons extend their axon through the organism in order to connect their final target. Axon navigation is tightly regulated by many cues allowing a stereotyped trajectory, and involves various steps. In bilaterians, commissures add another level of complexity. These structures are composed of a bundle of axons crossing the midline, thus interconnecting both halves of the central nervous system. Proper commissure formation is essential for the integration and coordination of motor commands and sensory modalities, but also for brain processing.

In the spinal cord, numerous sources provide attractive and repulsive cues to guide commissural axons to the floor plate (FP) where they cross the midline. The FP provide both attractive and repulsive cues. However, the latter do not prevent commissural axons from crossing the FP. Instead, they navigate through the basal end-feet of the FP's glial cells, where they gain sensitivity to repellents. Upon sensitization, axons are expulsed from the FP, they then turn rostrally to navigate alongside the FP without ever crossing back, in order to reach their final target. Various repulsive signalizations are involved in FP crossing, the main ones being: SlitN through Roundabout1 and 2 (Robo1 and 2) receptors; SlitC through PlexinA1 (PlxnA1) receptor; Semaphorin3B (Sema3B) through the PlxnA1-Neuropilin2 (Nrp2) complex. Analyzes of axon trajectories inside the FP – in mutants knocked out (KO) for the different proteins – suggest different mechanisms for the control of FP crossing by repellents. Still, little is known about the link between these mechanisms and signalizations. This can partly be explained by the complexity to differentiate between each signalization. Indeed, on one side, PlxnA1 KO affects both SlitC and Sema3B pathways. On the other side, both SlitN and SlitC comes from Slit cleavage, therefore Slit KO affects pathways mediated by PlxnA1 and Robo1-2.

My thesis involved the analyzes of a murine mutant line based on previous work, done by our team, showing that PlxnA1^{Y1815F} mutation specifically abrogate SlitC/PlxnA1 signaling *in vitro*. We were able to see crossing defects characteristic of this signalization. Therefore, we propose the SlitC/PlxnA1 specifically constrain axon navigation in a straight trajectory and prevents their turning back. In order to investigate the emergence of functional specificities, I followed the hypothesis of a difference in cue presentation. To do so, I developed various tools, the main allowing to follow Slit2 cleavage fragments *in vivo*. Thus, I was able to show that SlitN and SlitC are distributed in a similar manner within the FP, suggesting that functional specificities do not come from ligand presentation. Furthermore, this tool allowed me to observe a diminution in Slit cues diffusion, within FP basal compartment, in the absence

of cleavage. This result brings to light the importance of Slit cleavage in obtaining proper ligand presentation.

During my thesis, I also tried to better our understanding of FP crossing by studying the physical environment formed by the FP. To do so, I imaged individual glial cells, but also individual axons within a stained FP. Through 3D reconstructions, I was able to show the surprising complexity of FP cells morphology, but also the close contact between axons and the glial cells end-feet. This information is crucial to understand FP crossing for various reasons: 1) physical constraints can partly force a straight trajectory; 2) a cluttered environment affects the ligands diffusion; 3) close contact between axons and glial cells allows membrane to membrane signalizations.

Table des matières

Table des figures

Abréviations

Abl	Abelson
ALPS	Agrin-Perlecan-Laminin-Slit
APP	Protéine précurseur de l'amyloïde β
CAM	molécule d'adhésion cellulaire
CC	cône de croissance
Co-IP	co-immunoprécipitation
Col4a5	Collagen4a5
DEC	domaine extracellulaire
DIC	domaine intracellulaire
DRBZ	zone de bifurcation des axones des ganglions dorso-rachidiens
DREZ	zone d'entrée des axones des ganglions dorso-rachidiens
DRG	ganglions dorso-rachidiens
EGF	facteur de croissance épidermique
GAP	protéine activatrices de GTPase
GEF	facteur d'échange de guanine nucléotide
LP	longitudinaux primitifs
LRR	répétitions riches en leucine
MEC	matrice extracellulaire
Nrp	Neuropilin
PC2	Proprotéine Convertase 2
Plxn	Plexin
PP	plaque du plancher
Robo	Roundabout
Sema	Semaphorin
Shh	Sonic hedgehog
Slit2 DT	Slit2 double tag
SlitC	fragment C-terminal de Slit
Slit FL	Slit « full length »
SlitN	fragment N-terminal de Slit
SM	spectrographie de masse
SN	système nerveux
SNC	système nerveux central
Sos	Son of seven
TM	Domaine transmembranaire
VenusC	fragment C-terminal de Venus
VenusN	fragment N-terminal de Venus
VZ	zone ventriculaire

INTRODUCTION

I. Plaque du plancher et développement

Le développement d'un organisme est un processus complexe. Les cellules doivent se différencier au bon endroit et au bon moment, et s'organiser afin de former tissus et organes. En 1909, dans le but de comprendre comment ce processus est contrôlé, Browne greffe un hypostome (une structure adjacente de la tête de l'hydre) chez une hydre receveuse (Browne, 1909; Anderson and Stern, 2016). Elle observe ainsi l'induction d'un nouvel axe de développement composé des cellules de l'organisme receveur, mais dépourvu de cellules du donneur. Elle en conclut que l'hypostome est une structure qui va influencer le sort des cellules adjacentes, permettant ainsi d'organiser le développement de l'organisme. Quinze ans plus tard, Spemann et Mangold utilisent la même technique dans la salamandre (Anderson and Stern, 2016). Ils greffent ainsi une lèvre dorsale du blastopore d'un embryon A sur un embryon B. Au niveau du site de greffe, peu importe sa localisation, un embryon siamois se développe. En étudiant les cellules de ce dernier, ils observent que les cellules de l'embryon A vont uniquement se retrouver dans quelques structures (la notochorde, les somites et la plaque du plancher), alors que les cellules de l'embryon B vont composer la majorité de l'embryon siamois. Ces résultats montrent que le développement de certains tissus n'est pas une caractéristique intrinsèque des cellules qui les composent, mais est en fait contrôlé par des structures spécifiques adjacentes. Spemann et Mangold utilisent pour la première fois le terme d'organisateur pour désigner ces structures.

Aujourd'hui, ce terme regroupe différentes régions, ou groupes de cellules, ayant la particularité d'induire la différentiation des cellules adjacentes et de générer des structures organisées. Les organisateurs permettant l'émergence de structures complexes, il n'est pas étonnant d'en retrouver plusieurs contrôlant le développement du système nerveux (SN) (Anderson and Stern, 2016).Ce dernier doit en effet se développer selon plusieurs axes et à travers tout l'organisme, avec des structures aux formes variées.

La moelle épinière est l'une de ces structures. Elle relaie les informations sensorielles au cortex grâce à des interneurones et permet le contrôle des mouvements *via* des motoneurones. Son développement dépend de différents organisateurs : le nœud primitif (appelé nœud de Hensen chez les oiseaux) ; la notochorde (située ventralement par rapport la moelle épinière) ; la plaque du toit (dans la partie dorsale de la moelle) et la plaque du plancher (PP). Cette dernière est située au niveau de la ligne médiane dans la partie la plus ventrale de la moelle et c'est particulièrement sur cette structure qu'ont porté les travaux de ma thèse.

1. Composition de la plaque du plancher

C'est Wilhelm His, en 1888, qui nomme la PP et la décrit comme un groupe distinct de cellules à la ligne médiane de la plaque neurale (Kingsbury, 1920). Il observe que la PP ne contient pas de progéniteurs neuraux ou de neurones différenciés, mais uniquement des cellules gliales translucides. Les cellules de la PP sont fortement polarisées et présentent un noyau allongé, radialement orienté, et relativement éloigné de la lumière du tube neural (van Straaten *et al.*, 1985, 1988). Avec leur noyau au niveau de la lame basale, pendant les stades précoces de leur développement, elles possèdent une morphologie triangulaire. A des stades plus tardifs, les corps cellulaires sont séparés de la lame basale par les prolongements basaux des cellules (Charrier *et al.*, 2002). Ces prolongements sont fins dans l'axe rostro-caudal et allongés latéralement (Yaginuma *et al.*, 1991).

Afin de mieux comprendre la composition de la PP, Charrier *et al.* étudient différents marqueurs et en dressent une liste spécifique de la PP (Charrier *et al.*, 2002). Ils constatent cependant que les cellules neuroépithéliales, issues du neuroectoderme, en contact avec la PP expriment certains marqueurs de leur liste. Bien que ces cellules n'aient pas la morphologie des cellules de PP, l'expression de marqueurs de PP suppose que les deux domaines remplissent un rôle similaire. Charrier *et al.* montrent donc une hétérogénéité dans la composition de la PP et proposent les appellations PP latérale, pour les cellules neuroépithéliales, et PP médiane, pour les cellules gliales. Dans la suite de ce manuscrit, j'utiliserai le terme de PP pour désigner la PP médiane.

Le long de l'axe rostro-caudal, les cellules de la PP présentent également une hétérogénéité morphologique. La PP s'étend de la moelle épinière jusqu'au diencéphale, avec une limite antérieure au niveau de la *zona limitans intrathalamica*. En plus de leurs différences morphologiques, les cellules de la PP possède une temporalité d'induction plus lente en caudal qu'en rostral (Placzek, Jessell and Dodd, 1993). De plus, elles n'ont pas la même origine développementale en fonction de leur position le long de l'axe rostro-caudal (Placzek and Briscoe, 2005). Dans la partie suivante, je détaillerai les origines développementales de la PP dans la moelle épinière.

2. Développement de la plaque du plancher de la moelle épinière

a. La plaque du plancher possède une origine différente du reste de la moelle

Dans l'expérience de Spemann et Mangold, la PP et la notochorde de l'embryon siamois sont constituées des cellules greffées, contrairement au reste de la moelle. Cela suggère que les cellules de

la notochorde et de la PP ont une origine partagée, mais également que celle-ci diffère de l'origine du reste de la moelle. Différentes études chez l'embryon aviaire exploitent le « fate mapping » pour montrer que la PP et la notochorde proviennent de régions chevauchantes de l'épiblaste, confirmant ainsi l'hypothèse d'une origine partagée (Glenn C. Rosenquist, 1966; Nicolet, 1970; Smith and Schoenwolf, 1989; Selleck and Stern, 1991). Parmi ces études, certaines suggèrent également que la PP et la notochorde dérivent du nœud de Hensen. Pour étudier cette possibilité, Charrier *et al.* remplacent le nœud de Hensen d'embryons de poulet par celui d'un embryon de caille et observent que la notochorde et la PP sont toutes les deux composées de cellules de caille (Charrier *et al.*, 2002). A l'inverse, en remplaçant la future plaque neurale de l'embryon de poulet par celle d'un embryon de caille, en position caudale par rapport au nœud de Hensen, Charrier *et al.* montrent qu'au sein de la plaque neurale, composée de cellules de caille, la PP est constituée de cellules de poulet. L'ensemble de ces résultats montre que la PP possède une origine différente du reste de la plaque neurale, mais ils suggèrent également une séquence développementale spécifique : 1) alors qu'il se déplace caudalement, la prolifération des cellules du nœud de Hensen génère une corde médiane de cellules et 2) cette corde va rapidement se séparer en deux : une partie ventrale qui va générer la notochorde ; une partie dorsale qui va progressivement s'incorporer à la plaque neurale (issue du neuroectoderme), au niveau de la ligne médiane, pour devenir la notoplaque (future PP) (Fig. 1A) (Catala, Teillet and le Douarin, 1995; Catala *et al.*, 1996; Charrier *et al.*, 2002).

A ce stade du développement, la plaque neurale n'est qu'un simple épithélium. Ses extrémités vont se rapprocher, formant ainsi des plis neuraux, puis fusionner pour former le tube neural. Les cellules neuroépithéliales vont ensuite continuer de proliférer, puis elles se différencient. C'est à ce moment que l'on parlera de moelle épinière (Fig. 1B - 1F).

Lors de la fermeture du tube neural, les cellules dans la région de fusion forment une ligne médiane appelée la plaque du toit, alors que les cellules de la ligne médiane ventrale (notoplaque) se différencient pour former la plaque du plancher. Il est intéressant de noter que la notochorde et les cellules de la notoplaque sont en contact direct durant les trois premières étapes mentionnées précédemment, avant de s'éloigner une fois la PP différenciée et la moelle épinière formée. Cette observation suggère que la notochorde pourrait avoir un impact sur la notoplaque et son développement en PP.

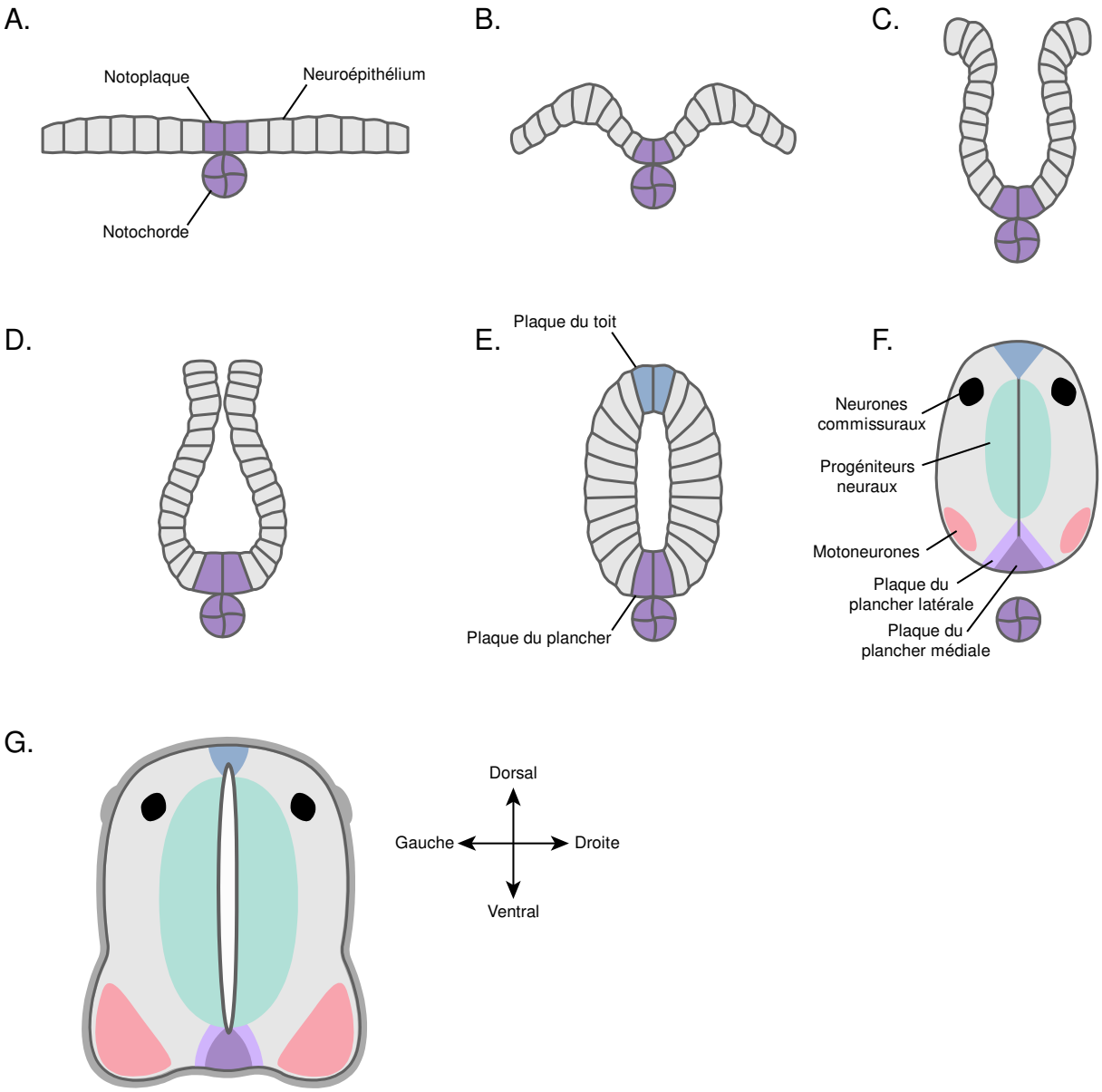

Figure 1. Représentation schématique de la formation de la moelle épinière

(**A**) **Plaque neurale.** Le mésoderme du nœud primitif donne les cellules de la notochorde et de la notoplaque. Ces dernières s'insèrent dans la plaque neurale, au niveau de la ligne médiane. A ce stade, la plaque neurale n'est qu'un simple épithélium avec des cellules du mésoderme à la ligne médiane. La notochorde est en contact direct avec la notoplaque. (**B, C, D**) **Plis neuraux.** Les cellules de la notoplaque adoptent une morphologie triangulaire. Ce changement participe aux forces mécaniques permettant aux extrémités de la plaque neurale de se rapprocher, mais n'est pas indispensable. (**E**) **Tube neural.** Les cellules des extrémités de la plaque neurale fusionnent. Les cellules de la ligne médiane dorsale se différencient pour former la plaque du toit, alors que celles de la notoplaque se différencient pour former la plaque du plancher (PP). (**F**) **Moelle épinière.** Les cellules neuroépithéliales prolifèrent et se différencient pour former les différents types cellulaires de la moelle. La notochorde n'est plus au contact de la PP. (**G**) Morphologie d'une moelle épinière de souris à E12.5 ou de poulet à E4. A ce stade, les axones des motoneurones sont déjà sortis de la moelle et la majorité des axones commissuraux traverse ou a déjà traversé la PP.

b. *La notochorde induit le développement de la plaque du plancher*

Pour confirmer cette théorie, des premières expériences d'ablation de la notochorde (chez des amphibiens, avant fermeture du tube neural) montrent que la PP ne se forme pas sans notochorde (Kitchin, 1949; van Straaten and Drukker, 1987; Jessell *et al.*, 1989). La conclusion de ces expériences est que la notochorde permet l'induction de la PP, mais un doute subsiste : n'est-ce pas seulement l'ablation d'une structure en contact direct avec la notoplaque qui va l'endommager et empêcher sa différenciation en PP ? Entre 1985 et 1987, grâce à des greffes ectopiques de notochorde, van Straaten et Drukker confirment que la notochorde induit un changement morphologique du tube neural similaire à la présence d'une PP supplémentaire. De plus, les cellules au contact de la notochorde adoptent une morphologie similaire à celle des cellules de la PP (van Straaten *et al.*, 1985; van Straaten and Drukker, 1987; Jessell *et al.*, 1989). Il faut attendre 1991 pour confirmer que les cellules à proximité de la notochorde greffée expriment des marqueurs de PP (Placzek *et al.*, 1991; Yamada *et al.*, 1991). Dans les travaux cités précédemment, les auteurs montrent qu'une faible distance (<30µm) entre la notochorde greffée et la moelle est nécessaire pour induire une PP. Tous ces travaux montrent donc que la formation de la PP dépend de la notochorde, et la faible distance requise pour cette induction suggère l'implication de signaux à forte concentration, ou bien de signaux piégés dans la matrice extracellulaire (MEC) de la notochorde (van Straaten *et al.*, 1985, 1988).

Une greffe de notochorde au contact de la moelle induit donc une PP exogène, mais greffer une PP de la même manière aura le même effet, soulignant le lien fort entre notochorde et PP (Yamada *et al.*, 1991). De plus, il est étonnant de voir que, si la PP endogène a une origine différente des autres cellules de la moelle, ces dernières peuvent toutefois se différencier en cellules de PP au contact d'une notochorde ou PP. Ce mécanisme d'induction homéogénétique permet potentiellement d'avoir une PP fonctionnelle et composée d'un nombre de cellules gliales suffisant, même en cas de malformation de la notoplaque. Cette caractéristique développementale sous-entend une importance de la PP dans le développement subséquent du reste de la moelle. Importance confirmée par le fait que, si la PP est dépendante d'organisateurs pour sa mise en place (nœud primitif et notochorde), elle est elle-même considérée comme un organisateur. Dans la prochaine sous-partie, je développerai les différentes caractéristiques permettant de la classifier en tant que tel.

3. D'influencé à influenceur

a. La notoplaque influence mécaniquement la morphologie de la moelle

Les cellules de la notoplaque présentent des propriétés mécaniques et adhésives particulières, en plus de leur forme triangulaire. Ces trois caractéristiques, ainsi que leur emplacement à ligne médiane de la plaque neurale – zone qui va fortement se plier pour former le tube neural – ont amené la théorie qu'elles seraient à l'origine des forces permettant les plis neuraux (Jacobson and Gordon, 1976; Jessell *et al.*, 1989; Schoenwolf and Smith, 1990). Cependant, le tube neural peut se fermer même sans notoplaque (Youn and Malacinski, 1981). Si les cellules de la notoplaque ne sont pas indispensables à la fermeture du tube neural, différents travaux ont montré qu'une fois que ces cellules prennent leur forme triangulaire, cela crée un sillon qui va faciliter la fermeture du tube neural et permettre d'obtenir la morphologie caractéristique de la moelle (Smith and Schoenwolf, 1989; Schoenwolf and Smith, 1990).

b. La plaque du plancher permet la structuration des territoires de la moelle

Si quelques études ont porté sur l'influence physique de la PP sur les tissus, un grand nombre se sont intéressées à son impact sur les cellules environnantes. Ainsi, plusieurs études ont suggéré que la PP restreint la prolifération neuroépithéliale (Grabowski, 1956; Youn and Malacinski, 1981; Malacinski and Youn, 1982). Cependant, la présence d'une PP exogène ne diminue pas pour autant le nombre de cellules (Yamada *et al.*, 1991). Ce résultat suggère que, si la PP est impliquée dans la prolifération neuroépithéliale, son rôle ne serait qu'indirect et limité. Une autre étude montre que l'absence de PP n'empêche pas la différenciation du neuro-ectoderme, ni la formation du tube neural, indiquant qu'elle n'est pas nécessaire pour l'induction neurale (Jessell *et al.*, 1989). Cependant, en 1991, Yamada *et al.* montrent que l'absence de notochorde et PP résulte en l'absence de motoneurones. Cela indique que la PP est impliquée dans leur développement (Yamada *et al.*, 1991). En parallèle, Placzek *et al.* montrent qu'une PP ectopique entraîne l'apparition de colonnes de motoneurones supplémentaires (Placzek *et al.*, 1991). Ces colonnes supplémentaires se développent par rapport à la PP ectopique avec la même symétrie que pour les colonnes physiologiques : une de chaque côté, espacée de la PP par une région de cellules non marquées. Dans le cas d'un développement physiologique, cette région (en violet clair sur la Fig. 1F) est notamment constituée de la PP latérale, décrite par Charrier *et al.*, et d'interneurones longitudinaux primitifs (LP). Charrier *et al.* montrent qu'une PP latérale est présente systématiquement lorsque qu'une PP, ectopique ou non, est induite (Charrier *et al.*, 2002). De plus, Yamada *et al.* observent que la PP induit également des interneurones LP – au moins dans le rhombencéphale, en l'absence de marqueur pour identifier ceux de la moelle (Yamada *et al.*, 1991). Ces résultats montrent que la PP permet la mise en place des domaines ventraux de la moelle : de la

PP latérale (en contact direct) jusqu'aux motoneurones (plus éloignés), en passant par les interneurones LP.

Pour étudier l'impact de la PP sur les domaines dorsaux de la moelle, Yamada *et al.* ont analysé l'expression de l'antigène AC4, marqueur des cellules neuroépithéliales de la plaque neurale (Yamada *et al.*, 1991). Pendant la neurulation, l'expression de ce marqueur disparaît en commençant dans le domaine ventral, jusqu'au domaine dorsal, pour ne rester qu'à proximité de la plaque du toit. L'induction d'une PP ectopique d'un côté du tube neural entraîne une diminution de l'expression d'AC4 du même côté, alors que l'absence de PP entraîne une expression d'AC4 tout le long de l'axe dorso-ventral. La PP aurait donc un rôle dans la différentiation des domaines dorsaux. Cependant, l'absence de PP n'empêche pas le développement des interneurones, qui ne sont alors plus restreints aux domaines dorsaux, mais se retrouvent jusque dans les régions habituellement occupées par les motoneurones et la PP (Yamada *et al.*, 1991). La PP n'est donc pas indispensable à la formation des neurones, mais est nécessaire pour structurer correctement les territoires de la moelle.

c. La plaque du plancher agit directement et indirectement sur la mise en place des territoires

La PP a-t-elle une action directe sur la différentiation des cellules du tube neural ou est-t-elle l'origine de transformations se transmettant par contact ? Sonic hedgehog (Shh) présente des preuves pour une action directe. *In vivo*, l'expression de ce morphogène par la PP et la notochorde va former un gradient au sein de la moelle (Briscoe and Ericson, 1999). *In vitro*, la culture d'explants en sa présence va provoquer la différentiation de types cellulaires variés en fonction de sa concentration (Ericson *et al.*, 1997). De plus, les concentrations relatives pour induire les différents types cellulaires correspondent à la distance de ces cellules par rapport à la PP *in vivo*. Ainsi, une faible concentration de Shh induira des types cellulaires éloignés de la PP et inversement. Cela suggère que la PP peut bien avoir un impact direct sur la différentiation de structures éloignées. Cependant, Briscoe et Ericson proposent un modèle de différentiation par Shh en trois étapes. Premièrement, Shh va induire l'expression de différentes protéines homéodomaines définissant des domaines de progéniteurs distincts. Deuxièmement, les interactions entre les différentes protéines homéodomaines voisines vont permettre d'affiner et de maintenir les différents domaines de progéniteurs. Enfin, alors que les cellules commencent à se différencier, les protéines homéodomaines des progéniteurs définissent l'identité des cellules. Ainsi, l'action directe de la PP sur les différents domaines dorso-ventraux est affinée par des interactions inter- et intra-domaines (Briscoe and Ericson, 1999).

II. Navigation des axones – Principes généraux

La moelle épinière est une structure du système nerveux faisant remonter les informations sensorielles au cortex. Pour remplir ce rôle, elle contient des interneurones dont le corps cellulaire est situé au niveau dorsal de la moelle. En plus de ce corps cellulaire, chaque interneurone possède des dendrites, pour capter les informations sensorielles afférentes, et un axone, pour transmettre ces informations jusqu'au cortex. Lors du développement, les axones des interneurones vont suivre une trajectoire stéréotypée grâce à divers signaux et structures leur permettant d'atteindre leur cible finale. Les différents mécanismes contrôlant cette navigation sont regroupés sous le terme de guidage axonal.

1. Le cône de croissance

a. Le cône de croissance est le moteur de la pousse axonale

Pendant sa navigation dans l'organisme, l'axone se termine par une structure élargie lui permettant de capter les signaux de guidage : le cône de croissance (CC). Cette structure est séparée en deux grandes régions, définies par leur cytosquelette : la région périphérique et la région centrale (Dent, Gupton and Gertler, 2011). La première est composée de lamellipodes – larges extensions – dont partent les filopodes – minces projections – les deux étant riches en actine. La région centrale, quant à elle, est riche en microtubules et connecte la région périphérique au reste de l'axone (Fig. 2A). Cependant, il est possible que la séparation entre un domaine actine et un domaine microtubule n'existe que pour les axones *in vitro* poussant sur un substrat 2D (Ren *et al.*, 2018). De même, si les CC sont souvent représentés en épouvantail à cause de leur forme *in vitro*, ils prennent en réalité des formes plus variées *in vivo*, en fonction de leur environnement (signaux présents, rigidité du milieu, structures physiquement contraignantes) (Yaginuma *et al.*, 1991). A la surface du CC se trouvent différents récepteurs lui permettant de capter et de répondre aux signaux de son environnement. *In fine*, les signalisations de guidage vont remodeler localement le cytosquelette afin d'acheminer l'axone jusqu'à sa cible. Pour contrôler la pousse de l'axone, le CC doit pouvoir construire l'axone, adhérer à un substrat, et s'orienter dans l'espace.

Les filaments d'actines et les microtubules du cytosquelette sont constamment en train de se polymériser et dépolymériser, modifiant les structures du CC (Fig. 2B). De plus, sur le dense réseau de microtubules du CC circulent différents moteurs moléculaires. Ce système permet un trafic vésiculaire intense amenant à une relocalisation du cytosquelette du CC, de ses membranes et des protéines à sa

surface (Fig. 2C) (Vitriol and Zheng, 2012). Au niveau cellulaire, ce remaniement se traduit par l'émission et la rétraction des filopodes et lamellipodes avec une vitesse importante (1 à 4 µm/min). Ce mécanisme permet au CC d'explorer rapidement son environnement, de relocaliser son cytosquelette en direction des territoires propices à la navigation, et de construire l'axone. Cependant, le CC a besoin d'exercer une force sur un support physique pour avancer et allonger l'axone.

Ce support physique, appelé substrat, est médié par un ensemble de molécules d'adhésion cellulaires (CAM) – situées dans la MEC, sur la surface de cellules de l'environnement, mais aussi à la surface des axones – ainsi que des récepteurs à ces molécules. Parmi les CAM du système nerveux central (SNC), on trouve les laminines, les intégrines, les cadhérines et la superfamille des immunoglobulines. Les récepteurs et CAM du CC, couplés au réseau d'actine, vont lui permettre de s'ancrer au substrat et d'utiliser le flux rétrograde d'actine pour se tirer vers l'avant (Fig. 2D) (Mitchison and Kirschner, 1988; Jay, 2000; Kamiguchi, 2007). Cependant, la pertinence de cette vision *in vivo* est remise en question. En effet, l'efficacité de ce mécanisme va dépendre de la rigidité de l'environnement (Chan and Odde, 2008; Koser *et al.*, 2016). Ainsi, les forces internes et externes au CC vont réguler sa pousse. Le dynamisme du CC et son adhésion au substrat rendent possible la pousse de l'axone dans des directions aléatoires. Cependant, pour atteindre sa cible, il doit suivre une direction précise en percevant différents signaux de guidage dans l'environnement.

b. Les signaux de l'environnement dirigent le cône de croissance

A la surface du CC se trouve également un éventail de récepteurs lui permettant de capter ces signaux. Ces derniers sont classés en deux catégories, attractif ou répulsif, en fonction de la réponse qu'ils provoquent : 1) en réponse à un attractant, des vésicules apportent des molécules d'adhésion par exocytose, permettant au cytosquelette de se polymériser vers l'avant, prolongeant la membrane et formant de nouveaux filopodes et lamellipodes ; 2) en réponse à un répulsif, les molécules d'adhésion sont endocytées, le cytosquelette se dépolymérise, la membrane est recyclée et le CC perd filopodes et lamellipodes – on parle alors de CC effondré (Fig. 2E) (Kamiguchi, 2007; Kerstein, Nichol and Gomez, 2015). Cependant, des travaux viennent nuancer cette vision, en montrant que certaines signalisations répulsives induisent et requièrent la formation de nouveaux filopodes (McConnell *et al.*, 2016). Les signaux de guidage peuvent être présents sur des cellules de l'environnement, séquestrés dans la MEC, ou bien diffusés dans l'environnement (formant des gradients). De plus, les CAM de l'environnement peuvent aussi médier des répulsions ou des attractions, et les CAM d'axones pionniers permettent aux suivants de s'y rattacher et de suivre la trajectoire des pionniers (Kamiguchi, 2007).

Le mélange de signaux répulsifs et attractifs présentés au CC de différentes façons va orienter la pousse de l'axone. De plus, l'adressage des CAM et des récepteurs de guidage et d'adhésion dans les différentes structures du CC est spécifique, polarisé et dynamique. Cela permet un contrôle local du cytosquelette et, *in fine*, l'émergence de trajectoires complexes de l'axone, comme des virages serrés.

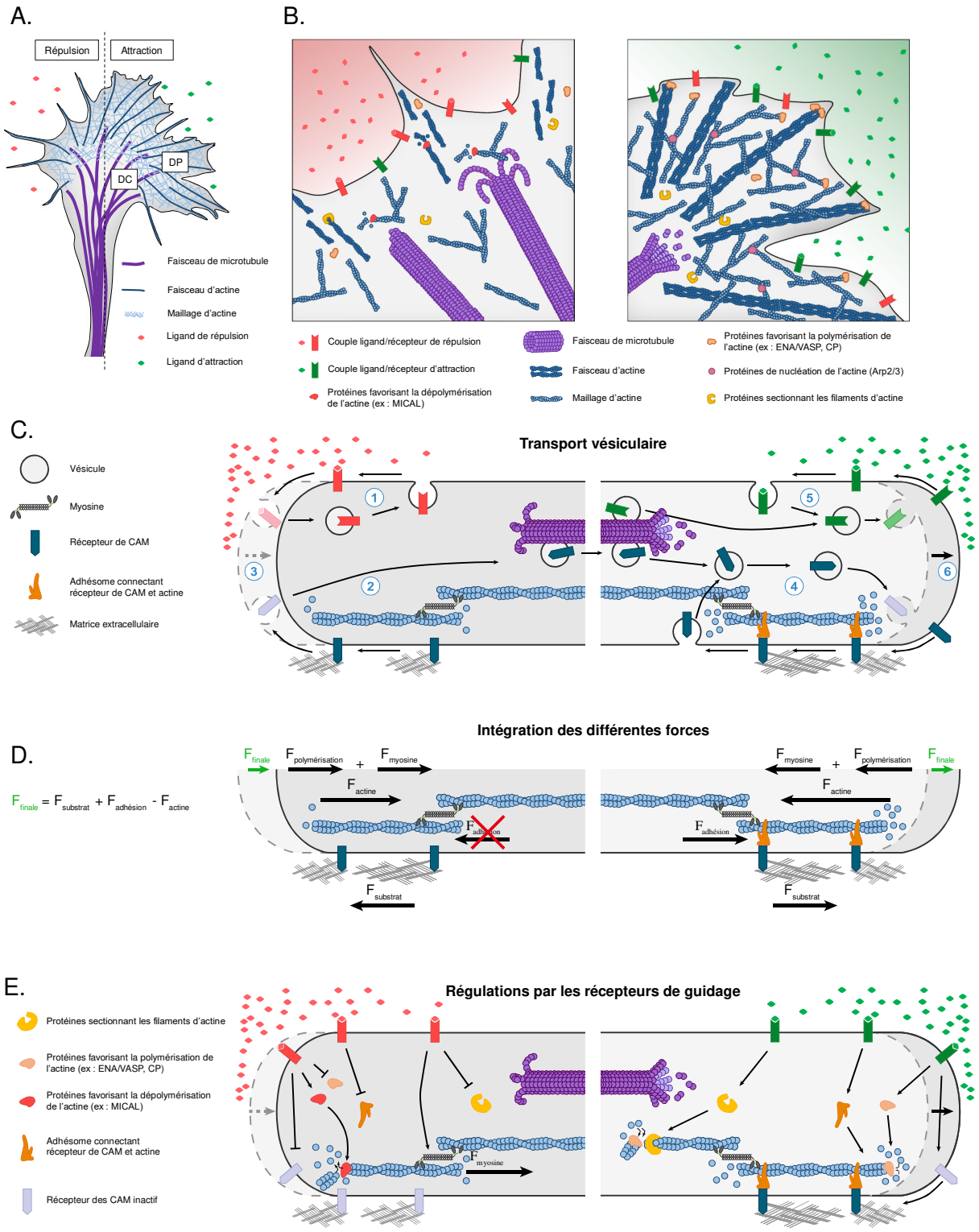

Figure 2. Le cône de croissance : moteur de la navigation axonale

(**A**) Représentation schématique d'un cône de croissance (CC) sous l'influence de signaux répulsifs (à gauche) et attractifs (à droite). Le domaine central (DC) est occupé majoritairement par les microtubules, alors que le domaine périphérique (DP) est occupé principalement par des faisceaux et un maillage d'actine. (**B**) Agrandissement des zones en rétraction (à gauche) et en croissance (à droite) avec les acteurs moléculaires impliqués. Au niveau de la zone en rétraction, les filaments d'actine sont sectionnés par différentes protéines et les extrémités (+) (propices à la polymérisation) sont déstabilisées et dépolymérisent. Les microtubules sont également sectionnés et subissent des évènements de catastrophe (dépolymérisation rapide). La dépolymérisation accrue des molécules du cytosquelette entraîne la rétraction, voire l'effondrement du CC. Du côté de la zone en croissance, les filaments d'actine sont également sectionnés, mais les extrémités (+) sont stabilisées et des protéines de nucléation de l'actine favorisent la polymérisation. Ce mécanisme permet notamment d'augmenter la ramification du maillage d'actine et de stabiliser le DP. Les microtubules sont polymérisés et envahissent le DP. (**C-E**) Représentation schématique de différents mécanismes permettant la pousse et la navigation axonales au niveau des zones en rétraction (à gauche) et en croissance (à droite). (**C**) Le trafic vésiculaire du CC participe à sa restructuration. **1.** Un mécanisme de « tapis roulant » va recycler les récepteurs des signalisations répulsives pour descendre les gradients de répulsifs. **2.** Les récepteurs des molécules d'adhésion cellulaires (CAM) sont également endocytés et transportés par des machineries moléculaires le long des microtubules. **3.** Ces mécanismes d'endocytose participent à la rétractation de la membrane. **4.** Les récepteurs des CAM sont transportés au niveau de la zone en croissance par les microtubules pour augmenter le contingent disponible. Un mécanisme de « tapis roulant » permet le recyclage des CAM vers l'avant. **5.** Le même mécanisme permet de recycler les récepteurs des signalisations attractives pour remonter le gradient d'attractants. **6.** L'intégration des vésicules à l'avant permet l'élargissement de la membrane plasmique et la formation de nouveaux territoires qui vont être envahis par les filaments d'actine. Ces mécanismes participent à la croissance. (**D**) La pousse de l'axone repose sur des forces mécaniques. La polymérisation des filaments d'actine contre la membrane plasmique va les pousser vers l'arrière. La contraction des molécules de myosine va également tirer les filaments vers l'arrière. Les deux forces s'additionnent pour former le flux rétrograde d'actine. Les récepteurs des CAM couplés à l'actine (*via* l'adhésome) et ancrés à la matrice extracellulaire (MEC) vont être tirés vers l'arrière et étirer la MEC. Ainsi, ces récepteurs génèrent des forces de traction au niveau de leur adhésome et sur le substrat, permettant de retenir les filaments d'actine et de se tirer vers l'avant. La diminution du flux rétrograde d'actine permet également d'augmenter la force de polymérisation contre la membrane plasmique, pour la pousser localement. En l'absence de couplage actine/récepteur, les forces de traction ne sont pas formées. (**E**) Présentation de certains mécanismes permettant aux récepteurs de guidage de contrôler la direction de la navigation. (**A, B**) Adaptées de Dent *et al.*, 2011 ; (**D**) Adaptée de Kerstein *et al.*, 2015.

2. Signalisations en aval des récepteurs de guidage

a. Les signalisations de guidage partagent de nombreux acteurs en aval

Le contrôle du cytosquelette par les signaux de guidage et des molécules d'adhésion implique des cascades de signalisation en aval de leur récepteur. Bien que ces voies de signalisation ne soient pas complètement élucidées, de nombreux acteurs et mécanismes sont connus. Les principales signalisations de guidage, aussi bien répulsives qu'attractives, vont contrôler l'activité de petites

GTPases de la famille Rho – notamment RhoA, Rac et CDC42 – et leurs effecteurs – les facteurs d'échange de guanine nucléotide (GEF) et les protéines activatrices de GTPase (GAP) (Wen and Liu, 2014; Niftullayev and Lamarche-Vane, 2019). Il est intéressant de noter que chaque signalisation a un impact différent sur ces GTPases, mais que des signalisations répulsives et attractives peuvent avoir un impact similaire. Il est donc difficile de relier l'activité d'une GTPase à un comportement de guidage spécifique. Cela suggère également que les réponses aux signaux attractifs et répulsifs sont croisées et pourraient reposer sur des mécanismes communs de remodelage du cytosquelette. Ces mécanismes communs pourraient donc résulter en des comportements différents, soulignant l'importance du contexte moléculaire global du CC.

Les kinases – connues pour leur rôle dans les cascades de signalisation – sont également des acteurs importants dans la réponse aux signaux de guidage (Bashaw and Klein, 2010). De nombreuses études *in vitro* montrent aussi l'implication de seconds messagers – principalement le calcium et les nucléotides cycliques (cAMP, cGMP) – et de plus en plus d'études *in vivo* semblent confirmer leur importance (Song *et al.*, 1998; Nishiyama *et al.*, 2003; Gomez and Zheng, 2006; Bashaw and Klein, 2010; Niftullayev and Lamarche-Vane, 2019).

Tous ces acteurs partagés et ces processus croisés entre les signalisations attractives et répulsives, font du guidage axonal un réseau de signalisations complexe permettant une régulation fine du comportement des axones et, finalement, de leur trajectoire (Fig. 2E). La régulation de cette trajectoire est essentielle pour que l'axone atteigne sa cible, d'où l'importance de posséder des mécanismes résilients. De plus, les neurones étant plus ou moins éloignés de leur cible, certains axones doivent naviguer moins d'un millimètre, d'autres naviguent plus d'un mètre. Pour pallier les longues distances incompatibles avec la diffusion de signaux uniquement par la cible, les axones exploitent plusieurs stratégies.

3. Guidage axonal et distance

a. Différentes sources de signaux jalonnent la trajectoire de l'axone

Quelques études – et notamment des travaux en cours dans notre équipe – indiquent que des signaux électriques pourraient permettre d'orienter les axones vers leur cible sur de longues distances, s'additionnant aux signaux chimiques dont la diffusion est plus restreinte (Yamashita, 2013, 2015). Cependant, la stratégie la plus connue et étudiée est la multiplication des sources de signaux chimiques. De fait, il existe plusieurs territoires jalonnant la trajectoire de l'axone jusqu'à sa cible finale

et émettant des signaux de guidage. On en discerne deux types : les « guideposts » et les cibles intermédiaires. Les premiers émettent essentiellement des signaux répulsifs et vont empêcher l'égarement de l'axone à travers trois actions principales : 1) la répulsion, au sens littéral, pousse les axones à se diriger dans le sens opposé aux guideposts ; 2) le confinement empêche les axones de sortir d'un territoire ; 3) la canalisation entre deux guideposts permet de restreindre les axones dans un passage étroit (Palka, Whitlock and Murray, 1992; Ducuing *et al.*, 2017). Les cibles intermédiaires se différencient des guideposts par leur comportement attractif. Les axones vont d'abord se diriger vers leur cible intermédiaire, l'atteindre (voire la traverser), puis vont se diriger vers la cible suivante (intermédiaire ou finale). La multiplication des sources de signaux permet les trajectoires stéréotypées qu'effectuent les axones, même sur de longues distances.

En plus de faciliter la navigation sur de longues distances, les cibles intermédiaires peuvent permettre de séparer différentes populations neuronales. Dans la moelle, c'est le cas de la PP qui va séparer les interneurones ipsilatéraux et commissuraux dont les cibles se trouvent, respectivement, du même côté du SNC que leur corps cellulaire ou du côté opposé. Si les deux populations atteignent la PP, les ipsilatéraux tournent alors rostralement sans jamais y pénétrer, quand les commissuraux traversent la PP, et donc la ligne médiane, pour *in fine* interconnecter les moitiés droite et gauche du SNC en formant une commissure (Ducuing *et al.*, 2017).

III. Plaque du plancher et guidage axonal

1. Les commissures

a. Les commissures interconnectent les moitiés droite et gauche du système nerveux

Ces commissures sont caractéristiques des bilatériens, vertébrés comme invertébrés, et se retrouvent tout le long de l'axe rostro-caudal (Fig. 3). Un exemple particulièrement étudié chez les invertébrés se situe dans la corde ventrale de la drosophile, où des faisceaux perpendiculaires à l'axe antéro-postérieur se répètent à chaque segment (Bashaw *et al.*, 2000).

Chez les vertébrés, des commissures distinctes se développent à différents niveaux du SNC. Au niveau du cerveau, on retrouve cinq commissures inter-hémisphériques principales. Le corps calleux est la plus volumineuse et interconnecte les aires corticales droite et gauche, permettant le transfert

d'informations, l'intégration des signaux, et facilitant l'activité corticale. Le fornix interconnecte les deux moitiés de l'hippocampe et joue un rôle crucial dans la mémoire déclarative. La commissure habénulaire relie les noyaux habénulaires et est impliquée dans la régulation de neurotransmetteurs du SNC. La commissure antérieure interconnecte les deux lobes temporaux, ainsi que les bulbes et régions olfactifs, et semble impliquée dans la communication *via* des signaux olfactifs et non-visuels. Et enfin la commissure postérieure interconnecte les noyaux prétectaux droit et gauche et médie les mouvements des yeux ainsi que le réflexe photomoteur (Lavrador *et al.*, 2019).

Il existe également d'autres commissures dans tout l'axe antéro-postérieur. Par exemple, chez les organismes à la vision bilatérale, on retrouve le chiasme optique qui va connecter œil gauche et thalamus droit, œil droit et thalamus gauche. Une autre est présente à la frontière entre *medulla oblongata* et moelle épinière, où des projections cortico-spinales relient des aires cérébrales. Dernier exemple, la commissure de la moelle épinière, tout le long de l'axe antéro-postérieur, interconnecte différents circuits moteurs et sensoriels (Fame, MacDonald and Macklis, 2011; Belle *et al.*, 2014).

L'importance des commissures est illustrée par différentes pathologies dont l'origine pourrait être liée à une malformation de ces structures. Par exemple, l'absence de développement du corps calleux est associée à divers syndromes développementaux (Andermann, Apert, *etc.*) (Kamnasaran, 2005; Fitsiori *et al.*, 2011). Des défauts du faisceau cortico-spinal induisent des syncinésies allant jusqu'aux mouvements miroirs – les patients effectuant un mouvement d'un côté vont involontairement réaliser le même de l'autre côté – alors qu'un défaut de commissure postérieure détériore les mouvements verticaux des yeux (Nugent, Kolpak and Engle, 2012; Strupp *et al.*, 2014).

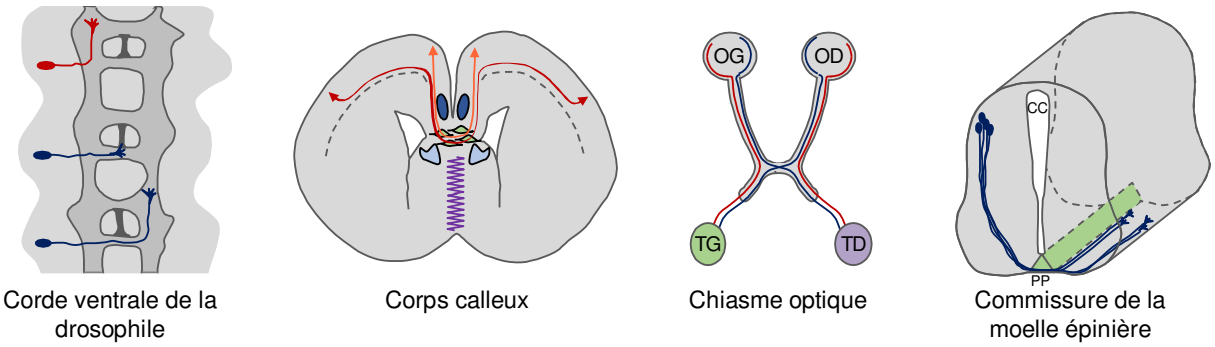

Corde ventrale de la drosophile | Corps calleux | Chiasme optique | Commissure de la moelle épinière

Figure 3. Représentations schématiques de différentes commissures

(**A**) Dans la corde ventrale de drosophile, les neurones ipsilatéraux (en rouge) et contralatéraux (en bleu) étendent leur axone médialement vers la ligne médiane, mais les axones ipsilatéraux tournent avant de traverser alors les que les axones contralatéraux tournent après avoir traversé. (**B**) Chez les mammifères, les axones néocorticaux calleux (en rouge) tournent médialement et naviguent vers la ligne médiane. Ils sont guidés par des signaux émanant de différentes sources : la fermeture éclair

gliale de la ligne médiane (en violet), les amas gliaux (en bleu clair), la glie *indusium griseum* (en bleu foncé), et des neurones en migration (en vert). (**C**) Les axones des neurones des ganglions sortant de la rétine connectent les deux moitiés du cerveau, formant ainsi des faisceaux ipsilatéral (en rouge) et contralatéral (en bleu), ce dernier traversant la ligne médiane au niveau du chiasme optique. OG = œil gauche, OD = œil droit, TG = thalamus gauche, TR = thalamus droit. (**D**) Chez les vertébrés, les axones commissuraux (en bleu) de la moelle épiniere naviguent ventralement vers la plaque du plancher (PP), en dessous du canal central (CC), traversent la ligne médiane et tournent ensuite rostralement. Les axones ipsilatéraux, quant à eux, tournent rostralement sans traverser la ligne médiane. Adaptée de Pignata, Ducuing and Castellani, 2016.

b. Les commissures sont un modèle du guidage axonal

Dans le domaine du guidage axonal, les commissures sont des modèles d'étude particulièrement attrayants de par la complexité de leur mise en place. En effet, dans un premier temps les axones commissuraux vont être attirés par la ligne médiane et s'en approcher, pour finalement la traverser. Au cours de leur traversée, ils vont subir des modifications moléculaires qui vont les amener à être expulsés de la ligne médiane. Par la suite, ils ne la traverseront plus jamais. Cette navigation stéréotypée cumule les deux aspects les plus basiques du guidage axonal, attraction et répulsion, en y ajoutant un degré de complexité supplémentaire à travers le changement de comportement des axones : d'abord attirés puis repoussés par la ligne médiane. L'étude de ces changements de comportement permet de mieux comprendre comment, d'un nombre relativement limité de signaux, peut émerger une organisation aussi complexe que le réseau neuronal.

2. Navigation des axones commissuraux – Exemple de la moelle épinière

Dans le cas de la moelle épinière, on retrouve différentes populations d'interneurones se situant toutes dans le domaine dorsal. Ces populations sont réparties de la plus dorsale, dI1, à la plus ventrale, dI6. Il existe également deux populations apparaissant tardivement : dIL_A et dIL_B. Chaque population peut ensuite être subdivisée en fonction de critères comme l'expression de marqueurs spécifiques, leur localisation finale, ou leur projection axonale. Ainsi, la population de dI1 est composée des dI1i (neurones ipsilatéraux) et dI1c (neurones commissuraux) (Chizhikov and Millen, 2005; Lai, Seal and Johnson, 2016). C'est sur la relation entre cette sous-population dI1c et la PP que portent mes travaux.

a. *Différents domaines permettent la navigation de l'axone jusqu'à la plaque du plancher*

Au sein de la moelle, la PP n'est pas la seule source de signaux de guidage axonal (Fig. 4A). Au début de leur croissance, les axones se dirigent ventralement en réponse aux signaux répulsifs émis par la plaque du toit. Deux signalisations entraînent cette orientation : GDF7 et BMP7 *via* le récepteur BMPR-IB (Augsburger *et al.*, 1999; Butler and Dodd, 2003) et Draxin *via* le récepteur DCC (Islam *et al.*, 2009; Ahmed *et al.*, 2011).

Une fois la croissance initiée, la Netrin-1 exprimée par la DREZ – zone d'entrée des axones des ganglions dorso-rachidiens (DRG) – et la DRBZ – zone de bifurcation des axones de DRG – va agir *via* DCC (pour la DREZ) et l'hétérodimère DCC/Unc (pour la DRBZ) afin de confiner les axones dans la moelle (Ducuing *et al.*, 2017; Varadarajan and Butler, 2017). Les méninges semblent également jouer un rôle répulsif de confinement, bien que les études *in vivo* soient encore rares (Suter, DeLoughery and Jaworski, 2017). S'ils y restent confinés, les axones n'envahissent pas pour autant toute la moelle, mais poussent le long de la surface piale. Ils évitent ainsi la zone ventriculaire (VZ), composée de progéniteurs neuraux. En 2017, deux études révèlent le rôle de confinement que jouent ces progéniteurs en exprimant de la Netrin-1 qu'ils transportent le long de leur prolongement basal pour la déposer sur la surface piale (Dominici *et al.*, 2017; Varadarajan *et al.*, 2017). L'expression de Netrin-1 par les progéniteurs restreint la pousse axonale le long de la surface piale, mais ce n'est sans doute pas la seule signalisation empêchant l'invasion de la VZ.

A l'approche du domaine des motoneurones, les axones vont s'éloigner de la surface piale pour se diriger vers la PP en évitant les motoneurones. Ces derniers expriment NELL-2 qui va agir *via* le récepteur Roundabout3 (Robo3) pour empêcher les axones de pénétrer dans le domaine des motoneurones (Jaworski *et al.*, 2015). D'autres signaux répulsifs sont exprimés par les motoneurones, notamment des Slits et Sémaphorines (Sema), mais leur implication directe n'a pas encore été démontrée (Brose *et al.*, 1999; Moret *et al.*, 2007; Sanyas *et al.*, 2012).

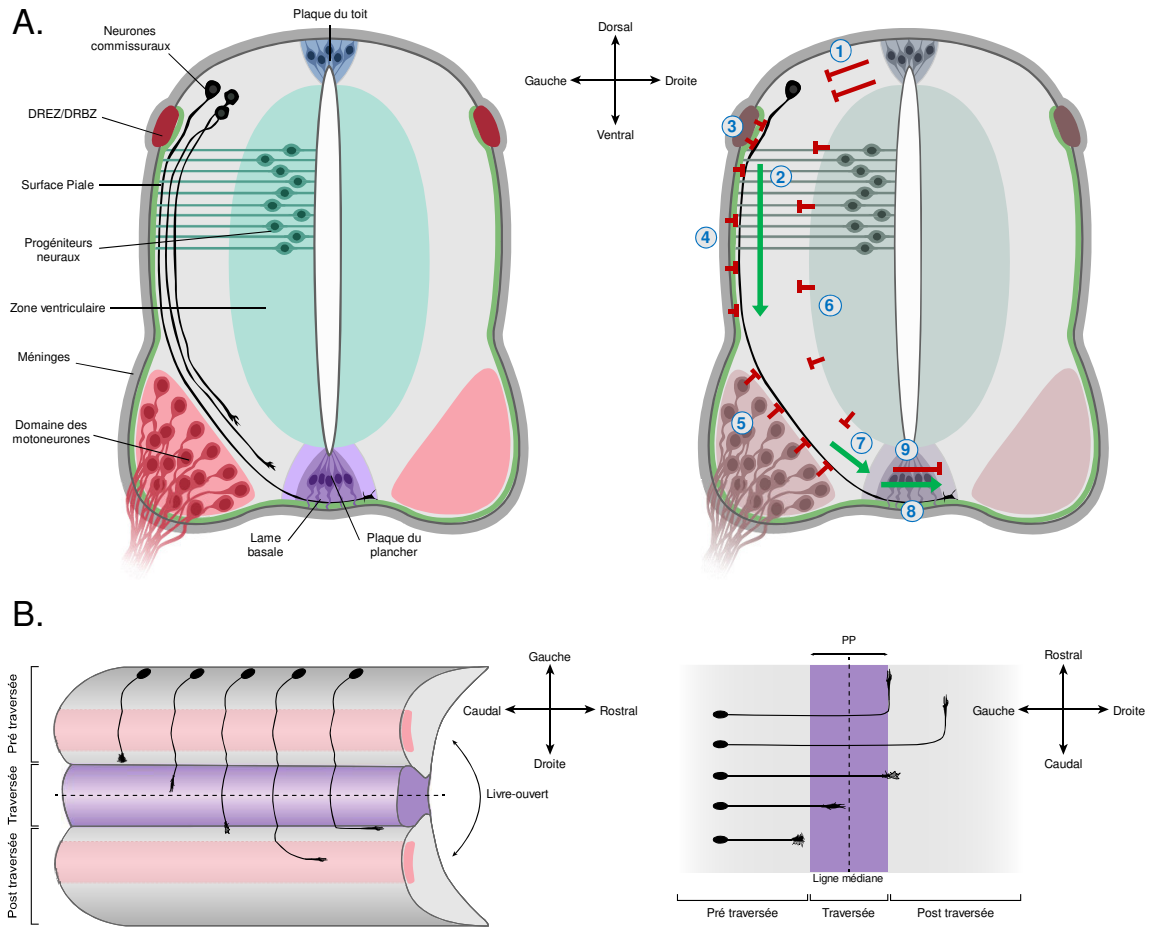

Figure 4. Navigation des axones commissuraux dans la moelle épinière

Les axones commissuraux naviguent ventralement, traversent la plaque du plancher (PP), puis tournent rostralement. (**A**) Cette trajectoire stéréotypée repose sur plusieurs sources de signaux. **1.** Les axones sont repoussés par les signaux répulsifs diffusant depuis la plaque du toit (en bleu à gauche). **2.** Ils poussent le long de la surface piale (en vert) où se situent des attractants déposés par les progéniteurs (en cyan). **3 et 4.** La DREZ/DRBZ (en rouge) et les méninges (en gris) confinent les axones dans la moelle. **5 et 6**. Les axones tournent ensuite en direction de la PP, et longent le domaine des motoneurones (en rose). Leur trajectoire est canalisée par des signaux provenant des motoneurones et de la zone ventriculaire (en cyan). **7.** Les axones sont ensuite attirés par des gradients de signaux provenant de la PP. **8.** Au niveau de la PP, les axones interagissent avec la lame basale (en vert) et naviguent à travers les pieds basaux des cellules gliales de la PP. Au cours de leur traversée, ils sont sensibilisés à différents signaux répulsifs de la PP et en sont expulsés. **9.** Certains effectuent alors un virage serré, rostralement, et naviguent dans le funicule ventral sans jamais retraverser la PP. D'autres vont continuer de naviguer tout droit, puis tourner dans le funicule latéral. Dans les deux funicules, les axones voyagent en faisceau. (**B**) Représentations en livre-ouvert permettant de visualiser les trajectoires dans les funicules ainsi que la morphologie des cônes de croissance (CC) dans les différents territoires. En pré-traversée, ils sont allongés dans l'axe rostro-caudal et présentent des lamellipodes, mais peu de filopodes. Dans la PP, ils adoptent des morphologies variées, mais toujours écrasée dans l'axe rostro-caudal. Ici, c'est une morphologie fusiforme qui est représentée. A la sortie de la PP, les CC possèdent une morphologie étalée similaire à celle des CC pré-traversée. Dans le funicule ventral, les CC possèdent des lamellipodes, mais peu de filopodes. Aucune donnée n'est disponible pour les CC dans le funicule latéral, celui présenté ici est donc le même cône que dans le funicule ventral. Les CC sont adaptés de Yaginuma *et al.* 1991.

b. *La plaque du plancher influence la navigation pendant et après la traversée*

Les axones commissuraux pénètrent ensuite la PP au niveau des pieds basaux des cellules gliales. Lors de cette traversée, les axones forment un faisceau plus compact et même leurs cônes de croissance changent de forme. Avant la traversée, ils présentent une structure aplatie perpendiculairement à la direction de la pousse (Fig. 4B). Pendant la traversée, ils présentent des morphologies variées du simple cône fusiforme au cône de croissance complexe avec filopodes et lamellipodes (Yaginuma *et al.*, 1991). Toujours pendant la traversée, les axones sont sensibilisés aux signaux répulsifs de la PP, ce qui leur permet d'être expulsés dans le domaine contralatéral. Chez les vertébrés, les axones commissuraux se séparent alors en deux : certains naviguent dans le funicule ventral, les autres dans le funicule latéral (Fig. 4B). Les mécanismes contrôlant ce choix ne sont pas encore connus, mais les récepteurs Robo, la molécule d'adhésion N-cadherin, et la signalisation EphB3/EphB semblent être impliqués (Imondi and Kaprielian, 2001; Kadison *et al.*, 2006; Jaworski and Tessier-Lavigne, 2012; Sakai *et al.*, 2012; Pignata *et al.*, 2019).

Une fois sortis de la PP et dans le funicule qui leur correspond, les axones commissuraux tournent rostralement et se dirigent vers le cortex, en suivant une trajectoire longitudinale. Cette trajectoire dépend de deux gradients chimiques établis par les cellules de la PP et s'étendant le long de l'axe rostro-caudal : un gradient attractif de WNT attire les axones rostralement, pendant qu'un gradient répulsif de Shh les empêche de se diriger caudalement (Lyuksyutova *et al.*, 2003; Bourikas *et al.*, 2005). Les axones du funicule ventral longent la PP sans jamais la retraverser, indiquant que leur sensibilisation aux signaux répulsifs est définitive.

3. Influence physique et moléculaire de la plaque du plancher sur la navigation des axones commissuraux

a. *Des signaux chimiques exprimés par la plaque du plancher attirent les axones*

Nous avons vu que la PP est une structure que les axones commissuraux vont d'abord approcher, traverser, puis longer. Ici, je détaillerai un peu plus le contrôle du guidage axonal par la PP. En effet, ce domaine exprime une grande quantité de signaux, attractifs et répulsifs, formant ainsi des gradients aussi bien rostro-caudaux que ventro-dorsaux au sein de la moelle. Shh, que j'ai cité en tant que répulsif précédemment, forme en fait deux gradients : un gradient dorso-ventral attractif pour amener les axones à la PP avant leur traversée, et un gradient un rostro-caudal répulsif pour diriger rostralement les axones (Charron *et al.*, 2003; Bourikas *et al.*, 2005). L'expression de VEGF par la PP participent également à l'attraction des axones par la FP (Ruiz de Almodovar *et al.*, 2011). La Netrin-1

exprimée par la PP a longtemps été considérée comme un exemple de gradient attractif. Cependant, deux études de 2017 réfutent ce modèle en montrant que les axones atteignent la PP sans présenter de défauts, malgré l'invalidation conditionnelle de la Netrin-1 dans la PP (Dominici *et al.*, 2017; Varadarajan *et al.*, 2017). Ces études ont eu un impact important sur la vision du guidage axonal, puisqu'elles ont remis en question le dogme des gradients et souligné l'importance des mécanismes de guidage locaux.

En plus de signaux attractifs, certaines molécules d'adhésion sont exclusivement présentes dans la PP. On y trouve p84 (Chuang and Lagenaur, 1990), N-CAM poly-sialylate (Bovolenta and Dodd, 1990; Griffith and Wiley, 1991), GP-90 (Moss and White, 1989), et F-spondin (Klar, Baldassare and Jessell, 1992). Ces molécules d'adhésion pourraient servir de substrat de croissance et favoriser la traversée des axones (Bovolenta and Dodd, 1990). Il est également possible que les axones commissuraux tournant dans le funicule ventral après la traversée soit influencés par une adhésion préférentielle aux cellules de PP (Bovolenta and Dodd, 1990).

b. La plaque du plancher est un environnement contraignant pour les axones

Une fois dans la PP, les cônes de croissance sont avant tout soumis à un environnement bien plus contraignant physiquement les empêchant possiblement de faire demi-tour pendant la traversée (Bovolenta and Dodd, 1990). De plus, des contraintes mécaniques externes peuvent réguler localement l'ouverture de canaux ioniques, modifiant ainsi la concentration de composants clefs du remodelage du cytosquelette (Tyler, 2012). Enfin, une contrainte de pression pourrait également favoriser la pousse vers l'avant en agissant directement sur l'actine et les microtubules (Heidemann and Buxbaum, 1990). L'impact de l'environnement physique sur la croissance axonale n'est pas encore bien compris, mais plusieurs études soulignent l'importance des contraintes mécaniques d'un environnement tridimensionnel pour un guidage axonal correct (Francisco *et al.*, 2007; Franze, 2013; Kerstein, Nichol and Gomez, 2015; Koser *et al.*, 2016; Thompson *et al.*, 2019). Des études de microscopie électronique suggèrent que les pieds basaux des cellules de PP, domaine de passage des axones, sont aplatis et en contact étroit avec les axones (Glees and LeVay, 1964; Yaginuma *et al.*, 1991). Une autre approche, basée sur un marquage *lacZ*, décrit également de fines excroissances latérales entourant les axones, mais les auteurs précisent qu'il pourrait s'agir d'artefact de marquage (Campbell and Peterson, 1993). Si la morphologie précise des cellules de la PP reste encore à élucider, leur contact direct avec les axones vient renforcer l'hypothèse selon laquelle les cellules de la PP et leurs molécules d'adhésion pourraient agir comme un substrat physique de pousse axonale.

c. *De nombreux signaux répulsifs sont exprimés par la plaque du plancher sans empêcher la traversée des axones commissuraux*

Au cours de la traversée, les axones vont également devenir sensibles à de nombreuses signalisations répulsives de la PP. On trouve entre autres les couples suivants (ligand de la PP/récepteur du CC) : EphrinB3/EphB3 (Kadison *et al.*, 2006), NOGO/NOGOR (Wang *et al.*, 2017), PlxnA2/Sema6B (Andermatt *et al.*, 2014), Sema3B/PlxnA1-Nrp2 (Charoy *et al.*, 2012), Slit2N/Robo1-2 (Kidd, Bland and Goodman, 1999) et Slit2C/PlxnA1 (Delloye-Bourgeois *et al.*, 2015). La présence d'une grande quantité de signalisations répulsives soulève plusieurs possibilités : 1) il y a beaucoup de redondance pour augmenter la robustesse, car la traversée est essentielle et il existe donc des mécanismes de contrôle renforcé ; 2) les différentes signalisations répulsives n'ont pas toutes le même rôle et permettent ainsi d'ajuster avec précision la traversée ; 3) la vision dogmatique qui considère ces signalisations comme répulsives est incorrecte ou incomplète ; 4) un mélange des trois premières possibilités.

Un dernier rôle essentiel de la PP a été observé par Placzek *et al.* En l'absence de PP et de notochorde, les axones se dirigent ventralement, mais projettent hors de la moelle au niveau ventral (Placzek *et al.*, 1991). La PP n'a donc pas qu'un rôle de cible intermédiaire, mais permet également le confinement des axones dans la moelle. Cependant, il n'est pas encore clair si ce rôle est directement joué par la PP ou si elle permet le développement d'une barrière. De plus, Placzek *et al.* effectuent une ablation de la notochorde pour empêcher la formation de la PP, il est donc possible que le confinement des axones dépende de la notochorde et non pas de la PP.

La traversée de la plaque du plancher est donc une étape essentielle permettant d'interconnecter les deux côtés du SNC, mais également complexe car théâtre de nombreuses signalisations. Le cas des signalisations répulsives est intrigant, car la présence d'un grand nombre de ces signaux dans la PP n'empêche pas la traversée des commissuraux. A première vue, le rôle des signaux répulsifs est encore plus paradoxal que leur présence, puisque leur absence engendre des défauts de traversée : certains axones mettent plus de temps à traverser, d'autres font même demi-tour. Les axones commissuraux semblent donc insensibles aux signaux répulsifs, avant leur traversée, mais un gain de sensibilité a lieu pendant qu'ils traversent la PP. Cette sensibilisation n'empêche pas la pousse de l'axone, mais va au contraire accélérer la sortie de la PP, indiquant qu'elle est possiblement importante pour contrecarrer l'affinité des axones pour la PP et les expulser. Cependant, elle ne doit pas être activée trop tôt pour permettre aux axones de pénétrer la PP. Le gain de sensibilité doit donc être finement contrôlé. J'exposerai ici certains mécanismes impliqués à travers quatre exemples : Shh, Sema3B/PlxnA1-Nrp2, SlitN/Robo, et SlitC/PlxnA1.

4. Régulations spatio-temporelles des signalisations répulsives

a. Sonic hedgehog : de l'attraction à la répulsion

Le cas de Shh est particulièrement intéressant puisque la molécule va d'abord médier l'attraction des axones commissuraux – à travers BOC, un de ses récepteurs, et SMO. Post-traversée, Shh va repousser les axones pour les diriger rostralement – à travers SMO seul (souris) ou Hhip1 (poulet) (Bourikas *et al.*, 2005; Yam *et al.*, 2012). Afin d'étudier le comportement intrinsèque des axones face à un gradient de Shh, Yam *et al.* ont réalisé des tests *in vitro* dans des chambres de Dunn (Yam *et al.*, 2012). Ils cultivent des jeunes neurones commissuraux pendant 2 jours *in vitro* (JIV) et observent que leurs axones s'orientent vers les concentrations de Shh les plus fortes. A l'inverse, les neurones à 3-4 JIV ont le comportement opposé. Les auteurs montrent que c'est l'accumulation, au cours du temps, de l'adaptateur 14-3-3 qui va provoquer ce changement de réponse. *In vivo*, l'inhibition de 14-3-3 cause une augmentation des axones tournant caudalement post-traversée. A l'inverse, sa surexpression amène les commissuraux à tourner rostralement avant d'avoir atteint la PP. Tous ces résultats suggèrent que les commissuraux vont répondre différemment à Shh selon une certaine temporalité, et non pas selon leur environnement.

En plus de ce mécanisme intrinsèque, la concentration de Shh semble également pouvoir contrôler le passage de l'attraction (faible concentration) à la répulsion (forte concentration) (Kolpak, Zhang and Bao, 2005). Shh diffusant depuis la PP, cette dernière présente une plus forte concentration de Shh et pourrait ainsi activer la signalisation répulsive de Shh. Les axones commissuraux possèderaient donc un mécanisme intrinsèque et un mécanisme extrinsèque de sensibilisation leur permettant d'être repoussés par la PP avec la bonne spatio-temporalité.

b. Slit, Robo, Plexin et Semaphorin : un contrôle des récepteurs

Slit2 est un ligand répulsif exprimé par la PP. La protéine est clivée en un fragment N-terminal (Slit2N) et un fragment C-terminal (Slit2C), avec Slit2N connu depuis 1999 pour interagir avec Robo1 et Robo2 (Brose *et al.*, 1999; Kidd, Bland and Goodman, 1999). Chez la drosophile, ces récepteurs sont dégradés par le lysosome dans les axones en pré-traversée. Comm, une protéine contrôlant le trafic cellulaire, médie l'adressage au lysosome. Pendant la traversée de la ligne médiane, son activité est inhibée permettant ainsi l'adressage des Robo à la membrane du CC et donc la sensibilisation à SlitN (Keleman *et al.*, 2002; Keleman, Ribeiro and Dickson, 2005). Toujours chez la drosophile, les cellules de la ligne médiane expriment Robo2 qui va s'associer en *trans* avec le Robo1 axonal – dont la dégradation diminue pendant la traversée – pour l'inhiber (Evans *et al.*, 2015). Ce mécanisme supplémentaire pourrait permettre d'augmenter la quantité minimale de Robo1 pour répondre à Slit, et donc de retarder la sensibilisation des axones. Il est également possible que ce mécanisme permette de présenter les récepteurs à la surface précocement pour ensuite obtenir une sensibilisation rapide par lever d'inhibition. Chez les vertébrés, un mécanisme analogue à Comm contrôlé par la protéine

adaptatrice Ndfip, va dégrader Robo1 *via* le recrutement d'ubiquitine ligases (Gorla *et al.*, 2019). A l'inverse, PRRG4, qui partage des similarités structurales avec Comm, relocalise Robo1 à la surface cellulaire, permettant ainsi la réponse à Slit2N *in vitro*, mais son rôle *in vivo* reste encore à démontrer (Justice, Barnum and Kidd, 2017). Une autre molécule impliquée dans le contrôle de Robo chez les vertébrés, RabGDI, permet l'adressage de Robo à la membrane, *in vivo* et *in vitro*, même si son rôle exact reste encore à élucider (Philipp *et al.*, 2012). Enfin, Robo3, un homologue de Robo sans site de liaison à Slit, va se lier à Robo1 pour inhiber son activité pré-traversée (Sabatier *et al.*, 2004). Robo possède également une capacité structurelle d'auto-inhibition qui va être renforcée par trans-dimérisation et levée par l'interaction avec SlitN (Barak *et al.*, 2019). L'ensemble de ces mécanismes dynamiques va permettre d'inhiber l'activité de Robo et de lever rapidement cette inhibition au moment de la traversée de la PP.

Le fragment SlitC, quant à lui, a longtemps été supposé inactif. Des travaux de notre équipe ont démontré qu'il avait une activité de répulsion. Delloye-Bourgeois *et al.* montrent ainsi que SlitC agit à travers PlexinA1, un récepteur déjà connu pour médier la signalisation répulsive de Sema3B (Delloye-Bourgeois *et al.*, 2015). PlxnA1 est exprimé dans les CC pré-traversée, mais son clivage par les calpaïnes l'empêche d'atteindre la surface du CC (Nawabi *et al.*, 2010). Pendant la traversée, les CC sont en contact avec les molécules GDNF et NrCAM de la PP qui vont inhiber les calpaïnes, stopper le clivage de PlxnA1 et permettre son adressage à la membrane (Nawabi *et al.*, 2010; Charoy *et al.*, 2012).

Si Robo1 et PlxnA1 sont adressés à la membrane lors de la traversée, la spatio-temporalité et la polarité de cet adressage ne sont pas les mêmes. Ainsi, des travaux de l'équipe montrent que PlxnA1 va arriver à la membrane au début de la traversée, alors que Robo1 arrivera au milieu (Fig. 5) (Pignata *et al.*, 2019). De plus, PlxnA1 s'accumule dans la partie la plus distale du CC, quand Robo1 s'accumule dans la partie la plus proximale. Ces différences de spatio-temporalité et polarité suggèrent des rôles différents des signalisations répulsives permettant une régulation fine de la trajectoire des axones.

Dans les cas présentés ici, la réponse aux signaux répulsifs va être inhibée dans le compartiment pré-traversée en dégradant le récepteur axonal. Une fois dans la PP la dégradation est inhibée, permettant ainsi au récepteur d'être adressé à la membrane, d'arriver en contact avec le ligand, et d'activer la signalisation associée. Contrairement à l'exemple de Shh, ce ne sont pas les signaux intrinsèques à l'axone, mais bien ceux exprimés dans l'environnement qui vont réguler la sensibilisation au répulsif.

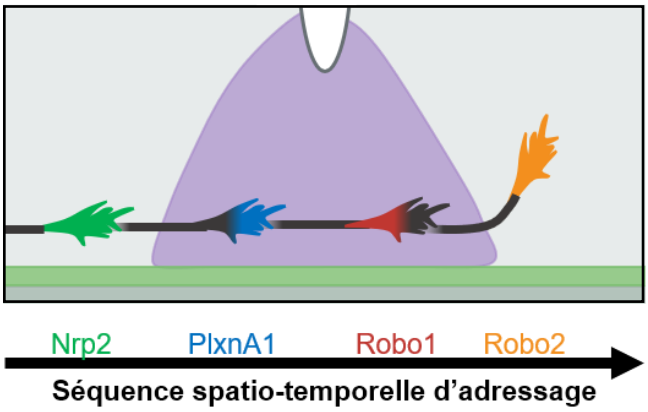

Figure 5. Spatio-temporalité de l'adressage des récepteurs à la membrane des cônes de croissance dans la plaque du plancher

Les récepteurs des signalisations répulsives de la PP ne sont pas intégrés à la membrane du CC au même moment de la navigatio, ni dans les mêmes compartiments du CC. Au niveau de la temporalité d'adressage à la membrane : Nrp2 est déjà présent avant la traversée de la PP ; PlxnA1 est adressé dès la première moitié de la traversée de la PP ; Robo1 est également adressé pendant la traversée, mais à partir de la seconde moitié ; Robo2 est adressé dans les CC au niveau du funicule latéral, au moment de leur virage rostral. Au niveau de la spatialité d'adressage à la membrane du CC : Nrp2 et Robo2 sont présents dans tout le CC ; PlxnA1 est majoritairement à l'avant ; Robo1 est majoritairement à l'arrière de la membrane du CC.

c. Régulations en aval des récepteurs

Un autre degré de régulation se situe cette fois en aval des récepteurs. On trouve deux types de régulation : 1) activation/inhibition et 2) transformation de l'attraction en répulsion (ou inversement). Un exemple de la première régulation est lié à Shh. En effet, si 14-3-3 médie la répulsion par Shh, Shh lui-même va activer la répulsion par les Sema. Pour ce faire, Shh interagit avec ses récepteurs Patched-1 et Smo. Cette signalisation va diminuer l'activité de la voie cAMP/protéine kinase A, et cette diminution est probablement à l'origine d'un contexte moléculaire favorable à la répulsion médiée par les Sema (Parra and Zou, 2010).

La seconde sorte de régulation est illustrée dans la réponse à SlitN. Des tests de pousse *in vitro* sur substrat permettent de moduler la réponse à SlitN en fonction de la présence de Fibronectin (attraction) ou de Laminin-1 (répulsion) (Ba-Charvet *et al.*, 2001). Les auteurs suggèrent que la Laminin-1 diminuerait les niveaux de cGMP, diminution induisant une réponse type répulsion chez l'axone. Ainsi, la réponse à SlitN dépend du substrat sur lequel pousse les axones.

La multiplicité des mécanismes régulant les différentes signalisations, ou régulant une même signalisation, soulignent l'importance de la spatio-temporalité de l'activation de ces signalisations.

Dans la partie suivante, j'explorerai plus en détail l'importance de ces signalisations à travers l'exemple de Slit. L'étude de ce ligand est particulièrement intéressante puisqu'un seul ligand va médier deux signalisations différentes grâce à ses fragments de clivage. De plus, SlitC va partager son récepteur avec Sema3B, mais ces signalisations semblent toutefois différentes. L'étude de Slit est donc pertinente pour comprendre l'émergence de la complexité à partir d'un nombre restreint d'acteurs.

IV. Le cas Slit

En 1984, Nüsslein-Vohlard *et al.* réalisent un crible génétique de facteurs impliqués dans la létalité et la structuration chez la drosophile et identifient la protéine Slit (Nüsslein-Volhard, Wieschaus and Kluding, 1984). Au cours de la décennie suivante, plusieurs études révèlent que Slit est également un ligand répulsif agissant à travers Robo pour contrôler la traversée de la ligne médiane (Rothberg *et al.*, 1988, 1990; Seeger *et al.*, 1993; Kidd, Bland and Goodman, 1999). Si la drosophile ne possède qu'une version de la protéine, la plupart des vertébrés possède trois homologues (Slit1-3). Ceux-ci possèdent une structure similaire composée de : quatre domaines de répétitions riches en leucine (LRR) ; sept à neuf domaines facteur de croissance épidermique (EGF) ; un domaine Agrin-Perlecan-Laminin-Slit (ALPS)/Laminin-G-like ; et un domaine nœud cystéine en C-terminal (Fig. 6A).

Entre les cinquième et sixième domaines EGF, on retrouve un site de clivage conservé – chez la drosophile, comme chez les homologues de la plupart des vertébrés – et c'est à ce niveau qu'aura lieu le clivage produisant SlitN et SlitC.

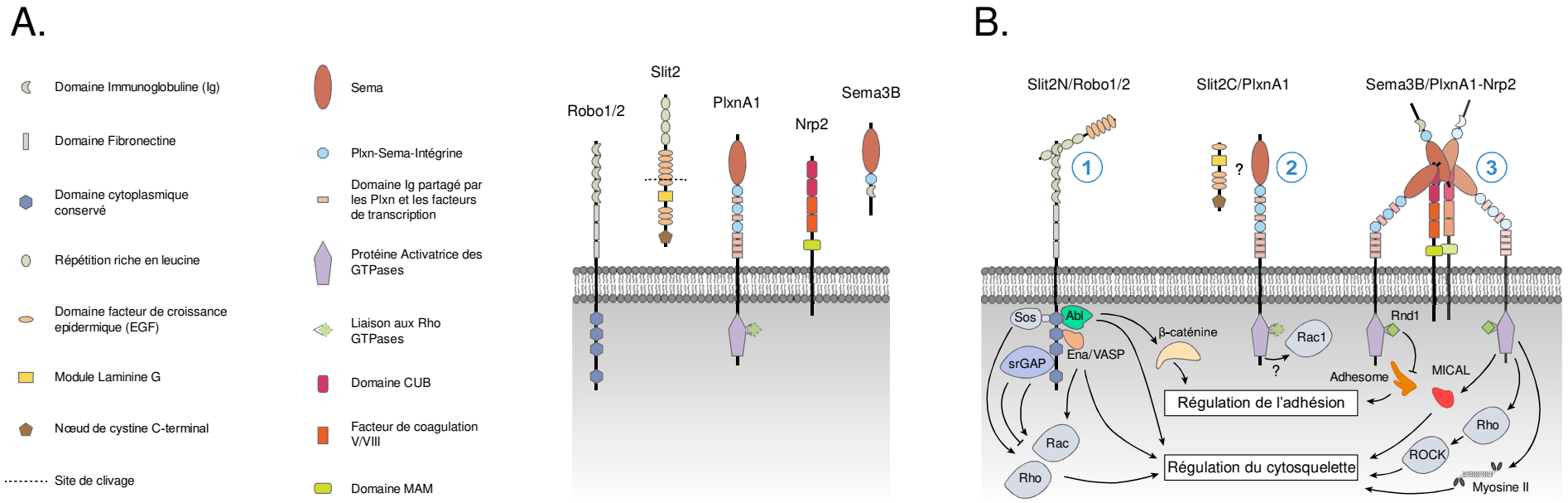

Figure 6. Représentation schématique des acteurs des principales signalisations répulsives de la PP et de leurs effecteurs

(**A**) Représentation des différents domaines des récepteurs Robo1/2, PlxnA1 et Nrp2, ainsi que des ligands Slit2 et Sema3B. Le clivage de Slit2 a lieu entre les domaines EGF 5 et 6. (**B**) Représentation de l'interaction entre Slit2N et Robo1/2 et entre Sema3B et PlxnA1-Nrp2. **1.** SlitN et Robo interagissent via leur domaine LRR 2 et Ig 1, respectivement. La signalisation Slit2N/Robo1/2 dépend de multiples effecteurs. Sos et Ena/VASP activent en aval la GTPase Rac pour réguler le cytosquelette. Des protéines Slit-Robo activatrices des GTPases (srGAP) contrôlent l'activation et l'inhibition de diverses GTPases, comme Rac1 ou Rho. Enfin, Ena/VASP régule la polymérisation des filaments d'actine, alors que Abl contrôle les filaments d'actine et les microtubules. Abl influe également sur l'adhésion cellulaire en phosphorylant la β-caténine, ce qui induit une perte de l'adhésion via N-cadherin. **2.** Peu d'informations sont disponibles sur la signalisation SlitC/PlxnA1. Cependant, Rac1 semble être activé par cette signalisation. **3.** Le complexe formé par l'interaction Sema3B/PlxnA1-Nrp2 comprend deux molécules de chaque protéine. Les deux Sema3B sont en interaction directe *via* leur domaine Sema. Chaque Sema3B interagit avec une molécule de Nrp2 *via* leur domaine Sema et a1, respectivement. Le domaine a1 des Nrp2 interagit également avec le domaine Sema d'une des PlxnA1. La formation de ce complexe permet le recrutement de la Rho GTPase Rnd1 qui va inhiber différents acteurs d'adhésome pour empêcher le couplage entre L1CAM et les filaments d'actine. Le domaine protéine activatrice des GTPase active Rho pour agir sur le cytosquelette, *via* ROCK, et active également la Myosine II. Enfin, MICAL est activé pour rompre les filaments d'actine et les dépolymériser.

1. Clivage de Slit : mécanisme et importance physiologique

a. Une protéase encore inconnue

Afin d'identifier la protéase impliquée, Ordan et Volk ont réalisé des invalidations de différents candidats chez la drosophile, puis des mutants homozygotes (Ordan and Volk, 2016). Ils ont ainsi observé une absence de clivage de Slit chez les mutants *amon*. Amontillado, la protéase codée par *amon*, semble donc être un bon candidat pour la protéase de Slit. Cependant, les auteurs n'ont pas pu montrer de lien direct entre Amontillado et le clivage de Slit. En effet, la surexpression d'Amontillado dans des cultures *in vitro* ne résulte pas en l'augmentation du clivage. De plus, l'analyse par western blot révèle que Slit non clivé – ou Slit « full-length » (Slit FL) – migre moins loin chez les embryons mutants *amon* homozygotes que chez les embryons sauvages. Ainsi, non seulement le rôle d'Amontillado dans le clivage de Slit pourrait n'être qu'indirect, mais il semble également qu'elle amorce ce clivage par une (ou des) modification(s) post-traductionnelle(s) de Slit.

Chez les vertébrés, la Proprotéine convertase 2 (PC2) est l'homologue d'Amontillado, mais son rôle potentiel dans le clivage de Slit n'a pas encore été montré. Cependant son expression est spécifique des tissus neuroendocriniens et du cerveau où elle va activer des prohormones et des précurseurs de neuropeptides (Smeekens and Steiner, 1991; Rouillé *et al.*, 1995; Seidah *et al.*, 1998; Zhou *et al.*, 1999). De plus, PC2 et d'autres convertases de la même famille sont impliquées dans l'épissage et l'activation de différentes métalloprotéases (Pei and Weiss, 1995; Sato *et al.*, 1996; Illman *et al.*, 2003; Stawowy *et al.*, 2005). Ces caractéristiques soutiennent l'hypothèse d'un potentiel rôle de PC2 dans le clivage de Slit2, soit directement soit indirectement à travers l'activation de métalloprotéases.

b. Le rôle du clivage dans le guidage axonal reste incertain

Si la protéase clivant Slit n'a pas encore été déterminée, le rôle physiologique du clivage ne l'a pas été non plus. En effet, chez la drosophile, les défauts de guidage axonal induits par l'absence de Slit sont secourus par l'expression d'une forme non clivable de Slit (Coleman *et al.*, 2010). Il est donc difficile de penser que le clivage est indispensable au guidage axonal, au moins chez la drosophile. Cependant, des études montrent que les deux fragments de clivage ont des propriétés physiques propres : Slit FL et SlitN diffuse peu et sont associés aux cellules, alors que SlitC (plus petit fragment) va diffuser et s'associer aux dystroglycans et avec la MEC (Wang *et al.*, 1999; Wright *et al.*, 2012; Bhat, 2017). De plus, les fragments se lient à des récepteurs différents – Robo1 et Robo2 pour SlitN, PlxnA1 pour SlitC – ce qui suggère que le clivage pourrait permettre d'augmenter le rayon d'action de SlitC/PlxnA1, tout en restreignant celui de SlitN/Robo. La protéine Slit FL peut également s'associer aux différents récepteurs, et induira aussi une répulsion (Brose *et al.*, 1999; Delloye-Bourgeois *et al.*, 2015).

A l'inverse, le processus de ramifications des axones sensoriels activé par SlitN va être inhibé par Slit FL (Wang *et al.*, 1999; Ba-Charvet *et al.*, 2001). Ainsi, certains processus développementaux semblent requérir le clivage de Slit pour être activés.

2. Slit et ses récepteurs : ménage à trois

a. Le fragment SlitN agit via les récepteurs Robo1 et 2

A travers leur domaine LRR2, Slit FL et le fragment SlitN vont se lier au domaine Ig1 des récepteurs Robo1 et Robo2 (Fig. 6) (Morlot *et al.*, 2007). La liaison des Robo à Slit entraîneraît des modifications structurelles de leur domaine extracellulaire et expose un site de clivage dans la région juxtamembranaire des Robo (Barak *et al.*, 2014, 2019). Le clivage, dépendant d'une métalloprotéase, est conservé chez le Robo1 humain et celui des drosophiles (Coleman *et al.*, 2010; Seki *et al.*, 2010). A l'aide d'une version non clivable de Robo1 chez la drosophile, Coleman *et al.* montrent que ce clivage est nécessaire pour la transduction du signal de SlitN/Robo1. Cependant, l'importance du clivage de Robo chez les vertébrés n'a pas encore été étudiée. En plus du clivage, Chance et Bashaw montrent que Slit peut entraîner l'endocytose de Robo1, *in vitro* chez la drosophile, et que cette endocytose permet également la transduction du signal SlitN/Robo *in vivo* (Chance and Bashaw, 2015). Ils soulignent également que les séquences permettant l'endocytose sont conservées chez l'humain, suggérant un mécanisme similaire. Il n'est pas encore clair si le clivage juxtamembranaire et l'endocytose sont liés, ou si les deux voies sont séparées.

En tout cas, l'interaction entre SlitN et Robo induit une cascade de signalisations, impliquant notamment des kinases cytoplasmiques, finissant par remodeler le cytosquelette d'actine et de microtubules (Fig. 6) (Blockus and Chédotal, 2016). Bien que la cascade exacte ne soit pas encore élucidée, plusieurs acteurs ont été identifiés – surtout chez la drosophile. On retrouve ainsi Abelson (Abl) qui joue un rôle double puisqu'il peut inhiber l'activité de Robo ou bien la promouvoir en présence de Capulet (Bashaw *et al.*, 2000; Wills *et al.*, 2002; O'Donnell and Bashaw, 2013). Son of seven (Sos) – un facteur d'échange de nucléotide guanine – va également être recruté par le récepteur endocyté (Chance and Bashaw, 2015). La liaison de Sos et d'autres effecteurs – comme Ena/VASP, Dock, Pak – permet l'activation de Rac et le remodelage du cytosquelette (Chédotal, 2007; McConnell *et al.*, 2016).

b. *La signalisation SlitN/Robo repose sur une élongation des filopodes*

Si la répulsion médiée par Slit/Robo provoque bien l'effondrement des lamellipodes, elle possède la particularité d'être précédée d'une élongation des filopodes en direction de la source de Slit, au moins *in vitro* (McConnell *et al.*, 2016). Cette élongation dépend du complexe Ena/VASP et est nécessaire pour la rétraction et la répulsion induite par Slit. S'il est contre-intuitif qu'un répulsif promeuve la pousse des filopodes, ce phénomène pourrait permettre au CC d'augmenter le volume qu'il explore et ainsi améliorer sa sensibilité aux gradients (Gallo and Letourneau, 2004). De plus, les filopodes sont également le lieu où s'organise la direction des mécanismes d'endo- et exocytose, et permettent des signalisations de guidage locales (Robles, Huttenlocher and Gomez, 2003; Dent, Gupton and Gertler, 2011; Ros *et al.*, 2015). Ainsi, il est également possible que cette élongation dépolymérise localement l'actine des lamellipodes, ce qui augmente le contingent d'actine disponible, et l'envoie du côté opposé à la source de Slit.

c. *Le fragment SlitC partage son récepteur avec Sema3B*

Si la signalisation SlitN/Robo a été beaucoup étudiée, ce n'est pas encore le cas de la signalisation SlitC/PlxnA1. Cette signalisation ayant été découverte récemment, le domaine de liaison ainsi que les acteurs en aval ne sont pas connus. Cependant, la signalisation SlitC/PlxnA1 semble activer Rac1 (Delloye-Bourgeois *et al.*, 2015). On pourrait supposer que la signalisation en aval soit similaire à celle de Sema3B/PlxnA1, cependant deux résultats laissent penser qu'elles sont différentes : 1) Nrp2 permet l'interaction de Sema3B et PlxnA1, alors qu'elle inhibe celle de SlitC et PlxnA1 ; 2) en présence de SlitC, PlxnA1 va être phosphorylé au niveau d'une tyrosine (Y1815, chez la souris), modification qui n'a pas lieu en présence de Sema3B. Ainsi, les signalisations SlitC/PlxnA1 et Sema3B/PlxnA1-Nrp2 pourraient avoir des effets différents sur les axones.

3. Rôles des signalisations répulsives dans la navigation des axones commissuraux

a. *Les signalisations répulsives contrôlent la traversée à différents niveaux*

L'analyse de la trajectoire d'axones commissuraux de souris Slit1/2/3 KO a permis d'observer différents comportements anormaux au sein de la PP : certains axones stagnent dans la PP (stalling), d'autres réalisent des demi-tours (Long *et al.*, 2004). Il est intéressant de noter que si les axones des souris Robo1 KO stagnent dans des proportions similaires, ils n'effectuent pas de demi-tour. Quant aux axones Robo2KO, ils ne présentent pas de défauts de traversée, alors que les axones PlxnA1 KO présentent à la fois stalling et demi-tour (Long *et al.*, 2004; Delloye-Bourgeois *et al.*, 2015). Au vu de ces phénotypes, il est possible que SlitN/Robo1 empêche la stagnation dans la PP et que SlitC/PlxnA1

empêche à la fois la stagnation et les demi-tours. Cependant, le récepteur PlxnA1 est aussi impliqué dans la signalisation de Sema3B. Or, les axones commissuraux des souris Sema3B KO stagnent dans la PP (Nawabi *et al.*, 2010). Il est donc possible que Sema3B/PlxnA1 empêche la stagnation, et que SlitC/PlxnA1 empêche soit uniquement les demi-tours, soit la stagnation et les demi-tours. Dans tous les cas, les signalisations répulsives de la PP vont influencer les axones de façons spécifiques, permettant un contrôle fin de leur trajectoire.

b. Slit est également impliqué dans la fasciculation post-traversée

Un autre rôle a été démontré, chez la drosophile, dans l'organisation des axones post-traversée de la ligne médiane. Slit est exprimé par les cellules gliales et est transporté au niveau des faisceaux compacts formés par les axones longeant la PP. Chez des embryons présentant des défauts d'expression de Slit, les axones post-traversée sont défasciculés et la réexpression de Slit permet de secourir ce phénotype (Bhat, 2017). L'auteur montre également que Robo1 va co-immunoprécipiter avec le Slit et SlitN des faisceaux, suggérant que l'interaction SlitN/Robo1 permet la fasciculation. Cependant, aucune étude fonctionnelle n'a prouvé l'implication de Robo1 dans la fasciculation. De plus, la diffusion depuis la PP et le rôle de Slit dans la fasciculation post-traversée n'a pas encore été observée chez les vertébrés.

Tous ces résultats montrent que les différentes signalisations répulsives ont des rôles spécifiques dans le contrôle de la traversée de la PP. Cela permet d'affiner une vision encore trop manichéenne du guidage axonal, basée sur des expériences *in vitro*, où les attractants attirent et les répulsifs repoussent. En réalité, il est important de prendre en compte l'environnement, qui va modifier la réponse de l'axone aux signaux de guidage, ainsi que la façon dont ces signaux remodèlent le CC.

4. Slit et pathologies

En tant que molécules du guidage axonal, Slit, Robo et Plxn se retrouvent également impliqués dans des troubles de l'autisme et des pathologies neuro-dégénératives (Pérez, Sawmiller and Tan, 2016). En plus de leur rôle dans le guidage axonal, ces signalisations ont également des rôles dans d'autres processus développementaux. Ainsi, l'organogenèse des reins, du diaphragme et du cœur impliquent ces molécules (Liu *et al.*, 2003; Lu *et al.*, 2007; Hwang *et al.*, 2015; Vogler and Bodmer, 2015; Blockus and Chédotal, 2016). Il n'est donc pas étonnant de retrouver des mutations de ces protéines chez des patients présentant des anomalies congénitales des organes cités. Ces molécules jouent également un rôle dans l'angiogenèse et couvrent ainsi un large spectre d'actions pour le

développement. Cela en fait des cibles privilégiées pour les cancers qui les détournent afin de : métastaser, envahir certains territoires, ou effectuer leur angiogenèse (Gara *et al.*, 2015; Blockus and Chédotal, 2016; Koohini, Koohini and Teimourian, 2019). L'étude du comportement physiologique de ces signalisations permet ainsi de mieux comprendre leurs rôles dans différentes pathologies.

RESULTATS

Au cours de ma thèse, j'ai cherché à mieux comprendre la traversée de la PP par les axones. Le sujet a émergé pour donner suite à différents travaux de l'équipe, à commencer par ceux publiés en 2015 (Delloye-Bourgeois *et al.*, 2015). Comme explicité dans l'introduction, ces travaux ont permis l'identification de SlitC comme ligand du guidage axonal dont l'action est médiée par PlxnA1 – le couple SlitN/Robo étant déjà connu en tant que signalisation répulsive. Ces résultats mettent l'accent sur l'étude du clivage de Slit, de la répartition des fragments de clivage et du rôle physiologique de la signalisation SlitC/PlxnA1. Nous avons étudié ces aspects *via* la création d'outils moléculaires innovants utilisés *in vivo*, ainsi qu'en générant un modèle murin invalidant spécifiquement la signalisation SlitC/PlxnA1.

J'ai également eu l'occasion de travailler sur le projet de thèse d'Aurora Pignata, dont les travaux portent sur la spatio-temporalité de l'adressage membranaire des récepteurs de guidage.

I. Participation au projet de thèse d'Aurora Pignata, doctorante dans l'équipe (2014-2018)

Au cours de la traversée de la plaque du plancher, les axones commissuraux vont être sensibilisés aux signaux répulsifs de la PP. Ces signalisations répulsives permettent d'expulser les axones de la PP et de les empêcher de retraverser la ligne médiane. De nombreuses études ont permis d'identifier trois signalisations principales impliquées dans la traversée : SlitN/Robo1-2, SlitC/PlxnA1, et Sema3B/PlxnA1-Nrp2. *In vitro*, ces signalisations induisent toutes l'effondrement des CC. Cependant, *in vivo*, les défauts de traversée observés chez les embryons mutants pour ces signalisations ne sont pas les mêmes. De telles différences fonctionnelles peuvent provenir d'un contrôle spécifique des récepteurs. Pour étudier cette hypothèse, Aurora Pignata a mis au point des techniques d'imagerie live et d'analyse en super-résolution permettant d'étudier les dynamiques d'adressage des récepteurs. Ces techniques d'imagerie utilisent la pHluorin, une GFP ne fluoresçant qu'à pH neutre. En clonant la pHluorin au domaine extracellulaire (DEC) de récepteurs de guidage, elle a pu étudier la spatio-temporalité de l'adressage à la membrane de ces récepteurs.

Ses travaux ont permis de montrer que PlxnA1 et Robo1 sont tous les deux adressés à la membrane du CC au cours de sa traversée. Cependant, la spatio-temporalité de cet adressage est spécifique de chaque récepteur : PlxnA1 est adressé à la membrane dès le début de la traversée alors que l'adressage de Robo1 a lieu en milieu de traversée. Elle a également montré que Robo2 est adressé après la traversée, dans les axones se dirigeant vers le funicule latéral. De plus, l'adressage à la membrane de

ces récepteurs s'accompagne d'un changement de comportement du CC. Ainsi, l'adressage de PlxnA1 corrèle avec une diminution de la vitesse de navigation, alors que l'adressage de Robo1 s'accompagne d'une augmentation du comportement exploratoire du CC. Enfin, l'adressage de Robo2 s'accompagne d'un changement d'angle pour le CC, suggérant que Robo2 pourrait permettre aux axones d'emprunter le funicule latéral.

Que des signalisations répulsives aient des impacts différents sur le comportement pourrait être expliqué par des différences de compartimentation des récepteurs. Grâce à une technique de super-résolution, cette étude a pu montrer que PlxnA1 se localise majoritairement à l'avant du CC, alors que Robo1 est majoritairement adressé à la base du CC. A l'inverse, Robo2 ne présente pas de localisation spécifique dans le CC. Ces différences de localisation pourraient permettre aux signalisations de remodeler le cytosquelette à des endroits précis, impactant ainsi le comportement du CC de façon spécifique.

J'ai contribué à approfondir ces résultats en concevant des outils permettant de perturber la séquence d'adressage : des chimères PlxnA1/Robo1 aux domaines extracellulaires (DEC) permutés. Ainsi, le DEC de PlxnA1 est fusionné aux domaines intracellulaire (DIC) et transmembranaire (TM) de Robo1 (PlxnA1^{DEC}-Robo1$^{TM\text{-}DIC}$), et inversement pour la seconde chimère (Robo1^{DEC}-PlxnA1$^{TM\text{-}DIC}$). Ces chimères ont été électroporées dans des axones commissuraux d'embryons de poulet à HH14. Les moelles ont ensuite été récupérées à E4, montées en livre-ouvert et imagées au spinning-disk. Ainsi, nous avons pu montrer que le récepteur Robo1^{DEC}-PlxnA1$^{TM\text{-}DIC}$ possède la même spatio-temporalité d'adressage que PlxnA1. A contrario, le CC présente le récepteur PlxnA1^{DEC}-Robo1$^{TM\text{-}DIC}$ à sa surface avant même d'atteindre la PP. Ces résultats donnent plusieurs informations. Tout d'abord, PlxnA1$^{TM\text{-}DIC}$ est nécessaire et suffisant pour réguler la spatio-temporalité de l'adressage de PlxnA1. Deuxièmement, Robo1^{DEC} et Robo1$^{TM\text{-}DIC}$ séparément ne sont pas suffisants pour contrôler la spatio-temporalité de l'adressage de Robo1.

Physiologiquement, les axones exprimant Robo1 ou PlxnA1 avant la traversée ne pénètrent pas dans la PP, mais tournent rostralement. Cependant, l'adressage anticipé de PlxnA1^{DEC}-Robo1$^{TM\text{-}DIC}$ à la membrane des CC n'empêche pas la majorité des axones de traverser sans défaut, suggérant que la chimère est inactive. A contrario, l'électroporation de Robo1^{DEC}-PlxnA1$^{TM\text{-}DIC}$ augmente la proportion d'axones stagnant dans la PP, suggérant que cette chimère agit comme un dominant négatif de Robo1. Les résultats obtenus grâce aux chimères sont présentés dans la figure 7 de l'article ci-dessous.

Article

Cell Reports

A Spatiotemporal Sequence of Sensitization to Slits and Semaphorins Orchestrates Commissural Axon Navigation

Graphical Abstract

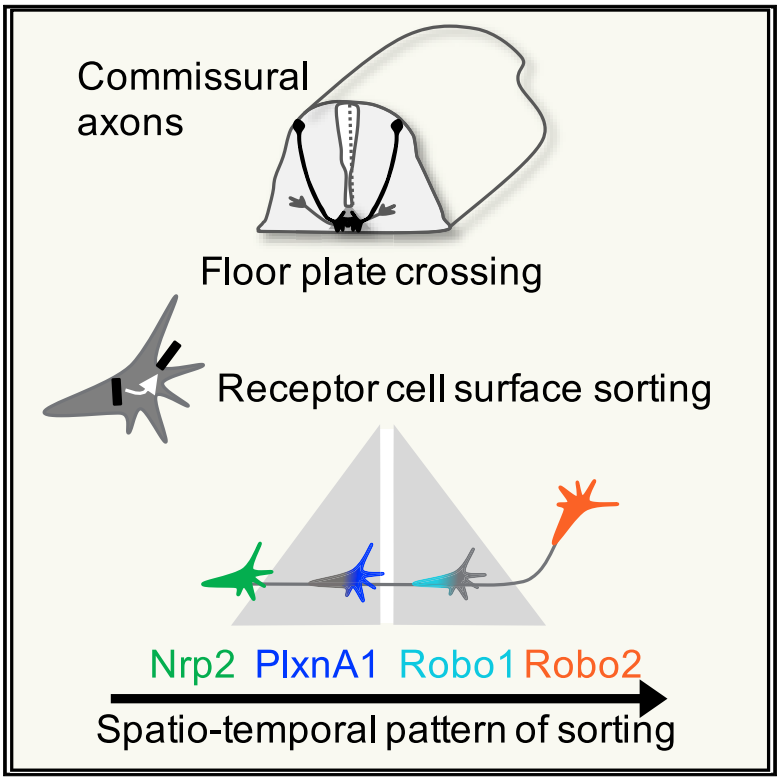

Authors

Aurora Pignata, Hugo Ducuing, Leila Boubakar, ..., Julien Falk, Olivier Thoumine, Valérie Castellani

Correspondence

valerie.castellani@univ-lyon1.fr

In Brief

Pignata et al. developed a setup to monitor the dynamics of receptors for midline repellents during commissural axon navigation across the floor plate. They find specific spatiotemporal patterns of receptor insertion at the growth-cone membrane. This suggests that differences of receptor dynamics can elicit functional specificities of midline repellents.

Highlights

- Live monitoring of guidance receptors reveals specific dynamics in commissural axons
- Slit and Semaphorin receptors have different temporal patterns of membrane insertion
- A front-rear polarity organizes PlxnA1 and Robo1 receptors at the growth-cone surface
- Robo1, but not Robo2, is sorted during midline crossing

Pignata et al., 2019, Cell Reports *29*, 347–362
October 8, 2019
https://doi.org/10.1016/j.celrep.2019.08.098

CellPress

Cell Reports
Article

A Spatiotemporal Sequence of Sensitization to Slits and Semaphorins Orchestrates Commissural Axon Navigation

Aurora Pignata,[1] Hugo Ducuing,[1] Leila Boubakar,[1] Thibault Gardette,[1] Karine Kindbeiter,[1] Muriel Bozon,[1] Servane Tauszig-Delamasure,[1] Julien Falk,[1] Olivier Thoumine,[2] and Valérie Castellani[1,3,*]
[1]University of Lyon, University of Lyon 1 Claude Bernard Lyon1, NeuroMyoGene Institute, CNRS UMR5310, INSERM U1217, 8 Avenue Rockefeller, 69008 Lyon, France
[2]Interdisciplinary Institute for Neuroscience, UMR CNRS 5297, University of Bordeaux 146 rue Léo Saignat, 33000 Bordeaux, France
[3]Lead Contact
*Correspondence: valerie.castellani@univ-lyon1.fr
https://doi.org/10.1016/j.celrep.2019.08.098

SUMMARY

Accurate perception of guidance cues is crucial for cell and axon migration. During initial navigation in the spinal cord, commissural axons are kept insensitive to midline repellents. Upon midline crossing in the floor plate, they switch on responsiveness to Slit and Semaphorin repulsive signals and are thus propelled away and prevented from crossing back. Whether and how the different midline repellents control specific aspects of this navigation remain to be elucidated. We set up a paradigm for live-imaging and super-resolution analysis of PlexinA1, Neuropilin-2, and Robo1/2 receptor dynamics during commissural growth cone navigation in chick and mouse embryos. We uncovered a remarkable program of sensitization to midline cues achieved by unique spatiotemporal sequences of receptor allocation at the growth-cone surface that orchestrates receptor-specific growth-cone behavior changes. This reveals post-translational mechanisms whereby coincident guidance signals are temporally resolved to allow the generation of specific guidance responses.

INTRODUCTION

In biological systems, cells are exposed to a complex array of environmental cues from which they receive specific instructions. This is well exemplified by the model of axon responses to guidance cues during the formation of neuronal circuits. Axons navigate highly diverse environments to reach their targets. Unique trajectories emerge from the perception by axon tips, the growth cones, of combinations of extracellular cues exposed in choice points along their paths. A typical case is provided by commissural neurons, which must project their axons across the midline to build circuits with contralateral target cells integrating left and right neuronal activities (Evans and Bashaw, 2010; Pignata et al., 2016; Stoeckli, 2018). Midline crossing of commissural axons in the floor plate (FP) of the developing spinal cord has been extensively studied to explore axon guidance mechanisms, especially those regulating growth-cone sensitivity to guidance cues. Various FP-derived repulsive forces are needed to prevent midline re-crossing, to expel the axons from the FP, and to organize their post-crossing lateral position (Long et al., 2004; Jaworski et al., 2010). They are mainly mediated by Semaphorin3B (Sema3B) acting via the Neuropilin2 (Nrp2)-PlexinA1 (PlxnA1) receptor complex, N-terminal and C-terminal Slit fragments resulting from Slit processing acting via Roundabout (Robo)1/2, and PlxnA1 receptors (Zou et al., 2000; Long et al., 2004; Jaworski et al., 2010; Nawabi et al., 2010; Delloye-Bourgeois et al., 2015).

Various manipulations in mouse and chicken embryo models suggested that the sensitivity of commissural axons to midline repellents must be silenced during an initial step, before midline crossing, and then switched on in a second step to allow repulsive forces to establish a midline barrier and expel the growth cones away. In agreement, inducing premature sensitization or preventing it resulted in failure of the FP crossing, with axons arrested before or within the FP, turning back or turning longitudinally before reaching the contralateral side (Chen et al., 2008; Nawabi et al., 2010). FP navigation is not a synchronous process, extending over several days, during which, the repellents are expressed in the FP (Wilson et al., 2008; Pignata et al., 2016). Thus, independent of ligand expression profiles, the switch toward sensitivity has to be set at the level of individual growth cones. Several mechanisms have been described to control the sensitivity of vertebrate commissural growth cones to midline repellents (Chen et al., 2008; Nawabi et al., 2010; Charoy et al., 2012; Philipp et al., 2012; Yang et al., 2018). A distinct and yet unanswered question concerns precisely when growth cones become sensitive and whether the sensitization to the various repellents occurs in synchrony or, rather, in a specific sequence or cascade. Moreover, when sorted in the growth cone, do repulsive guidance receptors distribute homogeneously or with a specific pattern of cell-surface expression? Insights into receptor dynamics are crucial for deciphering the exact behaviors triggered by guidance signaling, but data remain scarce because of the absence of experimental

paradigms allowing analysis of molecular events in single, living commissural axons during navigation in their native context.

To address these questions, we investigated the cell-surface dynamics of four receptors mediating repulsion by midline cues—Nrp2, PlxnA1, Robo1, and Robo2—in chick and mouse embryo models. Our study reveals unique spatial and temporal sequences of receptor cell-surface sorting during the navigation of spinal commissural axons. We propose that this enables growth cones to discriminate, in time and space, coincident guidance signals, allowing them to exert non-redundant and concerted actions.

RESULTS

Development of an Experimental Paradigm to Visualize Cell-Surface Receptor Dynamics in Navigating Commissural Axons

We set up time-lapse imaging to monitor the receptor cell-surface dynamics in commissural axons navigating the FP in native spinal cords of chicken embryos. Nrp2, PlxnA1, Robo1, and Robo2 receptors were fused to the pH-sensitive GFP, pHLuorin (pHLuo), which has a fluorescence at neutral pH that enables membrane protein pools to be identified, and cloned in vectors with ires-mb-tomato as a reporter of electroporation (Figure 1A) (Jacob et al., 2005; Nawabi et al., 2010; Delloye-Bourgeois et al., 2014). The pH dependency of receptor fluorescence was verified by *in vitro* cell-line transfections (Figure S1A; see Method Details) (Delloye-Bourgeois et al., 2014). The vectors were transferred to spinal cord commissural neurons of chick embryos using *in ovo* neural-tube electroporation. Commissural neurons prepared from dorsal spinal cords electroporated with pHLuo-PlxnA1 and pHLuo-Robo1 were imaged 2 days after electroporation at neutral pH, after acidification of the medium and washing, which confirmed that the pHLuo fluorescence reports cell-surface receptor pools (Figures S1B–S1E). Increasing concentrations of plasmid (0.5, 2, and 4 μg/μL) were electroporated to correlate in open books to the levels of the pHLuo-PlexinA1 signal with the FP navigation (Figures S1F and S2A–S2H). We selected the 2 μg/μL dose because it provided the better compromise of pHLuo signal and FP crossing. For the Robo1 condition, midline crossing was more sensitive to the electroporation dose; therefore, we decreased the plasmid concentration to 1.5 μg/μL.

PlxnA1 and Robo1 Are Specifically and Successively Sorted to the Growth-Cone Surface during FP Navigation

Isolated spinal cords were opened dorsally and imaged over several hours to map receptor cell-surface sorting reported by pHLuo fluorescence (Figure 1B). We analyzed individual growth cones from time-lapse sequences by plotting the position when they turned on the pHLuo fluorescence and built cartographies of receptor sorting during the navigation. First, we observed that Nrp2 is exposed at the commissural growth-cone surface from the pre-crossing stage and remains expressed over the FP crossing (Figures 1C, 1F, 1H, and 1I; Videos S1 and S2). In contrast, both PlxnA1 and Robo1 were sorted during FP navigation. Interestingly, the timing of their sorting differed significantly: occurring when commissural growth cones navigate the first FP half, thus, from the FP entry point to the midline for PlxnA1 (Figures 1D and 1G–1I; Videos S3 and S4) and during the navigation of the second FP half, thus, from the midline to the FP exit point for Robo1 (Figures 1E and 1G–1I; Videos S5 and S6).

PlxnA1 and Robo1 Temporal Expression Patterns Are Controlled by Cell-Surface Sorting

Next, we assessed whether these temporal patterns are profiled by control of receptor cell-surface sorting or, rather, of protein availability within the axon. Spinal cord open books were fixed with paraformaldehyde (PFA) at neutral pH to detect the total pHLuo receptor pool. When in live axons, the pHLuo signal was found restricted to the growth cones during FP crossing, we observed, in contrast, for both receptors that the total protein had much broader distribution. In 90% of the cases for PlxnA1 and 75% for Robo1, the pre-crossing axon segment immediately adjacent to the FP entry of growth cones navigating within the FP contained pHLuo-receptors (Figures 2A and 2B). We also measured $pHLuo^{+}$ pre-crossing segment length in the fixed samples and found a significant difference between the distribution of PlxnA1 and Robo1. The location of the latter was more restricted in length, and its expression was more punctate than the former (Figure 2C). These observations are consistent with previous studies, which reported that Robo1 undergoes intra-axonal vesicular trafficking in cultured commissural neurons (Philipp et al., 2012), and that PlxnA1 is processed within axons to prevent membrane expression (Nawabi et al., 2010). Thus, PlxnA1 and Robo1 are both available within commissural axons, but their cell-surface sorting is spatially and temporally controlled in a receptor-specific manner. We noted that the proportion of labeled axons was greater than that of axons found to sort pHLuo-tagged receptors in live imaging, possibly because axons sorted the endogenous receptors rather than the pHLuo-tagged ones.

We found in previous work that conditioned medium collected from cultured isolated FP tissues (FP^{cm}) could trigger PlxnA1 cell-surface expression (Nawabi et al., 2010). Such medium was also reported to induce the expression of Robo3.2, an isoform expressed in post-crossing axons in commissural growth cones (Colak et al., 2013), providing the evidence that local FP signals are implicated in synchronizing the sorting of these receptors with midline crossing. We thus examined whether the Robo1 process could also be under local FP control. We treated dorsal spinal-cord explants electroporated with pHLuo-Robo1-ires-mb-tomato with FP^{cm} and control medium and recorded Robo1 dynamics by measuring pHLuo fluorescence 20 min later in the growth cones at T0 and T1 (Figure 2D). We observed a significant increase of pHLuo fluorescence at T1 compared with T0 for the FP^{cm} but not the control condition (Figures 2E and 2F), thus indicating that FP cells release cues triggering Robo1 trafficking to the growth-cone surface.

Normal PlexA1 and Robo1 Receptor Expression Levels Are Critical for Proper Growth-Cone Guidance

Next, we assessed with live imaging whether disturbing the temporal pattern of receptor sorting affects growth cone

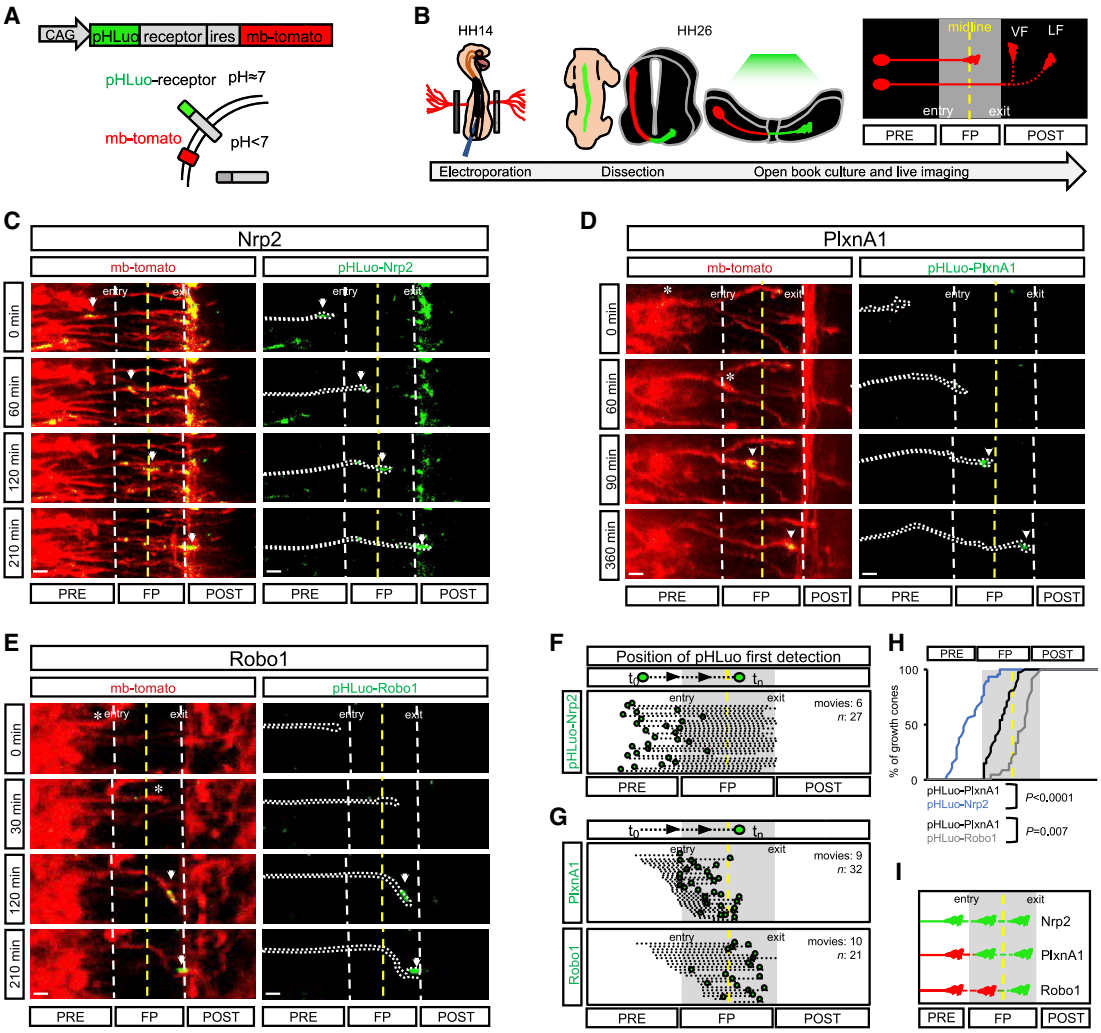

Figure 1. PlxnA1 and Robo1 Are Successively Sorted to the Growth Cone Surface during FP Navigation

(A) Representation of pHLuo vector and pH-dependent pHLuo fluorescence. pHLuo-receptor and mb-tomato coding sequences were cloned in pCAG vector, separated by an ires.

(B) *In ovo* electroporation procedure: 48 h after electroporation, spinal cords were dissected and mounted as open books for time-lapse microscopy. pHLuo fluorescence was monitored in three compartments: pre-crossing, FP, and post-crossing, in which commissural axons chose between ventral and lateral paths. VF, ventral funiculus; LF, lateral funiculus.

(C–E) Time-lapse sequences illustrating the dynamics of pHLuo-Nrp2 (C), pHLuo-PlxnA1 (D), and pHLuo-Robo1 (E) during FP navigation. Asterisks, growth-cone positions before pHLuo flashes; white arrowheads, pHLuo flashes and subsequent growth-cone positions.

(F) Cartography of pHLuo-Nrp2 dynamics from video analysis. Dashed lines, overall trajectory of single growth cones; green spots, the first pHLuo detection. Nrp2 is sorted from the onset of spinal-cord navigation (Nrp2: N = 5 embryos, 6 videos, 27 growth cones).

(G) Cartography of pHLuo-PlxnA1 and pHLuo-Robo1 dynamics. The top panel illustrates pHLuo-PlxnA1 sorting in the first FP half and the bottom panel that of pHLuo-Robo1 in the second FP half (PlxnA1, N = 5 embryos, 9 videos, 32 growth cones; Robo1, N = 9 embryos, 10 videos, 21 growth cones).

(H) Cumulative fractions showing differential pHLuo-Nrp2, pHLuo-PlxnA1, and pHLuo-Robo1 dynamics. p value is from the Kolmogorov-Smirnov (KS) test.

(I) Summary of the temporal sequence of pHLuo-Nrp2, pHLuo-PlxnA1, and pHLuo-Robo1 membrane sorting.

Scale bars: 10 μm in (C)–(E).

See also Figures S1–S3.

behaviors. Open books were electroporated with high concentration of vectors (3 and 4 μg/μL) to overcome the internal control of PlxnA1 and Robo1 surface sorting in commissural neurons and to force premature surface expression. We monitored individual growth cones and found that commissural growth cones that have premature cell-surface receptor exposure failed to cross the FP, either turning or stalling before entering, or within, the FP (Figure S3; Videos S7 and S8). These findings confirmed that the temporal pattern of receptor sorting is critical for proper FP navigation.

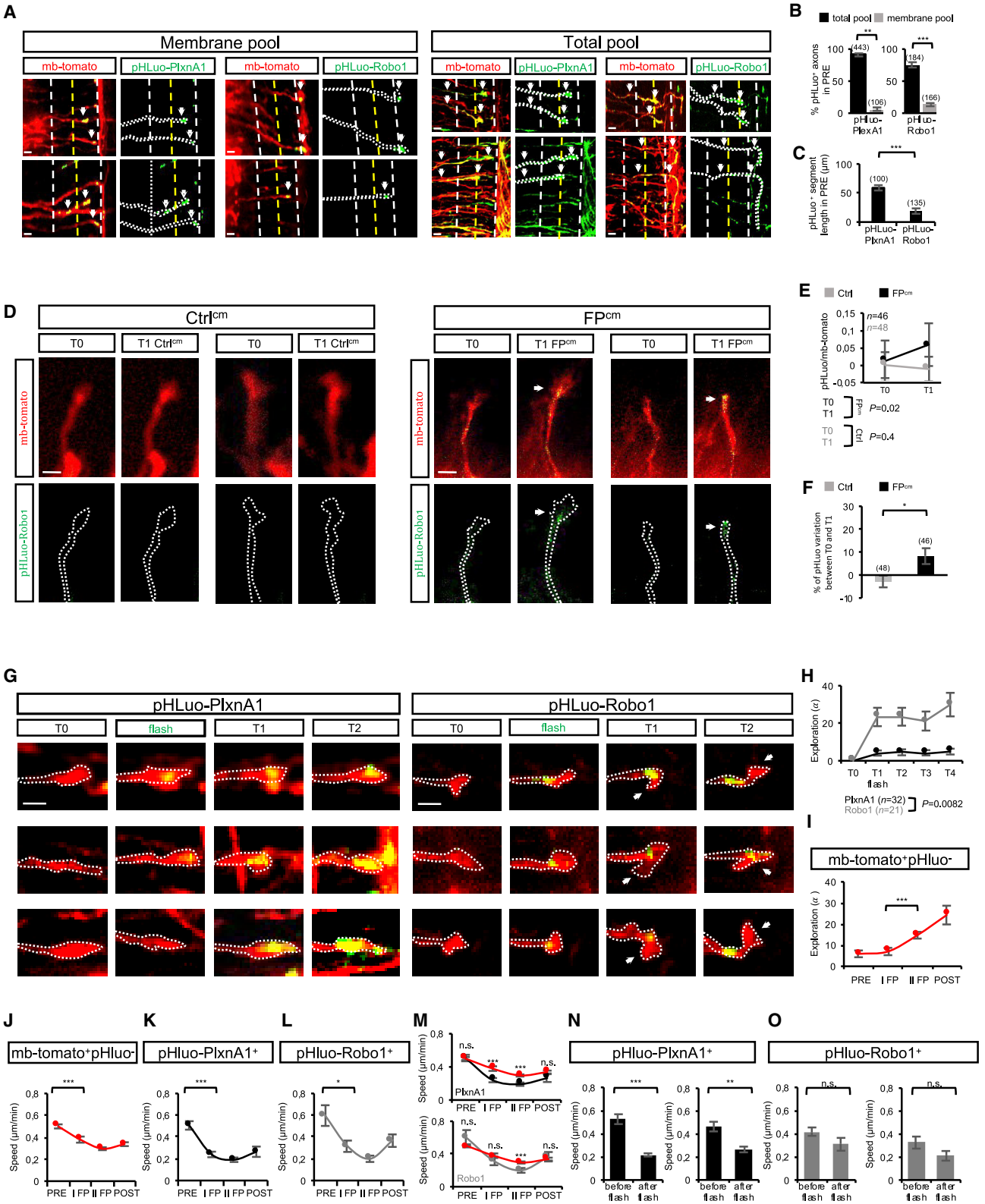

(legend on next page)

Surface Sorting of Robo1 and PlxnA1 Correlates with Changes of Growth-Cone Behaviors during the FP Navigation

We asked whether the increase of PlxnA1 and Robo1 levels at the cell surface could be correlated with acquisition of novel behavioral properties of the growth cones. We analyzed growth-cone trajectories in time-lapse videos at times preceding and succeeding the pHLuo flashes by measuring the deviation angles of growth-cone direction from the trajectory baseline (Figure 2G). Interestingly, for Robo1, we observed that the sorting was coincident with a significant increase in exploratory behavior along the rostro-caudal axis, as if the growth cones were beginning to sense cues that would direct their longitudinal turning at the FP exit (Figures 2G and 2H). In contrast, we found no difference of exploration correlating with the gain of PlxnA1 (Figures 2G and 2H). Remarkably, the increased exploration was observed in the mb-tomato$^+$pHLuo$^-$ condition in the second FP half (Figure 2I), thus, in the window of time when Robo1 is normally sorted, which, therefore, might reflect a physiological behavior of growth cones preparing for exit.

We next examined whether growth cones change their velocity during FP navigation, and if so, whether that could be achieved by surface addressing of PlxnA1 and Robo1. First, we studied the pattern of growth-cone speed. We calculated the average speeds by measuring the distance traveled by mb-tomato$^+$pHLuo$^-$ growth cones between time points in four different compartments: pre-crossing, first FP half (I FP), second FP half (II FP), and post-crossing. Interestingly, a marked slowing down of growth velocity was observed at the FP entry (Figure 2J). This slowing was also observed for mb-tomato$^+$pHLuo$^+$ growth cones. For PlxnA1, the amplitude of the slowing observed from the FP entry was, nevertheless, more pronounced in the pHLuo$^+$ condition than it was in the pHLuo$^-$ one (Figures 2K and 2M). For Robo1, the amplitude of the slowing at the FP entry was comparable for pHLuo$^+$ and pHLuo$^-$ conditions but was more pronounced for the pHLuo$^+$ condition in the second part of the FP (II FP) (Figures 2L and 2M).

Interestingly, the slowing at the FP entry occurs concomitantly to PlxnA1 surface sorting. To assess whether those two events are correlated, we calculated the average speed before and after pHLuo flashes for PlxnA1 and Robo1. As expected, we found that the average speed was significantly reduced when the growth cones gained PlxnA1 but not Robo1 (Figures 2N and 2O).

Robo2 Is Not Sorted in the FP but in the Post-crossing Lateral Funiculus

Next, we investigated the dynamics of Robo2. In sharp contrast with Robo1, we found that Robo2 was absent from the surface of commissural growth cones navigating the FP and turning longitudinally at the medial position in the ventral funiculus (VF). Instead, we observed that it was specifically sorted in post-crossing axons that chose to turn longitudinally in the lateral

Figure 2. Cell Surface Sorting of PlxnA1 and Robo1 and Functional Outcome

(A) Microphotographs of open books illustrating pHLuo-PlxnA1 and pHLuo-Robo1 membrane (left panel) and total (intracellular + membrane) receptor pools (right panel). Arrowheads indicate discrete pHLuo$^+$ growth cones and axon segments.

(B) Quantification of the percentage of growth cones navigating the FP and containing the pHLuo receptor in the pre-crossing segment immediately adjacent to the FP entry. Histograms show much broader total fluorescence than surface fluorescence (total PlxnA1, N = 6 embryos, 443 growth cones; membrane PlxnA1, N = 5 embryos, 106 growth cones; total Robo1, N = 4 embryos, 184 growth cones; membrane Robo1, N = 17 embryos, 166 growth cones. Error bars indicate means ± SEM; *p < 0.05, **p < 0.01, ***p < 0.001, p values are from Mann-Whitney tests.

(C) Histograms of lengths of total pHLuo-PlxnA1$^+$ or pHLuo-Robo1$^+$ pre-crossing segments of growth cones observed to navigate the FP, showing a more restricted pHLuo-Robo1 pattern than that of pHLuo-PlxnA1.

(D) Electroporated dorsal-explant cultures showing pHLuo-Robo1 increase at the growth-cone membrane after treatment with FP^{cm} (right panel) but not Ctrl^{cm} (left panel).

(E) Quantitative analysis of the increase after 20 min (T1) of FP^{cm} treatment. For each growth cone, pHLuo is normalized to the mb-tomato signal (three independent experiments; Ctrl, N = 19 explants, 48 growth cones; FP^{cm}, N = 18 explants, 46 growth cones). Error bars indicate means ± SEM; *p < 0.05, **p < 0.01, ***p < 0.001, p values are from paired Student's t test.

(F) Quantification of pHLuo-Robo1 signal variation between T0 and T1 in Ctrl^{cm} and FP^{cm} conditions showing the increase of surface Robo1 after FP^{cm} application. Error bars indicate means ± SEM; *p < 0.05, **p < 0.01, ***p < 0.001, p values are from Student's t test.

(G) Photomicrographs of pHLuo-PlxnA1 (left panel) and pHLuo-Robo1 (right panel) sorting at the growth-cone surface. Arrowheads in pHLuo-Robo1 condition indicate the exploratory behavior of growth cones after pHLuo sorting.

(H) Quantitative analysis of the average angle of growth-cone exploration from the time point preceding the flash (T0) to 1.5 h after the flash (T3) (PlxnA1, N = 3 embryos, 32 growth cones; Robo1, N = 10 embryos, 21 growth cones). Error bars indicate means ± SEM; p value is from the Kolmogorov-Smirnov (KS) test.

(I) Quantitative analysis of the average exploration angle of mb-tomato$^+$pHLuo$^-$ growth cones along spinal cord navigation (N = 9 embryos, 25 growth cones). Error bars indicate means ± SEM; p value is from the Mann-Whitney test between I FP and II FP.

(J) Average speed of mb-tomato$^+$pHLuo$^-$ in pre-crossing, first FP half, second FP half, and post-crossing, showing a significant decrease of growth-cone speed after the FP entry (N = 12 videos, 52 growth cones). Error bars indicate means ± SEM; p value is from the Mann-Whitney test between the pre-crossing and I FP.

(K) Average speed of pHLuo-PlxnA1$^+$ growth cones along the pre-crossing to post-crossing spinal-cord compartments (N = 9 videos, 17 growth cones). Error bars indicate means ± SEM; p value is from the Mann-Whitney test between pre-crossing and I FP.

(L) Average speed of pHLuo-Robo1$^+$ growth cones (N = 8 videos, 14 growth cones). Error bars indicate means ± SEM; p value is from the Mann-Whitney test between pre-crossing and I FP.

(M) Comparison between pHLuo-PlxnA1$^+$ and mb-tomato$^+$pHLuo$^-$ (top panel) and between pHLuo-Robo1$^+$ and mb-tomato$^+$pHLuo$^-$ (bottom panel) average speeds. p values are from Mann-Whitney tests between mb-tomato$^+$pHLuo$^-$ and pHluo$^+$ axons for each compartment.

(N) Left panel: average speed of pHLuo-PlxnA1$^+$ growth cones before and after pHLuo flash. Right panel: Time-restricted analysis comparing growth-cone average speed two time points preceding and two time points succeeding the pHLuo flash. p value is from the Mann-Whitney test.

(O) Left panel: average speed of pHLuo-Robo1$^+$ growth cones before and after pHLuo flash. Right panel: Time-restricted analysis comparing growth-cone average speed two time points preceding and two time points succeeding pHLuo flash. p value is from the Mann-Whitney test.

Scale bars: 10 μm in (A) and (D) and 5 μm in (G).

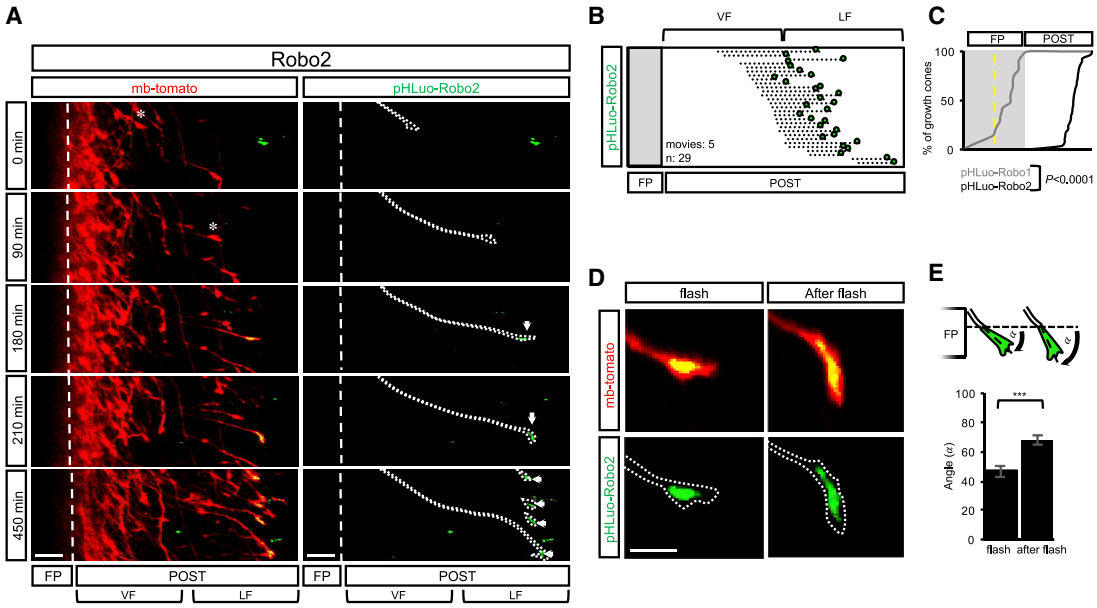

Figure 3. Robo2 Is Sorted during Post-crossing Pathfinding of the Lateral Funiculus

(A) Time-lapse sequences of open-books illustrating pHLuo-Robo2 dynamics. The asterisks indicate growth-cone positions before pHLuo flashes and the white arrowheads those of pHLuo flashes and subsequent growth-cone positions.

(B) Cartography of pHLuo-Robo2 flashes. Dashed lines indicate the overall trajectory of individual growth cones from imaging onset to the time point of flash occurrence (Robo2, N = 5 embryos, 29 growth cones).

(C) Cumulative fractions showing differential pHLuo-Robo1 and pHLuo-Robo2 dynamics during spinal-cord navigation. p value is from the Kolmogorov-Smirnov (KS) test.

(D) Representative time-lapse images illustrating a shift of growth-cone orientation subsequent to pHLuo-Robo2 flash.

(E) Schematic drawing and quantification of growth cone turning after pHLuo-Robo2 flashes (Robo2, N = 3 embryos, 30 growth cones). Error bars indicate means ± SEM; *p < 0.05, **p < 0.01, ***p < 0.001, p value is from the Mann-Whitney test.

Scale bars: 50 μm in (A) and 10 μm in (D).

funiculus (LF) (Figures 3A–3C; Videos S9 and S10). To assess whether Robo2 cell-surface sorting correlates with that change of trajectory, we measured the angle formed by a vector aligned along the axon tip and the FP axis at the two time points flanking the Robo2 pHLuo flash. We found that the angle was significantly more pronounced at post-flash times, compared with pre-flash ones, supporting a contribution to Robo2 sorting (Figures 3D and 3E). Thus, interestingly, signaling by Robo1 and Robo2 appears to have similar outcomes but at two different times in commissural navigation.

The Temporal Sequence of Receptor Sorting Is Conserved in the Mouse

Next, we studied whether the temporal control of guidance-receptor sorting during FP navigation uncovered in the chicken is conserved in the mouse and whether it also instructs growth-cone guidance choices. We electroporated pHLuo-PlxnA1 and pHLuo-Robo1 constructs into the developing spinal cord of E12 wild-type mouse embryos. We plotted the position of fluorescent growth cones in living open books at a fixed time point, 48 h after electroporation, when many FP crossing are occurring, as depicted by the distribution of mb-tomato^{+} growth cones (Figures 4C and 4D). In pHLuo-PlxnA1 electroporated spinal cords, growth cones expressing pHLuo were distributed almost homogenously in all FP and post-crossing compartments (Figures 4A–4C), whereas in the pHLuo-Robo1 electroporated littermates, most of the growth cones exposing Robo1 were situated between the midline and FP exit (Figures 4A, 4B, and 4D). Thus, the spatial and temporal cell-surface pattern of PlxnA1 and Robo1 observed in chick spinal cord is conserved in mice (Figure 4E).

Cell-Surface Sorting of Recombinantly Expressed Robo1 in Robo1/2$^{-/-}$ Embryos and PlxnA1 in PlxnA1$^{-/-}$ Embryos Rescues Commissural Guidance Errors

Next, we electroporated the pHLuo-Robo1 construct in spinal cord open books from Robo1/2$^{-/-}$ mice. We found that the profile of receptor sorting was identical to that observed in Robo1/2$^{+/+}$ embryos, indicating that the sorting pattern did not result from overexpression (Figures 4F–4H). Similarly, the distribution profiles of pHLuo-PlxnA1 fluorescent growth cones in PlxnA1$^{-/-}$ and PlxnA1$^{+/+}$ embryos were identical (Figures 4I–4K). Thus, recombinantly expressed pHLuo receptors seem to faithfully model the dynamics of endogenous receptors. These results also established that Robo1 sorting at the plasma membrane is independent of Robo2.

Then, we investigated whether the re-expression of pHLuo-Robo1 in Robo1/2$^{-/-}$ mice could rescue the previously reported stalling phenotypes resulting from Robo1/2 deletion (Long et al., 2004; Delloye-Bourgeois et al., 2015). We analyzed the

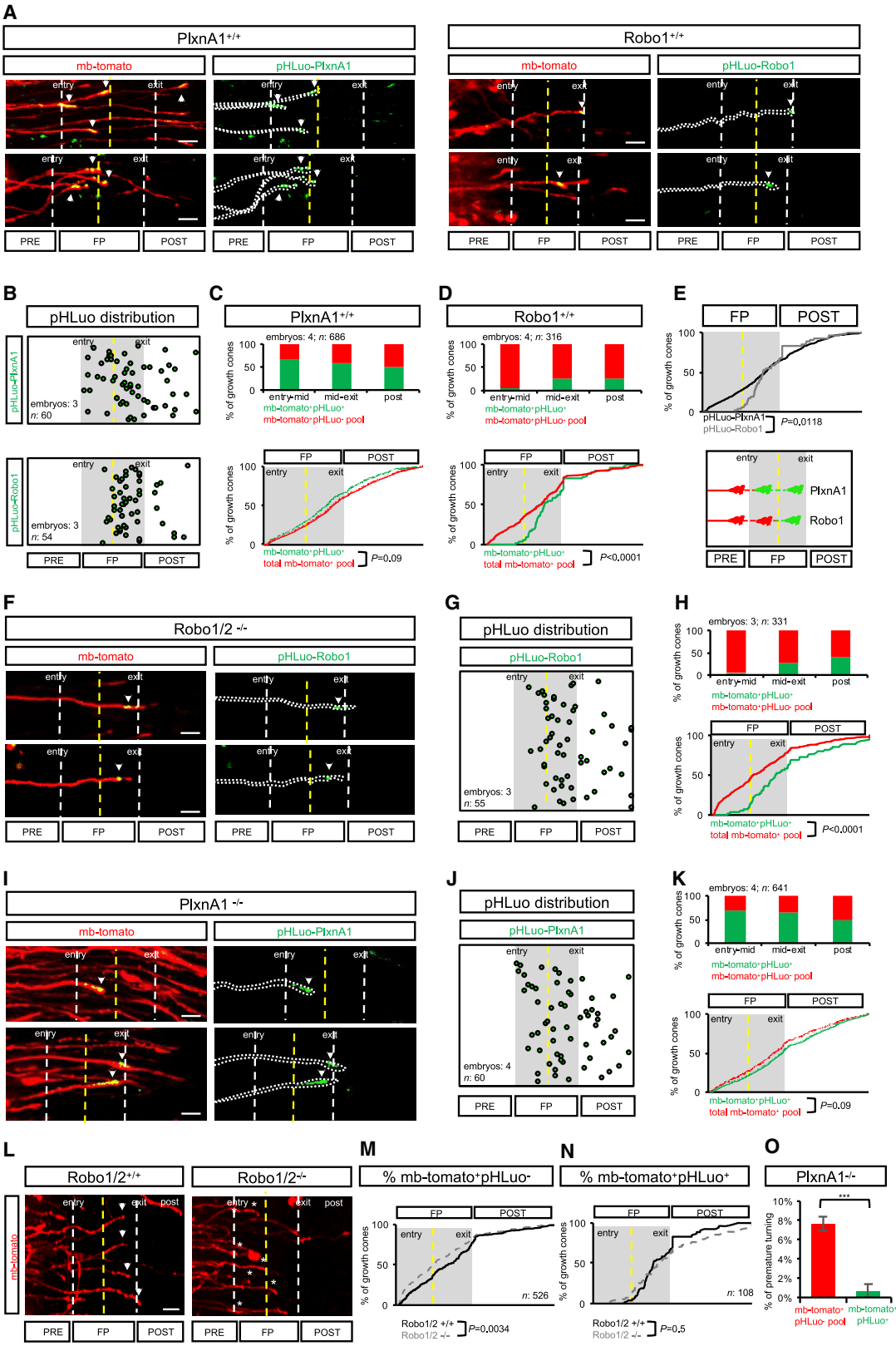

(legend on next page)

distribution of mb-tomato$^+$ growth cones over pre- to post-crossing steps, distinguishing growth cones that exposed Robo1 at their surface (mb-tomato$^+$pHLuo$^+$) from those that did not (mb-tomato$^+$pHLuo$^-$) in Robo1/2$^{+/+}$ and Robo1/2$^{-/-}$ embryos. We observed that Robo1/2 loss resulted in a significantly shifted distribution of mb-tomato$^+$pHLuo$^-$ toward the first FP half (Figures 4L and 4M). Interestingly, the expression of Robo1 at the growth-cone surface was sufficient to rescue the distribution observed in the wild-type (WT) condition, as observed by the matching of the distribution of mb-tomato$^+$pHLuo$^+$ growth cones in Robo1/2$^{-/-}$ and Robo1/2$^{+/+}$ embryos (Figure 4N). Moreover, and consistent with its observed sorting profile, Robo2 is dispensable for FP crossing. Next, we analyzed the guidance of mb-tomato$^+$ pHLuo$^-$ and mb-tomato$^+$pHLuo$^+$ growth cones in PlxnA1$^{-/-}$ open books. We focused on premature turning, which was particularly obvious in the mb-tomato$^+$pHLuo$^-$ condition and has already been reported in PlxnA1$^{-/-}$ mutants (Delloye-Bourgeois et al., 2015). We observed this phenotype was sharply reduced in the population of mb-tomato$^+$pHLuo$^+$ growth cones (Figure 4O). Thus, as for Robo1, rescuing the cell-surface PlxnA1 pool in PlxnA1$^{-/-}$ mutants was sufficient to prevent aberrant guidance behaviors during FP navigation.

STED Microscopy Reveals Differential Partition of PlxnA1 and Robo1 within Growth Cones

Next, we used super-resolution microscopy to assess whether Robo1 and PlxnA1 also differ in their spatial distribution at the growth-cone surface. Living open books were incubated with ATTO-647N-conjugated GFP nanobodies to label cell-surface pHLuo. After fixation, guidance-receptor pools were imaged in commissural growth cones at different FP navigation steps using stimulated emission depletion (STED) microscopy (Figure 5A). First, we measured the density of the fluorescent signal in individual growth cones. We found that PlxnA1 and Robo1 receptor clusters have differential cell-surface distributions. PlxnA1 predominantly accumulated at the growth-cone front and Robo1 at the rear (Figures 5B–5D). This was also confirmed by determining the center of mass of the signals, which segregated along the growth-cone front-rear axis (Figure 5E). Second, we studied whether the distribution patterns of PlxnA1 and Robo1 vary during FP navigation. According to their temporal sorting, we compared PlxnA1 distributions between FP entry and exit and those of Robo1 between midline and exit. Analysis of the number and size of individually labeled particles revealed modifications of Robo1, but not PlxnA1, patterns (Figures 5F and 5G). Although not differing in their numbers, the size of pHLuo-Robo1$^+$ particles increased from the midline to the exit, indicative of Robo1 diffusion at the surface (Figure 5G). Using the same experimental paradigm, we examined whether Robo2 was also distributed asymmetrically in a manner similar to Robo1 at the growth-cone surface. Strikingly, we found Robo2 cell-surface expression to be homogeneous in growth cones, the receptor covering all domains of the growth-cone surface, which was confirmed by center-of-mass quantitative analysis (Figures 5H and 5I).

Figure 4. Chick PlxnA1 and Robo1 Temporal Sequences Are Conserved in the Mouse

(A) Microphotographs of PlxnA1$^{+/+}$ and Robo1$^{+/+}$ open books illustrating pHLuo-PlxnA1$^+$ (left panel) and pHLuo-Robo1$^+$ (right panel) growth cones, indicated by white arrowheads.

(B) Top panel: cartography of pHLuo-PlxnA1$^+$ growth cones (N = 3 embryos, 60 growth cones); bottom panel: cartography of pHLuo-Robo1$^+$ growth cones (N = 3 embryos, 54 growth cones).

(C) Top panel: distribution of mb-tomato$^+$pHLuo$^+$ and mb-tomato$^+$pHLuo$^-$ populations in PlxnA1$^{+/+}$ open books. Bittin panel: cumulative fraction of mb-tomato$^+$pHLuo$^+$ and total mb-tomato$^+$ (composed of mb-tomato$^+$pHLuo$^+$ and mb-tomato$^+$pHLuo$^-$) populations showing that mb-tomato$^+$pHLuo$^+$ growth cones are detected from the onset of FP navigation. p value is from the Kolmogorov-Smirnov (KS) test.

(D) Top panel: distribution of mb-tomato$^+$pHLuo$^+$ and mb-tomato$^+$pHLuo$^-$ populations in Robo1/2$^{+/+}$ open books. Bottom panel: cumulative fractions of mb-tomato$^+$pHLuo$^+$ and total mb-tomato$^+$ (composed of mb-tomato$^+$pHLuo$^+$ and mb-tomato$^+$pHLuo$^-$) populations. The total mb-tomato$^+$ population distributes from the first FP half, whereas the mb-tomato$^+$pHLuo$^+$ growth cones are only detected from the second FP half. p value is from the Kolmogorov-Smirnov (KS) test.

(E) Cumulative fraction of pHLuo-PlxnA1$^+$ and pHLuo-Robo1$^+$ growth cones showing the differential timing of receptor sorting. p value is from the Kolmogorov-Smirnov (KS) test.

(F) Microphotographs of Robo1/2$^{-/-}$ open books illustrating pHLuo-Robo1$^+$ growth cones indicated by white arrowheads.

(G) Cartography of pHLuo-Robo1$^+$ growth cones (N = 3 embryos, 55 growth cones).

(H) Top panel: distribution of mb-tomato$^+$pHLuo$^+$ and the mb-tomato$^+$pHLuo$^-$ populations in Robo1/2$^{-/-}$ open books. Bottom panel: cumulative fractions of mb-tomato$^+$pHLuo$^+$ and total mb-tomato$^+$. p value is from the Kolmogorov-Smirnov (KS) test.

(I) Microphotographs of PlxnA1$^{-/-}$ open books illustrating pHLuo-PlxnA1$^+$ growth cones indicated by white arrowheads.

(J) Cartography of pHLuo-PlxnA1$^+$ growth cones (N = 4 embryos, 60 growth cones).

(K) Top panel distribution of mb-tomato$^+$pHLuo$^+$ and the mb-tomato$^+$pHLuo$^-$ populations in PlxnA1$^{-/-}$ open books. Bottom panel: cumulative fractions of mb-tomato$^+$pHLuo$^+$ and total mb-tomato$^+$. p value is from the Kolmogorov-Smirnov (KS) test.

(L) Representative images of mb-tomato$^+$ growth cones illustrating reduced numbers of growth cones (asterisks) on their way for the FP exit in Robo1/2$^{-/-}$ compared with Robo1/2$^{+/+}$ open books.

(M) Cumulative fractions reporting the distribution of mb-tomato$^+$pHLuo$^-$ growth cones in Robo1/2$^{+/+}$ and Robo1/2$^{-/-}$ embryos showing a significantly shifted distribution of tomato$^+$pHLuo$^-$ growth cones toward the first FP half in Robo1/2$^{-/-}$ embryos.

(N) Cumulative fractions reporting similar distribution of pHLuo-Robo1$^+$ growth cones in open books of Robo1/$^{+/+}$ and Robo1/2$^{-/-}$ embryos. p value is from the Kolmogorov-Smirnov (KS) test.

(O) Histograms showing the percentage of axons turning rostrally prematurely in PlxnA1$^{-/-}$ embryos electroporated with mb-tomato alone or in combination with pHLuo-PlxnA1. The quantification shows the reduction in the percentage of premature turning in embryos electroporated with pHLuo-PlxnA1 compared with the mb-tomato-electroporated littermate (mb-tomato$^+$pHLuo$^-$, N = 2 embryos, 18 stacks, 513 growth cones analyzed; mb-tomato$^+$pHLuo$^+$, N = 4 embryos, 40 stacks, 259 growth cones. p value is from the Mann-Whitney test.

Scale bars: 20 μm in (A), (F), and (I) and 50 μm in (L).

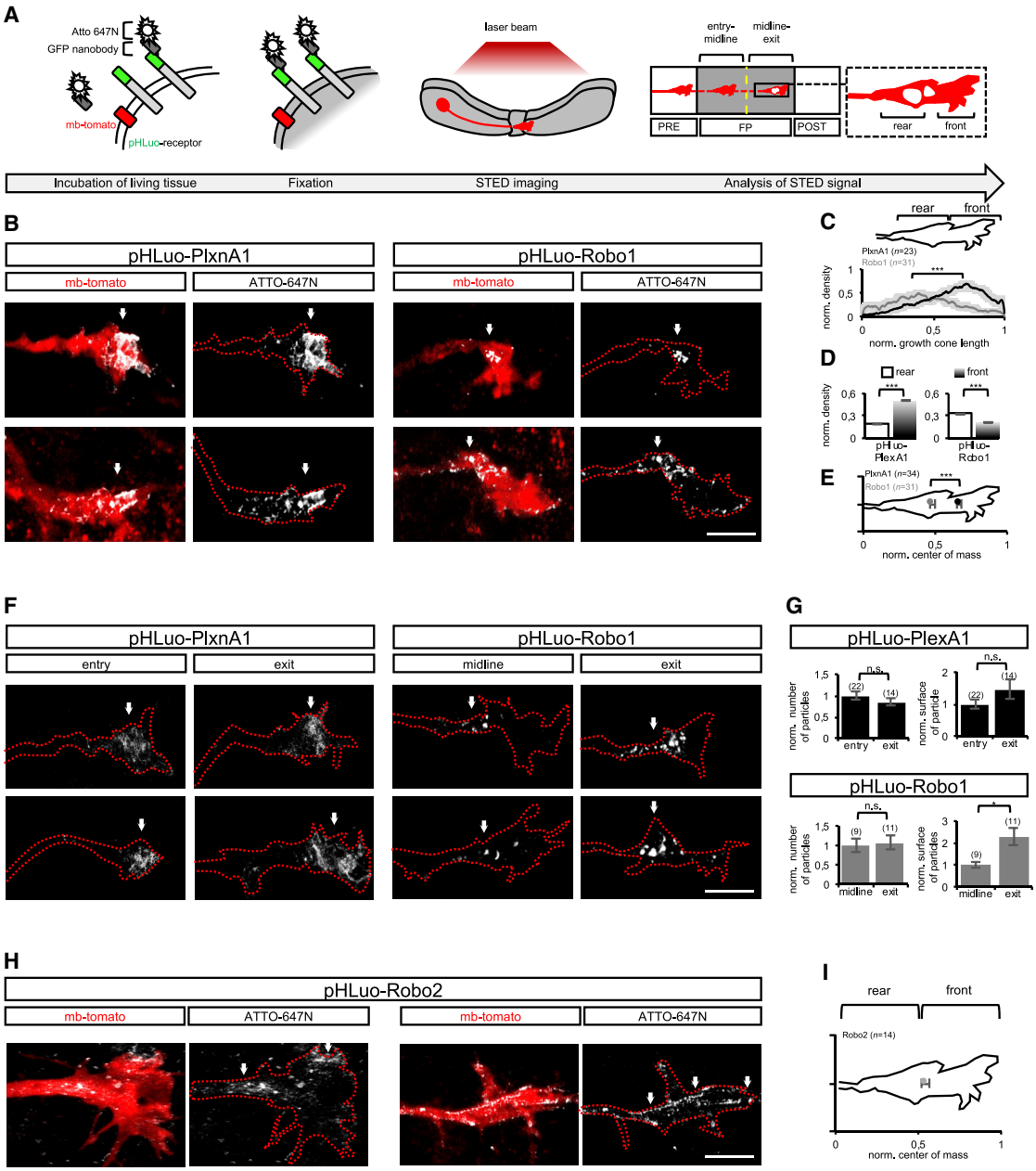

Figure 5. PlxnA1 and Robo1 Are Partitioned at the Cell Surface of Commissural Growth Cones

(A) Super-resolution imaging procedure. Open books of embryos electroporated with pHLuo vectors were live-labeled with ATTO-647N-conjugated GFP nanobodies and fixed with PFA before STED imaging. Membrane pHLuo density and distributions were analyzed in the growth cones navigating the first (entry to midline) and the second (midline to exit) FP halves. The growth cone was segmented into front and rear sub-domains.

(B) Microphotographs of representative commissural growth cones delineated with mb-tomato and labeled with ATTO-647N-conjugated GFP nanobodies. White arrowheads indicate ATTO-647N signal.

(C) Densities of membrane pHLuo-PlxnA1 and pHLuo-Robo1 signals normalized to the growth-cone length showing their differential distribution along the rear-front axis (PlxnA1, N = 8 embryos, 23 growth cones; Robo1, N = 12 embryos, 31 growth cones). Error bars indicate means ± SEM; *p < 0.05, **p < 0.01, ***p < 0.001, p is from Kolmogorov-Smirnov (KS) test.

(D) Histograms showing the comparison between normalized density of pHLuo signal in the front and the rear domains for both pHLuo-PlxnA1 and pHLuo-Robo1. p value is from the Mann-Whitney test.

(E) Positions of pHLuo-PlxnA1 and pHLuo-Robo1 center of mass normalized to growth-cone length (PlxnA1, N = 34 growth cones; Robo1, N = 31 growth cones).

(F) Microphotographs of mb-tomato$^+$pHLuo$^+$ commissural growth cones labeled with ATTO-647N-conjugated GFP nanobodies.

(G) Top panel: histograms of normalized numbers and surfaces of pHLuo-PlxnA1 individual clusters detected in the growth cones showing no changes during the FP navigation (PlxnA1, 22 growth cones in entry, 14 growth cones in exit). Error bars indicate means ± SEM; *p < 0.05, **p < 0.01, ***p < 0.001, p value is from the

(legend continued on next page)

We then investigated whether the distinct compartmentalization of PlxnA1 and Robo1 is generated at the surface or, rather, results from pre-patterns of intracellular receptor pools. To address that question, living open books where fixed, permeabilized, and incubated with anti-GFP antibodies to reveal the total pool of pHLuo at high resolution with STED microscopy (Figures 6A–6C). We quantified the receptor distribution within growth cones. Interestingly, both PlxnA1 and Robo1 occupied similar growth-cone areas and had equal centers of mass within the cone. Thus, the intracellular receptor pool is likely to be uniformly distributed (Figure 6D). This result suggests that PlxnA1 and Robo1 are either delivered at the surface of different growth-cone sub-domains or that their partitioning arises from selective membrane diffusion (Figure 6E).

FRAP Reveals Differential Dynamics of PlxnA1 and Robo1 at the Growth-Cone Surface

To get further insight into PlxnA1 and Robo1 sorting, we performed fluorescence recovery after photobleaching (FRAP) experiments, targeting commissural growth cones expressing pHLuo-tagged receptors and navigating the FP in living open books. To specifically assess the dynamics of membrane insertion of PlxnA1 and Robo1, the pHLuo-receptor fluorescence in an area of 15 to 20 μm^2 covering the entire growth cone surface was bleached to 80–90% at time zero, then, the fluorescence recovery was recorded for 20 min (Figures 6F and 6G). After 200 s, the fluorescence recovery represented less than 1% of the initial fluorescence, indicating that most of the surface-associated and freely diffusing receptors had been photobleached (Figure 6H). Instead, we observed a gradual increase in fluorescence (over 17 min), most likely reflecting receptor export from intracellular pools. The recovery of pHLuo-Robo1 was modest, rapidly reaching a plateau at around 17% of the initial fluorescence level. In contrast, the recovery level of PlxnA1 was significantly greater (Figure 6I; Videos S11 and S12 for PlxnA1 and Videos S13 and S14 for Robo1), although it still did not reach a plateau attaining 38% of the initial fluorescence at the end of the recording period. Thus, the dynamics of membrane insertion differs between Robo1 and PlxnA1: although intracellular PlxnA1 can be rapidly mobilized for externalization, the Robo1 intracellular pool might be almost depleted when commissural growth cones sort Robo1, strongly limiting the additional supply of receptors to the cell surface.

Intracellular Domain of PlxnA1, but Not Robo1, Controls Receptor Temporal Patterns

Lastly, to gain insight into the mechanisms controlling the specific temporality of Robo1 and PlxnA1 sorting, we constructed chimeric receptors in which the extracellular domain (ECD) and intracellular domain (ICD) were swapped (Figure 7A). pHLuo-PlxnA1^{ECD}-Robo1^{ICD} and pHLuo-Robo1^{ECD}-PlxnA1^{ICD} were introduced in the neural tube of chicken embryos, and the position of growth cones with pHLuo fluorescence was plotted to build cartographies of receptor cell-surface sorting.

We found that pHLuo-Robo1^{ECD}-PlxnA1^{ICD} was sorted at the FP entry, as observed for the PlexinA1 native receptor. In contrast, pHLuo-PlxnA1^{ECD}-Robo1^{ICD} was already detected at the surface of growth cones before FP entry. Thus, the temporal profile of PlxnA1 was preserved in a context in which the chimeric receptor contains the PlxnA1 ICD, but not the PlxnA1 ECD (Figures 7B–7E). In contrast for Robo1, neither Robo1 ICD nor ECD alone was sufficient to confer the temporal sorting of the native receptor in the second half of the FP navigation. Moreover, expression of PlxnA1^{ECD}-Robo1^{ICD} led to premature sorting of the receptor before FP entry, thus also revealing that PlxnA1 ICD is required to prevent the native receptor being sorted at the pre-crossing stage (Videos S15 and S16 for pHLuo-PlxnA1^{ECD}-Robo1^{ICD} and Videos S17 and S18 for pHLuo-Robo1^{ECD}-PlxnA11^{ICD}).

Next, we examined whether expression of these chimeric receptors affected the FP navigation. We monitored individual growth cones from the pre-crossing compartment and correlated their behavior with the timing of pHLuo-receptor sorting.

In the pHLuo-PlxnA1^{ECD}-Robo1^{ICD} condition, we found that most (81%) of the recorded growth cones exhibited a standard behavior, entering and crossing the FP, as observed for the integral PlxnA1 receptor (Figures S4A and S4B). Interestingly, 41% of these cases had prematurely sorted the chimeric receptor before the FP entry, which, in PlexinA1 and Robo1 integral receptor conditions, led, in all cases, to a failure of FP navigation (Figure 7G). In the pHLuo-Robo1^{ECD}-PlxnA1^{ICD} condition, 63% of the cases navigated the FP properly, with 93% of them sorting the receptor at the FP entry (Figure 7H). Stalling was slightly more frequent than in the pHLuo-PlxnA1^{ECD}-Robo1^{ICD} condition but occurred in growth cones that sorted the chimeric receptor before FP entry (Figure 7H). These results suggest that the chimeric receptor pHLuo-Robo1^{ECD}-PlxnA1^{ICD} is active, whereas pHLuo-PlxnA1^{ECD}-Robo1^{ICD} apparently is not.

DISCUSSION

During growth-cone guidance, focal and timed patterns of signaling are thought to be crucial, but their visualization remains highly challenging, requiring experimental paradigms that preserve the topography of guidance molecules and their proper perception by the growth cones. Our live-imaging procedure of receptor dynamics allows access to the temporal and spatial resolution of signaling activities in navigating growth cones. We report here that, beyond their synthesis and trafficking to the axon, guidance receptors are exposed at the surface of the

Mann-Whitney test). Bottom panel: histograms of the normalized numbers and surfaces of pHLuo-Robo1 individual clusters detected in growth cones navigating the FP midline and exit. Note that the particle number was unchanged, whereas the particle surface increased between the midline and the exit (Robo1, nine growth cones at midline, 11 cones at exit). Error bars indicate means ± SEM; *p < 0.05, **p < 0.01, ***p < 0.001, p value is from the Mann-Whitney test.
(H) Microphotographs of representative commissural growth cones electroporated with pHLuo-Robo2, delineated with mb-tomato and labeled with ATTO-647N-conjugated GFP nanobodies. White arrowheads point indicate ATTO-647N signal.
(I) Position of pHLuo-Robo2 center of mass normalized to growth-cone length suggesting no asymmetrical receptor distribution (Robo2, N = 14 growth cones).
Scale bars: 5 μm in (B), (F), and (H).

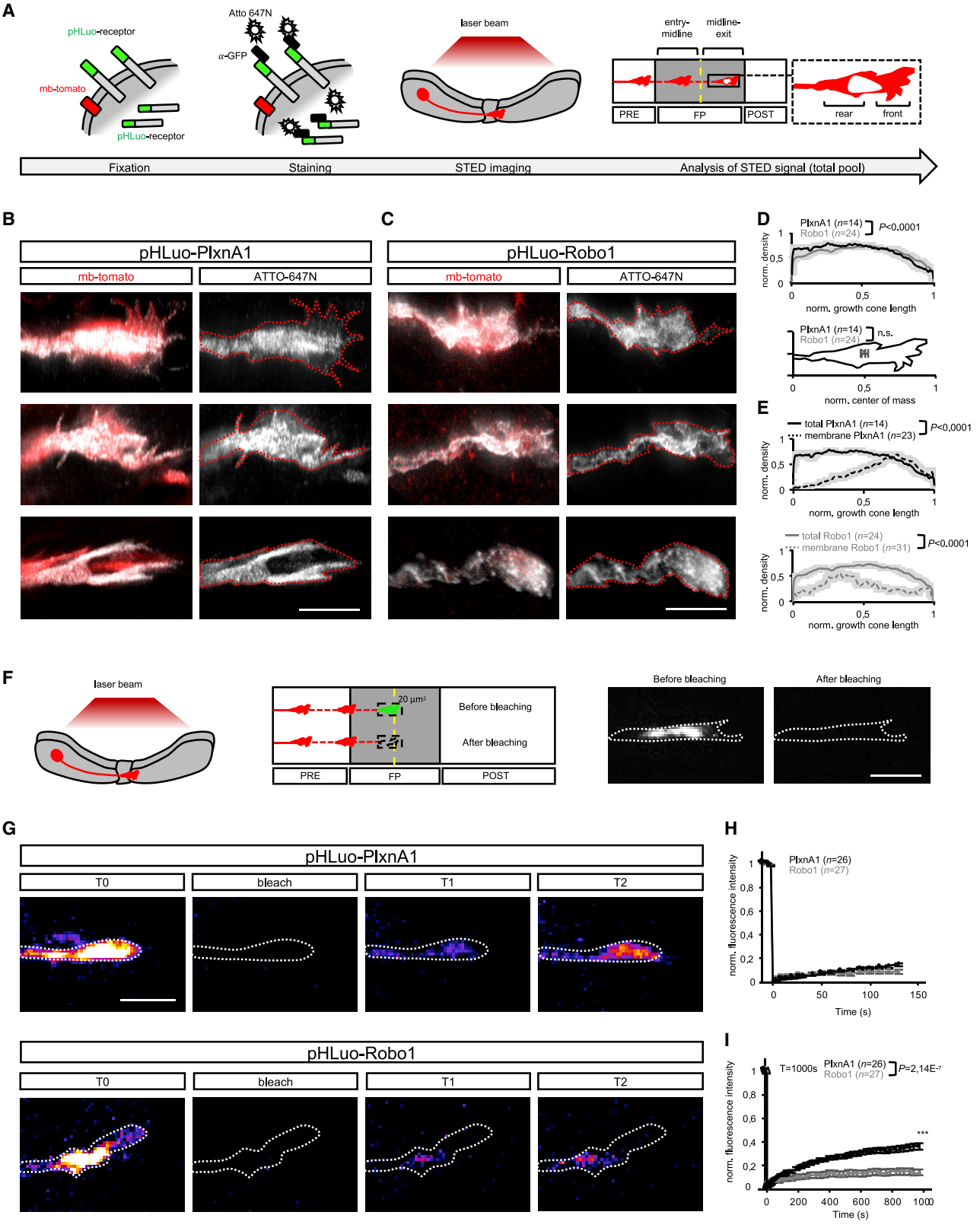

(legend on next page)

growth cones at precise times and locations. During commissural axon navigation, these receptor-specific cell-surface codes can thus shape spatially and temporally distinct signals from coincident midline cues. Our findings that the membrane sorting of PlxnA1, Robo1, and Robo2 coincides with changes of growth-cone behaviors also strengthen the view that temporally controlling the availability of the receptors at the growth-cone surface is a general mechanism to accommodate the growth cones to novel guidance challenges.

Sequential Sorting of Guidance Receptors at the Commissural Growth-Cone Surface Sets Specific Functions of Midline Repellents during and after Midline Crossing

Our data reveal a temporal sequence of Nrp2, PlxnA1, Robo1, and Robo2 surface sorting, which equip commissural growth cones at successive steps of their navigation. This could result in sequential growth-cone sensitization of the various local repellents. Accordingly, PlxnA1/Nrp2-mediated Sema3B and PlxnA1-mediated SlitC activities could be initiated on FP entry. Robo1-mediated SlitN signaling would start after the midline, and Robo2-mediated signaling at a next post-crossing choice point. Our data from super-resolution microscopy, showing that surface pools of Robo1 and PlxnA1 concentrate in distinct growth-cone domains, suggest, in addition, that the repellents might have distinct modes of action, regulating different steps or aspects of the navigation through specific downstream signaling cascades. The front-rear partitioning of PlxnA1 and Robo1 correlates with the spatial organization of growth-cone cytoskeletal components and could serve as a mechanism for generating focal signaling onto different cytoskeletal components. Indeed, growth-cone responses to guidance cues rely on regulations of both microtubule and actin dynamics, which physically occupy mainly the central and the filopodia-rich peripheral domains, respectively (Cammarata et al., 2016; Kahn and Baas, 2016).

Interestingly, our live-imaging analysis also supports signaling via these receptors having different functional outcomes. The gain of cell-surface expression of Robo1, but not PlxnA1, coincided with increased rostro-caudal exploration behavior of the growth cones. This did not result in premature deviation from the trajectory in the FP but appeared, rather, to pre-figure the longitudinal turning decision that will be taken at the FP exit. Interestingly, increased exploration in the second FP half was observed in the mb-tomato^{+} pHLuo^{-} condition, when endogenous Robo1 is presented at the cell surface, which thus supports that this might be a physiological behavior of growth cones preparing for exit. Either Robo1 contributes to this rostro-caudal turning or perhaps counteracts rostro-caudal guidance signals to prevent their activation until the FP crossing is achieved. Conversely, gain of PlxnA1, but not Robo1, coincides with the slowing of growth-cone velocity. Such a fluctuation was also observed in the mb-tomato^{+}pHLuo^{-} condition at the FP entry. It was, nevertheless, less pronounced, which likely reflects that receptor sorting in the mb-tomato^{+}pHLuo^{+} context led to an exacerbated functional outcome. Thus, PlxnA1 might contribute to the adaptation of growth-cone velocity during navigation. Whether exploratory behavior and growth speed are the sole functional outcomes of PlxnA1 and Robo1 ligands is unlikely. The timing of Robo1 sorting and activity after midline crossing is compatible with Slit-mediated repulsion toward the FP exit. In contrast, the sorting of PlxnA1, present from the FP entry, suggests a different mode of action of its ligands. Characterization of the ligand distributions at protein levels is still lacking and is instrumental for further elaboration of functional models.

We found that PlxnA1 and Robo1 have comparable dynamics in chick and mouse, suggesting that the role of these receptors and the mechanisms that regulate their dynamics are conserved. In addition, the rescue observed when re-expressing PlxnA1 and Robo1 coding sequences in commissural neurons of PlxnA1$^{-/-}$ and Robo1/2$^{-/-}$ embryos demonstrate that both receptors are required, cell autonomously, for FP navigation or at least for the parameters of the navigation that were examined in the present study.

Figure 6. PlxnA1 and Robo1 Partitioning at the Cell Surface Is Not Generated via Pre-patterns of Intracellular Receptor Pools

(A) Super-resolution procedure for total receptor-pool detection. Before STED imaging, open books of embryos electroporated with pHLuo vectors were fixed, permeabilized, and immunolabeled with a primary anti-GFP antibody recognizing pHLuorin, followed by an ATTO-647N-conjugated secondary antibody. pHLuo density and distribution were analyzed in growth cones at different steps of the FP navigation. The growth cone was segmented into front and rear sub-domains.

(B and C) Microphotographs of representative commissural growth cones delineated with mb-tomato and labeled with ATTO-647N-conjugated GFP nanobodies for pHLuo-PlxnA1 (B) and pHLuo-Robo1 (C).

(D) Distribution of total pHLuo within the growth cones. Top panel: densities of total pHLuo-Plxna1 and pHLuo-Robo1 signals normalized to the growth-cone length. Bottom panel: positions of pHLuo-PlxnA1 and pHLuo-Robo1 centers of mass normalized to the growth-cone length. Note that PlxnA1 and Robo1 total pools have similar centers of mass (PlxnA1, N = 14 growth cones; Robo1, N = 24 growth cones). Error bars indicate means ± SEM. Top panel p is from the Kolmogorov-Smirnov (KS) test; bottom panel p is from the Mann-Whitney test.

(E) Densities of membrane and total pHLuo in pHLuo-PlxnA1 (top panel) and in pHLuo-Robo1 (bottom panel) electroporated conditions, normalized to the growth-cone length. Note the Robo1 and PlxnA1 differential distribution along the rear-front axis (membrane PlxnA1, N = 23 growth cones; total PlxnA1, N = 14 growth cones; membrane Robo1, N = 31 growth cones; total Robo1, N = 24 growth cones). p is from the Kolmogorov-Smirnov (KS) test.

(F) FRAP procedure. Growth cones navigating the FP and expressing either pHLuo-PlxnA1 or pHLuo-Robo1 were photobleached with a 488-nm diode laser, and fluorescence recovery was monitored. The dashed rectangle indicates the typical bleached area.

(G) Representative color-coded images from time-lapse sequences illustrating the bleaching and the fluorescence recovery of pHLuo-PlxnA1 and pHLuo-Robo1 in growth cones. T1 = 370 s, T2 = 970 s.

(H and I) Graphs of fluorescence recovery for pHLuo-PlxnA1 and pHLuo-Robo1 150 (H) and 1000 (I) s after photobleaching. Dots represents the means of three independent experiments (PlxnA1, N = 26 growth cones; Robo1, N = 27 growth cones). Error bars indicate means ± SEM. p is from Student's t test performed on values at 1,000s.

Scale bars: 5 μm in (B) and (C) and 10 μm in (F) and (G).

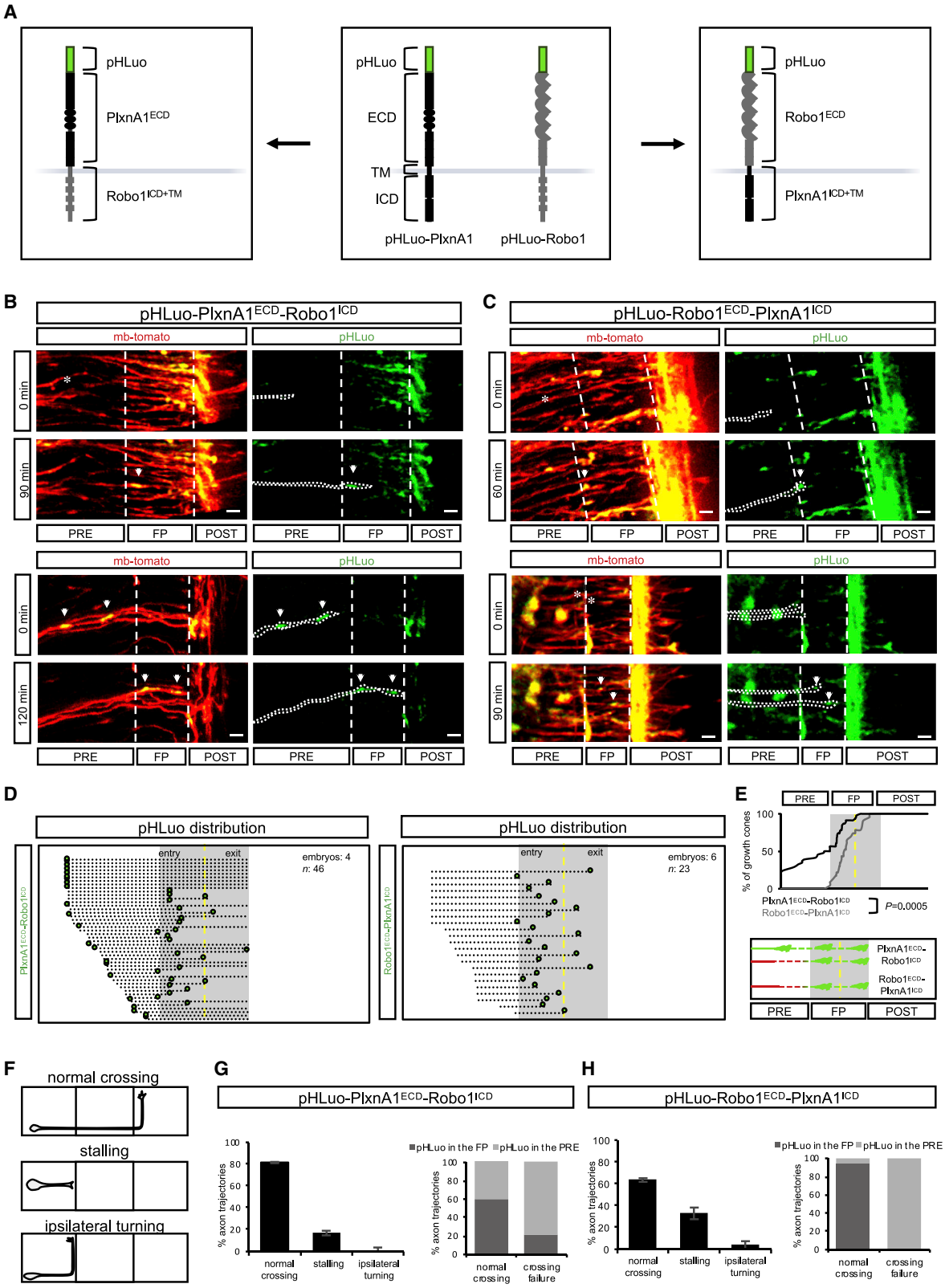

(legend on next page)

The Spatial and Temporal Specificity of Receptor Sorting Is Generated at the Membrane-Insertion Level

Several observations support Robo1 and PlxnA1 having specific membrane-insertion dynamics. In both cases, we observed receptors present in the growth cones but not yet sorted at their surface. Nevertheless, our FRAP revealed striking differences between Robo1 and PlxnA1 dynamics. They might rely on protein availability in the growth cone, which could be set through receptor-specific translational and post-translational regulations or trafficking pathways. Various mechanisms have been identified that regulate Robo levels in vertebrates. MicroRNA-mediated regulation of Robo1 synthesis was recently reported (Yang et al., 2018). It is unlikely responsible for specifying the timing of surface sorting because our expression vectors do not encode the regulatory sequences underlying microRNA regulation. Ndfip1/2 proteins recruiting Nedd4E3 ubiquitin ligases were discovered to target Robo1 in endosomes for degradation before FP crossing (Gorla et al., 2019). In the chicken embryo, Robo1 sorting from intracellular vesicles was found to occur through upregulation of RabGDI (Philipp et al., 2012). It would be interesting to determine whether these different regulatory mechanisms also determine the temporal pattern of Robo1 delivery. Interestingly, increases in Robo1 levels also occur in embryos lacking Robo3, which acts as a negative regulator of Robo1 before midline crossing, even though commissural axons are prevented from navigating the FP (Evans and Bashaw, 2010). This suggested that signals diffusing from the FP could act as triggers of Robo1 increase. Accordingly, recent work reported that Slit stimulation itself elevates Robo1 surface levels in axons of cultured commissural neurons through the endocytosis and recycling amplification loop (Kinoshita-Kawada et al., 2019). Our findings that FP-conditioned medium, which might contain Slits, induces Robo1 surface presentation in explant cultures are fully consistent with these data. It would be interesting to determine whether FP signals could suppress the Ndfip1/2-Nedd4E3 pathway to stop Robo1 degradation and allow its membrane insertion.

Concerning PlxnA1, we previously reported that regulation of its sorting depends on processing by calpains, with integral, but not cleaved, PlxnA1 undergoing cell-surface sorting (Nawabi et al., 2010; Charoy et al., 2012). Processing suppression, which results from calpain inhibition, occurs when commissural axons are exposed to local FP signals and allows rapid membrane insertion of integral PlxnA1. The findings from FRAP experiments, which revealed a capacity of the growth cones to deliver PlxnA1 to the surface after depletion of fluorescence in the entire growth cone are consistent with this model.

Our analysis of the total and membrane-receptor pools by STED microscopy suggests that the sorting mechanism controls not only controls the timing of membrane availability of the receptors but also their spatial distribution at the surface. Such membrane compartmentalization could emerge via polarized-receptor delivery or rearrangements at the membrane through selective retention or retrieval. Such rearrangements could depend on the local environment to which commissural growth cones are exposed. Noteworthy, Robo1 and Robo2, which are sorted at different steps of the navigation, also have distinct distribution at the growth-cone surface, with only Robo1 showing a front-rear polarity.

Robo1 and Robo2 Are Sorted at Different Steps of Commissural Axon Navigation

Despite various reports that Robo1 and Robo2 might have distinct contributions (Kim et al., 2011), the specific guidance decisions they control during commissural axon navigation have remained unclear. Both receptors transduce Slit signals and are expressed by commissural neurons. Both were found expressed at low levels in pre-crossing and crossing commissural axons and enriched at the post-crossing stage (Long et al., 2004), and their deletion in mice has a distinct effect on commissural axon navigation (Long et al., 2004; Reeber et al., 2008; Jaworski et al., 2010). Our study highlights novel drastic differences between Robo1 and Robo2 receptors, which could not be anticipated from their general expression patterns. Sorting occurs in the FP for Robo1 and in the LF for Robo2. Such temporally accurate Robo2 sorting appears unlikely to be dedicated to the perception of FP Slits. It suggests, rather, that the growth cone acquires perception of a signal precisely at the VF/LF transition, which suggests further examination of the

Figure 7. PlxnA1, but Not Robo1, Intracellular Domain Encodes Membrane Insertion Temporal Pattern

(A) Representation of pHLuo-PlxnA1 and pHLuo-Robo1 receptors. The pHLuo-PlxnA1-Robo1 chimera (left panel) consists of the PlxnA1^{ECD} fused to the Robo1 transmembrane (TM) and ICD. The pHLuo-Robo1-PlxnA1 chimera consists of the Robo1^{ECD} fused to PlxnA1 TM and ICD.

(B) Time-lapse sequences illustrating the dynamics of the chimera. Arrowheads indicate pHLuo detected in growth cones at the FP entry (top panel) and before their arrival to the FP (bottom panel).

(C) Time-lapses sequences showing the dynamics of the chimera. The flashes are detected at the FP entry.

(D) Cartographies of pHLuo-PlxnA1^{ECD}-Robo1^{ICD} (left panel) and pHLuo-Robo1^{ECD}-PlxnA1^{ICD} (right panel) dynamics from video analysis. Dashed lines indicate the overall trajectory of single growth cones; green spots, first pHLuo detection. Note that for both chimeras, flashes are detected at the FP entry. However, for pHLuo-PlxnA1^{ECD}-Robo1^{ICD} chimera, pHLuo is also detected in growth cones before their crossing.

(E) Top panel: cumulative fractions showing differential dynamics of pHLuo-PlxnA1^{ECD}-Robo1^{ICD} and pHLuo-Robo1^{ECD}-PlxnA1^{ICD} dynamics. p value is from the Kolmogorov-Smirnov (KS) test. Bottom panel: summary of the temporal sequence of PlxnA1^{ECD}-Robo1^{ICD} and pHLuo-Robo1^{ECD}-PlxnA1^{ICD}.

(F) Illustrations of the phenotypes observed in open books.

(G) Left panel: Histograms showing the percentage of normal and aberrant (stalling and ipsilateral turning) trajectories in the pHLuo-PlxnA1^{ECD}-Robo1^{ICD} condition. Right panel: Repartition, according to the axon trajectory (normal or aberrant) between axons starting to express pHLuo at their growth cone surface in pre-crossing or at the FP entry (N = 2 embryos, 49 growth cones).

(H) Left panel: Histograms showing the percentage of normal and aberrant (stalling and ipsilateral turning) trajectories in the pHLuo-Robo1^{ECD}-PlxnA1^{ICD} condition. Right panel: Repartition, according to the axon trajectory (normal or aberrant) between axons starting to express pHLuo at the surface of their growth cone in PRE-crossing or at the FP entry. Expression of this chimera in the pre-crossing prevented FP crossing (N = 3 embryos, 35 growth cones).

Scale bars: 10 μm in (B) and (C).

mechanisms controlling medio-lateral position choices of post-crossing axons is needed.

Overall, our study demonstrates that the generation of specific temporal sequences of receptor sorting represents a mechanism by which commissural growth cones functionalize guidance signals with precise timing during spinal-cord navigation. Such a dynamic regulation might be exploited in a variety of biological processes during which cells must adapt their perception of extracellular cues in a context-dependent manner. Particularly, establishing a fast and flexible perception of extracellular signals is a prerequisite for cells or axons that migrate along highly stereotyped, long-distance pathways, being exposed to fluctuating combinations of guidance cues (Te Boekhorst et al., 2016).

STAR★METHODS

Detailed methods are provided in the online version of this paper and include the following:

- KEY RESOURCES TABLE
- LEAD CONTACT AND MATERIALS AVAILABILITY
- EXPERIMENTAL MODEL AND SUBJECT DETAILS
  - Chick Embryos
  - Mice embryos
  - Cell Lines
- METHOD DETAILS
  - Receptor molecular biology
  - *In vitro* test of pH fluorescence dependency
  - In ovo electroporation
  - Open book culture
  - Mouse spinal cord electroporation and culture
  - Live imaging and data analysis
  - Detection of the total pool of pHLuorin
  - Chick explant cultures
  - Atto647N staining for surface receptor pool
  - Atto647N staining for total receptor pool
  - STED imaging and data analysis
  - Fluorescence Recovery After Photobleaching
  - Chimeric receptor molecular biology
- QUANTIFICATION AND STATISTICAL ANALYSIS
  - Number of Experimental Replicates
  - Data Exclusion
  - Statistical treatment of data
- DATA AND CODE AVAILABILITY

SUPPLEMENTAL INFORMATION

Supplemental Information can be found online at https://doi.org/10.1016/j.celrep.2019.08.098.

ACKNOWLEDGMENTS

We thank A. Chedotal for sharing the Robo mouse model, E. Derrington for input on the manuscript, and O. Raineteau for scientific discussions. STED and FRAP microscopy were performed at the Bordeaux Imaging Center (BIC), CNRS-INSERM-Bordeaux University, member of the national infrastructure France BioImaging supported by the French National Research Agency (ANR-10-INBS-04). We thank C. Poujol and M. Mondin (BIC) for advice, M. Sainlos for sharing the anti-GFP nanobody, and B. Tessier and S. Benquet for technical assistance. This work was conducted within the frame of the LabEx CORTEX and DEVWECAN of Université de Lyon, within the program ''Investissements d'Avenir'' (ANR-11-IDEX-0007) operated by the French National Research Agency (ANR). The study was supported by an ANR funding to V.C. and O.T., the Association Française contre les Myopathies (AFM) to V.C., and the Conseil Régional d'Aquitaine (Neurocampus funds).

AUTHOR CONTRIBUTIONS

Conceptualization, V.C.; Methodology, A.P., H.D., J.F., L.B., V.C., and O.T.; Investigation, A.P. (live imaging and STED microscopy, tool validation), H.D. (STED microscopy and FRAP experiments), K.K. and M.B. (molecular biology, tool validation), and S.T.-D. and T.G. (chimeric receptor constructions); Writing, A.P. and V.C.; Writing – Review & Editing, H.D. and J.F.; Formal Analysis, A.P., H.D., J.F., O.T., and V.C.

DECLARATION OF INTERESTS

Authors declare no competing interests.

Received: March 22, 2019
Revised: July 5, 2019
Accepted: August 28, 2019
Published: October 8, 2019

REFERENCES

Cammarata, G.M., Bearce, E.A., and Lowery, L.A. (2016). Cytoskeletal social networking in the growth cone: how +TIPs mediate microtubule-actin cross-linking to drive axon outgrowth and guidance. Cytoskeleton (Hoboken) *73*, 461–476.

Chamma, I., Letellier, M., Butler, C., Tessier, B., Kok-Hong, L., Gauthereau, D., Choquet, D., Sibarita, J., Park, S., Sainlos, M., and Thoumine, O. (2016). Mapping the dynamics and nanoscale organization of synaptic adhesion proteins using monomeric streptavidin. Nat. Commun. *7*, 10773.

Charoy, C., Nawabi, H., Reynaud, F., Derrington, E., Bozon, M., Wright, K., Falk, J., Helmbacher, F., Kindbeiter, K., and Castellani, V. (2012). gdnf activates midline repulsion by Semaphorin3B via NCAM during commissural axon guidance. Neuron *75*, 1051–1066.

Chen, Z., Gore, B.B., Long, H., Ma, L., and Tessier-Lavigne, M. (2008). Alternative splicing of the Robo3 axon guidance receptor governs the midline switch from attraction to repulsion. Neuron *58*, 325–332.

Colak, D., Ji, S.J., Porse, B.T., and Jaffrey, S.R. (2013). Regulation of axon guidance by compartmentalized nonsense-mediated mRNA decay. Cell *153*, 1252–1265.

Delloye-Bourgeois, C., Jacquier, A., Falk, J., and Castellani, V. (2014). Use of pHluorin to assess the dynamics of axon guidance receptors in cell culture and in the chick embryo. J. Vis. Exp. (*83*), e50883.

Delloye-Bourgeois, C., Jacquier, A., Charoy, C., Reynaud, F., Nawabi, H., Thoinet, K., Kindbeiter, K., Yoshida, Y., Zagar, Y., Kong, Y., et al. (2015). PlexinA1 is a new Slit receptor and mediates axon guidance function of Slit C-terminal fragments. Nat. Neurosci. *18*, 36–45.

Evans, T.A., and Bashaw, G.J. (2010). Axon guidance at the midline: of mice and flies. Curr. Opin. Neurobiol. *20*, 79–85.

Gorla, M., Santiago, C., Chaudhari, K., Layman, A.A.K., Oliver, P.M., and Bashaw, G.J. (2019). Ndfip proteins target Robo receptors for degradation and allow commissural axons to cross the midline in the developing spinal cord. Cell. Rep *26*, 3298–3312.

Jacob, T.C., Bogdanov, Y.D., Magnus, C., Saliba, R.S., Kittler, J.T., Haydon, P.G., and Moss, S.J. (2005). Gephyrin regulates the cell surface dynamics of synaptic GABAA receptors. J. Neurosci. *25*, 10469–10478.

Jaworski, A., Long, H., and Tessier-Lavigne, M. (2010). Collaborative and specialized functions of Robo1 and Robo2 in spinal commissural axon guidance. J. Neurosci. *30*, 9445–9453.

Kahn, O.I., and Baas, P.W. (2016). Microtubules and Growth Cones: Motors Drive the Turn. Trends Neurosci. *39*, 433–440.

Kim, M., Roesener, A.P., Mendonca, P.R., and Mastick, G.S. (2011). Robo1 and Robo2 have distinct roles in pioneer longitudinal axon guidance. Dev. Biol. *358*, 181–188.

Kinoshita-Kawada, M., Hasegawa, H., Hongu, T., Yanagi, S., Kanaho, Y., Masai, I., Mishima, T., Chen, X., Tsuboi, Y., Rao, Y., et al. (2019). A crucial role for Arf6 in the response of commissural axons to Slit. Development *146*, dev172106.

Long, H., Sabatier, C., Ma, L., Plump, A., Yuan, W., Ornitz, D.M., Tamada, A., Murakami, F., Goodman, C.S., and Tessier-Lavigne, M. (2004). Conserved roles for Slit and Robo proteins in midline commissural axon guidance. Neuron *42*, 213–223.

Nawabi, H., Briançon-Marjollet, A., Clark, C., Sanyas, I., Takamatsu, H., Okuno, T., Kumanogoh, A., Bozon, M., Takeshima, K., Yoshida, Y., et al. (2010). A midline switch of receptor processing regulates commissural axon guidance in vertebrates. Genes Dev. *24*, 396–410.

Philipp, M., Niederkofler, V., Debrunner, M., Alther, T., Kunz, B., and Stoeckli, E.T. (2012). RabGDI controls axonal midline crossing by regulating Robo1 surface expression. Neural Dev. *7*, 36.

Pignata, A., Ducuing, H., and Castellani, V. (2016). Commissural axon navigation: Control of midline crossing in the vertebrate spinal cord by the semaphorin 3B signaling. Cell Adhes. Migr. *10*, 604–617.

Polleux, F., and Ghosh, A. (2002). The slice overlay assay: a versatile tool to study the influence of extracellular signals on neuronal development. Sci. STKE *2002*, pl9.

Reeber, S.L., Sakai, N., Nakada, Y., Dumas, J., Dobrenis, K., Johnson, J.E., and Kaprielian, Z. (2008). Manipulating Robo expression *in vivo* perturbs commissural axon pathfinding in the chick spinal cord. J. Neurosci. *28*, 8698–8708.

Stoeckli, E.T. (2018). Understanding axon guidance: are we nearly there yet? Development *145*, 1–10.

Te Boekhorst, V., Preziosi, L., and Friedl, P. (2016). Plasticity of cell migration *in vivo* and *in silico*. Annu. Rev. Cell Dev. Biol. *32*, 491–526.

Wilson, S.I., Shafer, B., Lee, K.J., and Dodd, J. (2008). A molecular program for contralateral trajectory: Rig-1 control by LIM homeodomain transcription factors. Neuron *59*, 413–424.

Yang, T., Huang, H., Shao, Q., Yee, S., Majumder, T., and Liu, G. (2018). miR-92 Suppresses Robo1 Translation to Modulate Slit Sensitivity in Commissural Axon Guidance. Cell Rep. *24*, 2694–2708.e6.

Yoshida, Y., Han, B., Mendelsohn, M., and Jessell, T.M. (2006). PlexinA1 signaling directs the segregation of proprioceptive sensory axons in the developing spinal cord. Neuron *52*, 775–788.

Zou, Y., Stoeckli, E., Chen, H., and Tessier-Lavigne, M. (2000). Squeezing axons out of the gray matter: a 0role for slit and semaphorin proteins from midline and ventral spinal cord. Cell *102*, 363–375.

STAR★METHODS

KEY RESOURCES TABLE

REAGENT or RESOURCE	SOURCE	IDENTIFIER
Antibodies		
Atto 647N-GFP nanobody	Olivier Thoumine Lab. Chamma et al., 2016	N/A
Rabbit Anti-Green Fluorescent Protein (GFP) Polyclonal Antibody	Thermo Fisher Scientific	Cat# A-11122; RRID: AB_221569
Goat Anti-Mouse IgG, ATTO 647N	SIGMA Sigma-Aldrich	Cat# 50185, RRID: AB_1137661
Chemicals, Peptides, and Recombinant Proteins		
Dulbecco's Modified Eagle Medium (DMEM) GlutaMAX	Thermo Fisher Scientific	31966-021
Fetal Bovine Serum (FBS)	Sigma-Aldrich-Aldrich	F7524
Penicillin Streptomycin	Sigma-Aldrich	P4333
PBS 10x	Fischer	12037539
Paraformaldehyde 32%	Electron microscopy science	15714-S
Hanks'Balanced Salt Solution (HBSS)	Fischer	14170138
F12 medium	ThermoFischer Scientific	11580546
L15 medium	Thermo Fisher Scientific	11415-049
Glucose	Sigma-Aldrich	G7821
HEPES	ThermoFischer Scientific	15630-049
BSA bovine serum albumin	Sigma-Aldrich	**A7638**
Agarose, low gelling temperature	Sigma-Aldrich	A9414
Amphotericin B	Sigma-Aldrich	A2942
SYLGARD 184	Dow Corning	DC184-1.1
Neurobasal	Thermo Fisher Scientific	21103049
B27	Thermo Fisher Scientific	17504-044
PLL	Sigma-Aldrich	P1399
Laminin	Sigma-Aldrich	L2020
Recombinant Mouse Netrin-1	R&D systems	1109-N1-025
Methyl cellulose	Sigma-Aldrich	M7140
Critical Commercial Assays		
JetPrime reagent	PolyPlus - Ozyme	Pol114-15
Deposited Data		
Raw and analyzed data	This paper	https://data.mendeley.com/datasets/fwcr3csbff/draft?a=93767d36-5553-48a3-a3ef-c5ff63637b29
Experimental Models: Cell Lines		
COS-7 cells	ATCC	ATCC Cat# CRL-1651, RRID:CVCL_0224
Experimental Models: Organisms/Strains		
Embryonated eggs, naked neck strain	Élevage avicole du Grand Buisson, Saint Maurice sur Dargoire, France	N/A
Robo and Robo2 double KO, C57 Black 6 mice	Alain Chedotal lab. Long et al., 2004 Delloye-Bourgeois et al., 2015	N/A
PlxnA1 KO Mice, OF1 mice	Yoshida et al., 2006	N/A
OF1 Mice	Charles River	RRID: IMSR_CRL:612
Recombinant DNA		
pCAGEN-pHluo-PlxnA1	Nawabi et al., 2010 Delloye-Bourgeois et al., 2014	N/A

(*Continued on next page*)

Continued

REAGENT or RESOURCE	SOURCE	IDENTIFIER
pCAGEN-pHluo-Robo1-ires-mb-tdtomato	This paper	N/A
pCAGEN-pHluo-Robo2-ires-mb-tdtomato	This paper	N/A
pCAGEN-pHluo-Nrp2-ires-mb-tdtomato	This paper	N/A
pCAGEN-tdtomato	This paper	N/A
pCAGGS-PlxnA1-GFP	Nawabi et al., 2010 Delloye-Bourgeois et al., 2014	N/A
Software and Algorithms		
iQ3 imaging software	Andor	RRID: SCR_014461
Image J64	NIH	RRID: SCR_003070
Prism 6.0e	GraphPad	RRID: SCR_002798
BiostaTGV	Institut Pierre Louis d'Epidémiologie et de Santé Publique UMR S 1136	https://biostatgv.sentiweb.fr/
Metamorph: MetaMorph Microscopy Automation and Image Analysis Software	Molecular Devices	RRID: SCR_002368

LEAD CONTACT AND MATERIALS AVAILABILITY

Further information and requests for resources and reagents should be directed to and will be fulfilled by the lead contact, Valérie Castellani (valerie.castellani@univ-lyon1.fr). All unique/stable reagents generated in this study are available from the Lead Contact with completed Materials Transfer Agreement.

EXPERIMENTAL MODEL AND SUBJECT DETAILS

Chick Embryos

Naked Neck strain embryonated eggs were obtained from "Elevage avicole du Grand Buisson," Saint Maurice sur Dragoire, France. Sanitary status of animals was regularly checked by the suppliers according to the French law. Embryonated eggs were stored at 18°C prior to incubation. Eggs were incubated at 38.5°C in an humidified incubator until HH14 developmental stage, for electroporation step. Embryos were dissected at HH26. The sex of chick embryos used in this study was not determined.

Mice embryos

Robo1 and Robo2 double KO mice (C57 Black6J inbred strain) were kindly provided by Alain Chedotal Lab. Animals were housed at "ALECS, Module Conventionnel," Lyon, were the sanitary status of animals was regularly checked by the facility staff. Embryos from fertilized mice were dissected at E12.5 developmental stage. Fertilized mice were first asleep with 1000mg/g Isoflurane and then sacrificed by cervical dislocation. PlxnA1 KO mice (OF1 strain) were kindly provided by Yutaka Yoshida Lab.

Animals were handled according to the French national regulations, and the protocols were validated by the European Research Council ethical committee.

Cell Lines

COS7 cells were obtained from ATCC. Cells were cultured in Dulbecco's Modified Eagle's Medium (DMEM) GlutaMAX (Life Technologies) supplemented with 10% fetal bovine serum (FBS), 25 U/ml Penicillin Streptomycin (SIGMA). Cell lines were maintained in sterile conditions in a 37°C-, 5% CO_2-incubator.

METHOD DETAILS

Receptor molecular biology

FL mouse pHLuo-PlxnA1 was generated by introducing in Nter the coding sequence of the pHLuo cloned from a vector encoding GABA A pHLuo-GFP (Jacob et al., 2005). pHLuo derived from this vector was fused to FL rattus Robo1 and Robo2 sequences, kindly provided by A. Chedotal laboratory, to obtain pHLuo-Robo1 and pHLuo-Robo2 vectors. Using the same strategy, FL mouse Nrp2 kindly provided by Püschel laboratory, was fused to pHLuo to obtain pHLuo-Nrp2 vectors. pHLuo-receptors where finally cloned into a PCAGEN vectors with an ires-mb-tomato sequence.

In vitro test of pH fluorescence dependency

Cos7 cells were plated in a glass-bottom dish 35mm in 2ml of complete Dulbecco's modified eagle medium (DMEM – 10% fetal bovine serum – 1 mM sodium pyruvate – 25 U/ml penicillin/streptomycin – 2.5 μg/ml Amphotericin B – pH7.4). 24h after, cells

were transfected with 2 μg of plasmid encoding pHLuorin-tagged receptors and the transfection reagent was added. 48h later, live imaging of the cells was performed at 40X magnification. Cells were first imaged at pH 7.4 then, 1.25ml of pH3.5 complete DMEM was added to achieve a pH of 5.5 in the culture medium. Next, 1.2ml of pH9.5 complete DMEM was injected to revert the pH of the medium to neutrality. Images were taken every 20 s for 10 minutes.

In ovo electroporation

In ovo electroporation of HH14/HH15 chick embryos was performed as described previously (Delloye-Bourgeois et al., 2014). Plasmids were diluted at the following concentration: 1.5 μg/μl pHLuo-Robo1-*ires*-tomato; 2.5 μg/μl pHLuo-Robo2-*ires*-tomato; 1 μg/μl pHLuo-Np2-*ires*-tomato; 2 μg/μl pHLuo-PlexA1 and 0.03 μg/μl mb-tomato. Plasmids were diluted in UP H_2O and the solution was injected into the lumen of the neural tube using picopritzer III (Micro Control Instrument Ltd., UK). Electrodes (CUY611P7-4, Sonidel) were placed along the back of the embryo, at the thoracic level, and 3 pulses (25V, 500ms interpulse) were delivered by CUY-21 generator (Sonidell). Electroporated embryos were then incubated at 38.5°C.

Open book culture

48 hours after electroporation, embryos at HH25/HH26 were harvested in cold HBSS and the spinal cords were dissected. Spinal cords were mounted in 0.5% agarose diluted in F12 medium and placed on glass bottom dishes (P35G-1.5-14-C, MatTek). After agarose solidification, spinal cords were overlaid with 3ml of F12 medium supplemented with 10% FCS (F7524; Sigma-Aldrich), 1% Penicillin/Streptomycin (Sigma-Aldrich) and 20mM HEPES buffer (15630-049, ThermoFischer Scientific).

Mouse spinal cord electroporation and culture

E12 mice embryos were collected and fixed on a SYLGARD (Dow Corning) culture plate in Leibovitzs 15 medium (ThermoFisher) supplemented with Glucose 1M (Sigma-Aldrich). Plasmids were injected into the lumen of the neural tube using picopritzer III (Micro Control Instrument Ltd., UK). Electrodes (CUY611P7-4, Sonidel) were placed along the back of the embryo, at the thoracic level, and 3 pulses (25V, 500ms interpulse) were delivered by CUY-21 generator (Sonidell). Spinal cords were dissected from the embryos and cultured on Nucleopore Track-Etch membrane (Whatman) for 48 hours in Slice Culture Medium (Polleux and Ghosh, 2002).

Live imaging and data analysis

Live imaging was performed with an Olympus IX81 microscope equipped with a spinning disk (CSU-X1 5000 rpm, Yokogawa) and Okolab environmental chamber maintained at 37°C. Image were acquired with a 20X objective by EMCCD camera (iXon3 DU-885, Andor technology). Usually for spinal cord culture, 15-30 planes spaced of 0,5-3μm were imaged for each spinal cord at 30-minute interval for 10 hours approximatively. To reduce exposure time and laser intensity, acquisitions were done using binning 2x2. Images were acquired using IQ3 software using multi-position and Z stack protocols. Z stack projections of the movies were analyzed in ImageJ software. The analysis of pHLuo-flashes was performed from time-lapse acquisitions *in vivo*. For cartography representation, the lengths of PRE-crossing and POST-crossing compartment were normalized on FP length.

Detection of the total pool of pHLuorin

48h after electroporation, at HH25/HH26, the embryos were harvested in cold HBSS and the spinal cords were dissected and fixed for 2 hours with PBS supplemented with 4% paraformaldehyde (PFA). The % of the commissural population expressing total pool of pHLuo in PRE-crossing was calculated by qualitative analysis of Z stack projections. The length of the PRE-crossing segments expressing total pHLuo was measured with ImageJ software.

Chick explant cultures

FPs were isolated from HH25/HH26 chick embryos and cultured in tridimensional plasma clots in B27-supplmented Neurobasal medium (GIBCO). The supernatant (FP^{cm}) was collected after 48h. Electroporated spinal cord were dissected, cut into explants and incubated for 30min at 37°C. Then explants were placed on glass bottom dishes, previously coated with 10 μg/ml Laminin and 50 μg/ml polylysine and cultured for approximately 30h at 37°C in F12 medium supplemented with 0.4 Methylcellulose, 1X B27, 100ng/ml Netrin, 1/1000 Penistreptomycin. Explants were imaged at T0, then FP^{cm} or Ctrl medium were used for the treatment and 20min after, a second time-point was recorded.

Atto647N staining for surface receptor pool

Spinal cords were incubated at 38°C for 20 minutes with F12 medium supplemented with 5% FCS (F7524; Sigma-Aldrich), 20mM HEPES buffer (15630-049, ThermoFischer Scientific) and 1/100 small monovalent highly-specific GFP-nanobodies Atto647N to prevent receptor cross-linking that would trigger internalization. Spinal cords were then rinsed 4 times with the same medium (not containing the GFP-nanobodies) and were fixed at room temperature for 2 hours with PBS supplemented with 4% paraformaldehyde (PFA) and 1% BSA (A7638 Sigma-Aldrich).

Atto647N staining for total receptor pool

Spinal cords were fixed at room temperature for 2 hours with PBS supplemented with 4% paraformaldehyde (PFA) and 6% BSA (A7638 Sigma-Aldrich). Spinal cords were then incubated 18h at room temperature with 1% BSA, rabbit 1/400 anti-GFP antibody (Invitrogen) and incubated over night at 4°C with 3% BSA, anti-rabbit ATTO647N.

STED imaging and data analysis

The staining was observed with a STED microscope (TCS SP8, Leica). STED illumination of ATTO 647N was performed using a 633-nm pulsed laser providing excitation, and a pulsed bi-photon laser (Mai Tai; Spectra-Physics) turned to 765 nm and going through a 100-m optical fiber to enlarge pulse width (100ps) used for depletion. A doughnut-shaped laser beam was achieved through two lambda plates. Fluorescence light between 650 and 740 nm was collected using a photomultiplier, using a HCX PL-APO CS 100/1.40 NA oil objective and a pinhole open to one time the Airy disk (60mm). Images were acquired with using Leica microsystem software and a Z stack protocol. Usually 10-20 planes spaced of 0,5μm where imaged for each growth cone. The growth cone perimeter was outlined basing on the mb-tomato signal. Average density of pHLuo-receptors in the growth cones was calculated from Z stack projections with MATLAB software. Particle numbers and surfaces were calculated from Z stack projections with ImageJ.

Fluorescence Recovery After Photobleaching

FRAP experiments were performed on spinal cord open-books electroporated with either pHLuo-Robo1-ires-mb-tomato or pHLuo-PlxnA1 and mb-tomato using a Leica DMI6000 (Leica Microsystems, Wetzlar, Germany) equipped with a confocal Scanner Unit CSU-X1 (Yokogawa Electric Corporation, Tokyo, Japan) and a scanner FRAP system, ILAS (Roper Scientific, Evry, France). Images were acquired in both green and red channels using a 63X objective and an Evolve EMCCD camera (Photometrics, Tucson, USA). Growth cones located in the FP were first monitored for 9 s each 3 s and then bleached using a 488nm diode laser at full power. This resulted in an 80%–90% loss of the signal at t = 0. Fluorescence recovery was then monitored for 1030s with acquisitions every 3 s for 30 s, then every 10 s for 100 s, and finally every 30 s for 900 s. The images were corrected for background noise, residual fluorescence right after the bleach was set to zero, and recovery curves were normalized to the fluorescence lost after the bleach. No other corrections were applied since unbleached growth cone fluorescence showed no significant decay during the acquisition period.

Chimeric receptor molecular biology

The pHLuo-PlxnA1^{ECD} and Robo1^{ICD} fragments were amplified by PCR from pHLuo-PlxnA1 vector (forward pHLuo-PlxnA1^{ECD} 5′-CATCATTTTGGCAAAGAATTCATGGGCTGGTTCACTGGGA-3′; reverse pHLuo-PlxnA1^{ECD} 5′-CAATGAAGGCCGGCAGTGT CAGCAGGCT-3′) and pHLuo-Robo1-*ires*-tomato vector (forward Robo1^{ICD} 5′-GACACTGCCGGCCTTCATTGCGGGCATC-3′; reverse Robo1^{ICD} 5′-CGCGATATCCTCGAGGAATTTTAGCTTTCAGTTTCCTCTAATTC-3′), respectively. The pHLuo-Robo1^{ECD} and PlxnA1^{ICD} were amplified by PCR from pHLuo-Robo1-*ires*-tomato vector (forward pHLuo-Robo1^{ECD} 5′-CATCATTTTGGCAAAGAATTCATGGGCTGGTTCACTGGGA-3′; reverse pHLuo-Robo1^{ECD} 5′- CCACAATGGCTGGCTGCTT CACCACGTC-3′) and pHLuo-PlxnA1 (forward PlxnA1^{ICD} 5′-GAAGCAGCCAGCCATTGTGGGTATCGGTGGT-3′; reverse PlxnA1^{ICD} 5′- CGCGATATCCTCGAGGAATTTCAGCTGCTCAGGGCCAT-3′), respectively.

For both PlxnA1 and Robo1, the transmembrane domain was included in the ICD.

The amplified PCR fragments were cloned into the EcoRI site of pCAGEN (Addgene plasmid # 11160) using the In-Fusion HD Cloning Plus kit (Clontech, Mountain View, CA, USA) and following the manufacturer's instructions.

QUANTIFICATION AND STATISTICAL ANALYSIS

Number of Experimental Replicates

Number of independent experiments, embryos, stacks and growth cones (n) are given in figure legends or indicated in the figures. All embryos which developed normally and which expressed pHLuo-vectors at the thoracic level were included in the time-lapse analysis of receptor sorting. Analysis were done in blind for the quantification of pHLuo signal increase after FP^{cm} treatment and for the quantification of phenotype rescue in mouse embryos electroporated with pHLuo vectors.

Data Exclusion

In the analysis of pHLuo fluorescence increase after FP^{cm} and Ctrl^{cm} treatment, we measured pHLuo/mb-tomato in growth cones showing limited fluctuation of mb-tomato signal over time. We decided to select growth cones having at most 25% positive or negative mb-tomato average intensity variation with respect to the T0.

Statistical treatment of data

The statistical tests used and the *p-value*s are indicated in figures and figure legends. Sample size and statistical significances are represented in each figure and figure legend. Statistical tests were performed using Biosta-TGV (CNRS) and Prism 6 software

(GraphPad). For parametric tests, normality was checked. In case of non-normality, non-parametric tests were used. Error bars indicate SEM, which is noted for each panel in figure legends. Error bars indicate mean ± SEM; significance was defined for p values inferior to * $p < 0.05$; ** $p < 0.01$; *** $p < 0.001$.

DATA AND CODE AVAILABILITY

Raw data are available through Mendeley Data via accession: https://data.mendeley.com/datasets/fwcr3csbff/draft?a=93767d36-5553-48a3-a3ef-c5ff63637b29.

A preprint version of the paper is available via accession: https://doi.org/10.1101/540690

II. Projet de thèse personnel

Au cours des dernières années, le guidage axonal a fait l'objet de nombreuses études. Ainsi, différents acteurs contrôlant la navigation des axones ont été identifiés. Ces acteurs peuvent être de natures différentes : physique ou chimique. Les acteurs chimiques sont les plus étudiés et plus particulièrement les signaux de guidage agissant en couple ligand/récepteur. Historiquement, ces derniers ont été classés en deux catégories, les signaux attractifs et les signaux répulsifs, selon les résultats de tests *in vivo* et *in vitro*. Un signal est considéré attractif si : 1) son invalidation *in vivo* entraîne des défauts de guidage avec des axones qui ne poussent plus en direction des territoires habituels, et 2) son action *in vitro* sur des neurones entraîne la formation de filopodes et lamellipodes, ou bien la navigation en direction de la source du signal. A l'inverse un signal est considéré répulsif si : 1) l'invalidation *in vivo* du signal entraîne des défauts de guidage avec des axones envahissant des territoires inhabituels, et 2) son action *in vitro* sur des neurones entraîne l'effondrement des CC, ou bien la navigation dans la direction opposée à la source du signal. Cependant, en analysant des défauts de trajectoires plus fins, les différentes signalisations répulsives n'ont pas la même influence sur les axones. Cette grille de lecture est nuancée et remise en question par différents phénotypes. Ainsi, au sein de la PP, des défauts de SlitN/Robo ou Sema3B/PlxnA1-Nrp2 vont induire des phénotypes de stagnation dans la PP. Ici, ce sont des défauts de signalisations répulsives qui vont ralentir la navigation axonale, suggérant que cette dernière peut être favorisée par des signalisations répulsives. Dans le cas de souris KO pour Slit1-3 ou PlxnA1, des phénotypes de demi-tours apparaissent en plus des défauts de stagnation. Ces demi-tours et leur absence chez les KO Robo ou Sema3B – donc possiblement liés à la signalisation SlitC/PlxnA1 – suggèrent que différentes signalisations répulsives pourraient contrôler différents comportements du CC. Ces résultats laissent supposer que la limite entre attractants et répulsifs n'est pas si manichéenne, mais surtout que les signalisations de guidage ont des actions spécifiques sur les CC *in vivo*. Pour faire émerger des comportements différents à partir de signalisations répulsives, plusieurs niveaux de contrôle sont imaginables : 1) au niveau de la répartition des différents ligands répulsifs ; 2) au niveau de la répartition des récepteurs, comme le montre les travaux de Pignata *et al.* ; 3) en aval des récepteurs.

Dans le cadre de ma thèse, j'ai étudié le premier niveau de contrôle à travers l'étude de Slit, de son clivage, et de ses fragments. Pour ce faire, j'ai développé différents outils, utilisables *in vivo*, permettant de suivre les fragments individuellement et d'étudier le clivage.

De plus, pour ce qui est du troisième niveau, j'ai étudié l'impact de la signalisation SlitC/PlxnA1 grâce à une lignée de souris mutantes, PlxnA1 Y1815F, générée par notre équipe. Le résidu tyrosine

1815 est phosphorylé après interaction SlitC/PlxnA1 et est essentiel pour la réponse à SlitC, mais n'est pas nécessaire pour la réponse à Sema3B. Dans notre modèle, ce résidu est remplacé par une phénylalanine, inhibant ainsi spécifiquement la signalisation SlitC/PlxnA1, tout en conservant les signalisations Sema3B/PlxnA1 et SlitN/Robo. J'ai réalisé l'analyse des trajectoires axonales dans ce modèle en collaboration avec un autre thésard, Hugo Ducuing. Et ce dernier a également étudié plus en détail l'impact de cette mutation sur le comportement du récepteur et ses partenaires en aval.

L'impact de l'environnement physique a été moins étudié que celui des signaux chimiques, de par la difficulté à le retranscrire *in vitro* et à l'altérer *in vivo*. Quelques études ont tout de même révélé que la PP constitue un environnement très contraignant pour les axones. Au cours de ma thèse, j'ai pu étudier la morphologie de cellules de la PP individuelles et observer la relation physique entre axone et cellule de la PP.

Mes travaux et ceux d'Hugo Ducuing étant complémentaires, ils feront l'objet d'une publication commune dans laquelle nous serons tous deux co-premiers auteurs. Les résultats de notre étude sont présentés sous la forme d'un article, auquel j'ajouterai les détails de la conception des outils et des résultats d'expériences complémentaires.

1. Rôle de SlitC/PlxnA1 dans la traversée de la plaque du plancher

Comme expliqué dans l'introduction, les souris avec une invalidation des Slit ou de PlxnA1 présentent des défauts de traversée particuliers : des axones font demi-tour dans la PP. Cependant, ce phénotype n'est pas retrouvé chez les souris invalidées pour Robo ou pour Sema3B. Cela laisse penser que les signalisations SlitN/Robo et Sema3B/PlxnA1-Nrp2 ne sont pas impliquées dans le contrôle des demi-tours. Ainsi, il est possible que les demi-tours soient prévenus par la signalisation SlitC/PlxnA1. Pour tester cette hypothèse et afin d'étudier le rôle de la signalisation SlitC/PlxnA1 dans la traversée de la PP, nous avons étudié la trajectoire d'axones dans la PP de la souris PlxnA1 Y1815F présentée précédemment. Nous avons observé que certains axones, chez la souris mutante, réalisent bien des demi-tours et ce dans la même proportion que les souris invalidées pour PlxnA1. De plus, les trajectoires d'axones dans la PP sont désorganisées. Cependant, la proportion d'axones stagnant dans la PP n'augmente pas par rapport aux souris sauvages. Ces résultats suggèrent que la signalisation SlitC/PlxnA1 agit comme une barrière forçant les axones à suivre une trajectoire rectiligne. A contrario, les phénotypes de stagnation observés chez d'autres mutants suggèrent que les signalisations SlitN/Robo et Sema3B/PlxnA1-Nrp2, mais pas SlitC/PlxnA1, expulsent les axones hors de la PP. Ainsi,

les signalisations répulsives de la PP n'ont pas toutes le même rôle dans la traversée de la PP. Grâce à nos résultats, nous pouvons en distinguer deux : les rôles de barrière et d'expulsion (Fig. 7).

A.

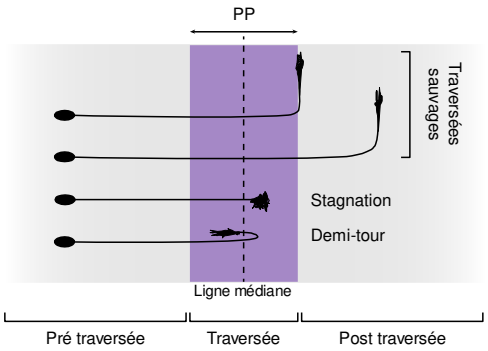

B.

Mutation	Stagnation	Demi-tour
PlexinA1$^{-/-}$	x	x
Sema3B$^{-/-}$	x	
Slit1/2/3$^{-/-}$	x	x
Robo1/2$^{-/-}$	x	
PlexinA1$^{Y1815F/Y1815F}$		x

Figure 7. Présentation des défauts de traversée de la PP

L'invalidation de signalisations répulsives induit des défauts de trajectoire pour les axones commissuraux, notamment dans la PP. Les principaux défauts observés sont la stagnation, visualisable par l'étalement des cônes de croissance (CC), et les demi-tours. (**A**) Représentation schématique des phénotypes de traversée, vus en livre-ouvert. (**B**) Tableau recensant les phénotypes observés chez les différentes lignées murines mutantes.

2. Diffusion de Slit FL, SlitN et SlitC

A travers ses fragments de clivage, le ligand Slit va contrôler des aspects différents de la traversée de la PP. Ainsi, SlitN a un rôle d'expulsion alors que SlitC a un rôle de barrière. Nous avons donc cherché à savoir l'origine de cette différence. Une hypothèse potentielle est que les CC ne ressentent pas les deux fragments de la même façon car ces derniers diffusent d'une façon spécifique. En effet les différences de propriétés physiques entre les fragments de Slit suggèrent que SlitN et SlitC pourraient se répartir différemment dans la PP. S'il est habituel de suivre la diffusion d'une protéine *in vivo* en exprimant une version taguée, le cas de Slit est particulier puisque sa diffusion va d'abord dépendre de Slit FL puis, après clivage, les fragments pourront diffuser de façon autonome. Pour prendre en compte cette particularité, j'ai donc développé une version de Slit fusionnée à deux protéines fluorescentes – la Cerulean en N-terminal et la Venus en C-terminal. Cet outil permet de suivre toutes les étapes de la diffusion des fragments en conservant l'influence des modifications post-traductionnelles. Ce principe de double fusion a déjà été utilisé pour suivre les fragments issus du clivage de la protéine précurseur de l'amyloïde β (APP) (Villegas et al. 2014). Afin de pouvoir approfondir des résultats obtenus précédemment par notre équipe et d'autres, j'ai utilisé l'homologue humain de Slit2 (Ba-Charvet *et al.*, 2001; Delloye-Bourgeois *et al.*, 2015). L'électroporation de ce Slit2

double tag (Slit2 DT) dans des PP d'embryons de poulet m'a permis d'imager sa répartition à E4, stade développemental auquel traverse la majorité des axones commissuraux. Ainsi j'ai pu déterminer que la majorité du signal est présente dans les corps cellulaires et pieds apicaux des cellules gliales, zone que ne traversent pas les axones. De plus, en calculant les coefficients de colocalisation (Pearson), j'ai pu déterminer que la colocalisation des fragments diminue dans la direction basale. Ces résultats reflètent la présence de Slit2 non clivé et/ou des fragments se chevauchant dans la partie apicale, ainsi que la séparation des fragments dans la partie basale où naviguent les axones.

A partir de ces résultats, deux hypothèses sont possibles : 1) le clivage a lieu dans le domaine apical, puis permet aux fragments de diffuser basalement, ou 2) le clivage a lieu dans le domaine basal et les fragments se séparent directement. Afin de départager ces deux hypothèses, j'ai utilisé une version de Slit2 DT avec une délétion de 9 acides aminés au niveau du site de clivage (Slit2 DT Δ). Cette mutation a déjà été utilisée pour empêcher le clivage de Slit2 sans modifier drastiquement la protéine (Ba-Charvet *et al.*, 2001). Ainsi, le signal basal de Slit2 DT Δ est diminué par rapport à Slit2 DT. Cela suggère que le clivage de Slit2 a lieu dans le domaine apical et que les fragments SlitN et SlitC vont ensuite diffuser dans le domaine basal. Grâce à cet outil, j'ai donc pu montrer que les fragments SlitN et SlitC sont tous les deux présents dans le domaine basal de la PP, mais ne colocalisent pas. De plus, j'ai pu montrer que le clivage de Slit2 est important pour la diffusion des signaux SlitN et SlitC.

J'ai également cherché à savoir si la distribution des fragments dépend uniquement de leurs propriétés intrinsèques ou si le passage par une étape de Slit FL modifie cette distribution. J'ai donc exprimé les fragments sous forme isolée et fusionnés à la GFP. Ainsi, j'ai pu montrer que les fragments isolés, comme les fragments issus du clivage de Slit, sont majoritairement présents dans le domaine apical. Cependant la diffusion dans le domaine basal de SlitC est plus importante lorsque le fragment est issu du clivage. Cela suggère que les propriétés de diffusion de SlitC vont être restreintes par la protéine complète. De plus, j'ai observé que le fragment isolé SlitC est enrichi au niveau de la lame basale, par rapport au fragment isolé SlitN. A l'inverse, en exprimant la protéine complète, les deux fragments sont présents à des niveaux similaires – inférieurs à celui de SlitC isolés, mais supérieurs à celui de SlitN isolé. Nous pouvons donc supposer que SlitC va permettre d'enrichir la lame basale en SlitN, mais également qu'il est important d'étudier la protéine complète, afin de reproduire les conditions physiologiques de diffusion et d'interaction.

3. Etude morphologique de la plaque du plancher

La morphologie générale de la PP et des axones qui la traversent a fait l'objet d'un nombre restreint d'articles (Glees and LeVay, 1964; Yaginuma *et al.*, 1991; Campbell and Peterson, 1993). Les auteurs y présentent que les axones dans la PP traversent un champ de pieds basaux aplatis dans l'axe de traversée. Afin d'approfondir leurs résultats et de comprendre comment se constitue ce champ de pieds basaux, j'ai cherché à étudier la morphologie de cellules de PP individuelles. Pour cela, j'ai utilisé des électroporations mosaïques permettant d'individualiser des cellules de PP, de les imager au confocal puis de les reconstruire en 3D. Si ces résultats ont permis de confirmer que les pieds basaux sont bien aplatis dans le sens de la traversée, ils ont surtout montré que chaque cellule de PP possède non pas un, mais plusieurs pieds basaux. De plus, les pieds d'une même cellule présentent des tailles et des morphologies différentes, et les cellules ne possèdent pas toutes le même nombre de pieds (Fig. 8). Enfin, au niveau du domaine apical de la PP, les cellules ne présentent qu'un unique prolongement apical. Les prolongements apicaux et les corps cellulaires forment un ensemble compact. Cette morphologie complexe pourrait permettre plusieurs choses : 1) la séparation d'un domaine apical compact et un domaine basal permissif va favoriser la pousse des axones dans le domaine basal et empêcher l'invasion du domaine apical ; 2) le faible espacement entre les pieds basaux va forcer le contact axones/pieds favorisant la capacité de ces derniers à servir de substrat de croissance ; 3) l'aplatissement des pieds dans le sens de la traversée va favoriser une trajectoire rectiligne et ainsi diminuer les défauts de traversée.

Après avoir étudié la morphologie des cellules de PP, je me suis intéressé à la relation physique entre les axones et les cellules de la PP. Pour étudier cette relation, j'ai exploité le même principe de reconstruction 3D présenté précédemment, mais cette fois en électroporant les axones (de façon mosaïque) et les cellules de la PP (en grand nombre). Cette technique m'a permis de confirmer que les axones naviguent bien sur les pieds basaux des cellules de PP et que ces derniers laissent peu d'espace libre pour la traversée des axones. Ainsi, ces résultats renforcent l'hypothèse que les pieds basaux servent de substrat physique et favorisent une trajectoire rectiligne pour les axones.

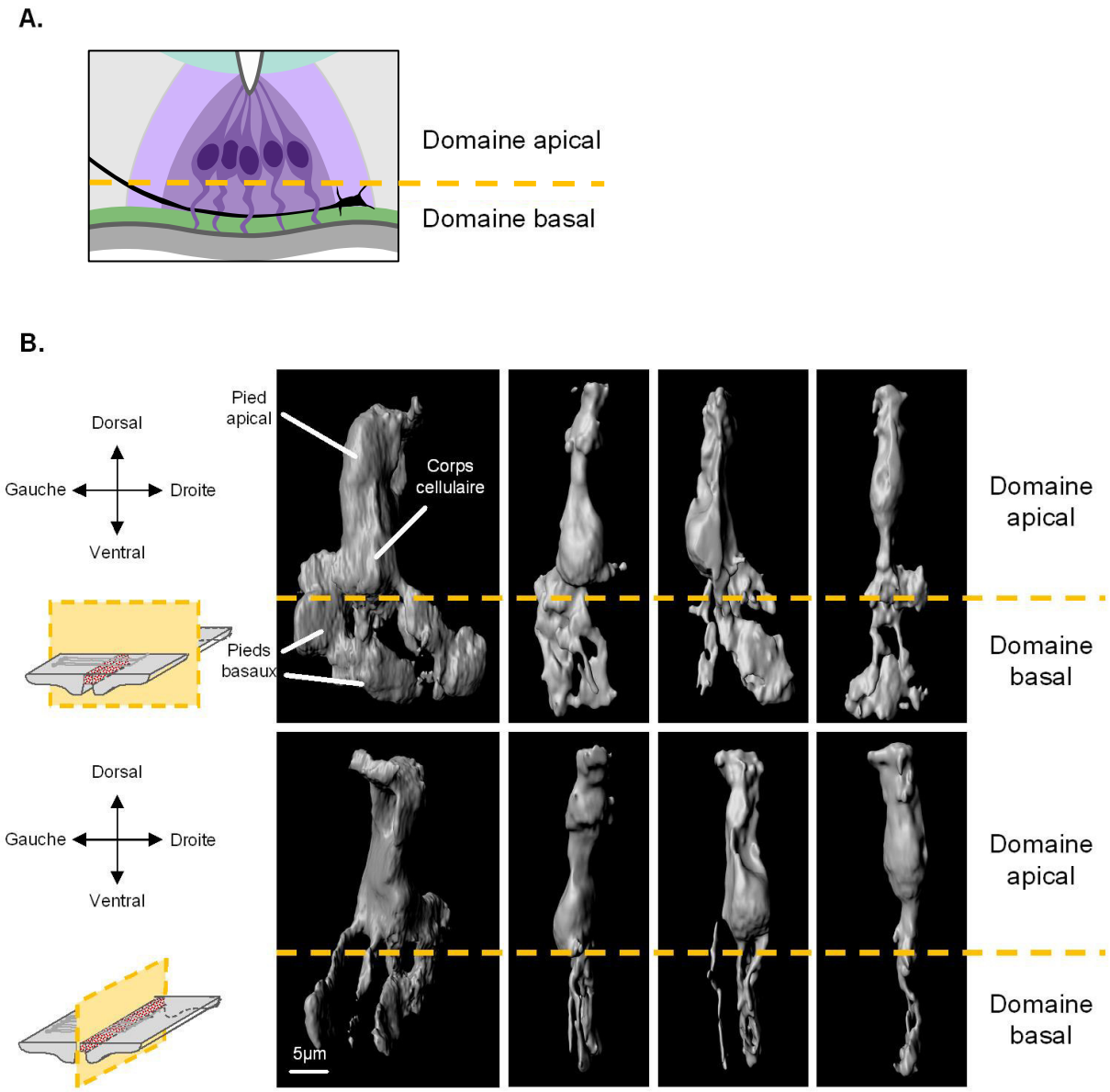

Figure 8. Variabilité morphologique des cellules de la plaque du plancher

(**A**) Représentation schématique répandue des cellules gliales de la plaque du plancher (PP). (**B**) Reconstructions 3D de cellules individuelles de PP de poulet à E4. L'imagerie de cellules individuelles est permise par une électroporation mosaïque de la tdTomato. Représentations en vue transversale (en haut) et sagittale (en bas).

Iterative inhibition of commissural growth cone exploration, not post-crossing barrier, ensures forward midline navigation through SlitC-PlxnA1 signaling

Hugo Ducuing[1]*, Thibault Gardette[1]*, Aurora Pignata[1], Karine Kindbeiter[1], Muriel Bozon[1], Olivier Thoumine[2], Céline Delloye-Bourgeois[1], Servane Tauszig-Delamasure[1], Valérie Castellani[1&]

* co-first authors

[1] Institut NeuroMyoGène - CNRS UMR 5310 - INSERM U1217 de Lyon- UCBL Lyon 1, Faculté de Médecine et de Pharmacie, 8 Avenue Rockefeller, F-69008 Lyon, France

[2] Interdisciplinary Institute for Neuroscience, UMR CNRS 5297 - University of Bordeaux, 146 rue Léo Saignat, F-33000 Bordeaux, France

& corresponding author: valerie.castellani@univ-lyon1.fr

Key words: midline crossing, axon guidance, commissural circuits, Slits, Plexins, floor-plate glia,

Summary

Sensitization to Slits and Semaphorin (Sema)3B floor plate repellents after midline crossing is thought to be the mechanism expelling commissural axons contralaterally and preventing their back-turning. We studied the role of Slit-C terminal fragment sharing with Sema3B the Plexin (Plxn) A1 receptor, newly implicated in midline guidance. We generated a knock-in mouse strain baring PlxnA1Y1815F mutation altering SlitC but not Sema3B responses and observed recrossing phenotypes. Using fluorescent reporters, we found that Slits and Sema3B form clusters decorating an unexpectedly complex mesh of ramified FP glia basal processes spanning the entire navigation path. Time-lapse analyzes revealed that impaired SlitC sensitivity destabilized axon trajectories by inducing high levels of growth cone exploration from the floor plate entry, increasing risk of aberrant decisions. Thus, FP crossing is unlikely driven by post-crossing sensitization to SlitC. Rather, SlitC limits growth cone plasticity and exploration through reiterated contacts, continuously imposing a straight and forward-directed trajectory.

Introduction

Extensive efforts have been put in the past decades into the identification of guidance cues and the receptors mediating their effects on navigating axons (Raper and Mason, 2010). Combinatorial expression of guidance cues at choice points along the path as well as versatile perception of these cues by growth cones were shown to largely contribute to coding the diversity of guidance decisions underlying the wiring of neuronal circuits (Raper and Mason, 2010; Stoeckli et al, 2019; Ducuing et al, 2019). In the recent years, a number of reports brought the evidence that guidance receptors have multiple binding partners, assembling into macro-complexes at the growth cone membrane under the influence of intrinsic or extrinsic triggers, and interacting in addition with more than a single ligand (Seiradake et al, 2016). This scheme significantly complexifies our understanding of axon guidance processes, making the characterization of functional outcomes downstream of each receptor module a central challenge. Noticeably too, the guidance sources controlling navigating axons appear to be much more diversified than anticipated. For instance, cell migration streams were

found to deliver guidance molecules to navigating axons at meeting points (Lopéz-Bendito et al, 2011). Bipolar progenitors were reported to contribute to commissural axon navigation by transporting Netrin on their basal processes, which then accumulates on the pial surface and is thought to serve as guidance support for axons pathing in its vicinity (Dominici et al, 2017; Varadarajan et al, 2017). These studies also highlight a lack of knowledge concerning the modes of action of the guidance cues. Indeed, how they are presented to the growing axons and how their patterns of distribution are regulated remain poorly addressed questions, leaving open whether the ligand topography takes a determinant part in the generation of specific guidance decisions.

The navigation of commissural axons across the spinal cord midline provides a very suited model to address these questions. Commissural axons navigate the midline ventrally in the floor plate (FP), guided by a wide range of cues. We reported in previous work that PlexinA1 (PlxnA1) is a receptor shared by different FP repulsive cues. When associated with Neuropilin2 (Nrp2), it mediates the response to Semaphorin3B (Sema3B) (Nawabi et al, 2010), and while unbound to Nrp2, it acts as a receptor for a second type of ligands, the Slit1-3-C (Delloye-Bourgeois et al, 2015). These C terminal fragments are generated from the processing of integral Slit1-3 proteins together with Slit1-3-N terminal fragments, whose effects are mediated by Roundabout (Robo) receptors (Evans and Bashaw, 2010). It turns out that at least three signaling pathways are thought to generate repulsive forces in the FP. They are considered indispensable to push the axons in the contralateral side and also to set a midline barrier preventing any turning back (Ducuing et al, 2019).

Genetic deletions of ligands or receptors to abrogate individual signaling were shown to alter the ability of commissural growth cones to exit the FP and interpreted as if repulsive forces were no longer sufficient to drive the growth forwards and prevent midline recrossing. Moreover, these phenotypic analyses also pointed out differences in guidance errors, suggesting that individual signaling pathways might regulate distinct aspects of the commissural navigation. Invalidation of Robo-SlitN or PlxnA1-Nrp2-Sema3B signaling were both reported to impair FP crossing by inducing stalling of commissural axons within the FP. An additional aberrant behavior - axons turning back towards the ipsilateral side - was found in mice lacking either PlxnA1 or all Slit

ligands. This indirectly suggested that the PlxnA1-SlitC signaling might specifically set the midline barrier that prevents commissural axons from crossing back (Ducuing et al, 2019, Chedotal, 2019).

In addition, various experiments suggested that the perception of repulsive forces is set at an appropriate timing, in order to synchronize ligands activity with commissural axon progression (Neuhaus-Follini and Bashaw, 2015; Pignata et al, 2016). Experimental manipulations leading to premature sensitivity were shown to induce commissural axons to stall at the FP entry or to undergo an ipsilateral turn (Chen et al, 2008; Nawabi et al, 2010; Ducuing et al, 2019). We recently reported that responsiveness to Slits and Sema3B is sequentially acquired through successive sorting of Nrp2, PlxnA1, Robo1, and Robo2 receptors at the growth cone membrane during the FP navigation (Pignata et al, 2019). This study however still leaves open several puzzling questions: What is the nature of the guidance forces generated by these signaling during the progression of commissural axons within the FP? How are the instructions from the different guidance cues present in the FP translated into directional information for axon growth? In particular, whether physical and/or chemical substrates build a midline barrier once the axons have crossed is still fully hypothetic. It is unclear as well whether commissural axons move away under the influence of ligands gradients. Moreover, so far, rare attention has been given to the topology of the FP territory in which commissural axons path, although increasing attention is given to physical properties exerted by environmental substrates during the formation of neuronal projections (Kerstein et al, 2015). FP glial cells are thought to have a typical progenitor-like bipolar morphology, with a dorsal apical anchor at the lumen of the central canal and a basal process laying ventrally on the basal lamina, even though some studies suggested these cells have much more complex morphology (Campbell et Peterson, 1993). The axon path is dorsally bordered by the soma and ventrally by the basal lamina (Figure 1A). Despite seminal studies performed with electronic microscopy, which described close contacts between the axons and glial cells (Yaginuma et al. 1991), little is known about the exact morphology of the basal processes and the putative physical constraints that axons might have to face during their FP navigation.

In the present study, we focused on the SlitC-PlxnA1 signaling and investigated its functional outcome during commissural axon navigation. Through combinations of *in vivo* analysis, live imaging and super resolution microscopy, we show that growth cone trajectories are actively kept straight over the FP navigation, through reiterated contacts with SlitC spots presented by ramifications of FP glia basal process that mark out the entire FP navigation path. PlxnA1 mutation altering perception of SlitC alleviates these constrains, resulting in highly dynamic growth cones that actively explore their local environment, which compromises efficient and straight navigation across the FP. This reveals that guidance forces preventing midline recrossing are not generated by post-crossing sensitization to repellents, but through continuous limitation of growth cone exploration to restrict the navigation direction forward.

Results

PlxnA1^{Y1815F} mutation in mice recapitulates PlxnA1$^{-/-}$ recrossing but not stalling phenotype

We identified in previous work a tyrosine residue of PlxnA1 cytoplasmic tail, whose phosphorylation was specifically triggered upon SlitC exposure (Delloye-Bourgeois et al, 2015). Expression of a mutant receptor form for this tyrosine, PlxnA1^{Y1815F}, in commissural neurons significantly reduced their growth-cone collapse response to SlitC, while their sensitivity to Sema3B was preserved (Delloye-Bourgeois et al, 2015). The presence of re-crossing phenotype in embryos lacking PlxnA1 or all Slit1-3 but not Robo1/2 or Sema3B led us to speculate that PlxnA1-SlitC signaling might provide the specific force that prevents commissural axons from turning back in the FP. To test this model, we generated a PlxnA1^{Y1815F} mouse strain. Homozygous individuals were viable, fertile, having no obvious morphological alterations (Supplemental Figure 1A-D). PlxnA1 expression in the spinal cord was further validated in western blot on lysates of spinal cords isolated from PlxnA1$^{+/+}$, PlxnA1$^{Y1815F/+,}$ PlxnA1$^{Y1815F/Y1815F}$ and PlxnA1$^{-/-}$ embryos (Supplemental Figure 1E). To examine commissural axon trajectories, we traced the commissural tracts with fast 1,1′-dilinoleyl-3,3,3′,3′-tetramethylindocarbocyanine, 4-chlorobenzenesulfonate (DiI) crystals inserted in the dorsal domain of open-book mounted embryonic spinal cords

isolated from E12.5 embryos having +/+, Y1815F/+, and Y1815F/Y1815F genotypes. Axon trajectories were classified according to previous work (Delloye-Bourgeois et al, 2015). Interestingly, while no difference of stalling was observed between PlxnA1$^{+/+}$ and PlxnA1$^{Y1815F/Y1815F}$ embryos, the recrossing cases were exclusively associated with loss of one or two copies of the PlxnA1 gene, reaching the proportion reported in PlxnA1$^{-/-}$ embryos (Figure 1A-C). Moreover, in the Y1815F context, axon trajectories appeared disorganized, with axons baring a tortuous aspect, even in cases where they succeeded to cross the FP and reached the post-crossing compartment (Figure 1B).

To further examine how the Y1815F mutation affects commissural axon navigation, E12.5 embryos were immunolabeled with an antibody against Robo3 commissural marker, cleared, and imaged with light sheet microscopy. We observed in 3D analysis a clear disorganization of the Robo3^{+} commissural tracts in PlxnA1$^{Y1815F/Y1815F}$ embryos compared with wild-type littermates, with axons losing their straight and parallel trajectory when navigating the FP (3 embryos for each genotype, Figure 1D).

Thus, the ability of commissural axons to maintain a straight trajectory towards the FP exit requires a functional PlxnA1-SlitC signaling. In contrast, the lack of stalling phenotype in PlxnA1$^{Y1815F/Y1815F}$ embryos indicates that the guidance forces resulting from the unaffected PlxnA1-Nrp2-Sema3B signaling remain sufficient for pushing commissural axons towards the FP exit.

PlxnA1^{Y1815F} mutation does not obviously affect pre-crossing commissural navigation

To examine the pattern of commissural axon projections prior to the FP crossing, transverse sections of E12.5 embryos were immunostained with antibodies directed against known pre-crossing and post-crossing markers of commissural axons, such as Robo3 and L1CAM, respectively. Analysis of commissural axon patterns in confocal images revealed no obvious defects of coursing towards the FP, indicating that PlxnA1 Y1815 residue is dispensable for the pre-crossing navigation (Figure 1E). This is consistent with our previous finding that PlxnA1 is not delivered at the commissural growth cone surface prior to the FP entry, and is thus not expected to have prominent role at the pre-crossing stage (Pignata et al, 2019). The expression pattern of PlxnA1 was also not obviously different between WT and PlxnA1$^{Y1815F/Y1815F}$ embryos, being detected in both cases at highest levels in crossing and post-crossing

axons (Figure 1F). This indicated that the Y1815 mutation does not prevent neither the synthesis of PlxnA1 receptor nor its trafficking to the axon compartment.

PlxnA1^{Y1815F} expressing axons fail to maintain forward directed growth when navigating the FP

To gain insights into how the alteration of SlitC-PlxnA1 signaling impacts on the behavior of navigating axons, we first thought to re-introduce WT and mutated versions of PlxnA1 in E12.5 PlxnA1$^{-/-}$ murine embryos by *ex vivo* electroporation of their neural tube. We constructed a pHluo tagged version of PlxnA1^{Y1815F} receptor by fusing the pHluo to the N-terminal part of the coding sequence to take advantage of this pH sensitive GFP allowing reporting the presence of the receptor at the cell membrane (Pignata et al, 2019). The pHluo-PlxnA1^{Y1815F} and pHluo-PlxnA1^{WT} constructs were co-electroporated along with a mbTomato construct (Figure 2A). We took advantage of our previous work in which we compared the outcome of different plasmid concentrations on the FP navigation to select a concentration of 2μg/μl, allowing sufficient receptor expression level and navigation across the FP (Pignata et al, 2019). The pH dependency of the pHluo constructs was verified as in Pignata et al, (2019). Right after electroporation, the spinal cords were dissected out and open-books were incubated for two days and imaged at fixed time-point with a spinning disk confocal microscope to examine the aspect of commissural axon trajectories in the FP. We analyzed individual axon trajectories spanning the FP by counting the number of deviations they presented and classifying them from O (straight and slightly and regularly curved with no deviation angle), 1, 2 and up to 2 deviation angles. Interestingly, we observed that while pHluo-PlxnA1^{WT+}growth-cones exhibited a 73,4% of straight growth trajectories, this ratio dropped to 35,6% for commissural axons that had sorted PlxnA1^{Y1815F} at their surface, that displayed much more irregular curly aspects, with trajectories having significantly increased number of curvature (Figure 2B, C). Video-time lapse recording on these electroporated mouse open-books turned out to be highly challenging, mainly due to high and fast toxicity resulting from repeated laser exposure. We thus turned to the chicken embryo as an alternative model for video-microscopy of commissural axon navigation in a context of impaired SlitC signaling.

We thus electroporated pHluo-PlxnA1^{WT} and pHluo-PlxnA1^{Y1815F} in the neural tube of the chicken embryo and performed time lapse analysis of the commissural axon navigation as in Pignata et al (2019). We first plotted the trajectories of individual axons at successive time points, classifying them as straight or curved. We also took advantage of live imaging to assess growth cone stalling. We found in the PlxnA1^{WT} condition a majority of axons having a straight trajectory (79,7%), whereas in contrast PlxnA1^{Y1815F} + axons exhibited a more tortuous aspect in 64,5% of the cases (Figure 2D-F). The rate of growth cone stalling was comparable in the WT and Y1815F conditions, which was also consistent with the lack of increased stalling phenotype in PlxnA1$^{Y1815/Y1815}$ embryos, compared to wild-type littermates. Finally, expressing PlxnA1^{Y1815F} in chicken commissural neurons also resulted in pictures of growth cones turning back (Figure 2F). As done in our experiments with mouse open-books, we also analyzed commissural axon trajectories to quantify their degree of deviation. Consistent with our previous observations, we found the percentage of straight trajectories significantly decreased from 82.7% in the PlxnA1^{WT} condition to 52.6% in the PlxnA1^{Y1815}F one, with correlated increase in curved shapes (Figure 2G-I).

Altogether these experiments confirmed that PlxnA1^{Y1815F} is unable to ensure the forward growth direction that is normally taken by commissural axons to cross the FP and validated the use of the chicken embryo as a model for further investigations.

The temporal and spatial pattern of PlxnA1 membrane insertion during commissural axon navigation is impacted by the Y1815 mutation

Next, we investigated whether the Y1815 mutation alters the SlitC-PlxnA1 signaling by modifying the dynamics of PlxnA1 in commissural growth cones in living conditions. First, we analyzed the pattern of pHluo receptor introduced in PlxnA1$^{-/-}$ mouse embryos. As expected from our immunohistochemical labeling of PlxnA1 in PlxnA1^{Y1815F} transverse sections, pHluo-PlxnA1^{Y1815F} was trafficked to the axon and the growth cones. However, the cell surface patterns of PlxnA1^{Y1815F} and PlxnA1^{WT} strikingly differed in axons navigating the FP. While PlxnA1^{WT} was mostly restricted to the growth cone, PlxnA1^{Y1815F} occupied a much larger membrane domain, overflowing in the adjacent axon shaft compartment (Figure 3A-C). The difference was statistically significant, as shown by measures of the area of pHluo signal in both PlxnA1^{Y1815F} and

PlxnA1^{WT} axons (Figure 3B). Thus, the Y1815 mutation alters the cell surface pattern of PlxnA1 receptor in navigating commissural axons.

Second, we recently reported that PlxnA1 is specifically delivered at the growth cone surface when commissural axons navigate the first part of the FP, a timing that differs from that of Robo1, which is sorted later on, in the second FP half (Pignata et al, 2019). To examine whether the Y1815 mutation affects the temporal sequence of PlxnA1 membrane insertion, the pHluo-PlxnA1^{Y1815F} and pHluo-PlxnA1^{WT} constructs, along with the mbTomato construct, were electroporated in the neural tube of chicken embryos. Receptor dynamics were studied in video-microscopy of commissural axons navigating the FP in open-books. We analyzed the temporal pattern of membrane insertion by pointing the position of growth cones switching on the pHluo fluorescence. Interestingly, we found with this cartography analysis that in both PlxnA1^{WT} and PlxnA1^{Y1815F} conditions, nearly 100% of the growth cones navigating the FP had sorted the receptor before midline crossing, indicating that the temporal pattern of membrane insertion within the FP was unaffected by the Y1815 mutation (Figure 3D-F, movies S1-S2). Nevertheless, we also observed that a significant proportion of PlxnA1^{Y1815F}-growth cones, that could navigate the FP, had sorted the receptor prior to the FP entry (Figure 3E, movies S3-S4). This suggested that the mutated receptor might be sorted precociously, although it appeared not to arrest the growth cones at the FP entry.

Third, in recent work using this experimental paradigm, we observed using STED microscopy that the membrane pool of PlxnA1^{WT} concentrates at the front of the growth cone. Thus, we thought to examine how PlxnA1^{Y1815F} distributes at the surface of the commissural growth cone. Living open-books electroporated with mbTomato/pHluo-PlxnA1^{Y1815F} constructs were incubated with Atto-647N-conjugated GFP nanobodies to label cell surface pHluo. Open-books were fixed, and plxnA1^{Y1815F} was imaged in growth cones navigating the FP. Notably, in sharp contrast with our observations of PlxnA1^{WT}, we observed that PlxnA1^{Y1815F} distributed from the front to the rear. This apparent absence of polarity was confirmed by measurement of the signal intensity along the rear-front axis (Figure 3G-I).

Thus, overall, these analyses showed that PlxnA1^{Y1815F} spatial distribution in commissural axons navigating the FP is altered, which reveals that the mutation might interfere with SlitC-specific traffic and signaling mechanisms.

Y1815F results in increased membrane mobility of PlxnA1 receptor in navigating commissural growth cones

To gain further insights into the biological process impaired by theY1815F mutation, we conducted FRAP experiments to compare exocytosis and membrane motility of WT and mutated PlxnA1 in commissural growth cones navigating the FP. The pHluo-receptor fluorescence was bleached to 80-90% at time zero, in a 15 to 20µm^2 area, which allows covering the entire growth cone surface. Then, the fluorescence recovery was recorded for 20 min (Figure 3J, K, movies S5-S8). Strikingly in the PlxnA1^{Y1815F} condition, the fluorescence recovery was significantly higher over the first time points, than in the PlxnA1^{WT} one, and the difference established from this early step remains constant over time. The temporality of the recovery pattern difference indicates that the PlxnA1^{Y1815F} has a faster membrane diffusion in the membrane than wild-type receptor. The stability of the difference over time suggests in addition that exocytosis events might be unaffected by the mutation. Thus, Y1815F mutation results in relapse of PlxnA1 motility at the cell membrane which, either upstream or downstream of SlitC binding, affects the ability of the receptor to mediate SlitC signal.

FP glia cells elaborate complex ramified basal processes staking the axon path

Next, we investigated how SlitC maintains a straight growth of commissural axons. To gain insights, we first thought to get a precise analysis of the topology of the axon navigation path in the FP and to characterize the spatial distribution of the different ligands (Figure 4A). We first proceeded to an immunostaining of transverse sections of E4 chick embryos with an antibody recognizing the FP glial cell marker Ben. The staining revealed an unexpected dense network of processes in the basal compartment corresponding to the axon path, in particular with BEN+ structures aligned in the left-right axis (Figure 4B). We next performed a sparse electroporation of chick embryos with a plasmid encoding a membrane-bound mbTomato to observe individual cells. We set-up a position of the electrodes on both sides of E2 embryos, allowing to specifically target FP glial cells. Spinal cords were dissected two days later and imaged in open-books by confocal microscopy (Figure 4C). We observed that the glial cell elaborates a morphologically complex basal process (Figure 4D, E). 3D

reconstruction with IMARIS software after deconvolution treatment of the images revealed a “squid-like” structure, with a basal process subdivided into several pillars, with typically several anchored to the ventral pole (Figure 4F). The pillars appeared much larger in the left-right axis than in the rostro-caudal one, as suggested by previous data from electronic microscopy (Okabe et al, 2004; Figure 4E-F). To examine the commissural axon path, we stained E4 spinal cord open-books with NgCAM commissural marker, and FP cells with the nuclear DAPI staining. In the rostro-caudal axis, we observed a “ladder rungs”-type NgCAM staining with rows of nuclei regularly interspaced, that delineated rostro-caudal interspaced streams through which the axons navigate. In the dorso-ventral axis, axons were constrained by the nuclei in the basal compartment (Figure 4G-H). To examine the dorso-ventral organization of commissural axons, we measured the intensity of NgCAM staining in dorsal (basal A) and ventral (basal B) equal sub-compartments (Figure 4I-J). We found that NgCAM staining was slightly enriched in the more ventral compartment, suggesting more axons are taking a ventral route (Figure 4J). Next, we electroporated a mbTomato plasmid containing a Math1 promoter, which specifically drives the expression in dorsal commissural neurons (Helms, 1998) and proceeded to immuno-staining of electroporated spinal cords with an anti-BEN antibody. This allowed us to visualize more precisely that commissural growth cones are individually intercalated between glial cell processes (Figure 4K). We finally co-electroporated Math1-mbTomato plasmid with a plasmid encoding GFP under the control of HoxA1 promoter, which specifically drives the expression in FP glial cells (Li and Lufkin, 2000), (Figure 4L-M). From confocal images of Math1-mbTomato fluorescent signal we reconstructed the morphology of commissural growth cones. We observed them infiltrating the space between pillars, having an oblong shape, flattened in the left-right dimension and elongated in the dorso-ventral one (Figure 4N). This analysis revealed that the FP glia builds highly complex mesh of basal processes whose stereotypic spatial organization provides a physical frame for commissural growth cones, likely imposing numerous and repeated contacts all over the FP navigation (Figure 4O, movies S9-S12).

SlitC and SlitN are expressed as segregated clusters in the FP navigation path

Next, we studied the distribution patterns of PlxnA1 ligands in the FP. For Sema3B, we took advantage of a knock-in model of Sema3B-GFP fusion generated in

our previous work (Arbeille et al, 2015). Transverse sections were stained with anti-GFP antibodies to amplify the GFP signal, allowing detection of the protein deposited in the basal domain (Figure 5A). Quantitative analysis of the GFP signal along the mediolateral axis of the basal domain and along the dorso-ventral axis of the FP revealed protein clusters distributed evenly in the FP, arranged in columns reflecting their localization along the basal processes. We then concentrated on Slit proteins. Study of Slit fragments distribution pattern is limited by the lack of antibodies allowing their detection and their distinction from the full-length form. Thus, as in Xiao et al (2011) we developed an alternative strategy based on fluorescent reporters, whose distribution should approximate the pattern of endogenous proteins, since their physico-chemical properties might be highly similar. We constructed a plasmid encoding full-length Slit2 (Slit2 FL), fused to two distinct fluorescent proteins: Cerulean at its N-terminal part and Venus at its C-terminal part. Slit2 FL is visualized with both fluorophores overlapping (white signal). Upon cleavage, Slit N is reported by Cerulean fluorescence (here in purple) and Slit C by Venus (here in green) (Figure 5B). This construct was electroporated in the FP of E2 chicken embryos, which were dissected two days later (Figure 5C). Thick transverse embryonic sections were prepared and the FP observed by confocal microscopy. For analysis, the FP domain was subdivided into three compartments along the dorso-ventral axis: (i) the “apical” one, delimited by the central canal and the bottom of glial cells nuclei, (ii) the “basal a” encompassing the dorsal half of the axons path and (iii) the “basal b”, containing the ventral half of the axons path until the basal lamina (Figure 5D). Slit2 dual-tagged construct allowed us to observe that glial cells display a massive white staining in their apical part, reflecting the presence of the uncleaved Slit2 FL and/or overlapping Slit2N and Slit2C fragments. Conversely, the basal compartments, in particular the most ventral one in which commissural axons preferentially path, showed higher degree of separation of the Slit2 fragments, as quantified by a Pearson coefficient evaluation (Figure 5E). Analysis of cerulean (Slit2N) and Venus (Slit2C) fluorescence showed that both Slit2 fragments had a graded pattern, with higher levels in the basal a *versus* basal b compartment. Yet, Slit2C was significantly enriched in the basal b compartment, when compared to Slit2N (Figure 5F). Thus, Slit2C and Slit2N distribution patterns within the FP territory are close, although they present some specificities which could result from distinct structural properties and/or from active mechanisms regulating Slit2 prior to the generation of the fragments. To address this question, we examined whether Slit2C

and Slit2N patterns resulting from endogenous Slit2 processing were similar to those observed when the fragments are expressed individually. We thus constructed two plasmids encoding one fragment each in secreted fusion with a GFP (Figure 5G). The patterns of distribution of Slit2N-GFP and Slit2C-GFP were then analyzed as performed previously. Interestingly, whereas Slit2N displayed the same distribution pattern when expressed as an isolated fragment or generated from Slit2 cleavage, Slit2C diffused massively in the axon path when issued from Slit2 cleavage (Figure 6H-J). Furthermore, Slit2C-GFP isolated fragment was more prone to deposition along the FP basal membrane than Slit 2C processing product (Figure 5K). Thus, beyond physicochemical properties, Slit2C and Slit2N patterns likely result from additional mechanisms regionalizing full-length Slit2 protein and its processing within the FP glial cell compartments.

Proteolytic processing by PC2 convertase is required for proper patterns of Slit2N and Slit2C

To decipher whether Slit2 processing contributes to the regionalization of Slit fragments in the native context, we constructed a plasmid encoding a dual-tagged Slit2 FL, fused to Cerulean in its N-terminal part and to Venus in C-terminal part, having a deletion of the Slit cleavage site (Amino-acids 110 to 118 -SPPMVLPRT- Nguyen Ba-Charvet et al, 2001). We verified by western-blot that the expression of this Slit2 FL Δ in neuronal N2a cells was not compromised. As expected, using an anti-GFP antibody (recognizing both Cerulean and Venus), the Cerulean-Slit2N and Slit2C-Venus fragments were detected in the Slit2 FL condition but not in the Slit2 FL Δ condition (Figure 6A). Dual-tagged Slit2 FL and Slit2 FL Δ were then electroporated in chicken embryos and transversal sections were analyzed by confocal microscopy. Notably, preventing Slit2 cleavage resulted in strong depletion of Slit2 protein in the basal compartment in which commissural axons navigate (Figure 6B, C). Thus, Slit2 FL protein might not be addressed to the basal processes, rather distributed in the apical compartment of FP glia cells, where it might locally be processed, generating fragments that are subsequently deposited on the basal processes. Thus, this confirmed that the cleavage is determinant for proper localization of Slit2 fragments to the axon navigation path. While the protease responsible for Slit2 cleavage is still

unknown in vertebrates, the pheromone convertase Amontillado has been shown to cleave Slit during drosophila muscles and tendons development (Ordan and Volk 2016). Amontillado homolog in vertebrates is PC2, a proprotein convertase (PC) involved in the activation of endocrine peptides (Smeekens and Steiner, 1991). We treated N2a cells transfected with dual-tagged Slit2 FL with Chloromethylketone (CMK), a PC2 inhibitor, and found that it resulted in a loss of the Slit2C-Venus fragment and an accumulation of the FL form, as also observed in N2a cells transfected with Slit2 FL Δ. (Figure 6D-F). Thus, PC2 might either directly or indirectly be involved in Slit2 cleavage.

Transverse sections of E12.5 embryos were immunolabeled with an anti-PC2 antibody to examine PC2 expression at the spinal cord midline. We observed that PC2 was expressed in the FP, exhibiting a discrete and almost exclusive expression in this spinal cord territory (Figure 6G). We quantified the distribution of PC2 in the apical, basal a and b compartments and found that it is enriched in the apical compartment with modest expression in the basal compartments (Figure 6H, I). PC2 is thus properly expressed at an appropriate timing and location to mediate the cleavage of Slits and participate in the setting of their distribution patterns in the FP navigation path (Figure 6J)

Y1815F mutation releases SlitC-mediated constrains imposed by the basal processes, resulting in abnormally plastic and exploratory growth cones during FP navigation

Our analysis revealed that SlitC does not accumulate in specific regions, nor it appeared to form a sharp gradient within the FP. Rather it distributes in clusters that decorate a tight mesh of ramified basal processes which spans the entire commissural path. Guidance cues have versatile effects, that largely depend on the context in which cues are presented (Nawabi and Castellani, 2011). The repulsive activity attributed to Slits in the context of commissural axon navigation was deduced from both *ex vivo* culture assays in which cues were delivered as soluble molecules, and interpretation of phenotypes resulting from *in vivo* manipulations (Zou et al, 2000; Long et al, 2005; Delloye-Bourgeois et al, 2015). SlitC spots could mediate a repulsive effect. Alternatively, they could act differently, for example by providing a positive signal at each contact, stabilizing the growth cone forward trajectory. Both modes of action

should be reflected in the aspect of the growth cones. Thus, to get further insights, we thought to compare the morphologies of growth cones expressing PlxnA1^{WT} or PlxnA1^{Y1815F} during their navigation of the FP. E2 Chicken embryos were electroporated with plasmids encoding pHluo-PlxnA1^{WT} and pHluo-PlxnA1^{Y1815F}. Open-books were mounted, immunolabeled with anti-BEN antibody to delineate FP cells and observed using confocal microscope. Within the BEN^{+} expression domain, lying in the dorso-ventral dimension below the soma territory, in which commissural axons navigate, two classes of growth cone shapes were observed: those having an oblong shape, modestly enlarged compared with the adjacent axon segment, and those having a more complex morphology, with visible protrusions and being enlarged of more than 2 times that of the axonal tract size (Figure 7A). We observed that while in the pHluo-PlxnA1^{WT} condition the proportion of complex growth cones was very low, it was increased by 3-fold in the pHluo-PlxnA1^{Y1815F} condition, reaching more than 15% (Figure 7B). Strikingly, these differences of growth cone morphologies were also very apparent in open-books labeled with Atto-647N-conjugated GFP nanobodies observed using STEP microscopy (Figure 7C).

These findings were evocative of SlitC acting as a repulsive molecule for commissural growth cones navigating the FP. Such repulsive effect was also suggested by previous *in vitro* experiments, reporting that soluble SlitC and Sema3B both had a collapsing effect in condition when cultured commissural neurons were exposed to the FP signal GDNF, which induces cell surface sorting of PlxnA1 receptor (Charoy et al, 2012; Delloye-Bourgeois et al, 2015). In contrast, commissural neurons over-expressing PlxnA1^{Y1815F} were significantly less sensitive to this SlitC effect, while their collapse response to Sema3B was preserved (Delloye-Bourgeois et al, 2015). We examined the behaviors of commissural neurons isolated from PlxnA1$^{Y1815F/Y1815F}$ embryos when exposed to SlitC and Sema3B, in the absence or presence of GDNF. As expected from our previous over-expression experiments, the capacity of SlitC to collapse PlxnA1$^{Y1815F/Y1815F}$ commissural growth cones was significantly reduced, compared to that of Sema3B. Interestingly, beyond the binary collapsed/non collapsed classification, we noted in the SlitC/GDNF condition, growth cones having atypical shapes. Some had long filopodia, or appeared contracted with numerous reminiscent filopodia or were also visibly spread (Figure 7D, E). This suggested that under normal

condition, SlitC/plxnA1 signaling might negatively regulate the complexity of growth cone morphologies.

How could be translated this increased complexity of PlxnA1$^{Y1815F+}$ commissural growth cones into aberrant axon trajectories? To address this question, we recorded the FP navigation in open-books at high frequency of time-lapse image acquisition. pHluo-PlxnA1^{WT} and pHluo-PlxnA1^{Y1815F} plasmids were electroporated in chick embryos and their spinal cords mounted in open-book. Images were taken with a time interval of 8 minutes, that enabled monitoring the growth cones over a period of time covering the FP navigation with manageable toxicity (see method). Individual growth cones were traced over time and scored according to two types of behavior: “straight” (growth cones that maintained forward trajectory), and exploratory (growth cones that deviated from their straight axis) (Figure 8A). Strikingly, while exploratory behavior was observed in only 15% of the pHluo-PlxnA1^{WT+} population, this level reached 59% in the PlxnA1$^{Y1815F+}$ one (Figure 8B, movies S13-S16). Exploratory growth cones could either present a split aspect or could be “turned” (deviated from their straight axis, orienting in rostral or caudal directions). While turned growth cones were found equally represented in both conditions, split PlxnA1$^{Y1815F+}$ growth cones growth cones were much more frequent than PlxnA1^{WT} ones, representing 49% of the observed cases (Figure 8C, D). Moreover, exploratory behaviors were not appearing after midline crossing or after FP exit, but were present from the onset of the FP navigation. To refine our analysis, we measured the width of individual growth cones over time, as a read-out of morphological plasticity and exploratory behavior. We found that PlxnA1$^{Y1815F+}$ growth cones were significantly larger than those expressing PlxnA1^{WT}. In addition, their increased exploratory behavior was also reflected in the higher variations of width over time when compared with PlxnA1^{WT+} growth cones (Figure 8E-F).

Overall, these results support a model whereby SlitC patches presented by the basal processes network spanning the entire FP navigation path generate a straight trajectory of the growth cones by continuously limiting their exploration potential through inhibitory/repulsive repetitive contacts.

Discussion

Our results establish that commissural axons navigate the FP in a complex environment, composed of ramified FP basal processes with stereotypic spatial organization. These basal structures are decorated with segregated Slit2C, Slit2N, and Sema3B clusters, forming a mesh that forces multiple and reiterated contacts with the navigating growth cones. Through analysis of a knock-in mouse model baring a PlxnA1 mutation specifically altering Slit2C responses and a range of *ex vivo* and imaging analysis, we show that the Slit2C-PlxnA1 signaling is indispensable for the maintenance of forward-directed commissural axon trajectories. We also identify Y1815 of PlxnA1, highly-conserved across PlxnA family members, as a key residue for proper distribution at the cell membrane. Finally, our data do not support that midline recrossing is prevented through gain of sensitivity to repellents after midline crossing. On the contrary, they show that repulsive forces generate a forward polarity of commissural axon growth starting from the FP entry and being active over the entire FP navigation. We propose an alternative view of the mechanism ensuring FP crossing, which is to limit continuously over the FP navigation the exploration activity of commissural growth cones (Figure 8G).

Specific sub-cellular architecture of the FP glia conforms the presentation of FP ligands to the navigating commissural axons

The mode of presentation of the FP ligands to the navigating axons has remained largely ignored, although it is generally admitted that it is determinant for the final outcome of guidance cues. Hence, despite extensive studies of spinal cord and midbrain midline crossing, very little is known on the tridimensional organization of the FP. Early electronic microscopy images revealed close contacts between FP glia surfaces and axons, and suggested complex shapes of basal processes (Yaginuma et al. 1991; Campbell and Peterson, 1993; Okabe et al. 2004). To which extent, and if so how, the spatial organization of the FP glia generates specific ligand patterns has been left open. Our study sheds novel light on this issue. Analysis of ligands distribution with fluorescent reporters whose expression was specifically driven in FP cells and immunolabeling of the FP-specific marker, BEN, allowed us to reconstruct in 3D the FP glia morphology. A particularly striking observation was the asymmetric apico-basal

polarity of the FP cell, with a single apical anchor and an enlarged basal process subdivided into several oblong pillars. In addition to this morphological complexity, we found that the basal ramified structures have a stereotypic spatial position. Their larger sides align along the left-right and rostro-caudal axes, parallel narrow corridors in which commissural axons navigate. Finally, in the dorso-ventral axis, ramifications of the main pillars also provide to the axons a net-shaped roof. Notably, this sub-cellular architecture of the FP glia provides a physical frame for the presentation of the ligands. We found that SlitC, SlitN, and Sema3B have resembling distribution patterns, prominently deposited in columnar clusters covering the ramified basal processes of FP glia cells. Nevertheless, our analysis using dual tagged Slit2 construct indicated that SlitC and SlitN clusters occupy physically distinct locations.

The molecular scaffold that localizes the ligands in such a way is still to be explored. Extracellular matrix components and their interactors are well acknowledged for their critical role in setting molecular patterns (Walter et al, 2018). Interestingly in the *zebrafish* developing brain, apical end feet of radial glial cells extend at the surface of the tectum, organizing through collagen IV the lamination of the neuropil by exposing Slits and heparan sulfate proteoglycans to axon terminals (Xiao et al, 2011). Morphogenesis of the *drosophila* heart tube lumen was found to rely on polarized localization of the collagen XV/XVIII orthologue Multi-Plexin forming a macro-complex with Slit (Harpaz et al, 2013). In the context of midline crossing, loss of the heparan sulfate carrier (Heparan sulfate proteoglycan) Syndecan results in modification of Slit distribution and activity in *drosophila* (Johnson et al, 2004). In the vertebrate spinal cord, dystroglycan was identified as a Slit binding partner, localizing the proteins in the basal lamina through non-cell autonomous action (Wright et al, 2012; Lindenmaier et al, 2019). Consistently, we detected the presence of SlitC, whose sequence contains dystroglycan binding motif, in the basement membrane, as well as that of SlitN, possibly sequestrated by additional components of the FP basal lamina. For example, proteolysis of the extracellular matrix protein F-spondin, reported to contribute to commissural axon guidance (Burstyn-Cohen et al, 1999), was found to generate two fragments, among which one is deposited at the basement membrane (Zisman et al, 2007). Patterning of guidance molecules by morphological specificities of producing cells was also nicely exemplified on Netrin-1. Synthesized by progenitor soma in the ventricular zone of the neuroepithelium, Netrin-1 was proposed to be transported on

or within the basal process for relocalization at the basal membrane, where it might serve as a growth-promoting substrate for pre-crossing commissural axons (Varadarajan et al, 2017).

Beyond the molecular components localizing the ligands, our analysis of Slit fragments distribution also revealed that Slit cleavage is a pre-requisite for the detection of Slits in the commissural axon navigation path, since uncleavable Slit2 almost exclusively localized in the FP apical domain. This suggests that, unlike in *drosophila* midline guidance for which Slit processing was reported to be dispensable (Coleman et al, 2010), under their full-length form, Slits likely play limited role, if not no role at all, in the guidance of spinal cord commissural growth cones. We also found that SlitC, when synthesized as a cleaved fragment, was significantly more prone to basement membrane deposition than its equivalent form resulting from endogenous processing. These findings support the intervention of a series of post-translational processes to properly present the ligands to the commissural axons, in particular those controlling the addressing of full-length Slit in the FP glia sub-cellular compartments, as well as those regulating the protease action. This is consistent with previous studies of the process of muscle anchorage to tendons in *drosophila*, that reported the importance of Slit processing for subsequent distribution of the fragments and proper functional outcome (Ordan and Volk 2015).

Commissural axon navigation is driven by restriction of growth cone exploration resulting from reiterated contacts with ligands deposited on the FP basal processes

A puzzling question of commissural axon navigation across the FP relates to the mode of action by which FP cues exert their effect. Proper FP crossing is thought to rely on a balance of positive and negative forces that support growth cone attachment, motility and direction (de Ramon Francàs et al, 2017). Early experiments conducted in the chicken embryo demonstrated that contacts engaging various Ig Superfamily Cell Adhesion Molecules expressed by growth cones and glia cells control the entry in the FP (Stoeckli et al, 1997; Fitzli et al, 2000). Complementarily, growth-promoting effect exerted by the Stem Cell Factor (SCF) under its transmembrane isoform acting via its KIT receptor was shown to be switched on after midline crossing to facilitate the growth

towards the FP exit (Gore et al, 2008). Finally, studies of midline crossing in *drosophila* inspired the view that in vertebrates as well commissural axons must acquire sensitivity to local repellents after midline crossing, in order to get directional information for exiting the FP and for not turning back to the ipsilateral side (Evans and Bashaw, 2010). Consistently, differential sensitivity of commissural growth cones to FP cues before and after FP crossing was reported in numerous experimental paradigms (Zou et al, 2000; Nawabi et al, 2010; Delloye-Bourgeois et al, 2015). Nevertheless, in vertebrates, the physical territory of midline navigation, the FP, is much larger and complex than that in invertebrates, which might impose particular constraints and require specific guidance forces that remain uncharacterized. Indeed, the exact mechanisms by which SlitC, SlitN, and Sema3B exert their action in the FP are unknown, although they are all considered as chemorepellents. However, this has yet to be demonstrated since they were studied using only *ex vivo* paradigms that neither recapitulated the architecture of the FP navigation path, nor the coincident information that the growth cones receive from their local environment when navigating in their native context (Zou et al, 2000; Nawabi et al, 2010; Delloye-Bourgeois et al, 2015). Functional outcomes of guidance signals are indeed highly versatile and shown to depend on many intrinsic and extrinsic variables (Nawabi et al, 2011). *In vitro*, context-dependent switch from attraction to repulsion and vice-versa were evidenced for a large range of guidance molecules including Netrins, Semaphorins, and Slits (Höpker et al, 1999; Castellani et al, 2000; Nguyen-Ba-Charvet et al, 2001; Castellani et al, 2002; Ma et al, 2007). *In vivo*, although considered as repellents, Sema2a and Sema3B were recently reported to promote midline crossing in *drosophila,* acting as chemoattractant via Sema1a (Hernandez-Fleming et al, 2017).

Our findings provide the first evidence that specific FP guidance forces ensure commissural axons a continuous straight trajectory, from the FP entry to the exit. With our analysis of PlxnA1^{Y1815F} model and live imaging paradigms, we show that SlitC brings a major contribution to this guidance mechanism, acting by restricting the exploratory capacity of commissural growth cones. This function is served by the particular morphology of the FP glia cells that might impose repeated contacts of the growth cones with spots of ligands spanning the navigation path. Our functional analyses are all consistent with SlitC mode of action restricting the formation or the stabilization of peripheral growth cone protrusions to constrain them in a non-

exploratory state, thus favoring forwards growth direction. Such effect is also reflected in the shape of wild-type crossing growth cones, which we observed are rostro-caudally thin and dorso-ventrally elongated. Notably, PlxnA1$^{Y1815F+}$ growth cones have a much more complex morphology than WT growth cones, and they also sense the environmental content much more actively. In recent work, axon growth was modeled using microcontact printing culture devices developed to examine individual growth cone responses to dots of guidance molecules (Ryu et al, 2018). Axons were challenged to grow on micropatterned surfaces consisting in uniform Sema3F substrate interrupted by permissive dots. They were found able to efficiently extend in such surfaces, having, in addition, a straight trajectory resulting from jumping from one permissive dot to the next one. Interestingly, perturbing the distance between dots or their size modified the shape of the axons by disorganizing their cytoskeleton and their trajectory, inducing curved growth patterns (Ryu et al, 2018). Thus, a “salt and pepper” context as in the FP with repulsive ligands localized in spots and intercalated with permissive regions might build an appropriate topographic environment for limiting the possibilities of growth deviations.

Such constrain of growth cone exploration might also be required for counteracting other local coincident guidance forces that would disturb axon trajectories during FP crossing. In our recent work, we found in live imaging that the exploration is increased when growth cones start navigating the second FP half, although we observed they still keep a clear straight growth (Pignata et al, 2019). This exploratory behavior could reflect an increasing sensitivity to FP-derived SHH and WNT rostro-caudal gradients that were found to drive the longitudinal turning after the crossing (Zuñiga and Stoeckli, 2017). The exact timing at which the axons become sensitive to these gradients is unclear. In Robo3 knockout embryos, commissural axons totally fail to cross the FP but turn longitudinally in the ipsilateral side. This argues that non-crossing commissural axons can get sensitized to longitudinal gradients, which also reflects the need for guidance constrains to counteract premature turning during the FP navigation (Friocourt and Chedotal, 2017). One function of PlxnA1/SlitC signaling would thus be to prevent premature longitudinal turning until FP exit.

Tyrosine 1815 mutation alters the membrane mobility of PlxnA1 receptor

Tyrosine phosphorylation is a pivotal modification by which receptors can acquire key specific dynamics, trafficking, or signaling properties. Plxn cytoplasmic domain contains several tyrosine residues, some of them being phosphorylated during the signaling cascade downstream of Semaphorin ligands (Tamagnone *et al*, 1999). Apart from PlxnB (Swiercz et al, 2009), the characterization of the molecular events triggered by specific tyrosine phosphorylation and identification of kinases targeting the different residues is only beginning. Recently, two highly-conserved residues were shown as major targets of Fyn, a kinase known to phosphorylate PlxnA1 downstream of Semaphorins, and their phosphorylation is required for *zebrafish* eye development (St Clair et al, 2018). All Plxns share a set of thirteen tyrosine, but interestingly the Y1815 is restricted to the PlxnA subfamily (Franco and Tamagnone, 2008). Consistently, we showed that PlxnAs interact with SlitC while PlxnBs do not (Delloye-Bourgeois et al, 2015). The present study shows that mutating the Y1815 residue strongly impacts on the distribution of PlxnA1 at the cell membrane. First, we observed in mouse commissural axons navigating the FP in PlxnA1$^{-/-}$ open-books that the PlxnA1^{Y1815F} cell surface pool expanded to the adjacent axon shaft, whereas it was much more restricted to the growth cone compartment in the WT context. Second, when expressed in chicken open-books for STED imaging, PlxnA1^{Y1815F} was observed to distribute at the membrane of the entire growth cone, not accumulating at the front as normally observed for PlxnA1^{WT} (Pignata et al, 2019). Third, FRAP experiments revealed an increased membrane mobility of the PlxnA1^{Y1815F} receptor pool, compared with the WT one, with a pattern of fluorescence recovery suggesting that exocytosis-mediated sorting is in contrast unaffected by the mutation. Overall this raises the interesting possibility that PlxnA1 baring Y1815F mutation lacks an interactor whose function in stabilizing the receptor at the growth cone membrane is indispensable for SlitC signaling. Structural analysis established the ability of PlxnA1 to engage its extra-cellular domain in dimeric complexes (Janssen *et al.*, 2010; Kong *et al.*, 2016). Thus, Y1815 could be required for allowing the formation of macro-complexes of PlxnAs at the growth cone membrane. Neuropilins are unlikely involved since we found they are dispensable for SlitC-PlxnA1 binding and SlitC responses (Delloye-Bourgeois et al, 2015). Heparan sulfate proteoglycans are possible candidates since they bind PlxnA1 (Delloye-bourgeois et al, 2015). Y1815 could also be involved directly or indirectly for the receptor to recruit scaffolding proteins and intracellular partners. For example, a recent study reported a novel interface between PlxnB2 and the PDZ domain of PDZ-

RHO-GEF, whose activation downstream of Semaphorin binding increases GTP-bound RHOA activity, that maps at the C-terminus side engaging an amino-acid sequence close to the 1815 residue (Pascoe et al, 2015). Further studies are needed to elucidate the contributions of Y1815 residue to the PlxnA1 biological activity.

Is PlxnA1-SlitC signaling the only player of the guidance program generating straight trajectory across the FP?

In vivo re-crossing phenotypes have been observed when PlxnA1, Slit1-3, but not Robo1/2 or Sema3B, are inactivated and we show here that it is manifested when PlxnA1 is prevented to properly mediate SlitC activity. This does not exclude that the Slit/Robo signaling also contributes to this function. The lack of recrossing in context of Robo1/2 loss could be due to the specific temporal and spatial pattern of Robo1 receptor at the growth cone surface. According to our previous work (Pignata et al, 2019), growth cones navigating the first FP half express PlxnA1 but not yet Robo1, while in the second FP half, they express both. Robo2 was found to be sorted only during the post-crossing longitudinal navigation (Pignata et al, 2019). Thus, PlxnA1 and Robo loss cannot have the same observable outcome, whether or not both receptors have similar functions. PlxnA1 deletion results in lack of Slits and Sema3B receptors when the growth cones enter the FP, whereas Robo deletion manifests itself later when growth cones already completed half of their navigation through the FP, and have a preserved PlxnA1-SlitC signaling to navigate the second FP half. Moreover, recrossing is likely to be the more drastic growth cone behavior resulting from abrogation of forces counteracting rostro-caudal gradients. Interestingly in Robo1/2$^{-/-}$ embryos, cases of commissural axons aberrantly oriented within the FP were reported (Long et al, 2004). As well in PlxnA1$^{-/-}$ embryos, premature turning in the FP was also frequently observed (Nawabi et al, 2010; Delloye-Bourgeois et al, 2015). Such phenotypes could well be interpreted as resulting from alleviation of straight growth constrains. The equally plausible alternative scenario would be that Slit2C-PlxnA1 signaling does indeed specifically ensure the straight growth of commissural axons in the FP, through specific downstream signaling. In support, we found that PlxnA1 and Robo1 are not only sorted at different timing but also in different growth cone compartments, with PlxnA1 enriched at the front and Robo1 at the rear, thus able to generate spatially distinct functional outcomes (Pignata et al, 2019).

Whatever the case, our study raises a novel guidance model of midline crossing that might represent a general mechanism for the navigation at choice points. Limiting growth cone exploration through short-range signaling would efficiently allow inhibiting premature directional changes elicited by coincident guidance cues, until intermediate target navigation is completed.

Materials and Methods

Generation of the PlxnA1^{Y1815F} mouse line and genotyping

The PlxnA1^{Y1815F} mouse line was generated by the Mouse Clinical Institute (Strasbourg, France). Mice were back-crossed to obtain PlxnA1^{Y1815F} in a C57/BL6 background. Mice were hosted either in SPF (ALECS SPF, Lyon, France) or conventional (SCAR, Lyon, France) animal facility with *ad libitum* feeding. This study was covered by a Genetically Modified Organisms approval (number 561, French ministery for Research) and a local ethical comity (CECCAPP, Lyon). Genotyping was performed on dissected tails lysed in NaOH 1M solution for 25 min at 95°C and digested overnight with Proteinase K at 56°C with the following primers 5'- CTT ATA GAT CTA GAC AGG CAG GGA GAC CAT-3' and 5'- CGG TTG TCT TCT CGA GTA TCA CAC TCC TA-3'. The PCR kit used was FastStrat PCR Master (Roche, 04710436001). The amplification product from mutated allele has a 341bp size and the one obtained from a wild-type allele is 262bp. Genotyping of PlxnA1-/- was done as in Yoshida et al. (2006).

Molecular biology

FL mouse pHluo-PlxnA1 was generated by introducing in Nter the coding sequence of the pHluo cloned from a vector encoding GABA A pHluo-GFP (Jacob et al., 2005). FL mouse pHluo-PlxnA1^{Y1815F} was obtained by directed mutagenesis using the In-fusion HD Cloning Plus Kit (638909, Ozyme) with the following primers: 5' AGG TAC TTT

GCT GAC ATT GCC and 5’ GTC AGC AAA GTA CCT TTC AAC. The pH dependency of the fluorescence was validated as in Pignata et al (2019).

Dual-tagged Slit2 was designed using the human Slit2 sequence (NM_001289135.2) and ordered from Genscript Biotech. Briefly, Cerulean was inserted after Slit2 signal peptide (MRGVGWQMLSLGLVLAILNKVAPQACPA) and Slit2 FL sequence. Venus was fused to the C-terminal part of Slit2. Dual-tagged Slit2 Δ construct was obtained by Quickchange mutagenesis procedure (Agilent), deleting 9 amino acids (SPPMVLPRT) at the cleavage site. The primer used for the mutagenesis were 5’-CTT GTT CTG TGA GTTT AGC CCC TGT GAT AAT TTT G-3’ and 5’- CAA AAT TAT CAC AGG GGC T AAA CTC ACA GAA CAAG-3’. Both constructs were cloned into a PCAGEN vector using NotI and EcoRV digestion. The Hoxa1-GFP plasmid was a kind gift of Esther Stoeckli.

The fusion of Slit2N and Slit2C with GFP was performed in order to express the fusion proteins resulting from the cleavage of Slit2 Dual-tagged construct: GFP-SlitN (GFP in Nter) and SlitC-GFP (GFP in Cter). The fusion of Slit2N with GFP was done by cloning the Slit2 signal peptide, the eGFP and the Slit2N sequences in a pCAGEN backbone using the In-Fusion HD cloning Plus Kit (638909, Ozyme) with the following primers : 5’-GCA AAG AAT TCC TCG AGG ATA TCA TGC GCG GCG TTG GCT GG-3’ and 5’-TGC TCA CGT TAA CCG CCG GGC ACG CCT G-3’ for the signal peptide; 5’-CCC GGC GGT TAA CGT GAG CAA GGG CGA GG-3’ and 5’-AGC ACT GAC GCG TCT TGT ACA GCT CGT CCA TGC-3’ for eGFP; 5’-GTA CAA GAC GCG TCA GTG CTC TTG CTC GG-3’ and 5’-CTG AGG AGT GCG GCC GCG ATT TAA CGA GGG AGG ACC ATG GG-3’ for Slit2N. The CAG promoter was then replaced by the Hoxa1 promoter using In-Fusion with the following primers: 5’- GTG CCA CCT GGT CGA CGC TTC TTC TAG CGA TTA AAT C-3’ and 5’- AAC GCC GCG CAT GAT ATC CCC ACT AGT AAG CTT GGA GGT G-3’. The fusion of Slit2C with GFP was done by cloning the sequences into a pEGFP-N3 vector after the addition of KpnI and BamHI restriction sites using the following primers: 5’-cg GGTACC acc agc ccc tgt gat aat ttt g-3’ and 5’-cg GGATCC gga cac aca cct cgt aca gc-3’. The Igκ Leader peptide signal was added for correct secretion by cloning the fusion fragment into a pSecTagB plasmid using KpnI and NotI digestion. The resulting sequence was cloned into a pCAGEN vector using XhoI and NotI digestion, and the In-Fusion HD Cloning Plus Kit (638909, Ozyme) with the following primers: 5’-caa aga att cct cga gat gga gac aga

cac act cct gc-3' and 5'-ctg agg agt gcg gcc gct tac ttg tac agc tcg tcc atg cc-3'. The CAG promoter was replaced by the Hoxa1 promoter using SalI and XhoI digestion, and the In-Fusion HD Cloning Plus Kit with the following primers: 5'-gtg cca cct ggt cga cgc ttc ttc tag cga tta aat caa ag-3' and 5'-ctg tct cca tct cga gcc cac tag taa gct tgg agg tg-3'. Math-1-mbTomato construct was described previously (Pignata et al, 2019).

DiI staining in spinal cord open-books

Spinal cords from E12.5 murine embryos were dissected and mounted as open-books prior to fixation in 4% paraformaldehyde (PFA) for 18 hrs. DiI crystals (D3911, ThermoFisher) were inserted in the most dorsal part of one hemi-spinal cord for anterograde labeling of commissural tracts. Axon trajectories were analyzed 24 hrs later with a spinning disk microscope (Olympus X80). For each DiI crystal, a range of phenotypes can be observed. Classes were made representing the percentage of DiI crystals showing the phenotype over the total number of observed DiI crystals. Classes were assessed independently, with percentage ranging from 0% to 100%.

Immunofluorescence labeling

Cryosections from embryos collected at E12.5 were prepared and processed for staining as in Charoy et al, (2012). For some experiments, chick embryos sections and open-book spinal cords were blocked in 6% BSA (A7906, Sigma) and 0.5% Triton (T9284, Sigma) diluted in PBS for 5 hours at room temperature. Sections were incubated overnight at room temperature with anti-PlxnA1 antibody (gift from Y. Yoshida), anti-Robo3 antibody ((1/100, R&D, AF3076); anti-L1CAM antibody (1:100, A439 Abcam 123990), anti-NgCAM antibody (1:50, 8D9, DSHB), anti-BEN (1:50, BEN, DSHB) or an anti-PC2 antibody (1:100, 3533, Abcam) in 1% BSA diluted in PBS**.** Alexa 488, Alexa 555 (1/500, Invitrogen) and Fluoroprobe 546 (1/400) were used as secondary antibodies.

***In ovo* electroporation, open-book mounting and imaging**

The neural tube of HH14/HH15 chick embryos was electroporated as described previously (Delloye-Bourgeois *et al.,* 2015, Pignata et al, 2019). Plasmids were diluted in PBS with Fast Green (F7262, Sigma) at the following concentration:

- 1.5mg/mL for dual-tagged Slit2 and dual-tagged Slit2 Δ. Lower concentration did not allow correct imaging with confocal microscopy.

- 1.34mg/mL for Hoxa1-Slit2N-GFP and 0.94mg/mL for Hoxa1-Slit2C-GFP. Both concentrations match the dual-tagged plasmid molarity in order to electropore the same amount of plasmid.
- 0.5mg/mL for Math1-mbTomato and 2 µg/µl for pHluo-PlxnA1 and pHluorin-PlxnA1^{Y1815F} and 0,05mg/mL for mbTomato and Hoxa1-GFP. These concentrations were selected according to our previous work (Pignata et al, 2019) in which we compared the outcome of different concentrations on the FP navigation and selected the conditions that gave the better compromise between receptor expression and ability of FP crossing. The pHluo dependency was controlled by *in vitro* cell line transfection as in Pignata et al, (2019).

The plasmid solution was injected into the lumen of the neural tube using picopritzer III (Micro Control Instrument Ltd., UK). Using electrodes (CUY611P7-4, Sonidel) 3 pulses (25V, 500ms interpulse) were delivered by CUY-21 generator (Sonidell). Electroporated embryos were incubated at 38.5°C. In ovo electroporation of floor plate cells was done on HH17/18 chick embryos as described by Wilson et al. (2012). Briefly, electrodes (CUY611P7-4, Sonidel) were placed at the thoracic level dorsally (cathode, negative electrode) and ventrally (anode, positive electrode), and 3 pulses (18V, 500ms interpulse) were delivered by CUY21 electroporator (Sonidell). Embryos at HH25/HH26 were harvested in cold HBSS (14170-088, Gibco) and the spinal cords were dissected out. They were mounted in 0.5% agarose diluted in F12 medium on glass bottom dishes (P35G-1.5-14-C, MatTek). After agarose solidification, spinal cords were overlaid with 3ml of F12 medium supplemented with 10% FCS (F7524; Sigma-Aldrich), 1% Penicillin/Streptomycin (Sigma-Aldrich) and 20mM HEPES buffer (15630-049, ThermoFischer Scientific). For section imaging, embryos were then fixed for 2 hours at room temperature in 4% paraformaldehyde diluted in PBS. For open-book imaging, spinal cords were dissected and then fixed 45 minutes in 4% paraformaldehyde diluted in PBS. For vibratome sectioning, embryos were embedded in 3% low gelling agarose (A9414, Sigma) diluted in PBS. The embryos were then sectioned in 80μm slices using Leica VT1000S vibratome.

Mouse spinal cord electroporation and open-book mounting

E12 mice embryos were collected and fixed on a SYLGARD (Dow Corning) culture plate in HBSS medium (ThermoFisher) supplemented with Glucose 1M (Sigma-Aldrich). Injection of plasmids into the lumen of the neural tube was performed using

picopritzer III (Micro Control Instrument Ltd., UK). Using electrodes (CUY611P7-4, Sonidel) 3 pulses (20V, 500ms interpulse) were delivered by CUY-21 generator (Sonidell). Spinal cords were dissected from the embryos and cultured on Nucleopore Track-Etch membrane (Whatman) for 48 hours in Slice Culture Medium (*Polleux and Ghosh., 2002*).

Imaging and data analysis

Live imaging was performed with an Olympus IX81 microscope equipped with a spinning disk (CSU-X1 5000 rpm, Yokogawa) and Okolab environmental chamber maintained at 37°C. Image were acquired with a 20X objective by EMCCD camera (iXon3 DU-885, Andor technology). 15-30 planes spaced of 0,5-3μm were imaged for each open-book at 30-minute interval for 10 hours approximatively. To reduce exposure time and laser intensity, acquisitions were done using binning 2x2. Images were acquired using IQ3 software using multi-position and Z stack protocols. Z stack projections of the movies were analyzed in ImageJ software. The analysis of pHluo-flashes was performed from time-lapse acquisitions. In some experiments, the time interval was reduced for faster image acquisition. Time intervals of 3 minutes, 5 minutes, 8 minutes and 12 minutes were tested. At 3 and 5 minutes, the tissues were rapidly damaged. We thus selected time interval of 8 min as the better compromise between time resolution and phototoxicity.

Confocal imaging was performed with either an Olympus FV1000 with a 40x objective and zoom or a Leica TCS SP5 with a 63x objective. Deconvolution was done using the Huygens software. 3D surface reconstructions were done using the Imaris software.

Atto647N staining and STED microscopy

Spinal cords were incubated at 38°C for 20 minutes with F12 medium supplemented with 5% FCS (F7524; Sigma-Aldrich), 20mM HEPES buffer (15630-049, ThermoFischer Scientific) and 1/100 GFP-nanobodies Atto647N. They were then rinsed 4 times with the same medium free of GFP-nanobodies and fixed at room temperature for 2 hours with PBS supplemented with 4% paraformaldehyde (PFA) and 1% BSA (A7638 Sigma-Aldrich). Open-books were observed with a STED microscope (TCS SP8, Leica). STED illumination of ATTO 647N was performed using a 633-nm pulsed laser providing excitation, and a pulsed bi-photon laser (Mai Tai; Spectra-

Physics) turned to 765 nm and going through a 100-m optical fiber to enlarge pulse width (100ps) used for depletion. A doughnut-shaped laser beam was achieved through two lambda plates. Fluorescence light between 650 and 740 nm was collected using a photomultiplier, using a HCX PL-APO CS 100/1.40 NA oil objective and a pinhole open to one time the Airy disk (60mm). Images were acquired with using Leica microsystem software and a Z stack protocol. Usually 10-20 planes spaced of 0,5μm where imaged for each growth cone. The growth cones were delineated and the intensity signal was calculated using ImageJ.

Fluorescence Recovery After Photobleaching (FRAP)

FRAP experiments were conducted on spinal cord open-books electroporated with either pHluo-receptor and mbTomato, using a Leica DMI6000 (Leica Microsystems, Wetzlar, Germany) equipped with a confocal Scanner Unit CSU-X1 (Yokogawa Electric Corporation, Tokyo, Japan) and a scanner FRAP system, ILAS (Roper Scientific, Evry, France). Images were acquired in both green and red channels using a 63X objective and an Evolve EMCCD camera (Photometrics, Tucson, USA). Growth cones located in the FP were first monitored for 12s each 3s and then bleached using a 488nm diode laser at full power. This resulted in an 85-95% loss of the signal (mean of 89%) at t=0. Fluorescence recovery was then monitored for 730s with acquisitions every 3s for 30s, then every 10s for 100s, and finally every 30s for 600s. The images were corrected for background noise, residual fluorescence right after the bleach was set to zero, and recovery curves were normalized to the fluorescence lost after the bleach. No other corrections were applied since unbleached growth cone fluorescence showed no significant decay during the acquisition period.

Western blot

To observe Slit cleavage, N2a cells were seeded into 6-wells plates ($2.5.10^5$ cells per well). 24 hours later, cells were transfected using jetprime transfection reagent (114, Polyplus transfection). 4 hours after starting the transfection, cell medium was changed and CMK (ALX-260-022, Enzo) was added to a final concentration of 100μM if needed. Two days after transfection, CMK treatment was repeated. Two hours after, cells were harvested. Whole cells extract was isolated using RIPA buffer (NaCl 150mM – Tris HCL pH7,35 50mM – DOC 1% – N-P40 1% – H_2O) supplemented with protease

inhibitor (04 693 116 001, Roche). Isolated protein concentration was determined using Bradford assay (500-0006, Bio-Rad).
Spinal cords were isolated from E12.5 embryos and dissected tissues were lyzed in RIPA buffer supplemented with protease inhibitor. Samples were analyzed in western blot using anti-PlxnA1 antibody (Gift from Y Yoshoda), anti-GFP (1:1000, 11814460001, Sigma), anti-Tubulin (1:10000, T5168, Sigma) and anti-PC2 (1:100, 3533, Abcam). Western blot quantification was performed using Image Lab4.0 software (Bio-Rad).

Commissural neuron cultures and collapse

Dorsal spinal cord tissue was dissected out from isolated spinal cord and dissociated. Neurons were grown on laminin-polylysine-coated coverslips in Neurobasal supplemented with B27, glutamine (Gibco), and Netrin-1 (R&D) medium for 24 to 48 hrs, as in Nawabi et al, (2010). Immunolabeling was performed with anti-PlxnA1 antibody (gift from Y. Yoshida). Nuclei were stained with bisbenzimide (Promega) and actin with TRITC-phalloidin. GDNF was applied to the cultures as in Charoy et al (2012). Collapse assays were performed as in Delloye-Bourgeois et al, 2015.

Quantification and Statistical analyses

Protein diffusion quantification: The background noise was removed by measuring it, then subtracting it in ImageJ. The electroporated zone was then divided into two different compartments along the dorso-ventral axis. The glial cells' apical feet and cellular bodies were included in the apical compartment. The axons path was divided in two, the most apical compartment being basal 1, the most basal compartment being basal 2. The mean intensity of Cerulean, Venus or GFP was measured using ImageJ in each compartment. The mean intensity was then normalized by the mean intensity in the apical compartment.

Pearson coefficient: The background noise was removed by measuring it, then subtracting it in ImageJ. The electroporated zone was then divided into three different compartments as mentioned previously. Each compartment was then analyzed using

the JACoP plugin in ImageJ. An empirical threshold was used, and the Pearson's coefficient calculated.

All embryos which normally developed and expressing pHluo-vectors at the thoracic level were included in the analysis. Number of independent experiments, embryos, stacks and growth cones (n) are indicated in figures or legends. Analysis were done in blind for the quantification of phenotype in mouse embryos and the collapse assays. Sample size and statistical significances are represented in each figure and figure legend. For each set of data, normality was tested and Student t or Mann-Whitney tests were performed when the distribution was normal or not, respectively. Statistical tests were performed using Biosta-TGV (CNRS) and Prism 6 software.

Acknowledgments

We thank Samir Merabet for helpful advices on the construction of fluorescent reporters, Julien Falk and Frédéric Moret for help with confocal microscopy, Camilla Lucardini, Dennis Ressnikoff, and Bruno Chapuis from the CIQLE platform of Lyon for advices on microscopy and deconvolution, Esther Stoeckli for Math1 and HoxA1 promoters constructs. STED microscopy was done in the Bordeaux Imaging Center (BIC), CNRS-INSERM-Bordeaux University, member of the national infrastructure France BioImaging supported by the French National Research Agency (ANR-10-INBS-04). We thank C. Poujol and M. Mondin (BIC) for advice, M. Sainlos for sharing the anti-GFP nanobody, and B. Tessier and S. Benquet for technical assistance. This work was conducted within the frame of the LabEx CORTEX and DEVWECAN of Université de Lyon, within the program ''Investissements d'Avenir'' (ANR-11-IDEX-0007) operated by the French National Research Agency (ANR). The study was supported by an ANR funding to VC and OT, the Association Française contre les Myopathies (AFM), the Fondation pour la Recherche Médicale (FRM) to VC, the Fondation Bettencourt-Schueller to VC, and Conseil Régional d'Aquitaine (Neurocampus funds).

References

Andermatt I, Wilson NH, Bergmann T, Mauti O, Gesemann M, Sockanathan S, Stoeckli ET. Semaphorin 6B acts as a receptor in post-crossing commissural axon guidance. Development. 2014 Oct;141(19):3709-20. doi: 10.1242/dev.112185.

Bellon A, Mann F. Keeping up with advances in axon guidance. Curr Opin Neurobiol. 2018 Dec;53:183-191. doi: 10.1016/j.conb.2018.09.004

Burk K, Mire E, Bellon A, Hocine M, Guillot J, Moraes F, Yoshida Y, Simons M, Chauvet S, Mann F. Post-endocytic sorting of Plexin-D1 controls signal transduction and development of axonal and vascular circuits. Nat Commun. 2017 Feb 22;8:14508. doi: 10.1038/ncomms14508

Burstyn-Cohen T, Tzarfaty V, Frumkin A, Feinstein Y, Stoeckli E, Klar A. F-Spondin is required for accurate pathfinding of commissural axons at the floor plate. Neuron. 1999 Jun;23(2):233-46.

Campbell, R M, and A C Peterson. 1993. “Expression of a LacZ Transgene Reveals Floor Plate Cell Morphology and Macromolecular Transfer to Commissural Axons.” *Development (Cambridge, England)* 119 (4): 1217–28.

Castellani V, De Angelis E, Kenwrick S, Rougon G. Cis and trans interactions of L1 with neuropilin-1 control axonal responses to semaphorin 3A. EMBO J. 2002 Dec 2;21(23):6348-57.

Castellani V, Chédotal A, Schachner M, Faivre-Sarrailh C, Rougon G. Analysis of the L1-deficient mouse phenotype reveals cross-talk between Sema3A and L1 signaling pathways in axonal guidance. Neuron. 2000 Aug;27(2):237-49.

Chance RK, Bashaw GJ. Slit-Dependent Endocytic Trafficking of the Robo Receptor Is Required for Son of Sevenless Recruitment and Midline Axon Repulsion. PLoS Genet. 2015 Sep 3;11(9):e1005402. doi: 10.1371/journal.pgen.1005402.

Chen, Z., Gore, B.B., Long, H., Ma, L., Tessier-Lavigne, M. (2008). Alternative splicing of the Robo3 axon guidance receptor governs the midline switch from attraction to repulsion. Neuron *58*, 325–332.

Coleman HA, Labrador JP, Chance RK, Bashaw GJ. The Adam family metalloprotease Kuzbanian regulates the cleavage of the roundabout receptor to control axon repulsion at the midline. Development. 2010 Jul;137(14):2417-26. doi: 10.1242/dev.047993.

de Ramon Francàs G, Zuñiga NR, Stoeckli ET. The spinal cord shows the way - How axons navigate intermediate targets. Dev Biol. 2017 Dec 1;432(1):43-52. doi: 10.1016/j.ydbio.2016.12.002

Dominici C, Moreno-Bravo JA, Puiggros SR, Rappeneau Q, Rama N, Vieugue P, Bernet A, Mehlen P, Chédotal A. Floor-plate-derived netrin-1 is dispensable for commissural axon guidance. Nature. 2017 May 18;545(7654):350-354. doi:10.1038/nature22331

Ducuing H, Gardette T, Pignata A, Tauszig-Delamasure S, Castellani V. Commissural axon navigation in the spinal cord: A repertoire of repulsive forces is in command. Semin Cell Dev Biol. 2019 Jan;85:3-12. doi: 10.1016/j.semcdb.2017.12.010. Epub 2018 Jan 3. Review. PubMed PMID: 29277684.

Evans, T.A., Bashaw, G.J. (2010). Axon guidance at the midline: of mice and flies. Curr Opin Neurobiol. *20*, 79-85

Fitzli D, Stoeckli ET, Kunz S, Siribour K, Rader C, Kunz B, Kozlov SV, Buchstaller A, Lane RP, Suter DM, Dreyer WJ, Sonderegger P. A direct interaction of axonin-1 with NgCAM-related cell adhesion molecule (NrCAM) results in guidance, but not growth of commissural axons. J Cell Biol. 2000 May 15;149(4):951-68.

Friocourt F, Chédotal A. The Robo3 receptor, a key player in the development, evolution, and function of commissural systems. Dev Neurobiol. 2017 Jul;77(7):876-890. doi: 10.1002/dneu.22478

Fothergill T, Donahoo AL, Douglass A, Zalucki O, Yuan J, Shu T, Goodhill GJ, Richards LJ. Netrin-DCC signaling regulates corpus callosum formation through attraction of pioneering axons and by modulating Slit2-mediated repulsion. Cereb Cortex. 2014 May;24(5):1138-51. doi: 10.1093/cercor/bhs395

Fournier AE, Nakamura F, Kawamoto S, Goshima Y, Kalb RG, Strittmatter SM. Semaphorin3A enhances endocytosis at sites of receptor-F-actin colocalization during growth cone collapse. J Cell Biol. 2000 Apr 17;149(2):411-22

Franco M, Tamagnone L. Tyrosine phosphorylation in semaphorin signalling: shifting into overdrive. EMBO Rep. 2008 Sep;9(9):865-71. doi: 10.1038/embor.2008.139.

Gore BB, Wong KG, Tessier-Lavigne M. Stem cell factor functions as an outgrowth-promoting factor to enable axon exit from the midline intermediate target. Neuron. 2008 Feb 28;57(4):501-10. doi: 10.1016/j.neuron.2008.01.006.

Harpaz, N., Ordan, E., Ocorr, K., Bodmer, R. and Volk, T. (2013). Multiplexin promotes heart but not aorta morphogenesis by polarized enhancement of slit/ robo activity at the heart lumen. PLoS Genet. 9, e1003597.

Helms AW, Johnson JE. Progenitors of dorsal commissural interneurons are defined by MATH1 expression. Development. 1998 Mar;125(5):919-28

Hernandez-Fleming M, Rohrbach EW, Bashaw GJ. Sema-1a Reverse Signaling Promotes Midline Crossing in Response to Secreted Semaphorins. Cell Rep. 2017 Jan 3;18(1):174-184. doi: 10.1016/j.celrep.2016.12.027

Höpker VH, Shewan D, Tessier-Lavigne M, Poo M, Holt C. Growth-cone attraction to netrin-1 is converted to repulsion by laminin-1. Nature. 1999 Sep 2;401(6748):69-73

Janssen BJ, Robinson RA, Pérez-Brangulí F, Bell CH, Mitchell KJ, Siebold C, Jones EY. Structural basis of semaphorin-plexin signalling. Nature. 2010 Oct 28;467(7319):1118-22. doi: 10.1038/nature09468.

Johnson KG, Ghose A, Epstein E, Lincecum J, O'Connor MB, Van Vactor D. Axonal heparan sulfate proteoglycans regulate the distribution and efficiency of the repellent slit during midline axon guidance. Curr Biol. 2004 Mar 23;14(6):499-504.

Kamiguchi H, Lemmon V. Recycling of the cell adhesion molecule L1 in axonal growth cones. J Neurosci. 2000 May 15;20(10):3676-86.

Kerstein PC, Nichol RH IV, Gomez TM. Mechanochemical regulation of growth cone motility. Front Cell Neurosci. 2015 Jul 7;9:244. doi: 10.3389/fncel.2015.00244.

Kinoshita-Kawada M, Hasegawa H, Hongu T, Yanagi S, Kanaho Y, Masai I, Mishima T, Chen X, Tsuboi Y, Rao Y, Yuasa-Kawada J, Wu JY. A crucial role for Arf6 in the response of commissural axons to Slit. Development. 2019 Feb 4;146(3). pii: dev172106. doi: 10.1242/dev.172106

Kolpak A, Zhang J, Bao ZZ. Sonic hedgehog has a dual effect on the growth of retinal ganglion axons depending on its concentration. J Neurosci. 2005 Mar 30;25(13):3432-41.

Kong Y, Janssen BJ, Malinauskas T, Vangoor VR, Coles CH, Kaufmann R, Ni T, Gilbert RJ, Padilla-Parra S, Pasterkamp RJ, Jones EY. Structural Basis for Plexin Activation and Regulation. Neuron. 2016 Aug 3;91(3):548-60. doi: 10.1016/j.neuron.2016.06.018

Lindenmaier LB, Parmentier N, Guo C, Tissir F, Wright KM. Dystroglycan is a scaffold for extracellular axon guidance decisions. Elife. 2019 Feb 13;8. pii: e42143. doi: 10.7554/eLife.42143.

Lochter A, Vaughan L, Kaplony A, Prochiantz A, Schachner M, Faissner A. J1/tenascin in substrate-bound and soluble form displays contrary effects on neurite outgrowth. J Cell Biol. 1991 Jun;113(5):1159-71

Long, H., Sabatier, C., Ma, L., Plump, A., Yuan, W., Ornitz, D.M., Tamada, A., Murakami, F., Goodman, C.S., Tessier-Lavigne, M. (2004). Conserved roles for Slit and Robo proteins in midline commissural axon guidance. Neuron 42, 213–223.

López-Bendito G, Cautinat A, Sánchez JA, Bielle F, Flames N, Garratt AN, Talmage DA, Role LW, Charnay P, Marín O, Garel S. Tangential neuronal migration controls axon guidance: a role for neuregulin-1 in thalamocortical axon navigation. Cell. 2006 Apr 7;125(1):127-42

Ma L, Tessier-Lavigne M. Dual branch-promoting and branch-repelling actions of Slit/Robo signaling on peripheral and central branches of developing sensory axons. J Neurosci. 2007 Jun 20;27(25):6843-51

Mire E, Hocine M, Bazellières E, Jungas T, Davy A, Chauvet S, Mann F. Developmental Upregulation of Ephrin-B1 Silences Sema3C/Neuropilin-1 Signaling during Post-crossing Navigation of Corpus Callosum Axons. Curr Biol. 2018 Jun4;28(11):1768-1782.e4. doi: 10.1016/j.cub.2018.04.026

Nawabi H, Castellani V. Axonal commissures in the central nervous system: how to cross the midline? Cell Mol Life Sci. 2011 Aug;68(15):2539-53. doi:10.1007/s00018-011-0691-9

Nguyen-Ba-Charvet KT, Brose K, Marillat V, Sotelo C, Tessier-Lavigne M, Chédotal A. Sensory axon response to substrate-bound Slit2 is modulated by laminin and cyclic GMP. Mol Cell Neurosci. 2001 Jun;17(6):1048-58.

Neuhaus-Follini. A, Bashaw. G.J. (2015). Crossing the embryonic midline: molecular mechanisms regulating axon responsiveness at an intermediate target. Wiley Interdiscip Rev Dev Biol. *4*(4):377-89

Okabe, Noriko, Kazuya Shimizu, Kumi Ozaki-Kuroda, Hiroyuki Nakanishi, Koji Morimoto, Masakazu Takeuchi, Hironobu Katsumaru, Fujio Murakami, and Yoshimi Takai. 2004. “Contacts between the Commissural Axons and the Floor Plate Cells Are Mediated by Nectins.” *Developmental Biology* (2): 244–56. https://doi.org/10.1016/j.ydbio.2004.05.034.

Ordan E, Volk T. Amontillado is required for Drosophila Slit processing and for tendon-mediated muscle patterning. Biol Open. 2016 Oct 15;5(10):1530-1534.doi: 10.1242/bio.020636

Pascoe HG, Gutowski S, Chen H, Brautigam CA, Chen Z, Sternweis PC, Zhang X. Secondary PDZ domain-binding site on class B plexins enhances the affinity for PDZ-RhoGEF. Proc Natl Acad Sci U S A. 2015 Dec 1;112(48):14852-7. doi:10.1073/pnas.1508931112.

Pignata A, Ducuing H, Boubakar L, Gardette T, Kindbeiter K, Bozon M, Tauszig-Delamasure S, Falk J, Thoumine O, Castellani V. A Spatiotemporal Sequence of Sensitization to Slits and Semaphorins Orchestrates Commissural Axon Navigation. Cell Rep. 2019 Oct 8;29(2):347-362.e5. doi: 10.1016/j.celrep.2019.08.098.

Pignata A, Ducuing H, Castellani V. Commissural axon navigation: Control of midline crossing in the vertebrate spinal cord by the semaphorin 3B signaling. Cell Adh Migr. 2016 Nov;10(6):604-617.

Raper J, Mason C. Cellular strategies of axonal pathfinding. Cold Spring Harb Perspect Biol. 2010 Sep;2(9):a001933. doi: 10.1101/cshperspect.a001933.

Ryu JR, Kim JH, Cho HM, Jo Y, Lee B, Joo S, Chae U, Nam Y, Cho IJ, Sun W. A monitoring system for axonal growth dynamics using micropatterns of permissive and Semaphorin 3F chemorepulsive signals. Lab Chip. 2019 Jan 15;19(2):291-305. doi: 10.1039/c8lc00845k.

Schaefer AW, Kamei Y, Kamiguchi H, Wong EV, Rapoport I, Kirchhausen T, Beach CM, Landreth G, Lemmon SK, Lemmon V. L1 endocytosis is controlled by a phosphorylation-dephosphorylation cycle stimulated by outside-in signaling by L1. J Cell Biol. 2002 Jun 24;157(7):1223-32.

Seiradake E, Jones EY, Klein R. Structural Perspectives on Axon Guidance. Annu Rev Cell Dev Biol. 2016 Oct 6;32:577-608. Epub 2016 Aug 24. Review. PubMed PMID: 27576119.

Smeekens SP, Steiner DF. Processing of peptide precursors. Identification of a new family of mammalian proteases. Cell Biophys. 1991 Oct-Dec;19(1-3):45-55

St Clair RM, Emerson SE, D'Elia KP, Weir ME, Schmoker AM, Ebert AM, Ballif BA. Fyn-dependent phosphorylation of PlexinA1 and PlexinA2 at conserved tyrosines is essential for zebrafish eye development. FEBS J. 2018 Jan;285(1):72-86. doi: 10.1111/febs.14313.

Stoeckli ET, Sonderegger P, Pollerberg GE, Landmesser LT. Interference with axonin-1 and NrCAM interactions unmasks a floor-plate activity inhibitory for commissural axons. Neuron. 1997 Feb;18(2):209-21

Stoeckli ET. Understanding axon guidance: are we nearly there yet? Development. 2018 May 14;145(10). pii: dev151415. doi: 10.1242/dev.151415

Swiercz JM, Worzfeld T, Offermanns S. Semaphorin 4D signaling requires the recruitment of phospholipase C gamma into the plexin-B1 receptor complex. Mol Cell Biol. 2009; 29:6321–6334. DOI: 10.1128/MCB.00103-09

Turner LJ, Nicholls S, Hall A. The activity of the plexin-A1 receptor is regulated by Rac. J Biol Chem. 2004 Aug 6;279(32):33199-205

Varadarajan SG, Kong JH, Phan KD, Kao TJ, Panaitof SC, Cardin J, Eltzschig H, Kania A, Novitch BG, Butler SJ. Netrin1 Produced by Neural Progenitors, Not Floor Plate Cells, Is Required for Axon Guidance in the Spinal Cord. Neuron. 2017 May 17;94(4):790-799.e3. doi: 10.1016/j.neuron.2017.03.007

Walker C, Mojares E, Del Río Hernández A. Role of Extracellular Matrix in Development and Cancer Progression. Int J Mol Sci. 2018 Oct 4;19(10). pii: E3028. doi: 10.3390/ijms19103028

Wu KY, He M, Hou QQ, Sheng AL, Yuan L, Liu F, Liu WW, Li G, Jiang XY, Luo ZG. Semaphorin 3A activates the guanosine triphosphatase Rab5 to promote growth cone collapse and organize callosal axon projections. Sci Signal. 2014 Aug 26;7(340):ra81. doi: 10.1126/scisignal.2005334.

Xiao T, Staub W, Robles E, Gosse NJ, Cole GJ, Baier H. Assembly of lamina-specific neuronal connections by slit bound to type IV collagen. Cell. 2011 Jul 8;146(1):164-76. doi: 10.1016/j.cell.2011.06.016.

Zisman S, Marom K, Avraham O, Rinsky-Halivni L, Gai U, Kligun G, Tzarfaty-Majar V, Suzuki T, Klar A. Proteolysis and membrane capture of F-spondin generates combinatorial guidance cues from a single molecule. J Cell Biol. 2007 Sep 24;178(7):1237-49

Zuñiga NR, Stoeckli ET. Sonic -'Jack-of-All-Trades' in Neural Circuit Formation. J Dev Biol. 2017 Feb 8;5(1). pii: E2. doi: 10.3390/jdb5010002

Figure legends

Figure 1: Y1815F mutation in PlxnA1 induces commissural axon recrossing and disorganized trajectories

(A) Schematic drawing of open-book preparations for DiI tracing of commissural axon trajectories. (B) (left panel) Microphotographs illustrating commissural tracts extending straight towards the FP, crossing the FP, and turning rostrally at the FP exit in PlxnA1$^{+/+}$ embryos. (right panel) Microphotographs and magnifications illustrating the phenotypes observed in the PlxnA1$^{Y1815F/Y1815F}$ embryos, with axons turning back during the navigation, and misdirected trajectories within the FP (indicated by green arrows). The FP is delimited by dashed green lines. (C) Quantitative analysis of commissural axon phenotypes showing that the Y1815F mutation induces recrossing, while it does not affect other aspects of the navigation such as the stalling (PlxnA1$^{+/+}$, N = 3 embryos; PlxnA1$^{+/Y1815F}$, N = 5 embryos; PlxnA1$^{Y1815F/Y1815F}$, N = 4 embryos). Data are shown as the mean ± s.e.m, Student test has been applied, *: P-value $p < 0.05$. (D) Light sheet imaging of the spinal commissural tracts in PlxnA1$^{+/+}$ and PlxnA1$^{Y1815F/Y1815F}$ embryos at E12.5, immunostained with anti-Robo3 antibody. Note the disorganized aspect of commissural axons crossing the FP. (E) Immunofluorescent labeling of Robo3 and L1CAM in transverse cryosections from E12.5 embryos illustrating the general patterns of pre-crossing commissural axons (revealed by Robo3 marker) and post-crossing axons (revealed by L1CAM marker) in PlxnA1$^{+/+}$ and PlxnA1$^{Y1815F/Y1815F}$ spinal cords. (F) PlxnA1 immunolabeling on E12.5 transverse sections of PlxnA1$^{+/+}$ and PlxnA1$^{Y1815F/Y1815F}$ embryos at E12.5 showing that the general pattern of the receptor is preserved in the mutated context. Scale bar: 10μm in (B), 50μm in (D, E, F).

Figure 2: Commissural neurons expressing PlxnA1^{Y1815F} at their surface fail to maintain straight growth during FP navigation

(A) Schematic drawing of the paradigm of electroporation of pHluo-PlxnA1 receptor forms in PlxnA1$^{-/-}$ mouse embryonic spinal cord and open-book preparations for live imaging. (B) Histogram depicting the analysis of axon trajectories, classified by counting curvatures according to the indicated criteria, showing that straight trajectories are less frequent when commissural neurons express PlxnA1^{Y1815F} than PlxnA1^{WT} (PlxnA1^{WT}, N = 10 embryos, 64 growth cones; PlxnA1^{Y1815F}, N = 7 embryos,

132 growth cones). Chi^2 test has been applied, ***: P-value $p < 0.001$. (C) Microphotographs illustrating navigating commissural growth cones expressing the mutated pHluo-receptor at their surface, reported by the green pHluo fluorescent signal. The red signal depicts the mbTomato, co-electroporated with the pHluo-receptor construct. Note that some axons have a curly aspect. (D) pHluo-receptor constructs were co-electroporated with the mbTomato in the chicken neural tube and spinal cords were mounted in open-books for time-lapse imaging. (E) Histogram quantifying axon trajectories reconstructed from time-lapse sequences of pHluo$^+$ growth cones navigating the FP, showing increased proportion of wavy axon shapes in the PlxnA1^{Y1815F} condition, compared with PlxnA1^{WT} one (PlxnA1^{WT}, N = 3 embryos, 188 growth cones; PlxnA1^{Y1815F}, N = 3 embryos, 249 growth cones). Chi^2 test has been applied, ***: P-value $p < 0.001$. (F) Snapshots of the movies illustrating the commissural growth patterns (white triangles) and an illustration of a PlxnA1$^{Y1815F+}$ growth cone turning back. The FP is delimited by dashed white lines. (G, H) Microphotograph illustrating traces of commissural axon trajectories. Example of traces patterns from several snapshots. (I) Histogram depicting the quantification and showing increased curvatures of axon shapes in the PlxnA1^{Y1815F} condition compared with PlxnA1^{WT} one (PlxnA1^{WT}, N = 3 embryos, 166 growth cones; PlxnA1^{Y1815F}, N = 3 embryos, 378 growth cones). Chi^2 test has been applied, ***: P-value $p < 0.001$. Scale bars: 10μm in (C, F, G).

Figure 3: the Y1815F mutation alters the spatio-temporal pattern of cell surface PlxnA1 distribution and membrane mobility at the growth cone

(A) Schematic drawing of the paradigm of electroporation of the mouse embryonic spinal cord. (B) Method and quantification of the pHluo signal in commissural axons navigating the floor plate (FP), showing an expansion of the expression domain in the PlxnA1^{Y1815F} condition, compared with the PlxnA1^{WT} one (PlxnA1^{WT}, N = 6 electroporated PlxnA1$^{-/-}$ embryos, 24 growth cones; PlxnA1^{Y1815F}, N = 4 PlxnA1$^{-/-}$ electroporated embryos, 18 growth cones). Data are shown as the mean ± s.e.m, Student test has been applied, *: P-value $p < 0.05$, **: P-value $p < 0.01$, ***: $p < 0.001$. (C) Microphotographs of commissural axons navigating the FP in living open-books, illustrating the difference of PlxnA1 cell surface distribution between the WT and Y1815F condition. The FP is delimited by dashed white lines. (D) Schematic drawing of the experimental paradigm of expression of PlxnA1 in the chicken spinal cord. (E)

Cumulative fractions of growth cones that sort PlxnA1 to their surface, reported by the pHluo fluorescence (pHluo-PlxnA1^{WT}, N = 2 electroporated embryos, 38 growth cones; pHluo-PlxnA1^{Y1815F}, 4 electroporated embryos, 53 growth cones). In the PlxnA1^{Y1815F} condition, 100% of the growth cone population has sorted the receptor when reaching the midline, but for a substantial amount of the growth cones, the sorting had already occurred prior to the FP entry. KS test has been applied, ***: P-value $p < 0.001$. (F) Microphotographs of live imaging movies illustrating the sorting of PlxnA1 receptor at the surface of commissural growth cones navigating the FP. The phase contrast image depicts the position of the FP in the open-books (delimited by dashed white lines). The green signal corresponds to the pHluo fluorescence, reporting the presence of PlxnA1 at the membrane. In the WT condition, PlxnA1 is sorted at the membrane from the FP entry to the midline. (G) Schematic representation of the paradigm of STED imaging in open-books. (H) Quantification of the center of mass of the signal, showing no polarity towards the rear or the front of the growth cones (N= 28 imaged growth cones from 5 electroporated embryos). Data are shown as the mean ± s.e.m. (I) STED microscopy images of pHluo-PlxnA1^{Y1815F} cell surface distribution in commissural growth cones navigating the FP. The signal distributes over the entire growth cone surface. (J) Schematic representation of the paradigm of FRAP experiments in open-books. Representative color-coded images from video time-lapse sequences illustrating photobleaching and fluorescence recovery of fluorescent growth cones navigating the FP. (K) Graphs of fluorescence recovery for pHluo-PlxnA1^{WT} and pHluo-PlxnA1^{Y1815F} (PlxnA1^{WT}, N = 2 embryos, 10 growth cones; PlxnA1^{Y1815F}, N = 2 embryos, 15 growth cones). Data are shown as the mean ± s.e.m, Student test has been applied at t=30s, t=280s, and t=580s, ns: non-significant, *: P-value $p < 0.05$, **: P-value $p < 0.01$. Scale bars: 5μm in (I), 10μm in (B, C, J), 50μm in (F).

Figure 4: Spatial organization of the commissural axon navigation path

(A) Schematic drawings of a spinal cord at E12.5 when commissural axons cross the floor plate (FP) (left panel) and close-up of the FP (right panel) with glial cells (light blue) and crossing axons (dark blue). (B) Immunostaining of an E4 FP transverse section with FP specific BEN antibody (left panel) and merged with DAPI staining (right panel). (C) *In ovo* FP electroporation procedure. 48h after electroporation, spinal cords are dissected and mounted as open-books for time lapse microscopy. Sparse electroporated mbTomato electroporated cells are visualized in red. (D) Open-book

imaging of E4 chick FP with sparse mbTomato electroporation. The dashed square highlights a glial cell. (E) Close-up of the single glial cell observed in (D), at three different positions along the dorso-ventral axis, as shown by the schematic representation on the upper right corner of each image. A single FP glial cell displays multiple basal feet. (F) 3D reconstruction (first and third panels) and surface modeling (second and last panels) of a single FP cell seen in a sagittal section (left panels) or transverse section (right panels). (G, H) Open-book view of E4 chick spinal cord floor-plate showing crossing axons stained with NgCAM at 20x magnification (first and third panels) and reconstruction of the corresponding sagittal view (second and last panels). In the open-book view, the depth shown is at the most dorsal part of the axon path. (I) 80μm transverse section of E4 chick spinal cord FP showing crossing axons stained with NgCAM. The FP basal domain was subdivided in two and NgCAM intensity was measured. (J) NgCAM in both basal subdomains (N= 3 embryos, 2 sections per embryo, 3 images analyzed per section). Data are shown as the mean ± s.d, paired Student test has been applied, **: P-value $p < 0.01$. (K) 3D reconstruction of axons navigating through the floor plate stained with DAPI (in blue), BEN (in white) and with mbTomato electroporated in axons (in red). The yellow dashed line corresponds to the cut plane resulting in the sagittal optic section shown in the lower panel. Yellow arrows point growth cones intercalated between BEN labeled glial cell processes when they navigate the FP (see also movies of this 3D reconstruction in Supplemental information movies S9-13). (L) Schematic drawings of an open-book with a sparse electroporation of commissural axons and a broad FP electroporation. Two plasmids are used: Math1-mbTomato drives the expression of a membrane anchored mbTomato in commissural neurons, while HoxA1-GFP drives the expression of GFP in FP glial cells. (M) Ventral longitudinal view from an open-book electroporated as described in (L). The yellow dashed square delineates a close-up of a crossing growth cone electroporated with Math1-mbTomato (in red) navigating along the basal feet of glial cells electroporated with Hoxa1-GFP (in white). (N) Surface reconstruction of a growth cone electroporated with Math1-mbTomato (in red) navigating along the basal feet of glial cells electroporated with Hoxa1-GFP (in white) as seen in a sagittal section (upper panel) or transversal section (lower panel). (O) Schematic drawing of a glial cell and two axons crossing through its basal end-feet, in a sagittal view (left panel) or transverse view (right panel). Scale bars: 5μm in (D, E, F, L, M), 20μm in (B, G, H).

Figure 5: Slit2N and Slit2C decorate the FP glia basal processes and have distinct diffusion properties conditioned by Slit2 FL processing

(A) Transverse section of Sema3B-GFP homozygous E12.5 embryo stained with DAPI. Endogenous GFP reports Sema3B expression and is quantified in the left-right axis of the FP (upper panel) and in the dorso-ventral axis (lower panel). Both distributions do not differ from a homogeneous distribution. The axon path is delineated by white dashed lines and the white arrows indicate the deposition of Sema3B-GFP along the glial cell processes. Data are shown as the mean ± s.e.m, KS test has been applied, n.s. (B) Schematic drawings of dual-tagged Slit2 construct and activity. Dual-tagged Slit2 coding sequence was cloned in pCAGEN vector. Full-length Slit2 (Slit2 FL) is fused to Cerulean at its N-terminal part and Venus at its C-terminal part. Slit2 FL is visualized with both fluorophores overlapping (white signal). Upon cleavage, Slit2N presence is reported by Cerulean fluorescence (here in purple) and Slit2C by Venus (here in green). (C) *In ovo* FP electroporation procedure. 48h after electroporation, embryos were fixed in PFA and sliced on vibratome. (D) 80μm transverse section of E4 chick spinal cord FP electroporated with dual-tagged Slit2. (E) Pearson coefficients quantify the degree of colocalization of Cerulean and Venus in FP electroporated with dual-tagged Slit2, through three compartments: apical, basal a, and basal b, as delimited by the dashed square in (D) (N= 3 embryos, 3 sections per embryo, 3 images analyzed per section). (F) Intensity ratio of the basal compartment over the apical compartment for Cerulean and Venus in FP electroporated with dual-tagged Slit2. (G) Schematic drawings of Slit2 isolated fragments fused to GFP. Both fusion protein coding sequence were cloned under the control of a HoxA1 promoter to drive the expression within the FP glial cells. (H) 80μm transverse sections of E4 chick spinal cord FP electroporated with isolated Slit2 fragments fused to GFP. The apical and basal compartment are delineated with yellow dashed lines. (I) Intensity ratio of the basal compartment over the apical compartment for GFP in FP electroporated with either Slit2N-GFP or Slit2C-GFP (N= 3 embryos, 3 sections per embryo, 3 images analyzed per section). (J) Comparison between the basal/apical intensity ratio of Slit2 isolated fragments compared to the basal/apical intensity ratio of Slit2N and Slit2C fragments generated by the cleavage of dual-tagged Slit2 FL. (K) Comparison between the basal membrane/apical domain intensity ratio of Slit2 isolated fragments compared to the basal membrane/apical domain ratio of Slit2N and Slit2C fragments generated by the cleavage of dual-tagged Slit2 FL. Data are shown as the mean ± s.d. in (E, F, I,

J, K), Student test has been applied, ns: non-significant, ***: P-value $p < 0.001$, ****: $p < 0.0001$. Scale bars: 10μm in (D, H), 50μm in (A).

Figure 6: Slit2 FL cleavage plays a role in the proper diffusion of the protein and is dependent on PC2

(A) Western blot detection of Cerulean and Venus in N2a cells transfected with either dual-tagged Slit2 FL or the uncleavable dual-tagged Slit2 FL Δ. An anti-GFP antibody was used, which recognizes Cerulean and Venus, two GFP derived fluorescent proteins. The protein sizes are indicated on the left (unit: kDa). (B) Thick transverse sections of E4 chick spinal cord FP electroporated with dual-tagged Slit2 FL or dual-tagged Slit2 FL Δ (uncleavable form deprived from the cleavage site generating Slit2N and Slit2C fragments). (C) Intensity ratio of the basal compartment over the apical compartment for Cerulean and Venus in FP electroporated with dual-tagged Slit2 FL or dual-tagged Slit2 FL Δ. (D) Western blot detection of Cerulean and Venus in N2a cells transfected with either dual-tagged Slit2 FL or the uncleavable dual-tagged Slit2 FL Δ and treated with PC2 inhibitor CMK. Tubulin is used as a loading control. (E-F) Ratio of the intensity of the Slit2 FL band (E) or the Slit2C band (F) over the intensity of tubulin band. (G) Immunofluorescent labelling of E4 chick spinal cord transverse sections using an antibody targeting PC2 (left panel) and DAPI (right panel). (H) Close-up of the PC2 labelling in the FP. (I) Quantification of the PC2 labelling in the three compartments delineated by yellow dashed lines. (J) Schematic representation of FP glial cells with Slit2 FL, Slit2 fragments, and PC2 distribution as seen in a transverse section (left side) or sagittal section (right side). Data are shown as the mean ± s.d. in (C-H) and Student test has been applied. ns: non-significant, *: $p < 0.05$, ***: $p < 0.001$. Scale bars = 10μm in (B, I), 80μm in (B, G, H).

Figure 7: PlxnA1Y1815F mutation confers to commissural growth cones navigating the FP a complex morphology

(A) Microphotograph of spinal cord open-books from chick embryo electroporated with pHluo-PlxnA1^{WT} or pHluo-PlxnA1^{Y1815F}, and immunolabeled with anti-BEN antibody and Atto-647 GFP nanobodies. BEN labeling delineates the FP. Note the complexification of growth cone morphology in the PlxnA1^{Y1815F} condition, with enlarged size and the presence of filopodia, compared with the PlxnA1^{WT} one. (B) Comparative analysis of the proportion of complex growth cones observed after

PlxnA1^{WT} and PlxnA1^{Y1815F} electroporation (PlxnA1^{WT}, N = 5 embryos, 367 growth cones; PlxnA1^{Y1815F}, N = 4 embryos, 199 growth cones). Spinal-cord open-books were subdivided in 3 fragments and observed by confocal microscopy as a dorso-ventral stack (27 stacks). A representative image for each condition is shown. Data are shown as the mean ± s.e.m, Student test has been applied, ***: P-value p < 0.001. (C) Microphotographs of representative growth cones from STEP microscopy of atto-647N-GFP nanobodies-labeled chick open-books. Note the complexity of PlxnA1^{Y1815F} growth cones compared to PlxnA1WT ones. Scale bar: 5 μm. (D) Microphotographs of cultured PlxnA1$^{Y1815F/Y1815F}$ commissural neuron illustrating representative growth cone morphologies exposed to different treatments. SlitC-GDNF-treated growth cones that were not collapsed exhibited a variety of shapes, some having a spread aspect, other long filopodia or forming a terminal branches pattern as shown with white arrows. (E) Histogram depicting the proportion of collapsed growth cones in the different experimental conditions (NB, N = 403; GDNF, N = 215; Sema3B, N = 215; SlitC, N = 197; GDNF+Sema3B, N = 406; GDNF+SlitC, N=363). The intermediate condition represents growth cones with a shrinked central domain but still having filopodia as shown in (D) with white arrows. Note that the presence of the Y1815F mutation in PlxnA1 reduced the growth cone collapse response, compared with Sema3B. Chi^2 test has been applied, ***: P-value p < 0.001. Scale bars: 5μm in (C,) 15μm in (D), 50μm in (A).

Figure 8: PlxnA1^{Y1815F} commissural growth cones have an increased exploratory behavior exerted through morphological split

(A) Analysis of growth cone behaviors with fast time-lapse sequences. Schematic representation of growth cone categories and microphotographs of representative growth cones. (B) Histogram of the quantification of exploratory growth cones in PlxnA1^{WT} and PlxnA1^{Y1815F} open-books (pHluo-PlxnA1^{WT}, N = 5 electroporated embryos, 89 growth cones; pHluo-PlxnA1^{Y1815F}, N = 3 electroporated embryos, 73 growth cones). Chi^2 test has been applied, ***: P-value p < 0.001. (C) Histogram depicting the mode of exploration adopted by PlxnA1^{WT} and PlxnA1^{Y1815F} growth cones. The percentage were calculated over the total growth cone population (pHluo-PlxnA1^{WT}, N = 5 electroporated embryos, 89 growth cones; pHluo-PlxnA1^{Y1815F}, N = 3 electroporated embryos, 73 growth cones). Chi^2 has been applied between non exploratory and split populations (**: P-value <0.01), and between non exploratory and

turned (ns: non-significant). (D) Time-lapse sequences of individual growth cones navigating the FP. The right panels show growth cone positions at time 0 and time 26. Note the simple, straight, and invariable aspect of the growth cone in the PlxnA1^{WT} condition. In contrast, the morphology of the PlxnA1^{Y1815F} growth cone is much complex and varies over time. Time interval: 8 min. (E) Quantification of growth cone width navigating the FP in PlxnA1^{WT} and PlxnA1^{Y1815F} open-books, showing significant enlargement of PlxnA1^{Y1815F} growth cones compared with PlxnA1^{WT} ones (pHluo-PlxnA1^{WT}, N = 4 electroporated embryos, 23 growth cones; pHluo-PlxnA1^{Y1815F}, N = 3 electroporated embryos, 25 growth cones). Data are shown as the mean ± s.e.m, Student test has been applied, ***: P-value $p < 0.001$. (F) Histograms of individual growth cone width, in μm, from t = 0 min to t = 122 min showing increased variations of width over time in the PlxnA1^{Y1815F} condition compared with the PlxnA1^{WT} one (pHluo-PlxnA1^{WT}, N = 4 electroporated embryos, 23 growth cones; pHluo-PlxnA1^{Y1815F}, N = 3 electroporated embryos, 25 growth cones). (G) Current and proposed novel model of the mechanisms ensuring proper midline crossing of spinal cord commissural axons. (a) In the current model, commissural axons acquire sensitivity to FP repellents after midline crossing, and whose graded expression drive their growth direction towards the FP exit. (b) In the proposed model, commissural axons perceive SlitC from their entry in the FP. The ligands are deposited on a mesh of basal process ramifications elaborated by the FP glia. Repeated contacts with the ligands prevent the growth cones from exploring the 3 dimensions of the territory, and are maintained straight. This mechanism is ensured by functional PlxnA1-SlitC signaling. (c) Growth cones expressing PlxnA1^{Y1815F} receptor failing to properly respond to SlitC elaborate a complex peripheral structure that enables them actively exploring their local environment, which disorganizes their trajectory, leading to drastic cases to back turning. Scale bars: 15μm in (A, D left), 50μm in (D right).

Supplementary Figure 1: generation of PlxnA1^{Y1815F} mutant strain

(A) Schematic representation of the PlxnA1^{Y1815F} allele. The selection cassette encoding neo is inserted in the region spanning exons 25 to 32. The homolog arms are indicated in 5′ and 3′. TAT>TTT (Y1815F) mutation is inserted in intron 30-31. The genotyping primers are indicated as yellow arrows. (B) Genotyping PCR products: the genotyping primers indicated in (A) amplify a 341bp fragment from the mutated allele (PlxnA1$^{Y1815F/Y1815F}$) and a 262bp fragment from the wild-type (PlxnA1$^{+/+}$) allele. (C)

Percentage of mice with each genotype coming from PlxnA1$^{Y1815F/+}$ x PlxnA1$^{Y1815F/+}$ crossing (N = 8 litters, 46 mice total). (D) Overall percentage of female and male mice (N = 41 litters, 220 mice total). Data are shown as the mean ± s.d, Student test has been applied, *: $p < 0.05$. (E) Representative electrophoresis of spinal cord lysates prepared from E12.5 PlxnA1$^{-/-}$, PlxnA1$^{+/+}$, PlxnA1$^{+/Y1815F}$, and PlxnA1$^{Y1815F/Y1815F}$ embryos, immunoblotted with anti-PlxnA1 and anti-actin antibodies. PlxnA1 is detected under two major forms, the integral form at 250kDa, and a short form at 55kDa. Black arrows point the 250kDa form found present at higher rate and the 55kDa form found present at lower rate in the PlxnA1^{Y1815F} condition, compared to the other genotypes.

Supplemental information

Movies S1-S4: pHluo-PlxnA1^{WT} (S1-S2) and pHluo-PlxnA1^{Y1815F} (S3-S4) are addressed to the cell surface of commissural growth cones during the FP navigation. White arrows point the growth cones during FP navigation. FP: floor plate.

Movies S5-S8: FRAP sequences of commissural growth cones in spinal cord open-books. The pHluo-receptor fluorescence in an area of 15 to 20μm^2 covering the entire growth cone surface was bleached at 80-90%. The recovery was measured over a period of 17 minutes.

Movie S9: 3D reconstruction with IMARIS software of axons navigating through the floor plate stained with DAPI (in blue), BEN (in white) and with mbTomato electroporated in axons (in red).

Movie S10: Same reconstitution as in Movie S1 but on a limited slice of spinal cord cut in the rostro-caudal axis.

Movie S11: The surface of a single axon from movie S2 has been reconstructed.

Movie S12: 3D reconstruction from a Math1-mbTomato and Hoxa1-GFP electroporation. A single Math1-mbTomato (in red) electroporated axon is navigating through the basal end-feet of a Hoxa1-GFP (in white) electroporated floor-plate cell.

Movies S13-S16: Sequences of time-lapse movies of chick open-books at fast time intervals (8 minutes) illustrating the navigation behaviors of PlxnA1^{WT} growth cones (S13-S14) and PlxnA1^{Y1815F} growth cones (S15-S16).

Figure 1

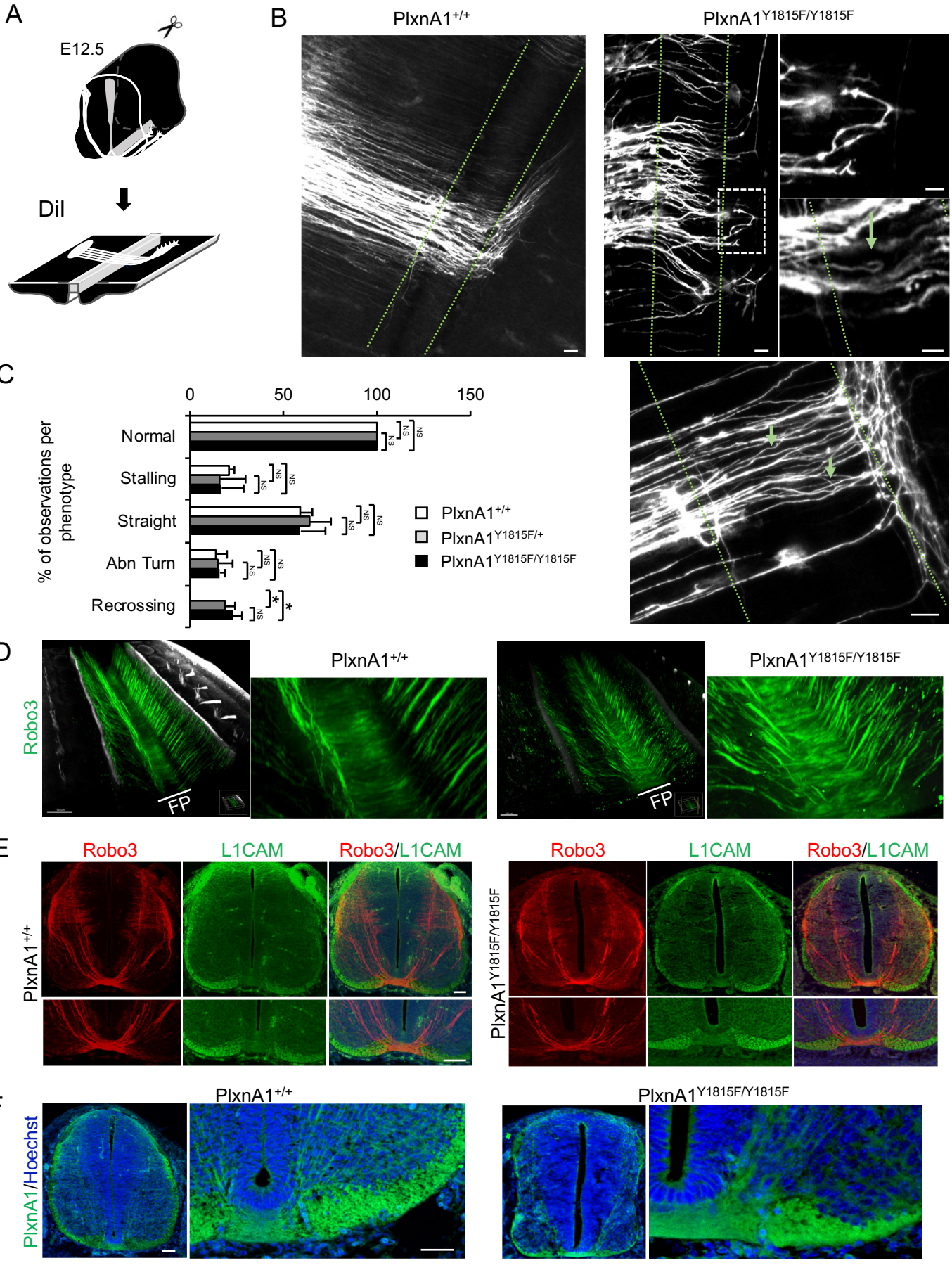
A
E12.5
DiI
B
PlxnA1+/+
PlxnA1Y1815F/Y1815F
C
% of observations per phenotype
Normal
Stalling
Straight
Abn Turn
Recrossing
0
50
100
150
NS
*
PlxnA1+/+
PlxnA1Y1815F/+
PlxnA1Y1815F/Y1815F
D
Robo3
FP
PlxnA1+/+
PlxnA1Y1815F/Y1815F
E
Robo3
L1CAM
Robo3/L1CAM
PlxnA1+/+
PlxnA1Y1815F/Y1815F
F
PlxnA1/Hoechst
PlxnA1+/+
PlxnA1Y1815F/Y1815F

Figure 2

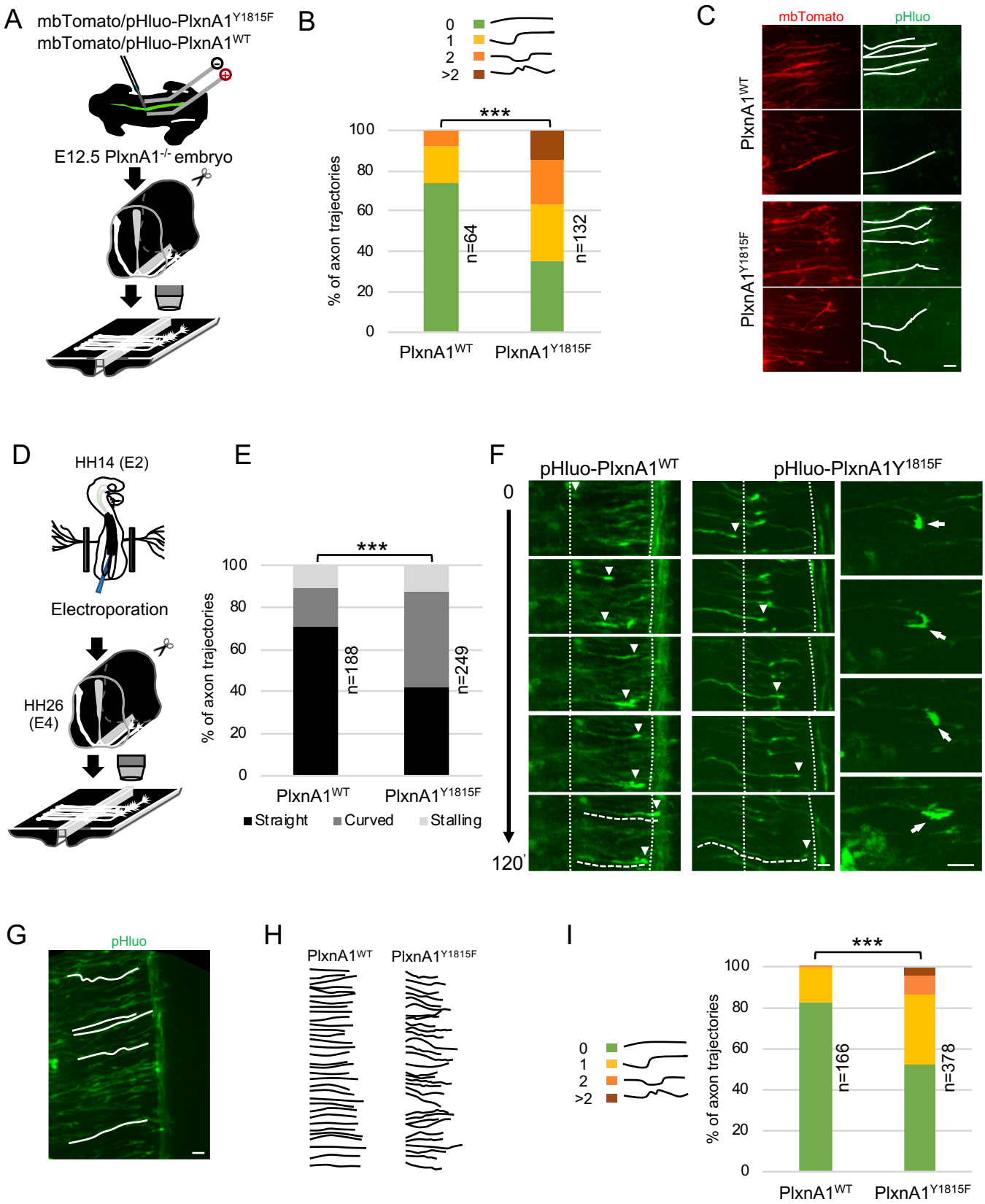
A
mbTomato/pHluo-PlxnA1Y1815F
mbTomato/pHluo-PlxnA1WT
E12.5 PlxnA1-/- embryo
B
0
1
2
>2
***
% of axon trajectories
n=64
n=132
PlxnA1WT
PlxnA1Y1815F
C
mbTomato
pHluo
PlxnA1WT
PlxnA1Y1815F
D
HH14 (E2)
Electroporation
HH26
(E4)
E
***
% of axon trajectories
n=188
n=249
PlxnA1WT
PlxnA1Y1815F
Straight
Curved
Stalling
F
pHluo-PlxnA1WT
pHluo-PlxnA1Y1815F
0
120'
G
pHluo
H
PlxnA1WT
PlxnA1Y1815F
I
0
1
2
>2
***
% of axon trajectories
n=166
n=378
PlxnA1WT
PlxnA1Y1815F

Figure 3

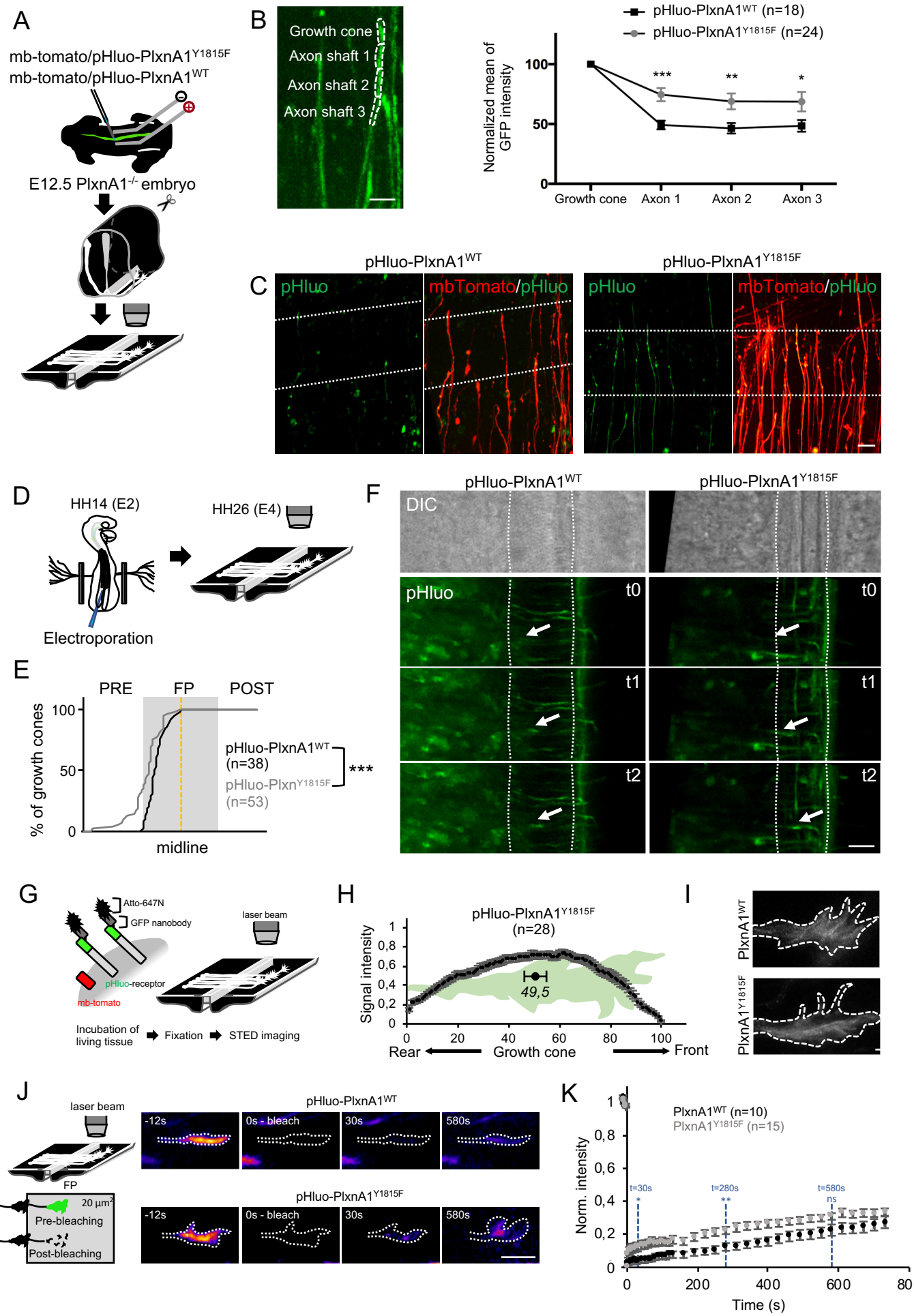
A
mb-tomato/pHluo-PlxnA1Y1815F
mb-tomato/pHluo-PlxnA1WT
E12.5 PlxnA1-/- embryo
B
Growth cone
Axon shaft 1
Axon shaft 2
Axon shaft 3
pHluo-PlxnA1WT (n=18)
pHluo-PlxnA1Y1815F (n=24)
Normalized mean of GFP intensity
100
50
0
***
**
*
Growth cone
Axon 1
Axon 2
Axon 3
C
pHluo-PlxnA1WT
pHluo-PlxnA1Y1815F
pHluo
mbTomato/pHluo
D
HH14 (E2)
HH26 (E4)
Electroporation
E
PRE
FP
POST
% of growth cones
100
50
0
pHluo-PlxnA1WT (n=38)
pHluo-PlxnY1815F (n=53)
***
midline
F
pHluo-PlxnA1WT
pHluo-PlxnA1Y1815F
DIC
pHluo
t0
t1
t2
G
Atto-647N
GFP nanobody
laser beam
pHluo-receptor
mb-tomato
Incubation of living tissue
Fixation
STED imaging
H
pHluo-PlxnA1Y1815F (n=28)
Signal intensity
1
0,8
0,6
0,4
0,2
0
49,5
0
20
40
60
80
100
Rear
Growth cone
Front
I
PlxnA1WT
PlxnA1Y1815F
J
laser beam
FP
20 µm2
Pre-bleaching
Post-bleaching
pHluo-PlxnA1WT
pHluo-PlxnA1Y1815F
-12s
0s - bleach
30s
580s
K
PlxnA1WT (n=10)
PlxnA1Y1815F (n=15)
Norm. intensity
1
0,8
0,6
0,4
0,2
0
t=30s
t=280s
t=580s
*
**
ns
0
200
400
600
800
Time (s)

Figure 4

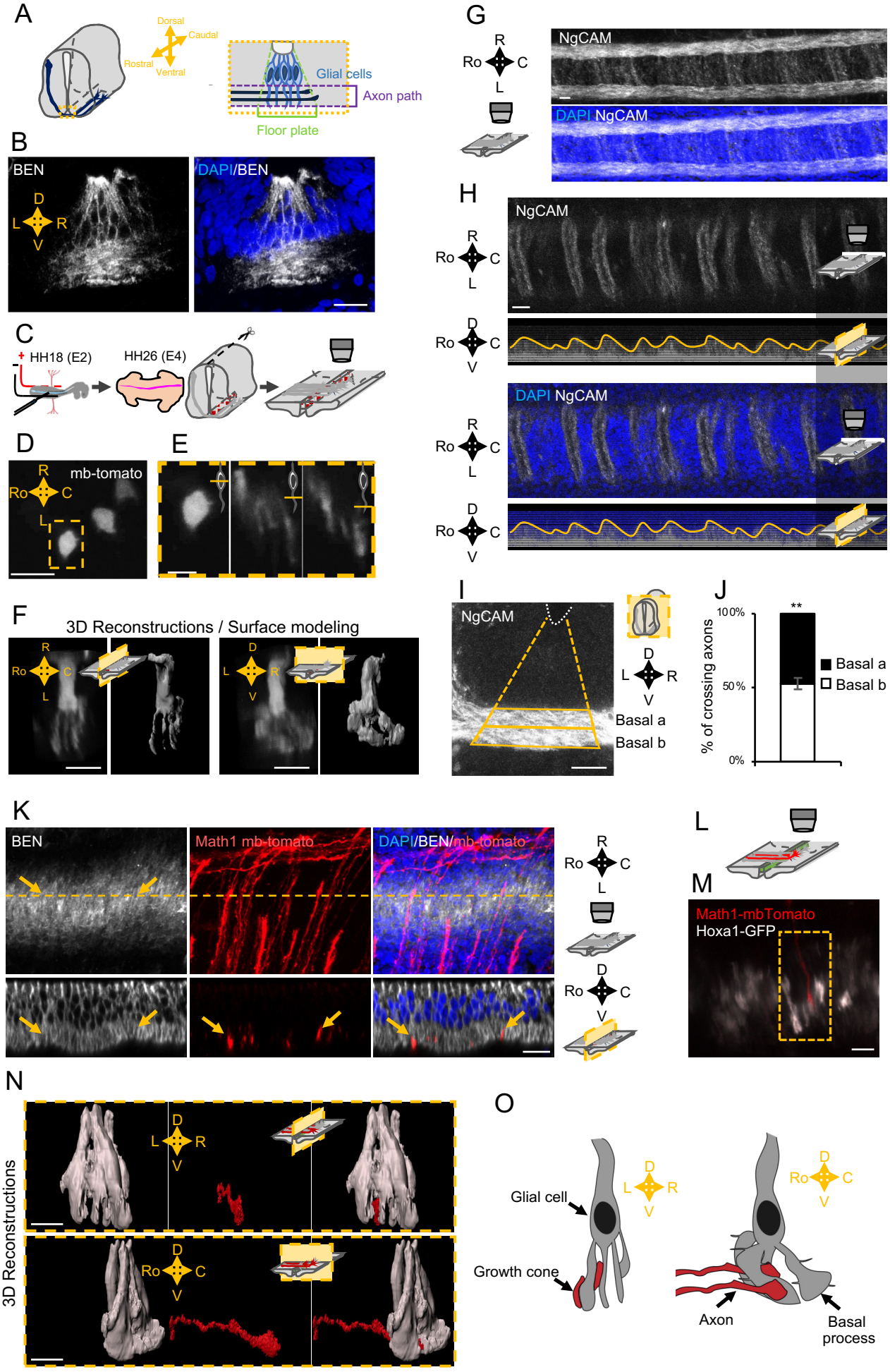
A
Dorsal
Caudal
Rostral
Ventral
Glial cells
Axon path
Floor plate
B
BEN
DAPI/BEN
C
HH18 (E2)
HH26 (E4)
D
mb-tomato
E
F
3D Reconstructions / Surface modeling
G
NgCAM
DAPI NgCAM
H
NgCAM
DAPI NgCAM
I
NgCAM
Basal a
Basal b
J
% of crossing axons
100%
50%
0%
**
Basal a
Basal b
K
BEN
Math1 mb-tomato
DAPI/BEN/mb-tomato
L
M
Math1-mbTomato
Hoxa1-GFP
N
3D Reconstructions
O
Glial cell
Growth cone
Axon
Basal process

Figure 5

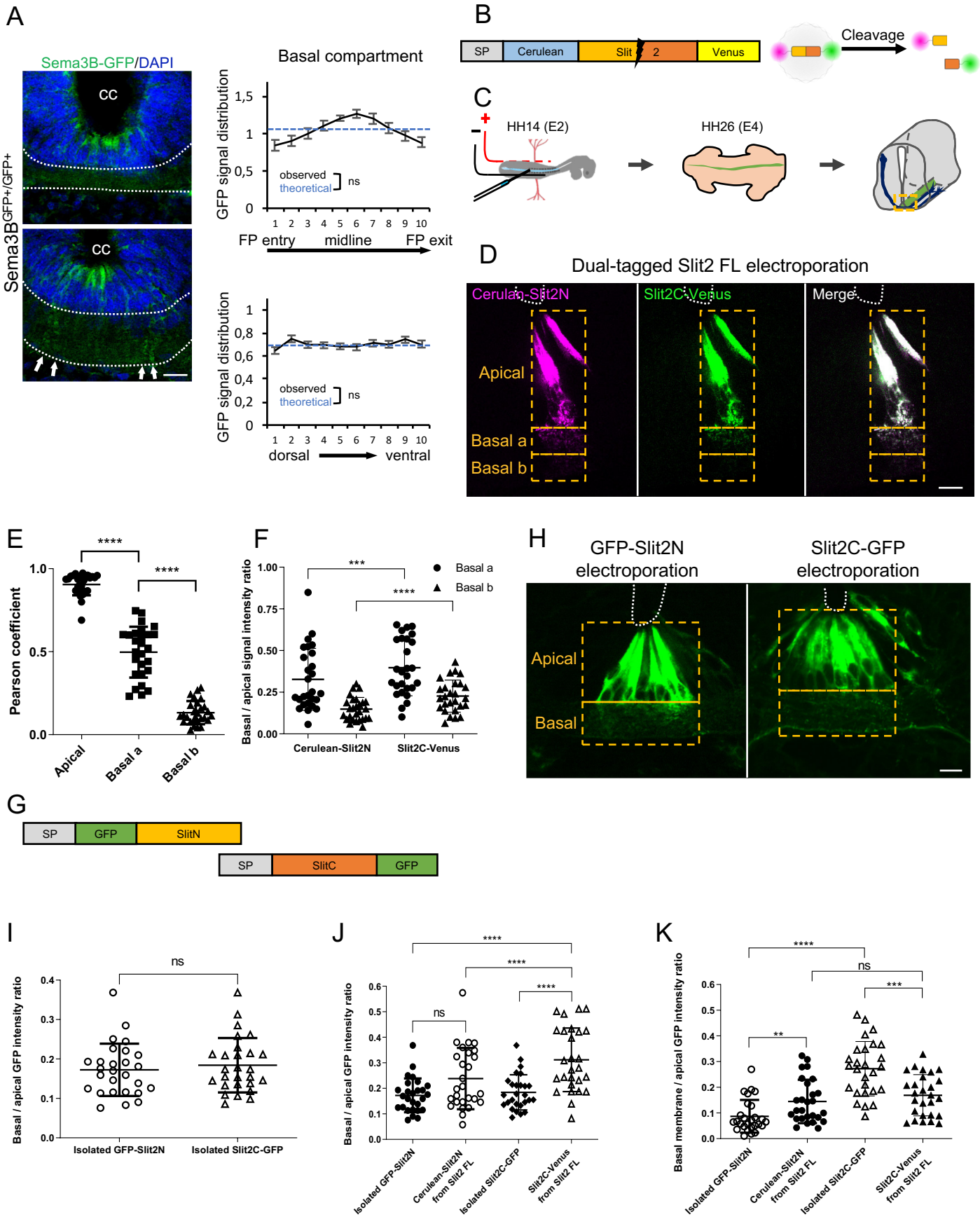
A
Sema3B-GFP/DAPI
Sema3BGFP+/GFP+
CC
CC
Basal compartment
GFP signal distribution
observed
theoretical
ns
FP entry
midline
FP exit
dorsal
ventral
B
SP
Cerulean
Slit
2
Venus
Cleavage
C
HH14 (E2)
HH26 (E4)
D
Dual-tagged Slit2 FL electroporation
Cerulean-Slit2N
Slit2C-Venus
Merge
Apical
Basal a
Basal b
E
Pearson coefficient
Apical
Basal a
Basal b
F
Basal / apical signal intensity ratio
Basal a
Basal b
Cerulean-Slit2N
Slit2C-Venus
H
GFP-Slit2N electroporation
Slit2C-GFP electroporation
Apical
Basal
G
SP
GFP
SlitN
SP
SlitC
GFP
I
Basal / apical GFP intensity ratio
ns
Isolated GFP-Slit2N
Isolated Slit2C-GFP
J
Basal / apical GFP intensity ratio
ns
Isolated GFP-Slit2N
Cerulean-Slit2N from Slit2 FL
Isolated Slit2C-GFP
Slit2C-Venus from Slit2 FL
K
Basal membrane / apical GFP intensity ratio
ns
Isolated GFP-Slit2N
Cerulean-Slit2N from Slit2 FL
Isolated Slit2C-GFP
Slit2C-Venus from Slit2 FL

Figure 6

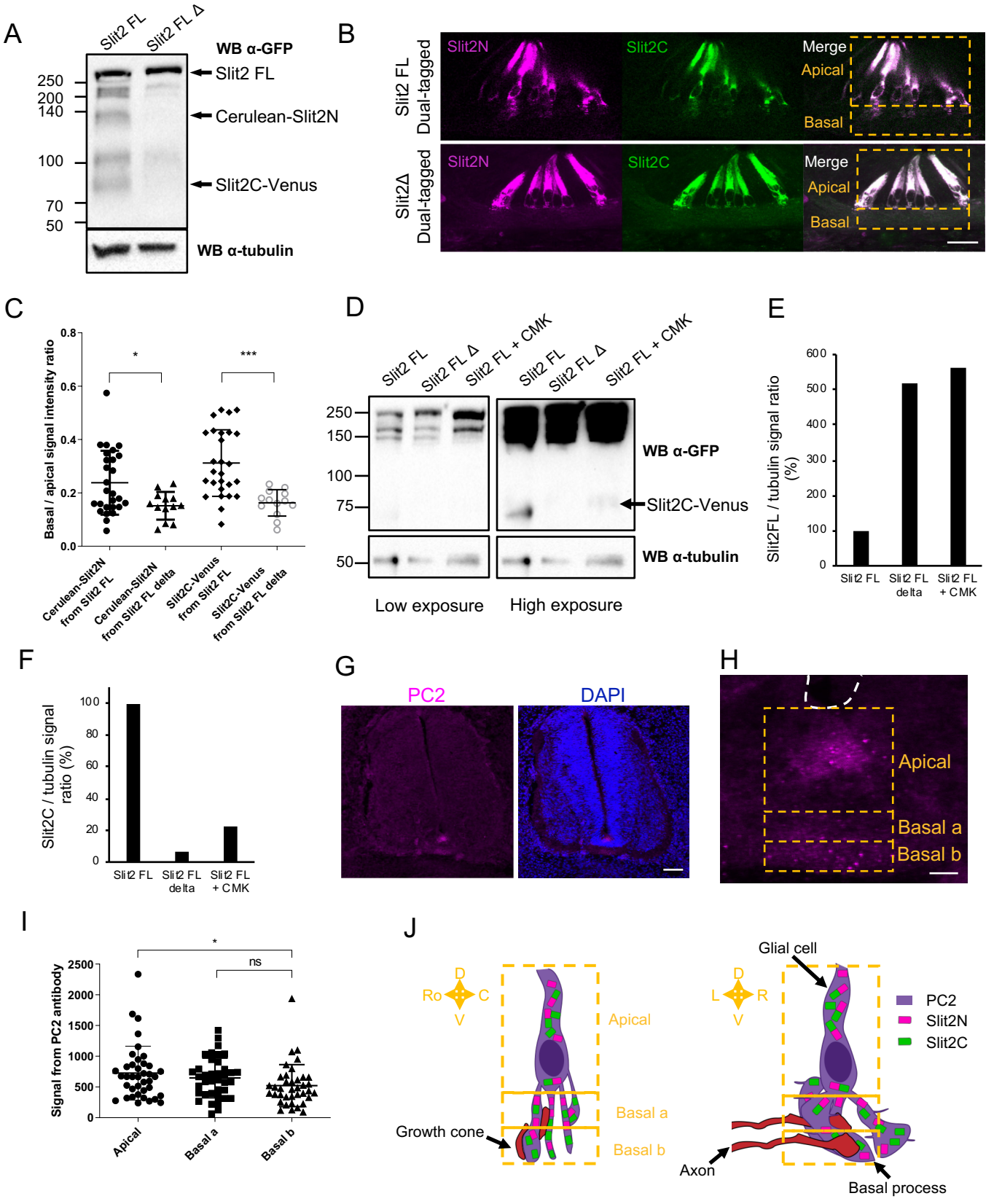
A
Slit2 FL
Slit2 FL Δ
WB α-GFP
250
200
140
100
70
50
Slit2 FL
Cerulean-Slit2N
Slit2C-Venus
WB α-tubulin
B
Slit2 FL Dual-tagged
Slit2Δ Dual-tagged
Slit2N
Slit2C
Merge
Apical
Basal
C
Basal / apical signal intensity ratio
0.8
0.6
0.4
0.2
0.0
*
***
Cerulean-Slit2N from Slit2 FL
Cerulean-Slit2N from Slit2 FL delta
Slit2C-Venus from Slit2 FL
Slit2C-Venus from Slit2 FL delta
D
Slit2 FL
Slit2 FL Δ
Slit2 FL + CMK
250
150
100
75
50
WB α-GFP
Slit2C-Venus
WB α-tubulin
Low exposure
High exposure
E
Slit2FL / tubulin signal ratio (%)
600
500
400
300
200
100
0
Slit2 FL
Slit2 FL delta
Slit2 FL + CMK
F
Slit2C / tubulin signal ratio (%)
100
80
60
40
20
0
Slit2 FL
Slit2 FL delta
Slit2 FL + CMK
G
PC2
DAPI
H
Apical
Basal a
Basal b
I
Signal from PC2 antibody
2500
2000
1500
1000
500
0
*
ns
Apical
Basal a
Basal b
J
D
Ro
C
V
Apical
Basal a
Basal b
Growth cone
Glial cell
D
L
R
V
PC2
Slit2N
Slit2C
Axon
Basal process

Figure 7

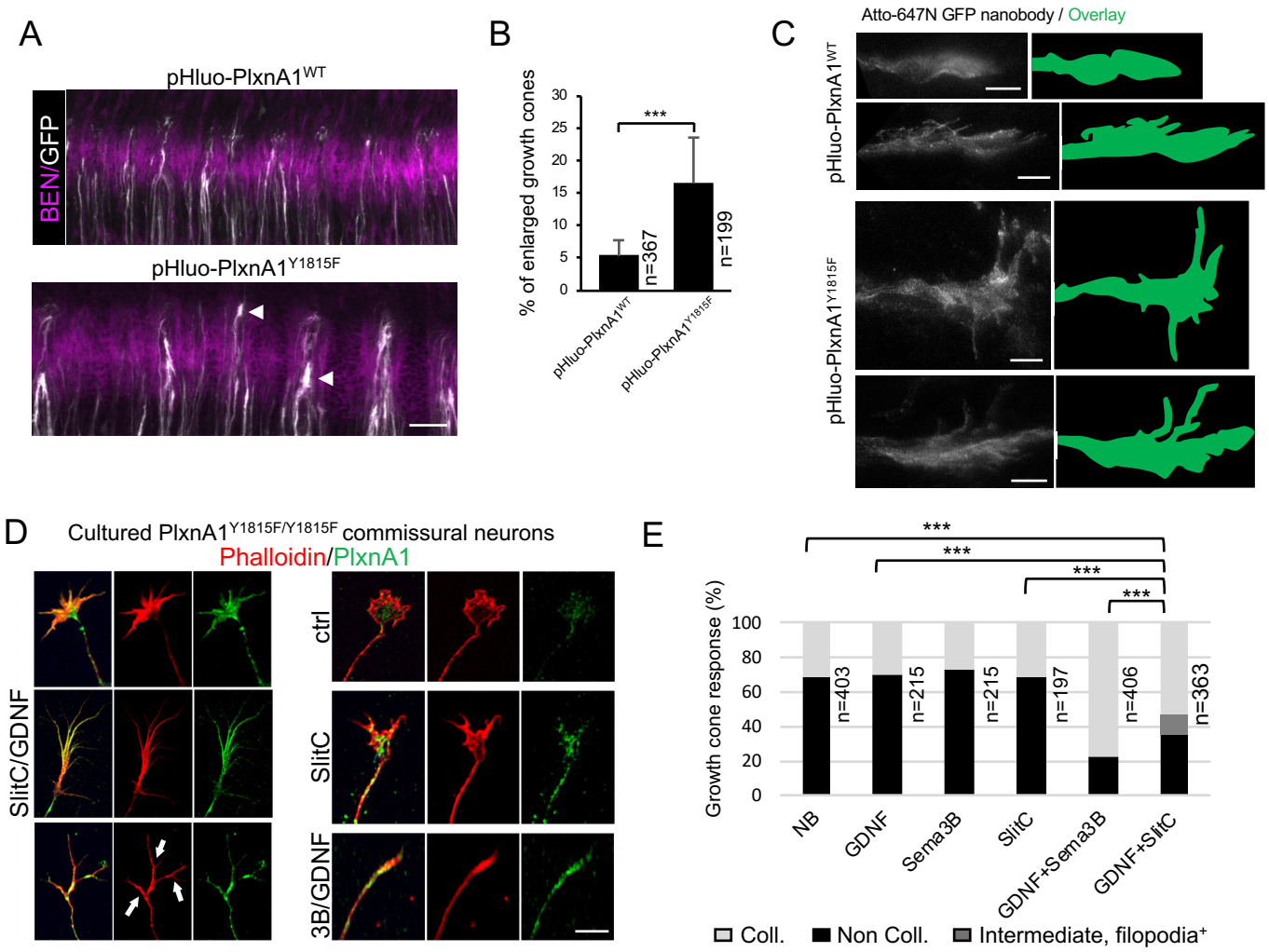
A
pHluo-PlxnA1WT
BEN/GFP
pHluo-PlxnA1Y1815F
B
% of enlarged growth cones
30
25
20
15
10
5
0
***
n=367
n=199
pHluo-PlxnA1WT
pHluo-PlxnA1Y1815F
C
Atto-647N GFP nanobody / Overlay
pHluo-PlxnA1WT
pHluo-PlxnA1Y1815F
D
Cultured PlxnA1Y1815F/Y1815F commissural neurons
Phalloidin/PlxnA1
SlitC/GDNF
ctrl
SlitC
3B/GDNF
E
Growth cone response (%)
100
80
60
40
20
0
***
***
***
***
n=403
n=215
n=215
n=197
n=406
n=363
NB
GDNF
Sema3B
SlitC
GDNF+Sema3B
GDNF+SlitC
Coll.
Non Coll.
Intermediate, filopodia+

Figure 8

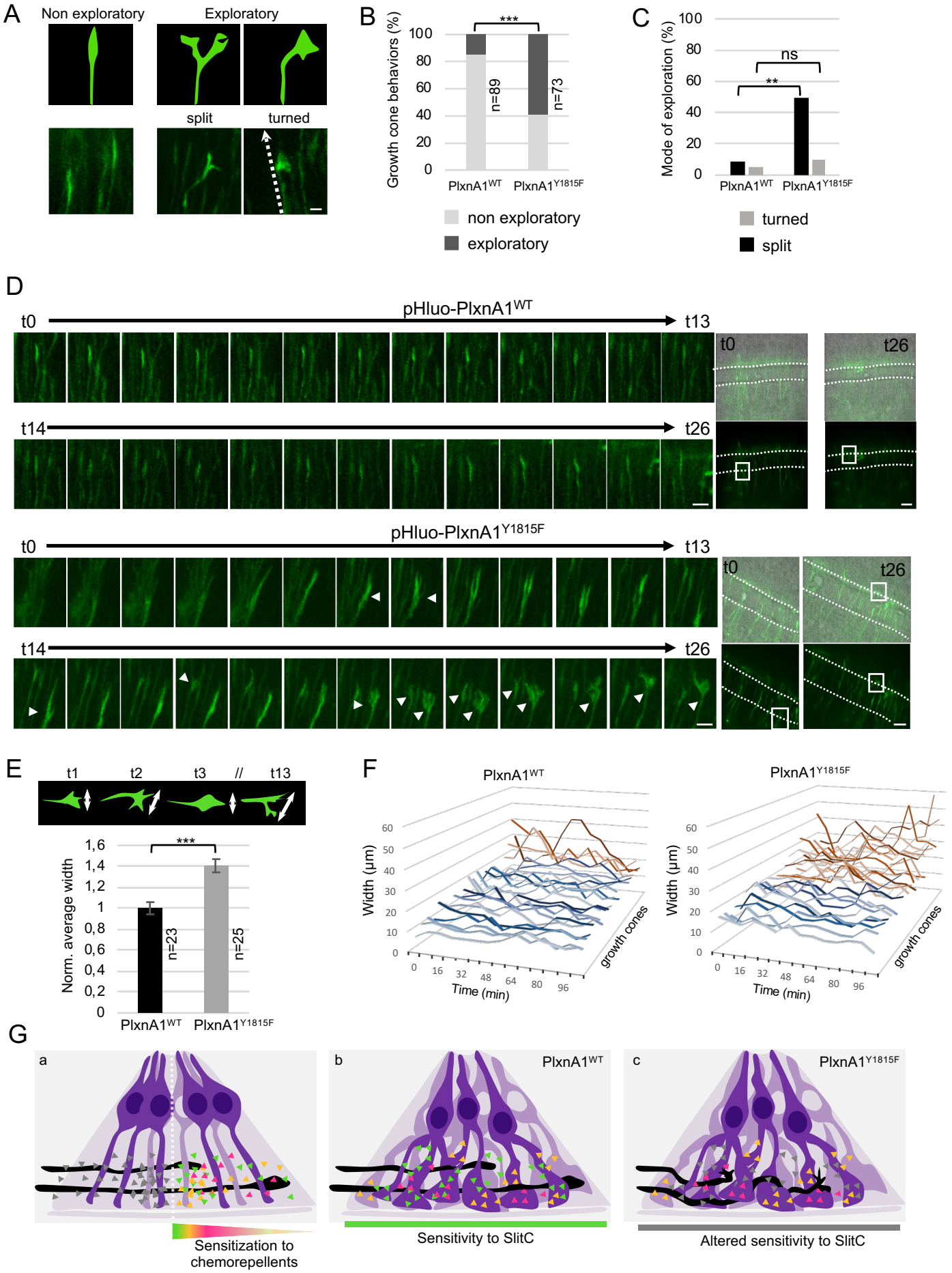
A
Non exploratory
Exploratory
split
turned
B
Growth cone behaviors (%)
***
n=89
n=73
PlxnA1WT
PlxnA1Y1815F
non exploratory
exploratory
C
Mode of exploration (%)
ns
**
PlxnA1WT
PlxnA1Y1815F
turned
split
D
pHluo-PlxnA1WT
t0
t13
t14
t26
pHluo-PlxnA1Y1815F
E
t1
t2
t3
//
t13
Norm. average width
***
n=23
n=25
PlxnA1WT
PlxnA1Y1815F
F
PlxnA1WT
PlxnA1Y1815F
Width (µm)
growth cones
Time (min)
G
a
b
PlxnA1WT
c
PlxnA1Y1815F
Sensitization to chemorepellents
Sensitivity to SlitC
Altered sensitivity to SlitC

Supplementary Figure 1

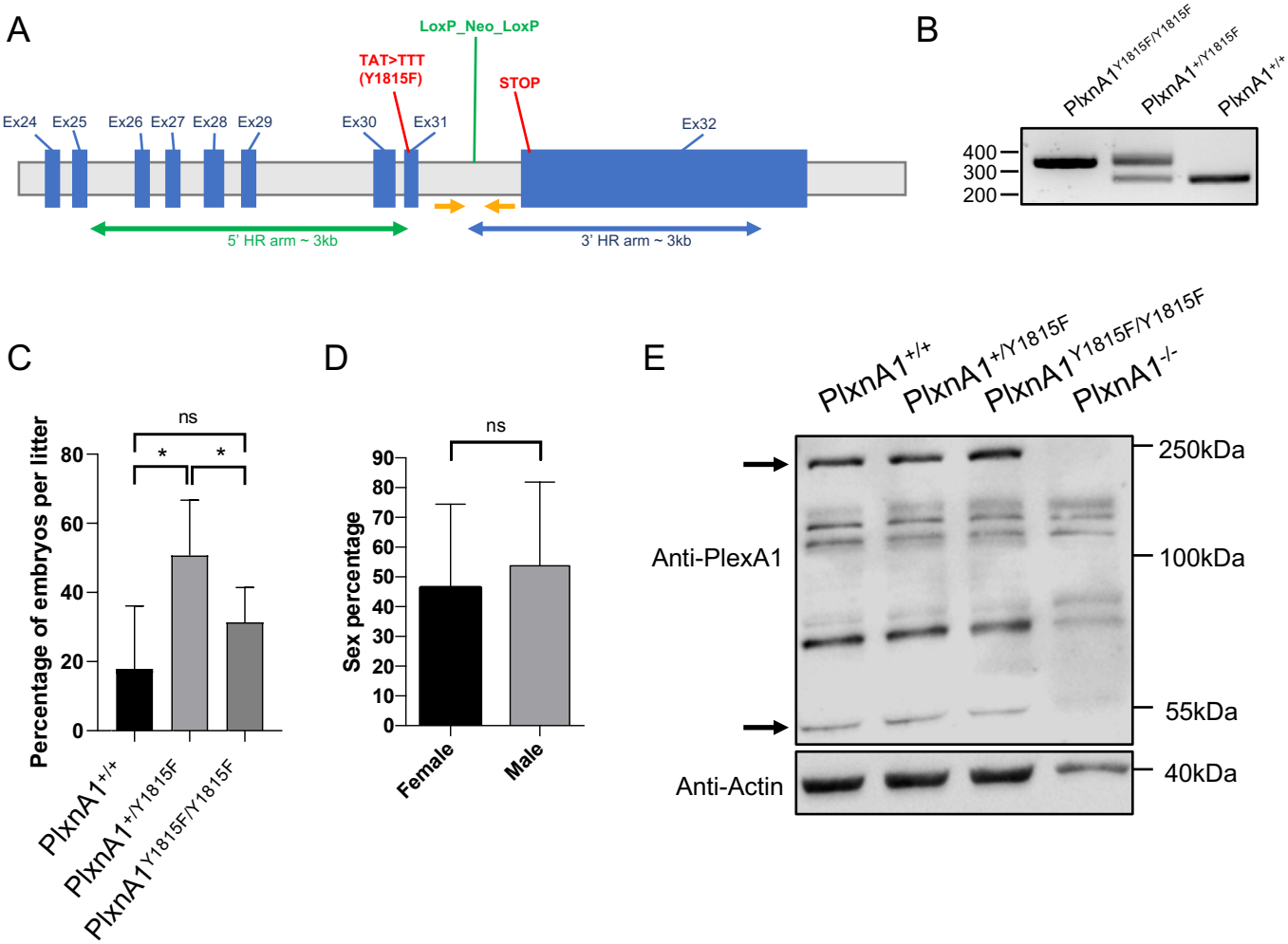

III. Résultats supplémentaires

1. Etude du clivage de Slit

D'après les résultats obtenus avec le Slit2 DT, le clivage de Slit permet la diffusion des fragments dans le domaine basal de la PP. Ainsi, une hétérogénéité de clivage de Slit pourrait contrôler un patterning local des signalisations Slit. Nous souhaitions donc déterminer si les cellules de la PP présentent toutes la même capacité à cliver Slit. Cependant, la protéase de Slit étant encore inconnue, il n'existe pas d'outil permettant d'étudier ce clivage *in vivo*. J'ai donc développé un biosenseur à partir du site de clivage de Slit. Pour cela, je me suis inspiré d'un rapporteur de l'activité des caspases (Wu, Nicholls and Hardy, 2013). La protéine GFP est reliée à un peptide quenchant qui va se tétramériser et empêcher la maturation de la GFP par gêne stérique, gardant ainsi la GFP dans un état « sombre » (Fig. 9A, 9B). La GFP et le peptide sont reliés par le site de clivage de la protéine d'intérêt. L'activité de la protéase va donc libérer la GFP du tétramère et permettre la maturation de son fluorophore puis sa fluorescence. Si Nicholls et Hardy ont nommé leur outil CA-GFP pour Caspase Activatable-GFP, j'utiliserai également le terme de CA-GFP pour Cleavage Activatable-GFP.

Le développement de cet outil était ambitieux puisque la séquence de clivage exacte n'est pas connue. De plus, la taille de la séquence séparant la GFP du peptide quenchant influence la gêne stérique. Ainsi, une séquence trop grande donnera une trop grande flexibilité à la construction et ne permettra pas d'empêcher la maturation de la GFP. A l'inverse, une séquence trop petite ne sera pas reconnue par la protéase. J'ai donc développé trois variantes différentes de cet outil (longue, moyenne et courte) pour obtenir le meilleur compromis entre gêne stérique efficace et clivage efficace. Ainsi, la séquence de clivage de la version longue est constituée des 40 acides aminés bordant le site de clivage, celle de la version moyenne est constituée de 16 acides aminés, et celle de la version courte est constituée de 8 acides aminés (Fig. 9B). Pour comparaison, les CA-GFP développées par Nicholls et Hardy présentent entre 4 et 8 acides aminés au niveau de la séquence de clivage. Notre version CA-GFP courte est donc celle qui se rapproche le plus de l'outil d'origine.

J'ai également utilisé un IRES-tdTomato comme témoin d'expression. Ainsi, il est possible de visualiser les cellules exprimant la CA-GFP mais ne pouvant pas cliver Slit. De plus, en normalisant l'intensité du signal CA-GFP par celle de la tdTomato, il est possible de comparer l'efficacité de clivage des cellules.

Afin de tester cet outil, j'ai électroporé les versions longue et courte dans des PP de poulet. A E4, les cellules électroporées présentent un signal GFP dans les deux conditions (Fig. 9C). J'ai décidé d'utiliser la version CA-GFP courte car elle permet une meilleure gêne stérique que la version longue, tout en pouvant présenter un signal GFP.

En parallèle, j'ai cherché à m'assurer de la spécificité de la CA-GFP. Le test le plus direct aurait été d'inhiber la protéase de Slit pour voir l'impact sur le signal GFP. Cependant, la protéase étant inconnue, je n'ai pu réaliser ce test. J'ai donc dû développer une version non clivable de notre outil. Pour cela, je n'ai pas pu réaliser la même délétion que pour Slit2 Δ pour plusieurs raisons : 1) les acides aminés délétés dans Slit2 Δ ne sont pas tous présents dans la séquence de clivage courte ; 2) la séquence de clivage jouant sur la gêne stérique, diminuer sa taille n'aurait pas été un bon témoin négatif. J'ai donc cherché à réaliser un témoin négatif en mutant la séquence de clivage – plus précisément en remplaçant les 2 résidus bordant le site du clivage en Proline (Slit2 PP) ou en Glycine (Slit2 GG) (Fig. 9D). J'ai d'abord effectué ces mutations sur le Slit2 DT afin de vérifier l'inhibition du clivage *in vitro*. Les WB obtenus m'ont indiqué que le premier mutant (Slit2 PP) ne s'exprime pas correctement – possiblement à cause d'un coude créé par la substitution en Proline – alors que le second mutant (Slit2 GG) s'exprime correctement. De plus, Slit2 GG permet l'inhibition incomplète du clivage (Fig. 9E). Ce résultat en fait un bon candidat pour tester la spécificité du signal CA-GFP.

Pour tester la spécificité de l'outil dans des conditions proches de l'*in vivo* tout en s'astreignant des variations rostro-caudale, j'ai développé un protocole *in vitro* utilisant des cellules de PP dissociées. Des résultats préliminaires ont permis de montrer que la CA-GFP GG possède une intensité du signal inférieure à celle de la CA-GFP clivable (Fig. 9F). Ainsi, la fluorescence de l'outil semble être liée à l'activité du clivage de Slit. Cependant, plus d'études restent nécessaires pour confirmer la corrélation.

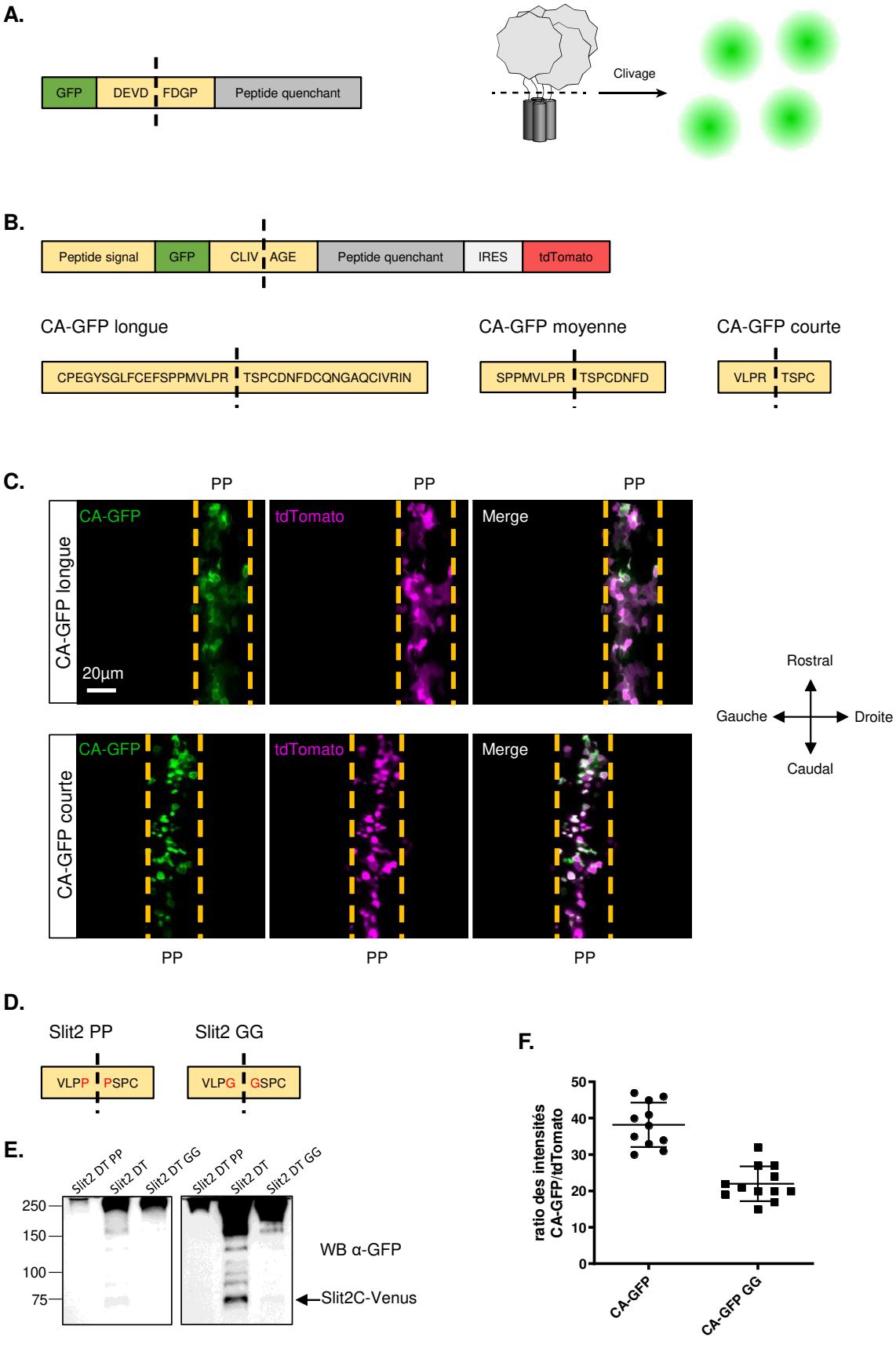
A.
GFP
DEVD
FDGP
Peptide quenchant
Clivage
B.
Peptide signal
GFP
CLIV
AGE
Peptide quenchant
IRES
tdTomato
CA-GFP longue
CPEGYSGLFCEFSPPMVLPR
TSPCDNFDCQNGAQCIVRIN
CA-GFP moyenne
SPPMVLPR
TSPCDNFD
CA-GFP courte
VLPR
TSPC
C.
PP
PP
PP
CA-GFP
tdTomato
Merge
CA-GFP longue
20µm
CA-GFP
tdTomato
Merge
CA-GFP courte
PP
PP
PP
Rostral
Gauche
Droite
Caudal
D.
Slit2 PP
Slit2 GG
VLPP
PSPC
VLPG
GSPC
E.
Slit2 DT PP
Slit2 DT
Slit2 DT GG
Slit2 DT PP
Slit2 DT
Slit2 DT GG
250
150
100
75
WB α-GFP
Slit2C-Venus
F.
ratio des intensités CA-GFP/tdTomato
50
40
30
20
10
0
CA-GFP
CA-GFP GG

Figure 9. Développement d'un biosenseur pour visualiser le clivage de Slit2 *in vivo*

(**A**) Présentation de la GFP Activable par les Caspase (CA-GFP) développée par Nicholls et Hardy. La GFP est fusionnée à un peptide quenchant dont la tétramérisation va empêcher la maturation du chromophore de la GFP. La séquence de clivage entre la GFP et le peptide quenchant va permettre, après l'activation des caspases, la libération de la GFP, puis la maturation de son chromophore et enfin sa fluorescence. (**B**) Présentation de notre outil CA-GFP adapté au clivage de Slit2. Un IRES-tdtomato sert de témoin d'expression. Trois versions différentes ont été développées en variant la taille de la séquence de clivage : la version longue contient les 40 acides aminés bordant le site de clivage de Slit2 ; la version moyenne en contient 16 ; la version courte en contient 8. (**C**) Imagerie livre-ouvert de plaques du plancher (PP) d'embryons de poulet à E4 électroporées avec les versions CA-GFP longue et courte. (**D**) Développement d'une version non clivable de la CA-GFP courte par mutation. (**E**) Western-blot des versions Slit2 double tag mutées pour vérifier l'inhibition du clivage. (**F**) Quantification de l'intensité CA-GFP dans des cellules de PP dissociées (n=1 expérience, 12 cellules par condition).

2. Saptio-temporalité des signalisations de guidage axonal dans la plaque du plancher

Les travaux d'Aurora Pignata ont montré que, lors de la traversée, les différents récepteurs de guidage ne sont pas adressés à la membrane au même moment, ni au même endroit du CC. Cela permet une régulation de l'activation des signalisations répulsives. Cependant, la présence d'un récepteur à la surface n'équivaut pas à son activation. Ainsi, des différences spatio-temporelles d'activation pourraient expliquer les différences d'effet des signalisations répulsives de la PP. Pour étudier la spatio-temporalité de ces signalisations, il est possible d'étudier l'interaction ligand/récepteur ou bien l'activation de facteurs en aval. Comme expliqué dans l'introduction, les signalisations du guidage axonal partagent de nombreux acteurs en aval des récepteurs ce qui rend difficile l'association d'un acteur avec une signalisation particulière. De plus, dans le cas de SlitC/PlxnA1, ces acteurs ne sont pas connus. Nous avons donc choisi d'étudier l'activation des signalisations de guidage en suivant les interactions ligand/récepteur. Pour ce faire, j'ai développé un test d'interaction protéine/protéine basé sur la complémentation de fluorescence bimoléculaire (ou BiFC pour Bimolecular Fluorescence Complementation). Dans ce test, une protéine rapportrice fluorescente est séparée en deux et les fragments sont fusionnées aux deux partenaires d'intérêts. L'interaction des partenaires rapproche les fragments ce qui permet la reconstitution de la protéine rapportrice et, *in fine*, sa fluorescence (Fig. 10A).

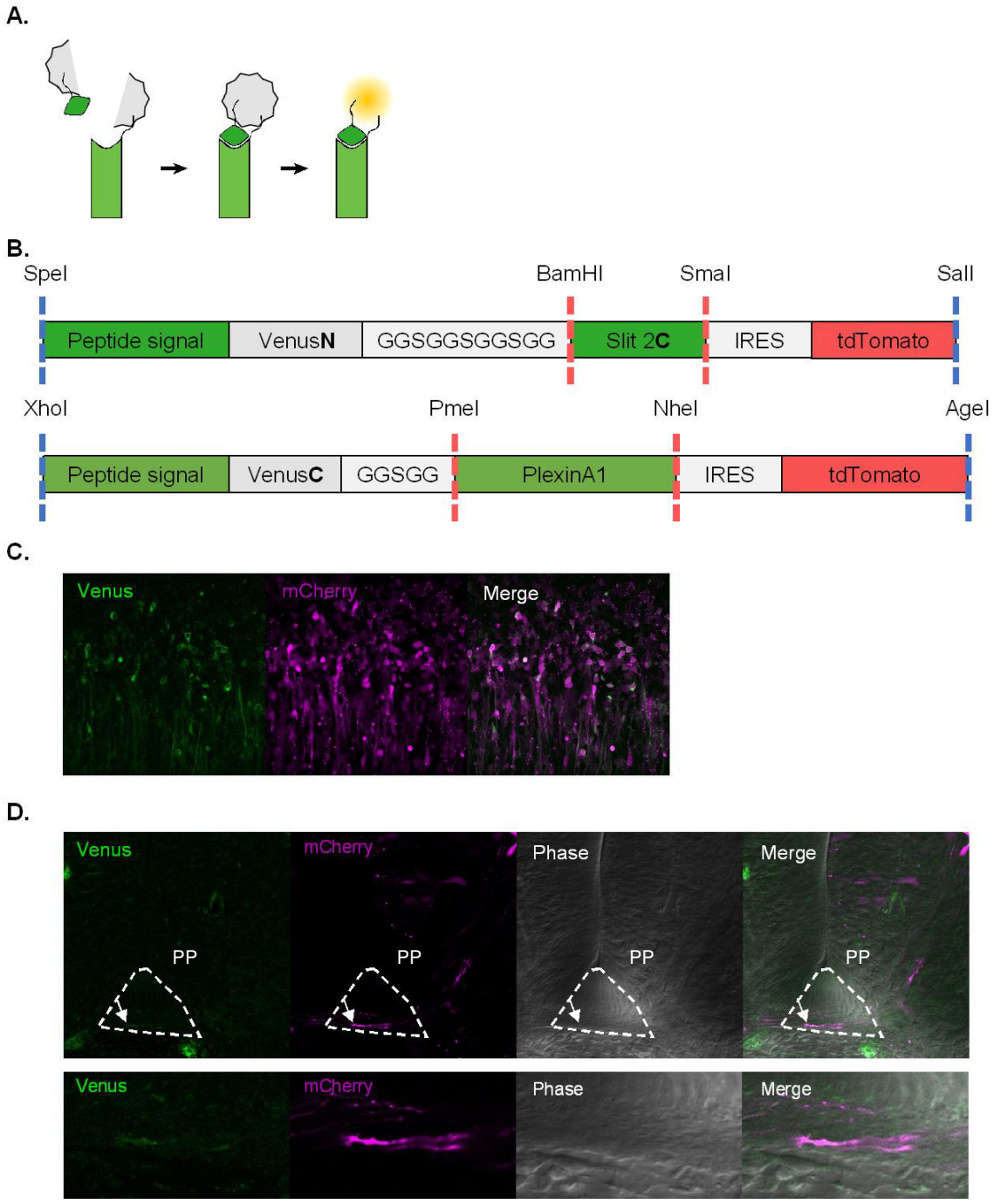

Figure 10. Développement d'une technique de complémentation de fluorescence bimoléculaire pour cartographier *in vivo* l'interaction entre ligand et récepteur du guidage axonal

(**A**) Représentation schématique de la complémentation de fluorescence bimoléculaire (BiFC). Une protéine fluorescente rapportrice est séparée en deux fragments et chaque fragment est fusionné à un partenaire du complexe d'intérêt. L'interaction des deux partenaires permet la reconstitution de la protéine rapportrice, puis sa fluorescence. (**B**) Constructions développées pour étudier l'interaction Slit2C/PlxnA1 tout en permettant un clonage facile pour étudier d'autres couples. (**C**) Imagerie en livre-ouvert de neurones exprimant le ligand et le récepteur de BiFC pour contrôler la reconstitution de la protéine rapportrice. (**D**) Coupe d'un embryon de poulet à E4 dont les neurones ont été électroporés avec le ligand et le récepteur de BiFC. La flèche montre un cône de croissance navigant dans la plaque du plancher et présentant un signal BiFC. La rangée du bas est un agrandissement au niveau du CC.

La conception de cet outil a nécessité une réflexion particulière de par sa complexité. Nous avons ainsi eu l'occasion de travailler avec Samir Merabet, référence lyonnaise de la BiFC, qui nous a aiguillés sur les différents paramètres à prendre en compte :

- La protéine rapportrice : certaines protéines fluorescentes se reconstituent plus facilement que d'autres et donnent un signal plus important. Ainsi, nous avons choisi d'utiliser la protéine Venus ;
- La séquence des fragments : en fonction de la séparation des fragments, la protéine fluorescente se reconstituera plus ou moins facilement. De plus, en conservant une partie chevauchante entre les deux fragments, la reconstitution est améliorée. Notre fragment N-terminal (VenusN) est donc constitué des acides aminés 1 à 173, et notre fragment C-terminal (VenusC) des acides aminés 155 à 243 ;
- Le choix du fragment à fusionner aux protéines d'intérêt : les deux fragments n'ayant pas la même taille, nous avons décidé de fusionner le plus petit au récepteur pour ne pas perturber la temporalité de son adressage à la membrane ;
- La taille du linker : il est important de placer une séquence de liaison permettant une mobilité des fragments de Venus, ce qui facilite leur interaction. Cependant, une séquence trop grande va permettre la reconstitution de la Venus, même en l'absence d'interaction des protéines d'intérêt. En revanche, un linker trop court pourrait rendre la construction trop rigide et empêcher la reconstitution. C'est pourquoi nous avons choisi d'utiliser un linker double pour l'un des fragments et un linker simple pour le second. Le linker simple a été choisi pour le récepteur, toujours dans le but de minimiser l'impact de la fusion.

En plus de ces considérations, j'ai conçu les séquences dans l'optique de faciliter la permutation des fragments de Venus, et l'utilisation de l'outil pour l'étude de futurs couples protéine/protéine en insérant des sites d'enzyme de restrictions permettant de modifier facilement les constructions (Fig. 10B).

Si l'objectif final était d'exprimer le ligand au niveau de la PP et le récepteur dans le CC, nous avons d'abord effectué des tests en coexprimant les deux dans les axones. Nous avons obtenu de premiers résultats encourageants en détectant le signal Vénus au niveau des CC dans la PP (Fig. 10C). Cependant, l'expression ciblée des protéines de fusion a diminué le nombre de cellules électroporées. Cette diminution a grandement impacté la probabilité d'obtenir un axone, avec le récepteur de BiFC, rencontrant le ligand de BiFC. La quantité de travail requise pour améliorer cette probabilité, obtenir

des résultats robustes et contrôler les faux positifs aurait représenté un projet entier. Nous avons donc décidé de mettre de côté cet outil pour nous concentrer sur la répartition et le clivage de Slit, ainsi que sur la morphologie de la PP. Cependant, les outils développés pourront être utilisés par d'autres projets de l'équipe, que ce soit pour des études de guidage axonal ou des études de cancérologie.

DISCUSSION

Ma thèse portait sur la navigation des axones commissuraux de la moelle épinière dans la PP, et comportait trois axes. Le premier visait à améliorer notre visualisation du processus physique de traversée de la PP. A l'aide de reconstructions 3D, j'ai pu montrer la complexité de la morphologie des cellules de la PP, mais aussi renforcer l'hypothèse que les cellules de PP servent de substrat physique pour la pousse. Une meilleure représentation de l'environnement physique permet de mieux comprendre la navigation des axones, non seulement car un substrat et des obstacles physiques vont influencer directement la navigation, mais également car un environnement encombré va influencer la distribution des signaux chimiques.

Le second axe, en collaboration avec un autre doctorant de l'équipe (Hugo Ducuing), concernait l'étude du rôle de la signalisation SlitC/PlxnA1 au cours de la traversée de la PP. Nous avons pu montrer que cette signalisation empêche les axones de faire demi-tours dans la PP et les contraint à traverser en ligne droite. Cette étude fait partie des premières preuves que les différentes signalisations répulsives de la PP possèdent des fonctions spécifiques. Cette information permet de mieux comprendre comment un axone traverse un champ de répulsifs, mais apporte également une nuance supplémentaire dans notre compréhension des signalisations répulsives.

Le troisième axe concernait l'étude du champ de répulsifs *via* l'analyse de Slit2. Pour cet axe, nous avons dû développer différents outils permettant d'étudier plusieurs caractéristiques de Slit2 *in vivo*. J'ai ainsi pu montrer que les différences fonctionnelles des fragments de Slit2 ne proviennent pas d'une différence de répartition de ces derniers. Cependant, j'ai observé que leur diffusion dans le domaine basal de la PP, dépend du clivage de Slit2. Ces informations permettent d'éliminer l'hypothèse que la diffusion des fragments est à l'origine des spécificités fonctionnelles observées. Elles apportent également des informations supplémentaires sur le rôle physiologique du clivage de Slit2.

I. Les cellules de la plaque du plancher forment un environnement contraignant pour la navigation axonale

a. Chaque cellule gliale possède une morphologie complexe et unique

Lors d'un voyage en voiture, nous utilisons différents signaux pour nous diriger : des panneaux, des points de repères, des cartes/GPS, *etc*. Cependant, sans infrastructures favorables à la voiture, notre voyage n'aurait pas lieu. De la même manière, la navigation des axones dépend de son environnement physique. Cependant, peu d'études se sont intéressées au guidage à travers ce prisme. Dans le cas de la plaque du plancher, le peu d'informations disponibles sur sa structure est d'autant plus paradoxal

que son apparence physique est bien connue, et facilement reconnaissable, par toutes celles et ceux travaillant sur le neurodéveloppement. C'est d'ailleurs cette apparence particulière qui a permis son identification par Wilhelm His (Kingsbury, 1920). Depuis, des études ont permis de révéler que les axones traversant la PP sont en contact étroit avec les cellules gliales, d'autres ont montré que les processus basaux possèdent une morphologie complexe (Yaginuma *et al.*, 1991; Campbell and Peterson, 1993; Okabe *et al.*, 2004). Nos reconstructions 3D confirment que les axones poussent sur les pieds basaux, mais également que la morphologie de ces derniers est particulière. En effet, ces prolongements sont élargis dans l'axe de la traversée, et aplatis dans l'axe rostro-caudal.

Les travaux de Campbell et Peterson sont fondés sur un rapporteur *lacZ*, sous la dépendance du promoteur de la protéine à choc thermique Hsp68 permettant d'exprimer spécifiquement le rapporteur dans la PP (Campbell and Peterson, 1993). Ainsi, les auteurs ont pu observer les pieds basaux des cellules de la PP et montrent que certains n'atteignent pas la lame basale. Ils notent également la présence d'une multitude de fines ramifications, partant des pieds basaux et alignées dans le sens de traversée. Cependant, les auteurs nuancent ces observations en précisant que les ramifications pourraient provenir d'artefacts de marquage. Nos reconstructions 3D de cellules individuelles confirment que certains prolongements n'atteignent pas la lame basale. Cependant, l'imagerie en livre-ouvert, propice à la reconstruction 3D, ne permet pas de voir les fines ramifications décrites par Campbell et Peterson. Nous avons toutefois pu les observer en coupe transversale, mais leur présence ne semble pas systématique ce qui suggère une hétérogénéité morphologique entre les cellules de PP.

Si notre étude corrobore les quelques informations déjà publiées, elle révèle surtout qu'une cellule individuelle possède non pas un, mais plusieurs prolongements basaux. De plus, nous avons observé que chaque cellule de PP est unique de par son nombre de pieds basaux (deux à quatre, d'après nos observations) et leur morphologie. Ainsi, certains pieds vont atteindre la lame basale, d'autres non ; certains pieds vont être très élargis, d'autres très peu. Ces différences permettent un entremêlement de prolongements, formant ainsi un environnement physique contraignant pour les axones. En complément, nous avons pu noter que les CC dans la PP adoptent une morphologie étalée dans le plan transversal, mais également que les axones semblent naviguer dans les interstices des pieds basaux en longeant ces derniers.

b. *L'étude de l'environnement physique est un aspect important pour notre compréhension du guidage axonal*

Ces observations suggèrent que l'environnement physique exerce une forte contrainte mécanique sur les axones, contrainte pouvant modifier le comportement du CC (Fig. 11) (Tyler, 2012; Kerstein, Nichol and Gomez, 2015). L'environnement physique va également jouer sur la façon dont les molécules de guidage sont présentées. En effet, le contact étroit entre les cellules suggère que les molécules peuvent être présentées à de fortes concentrations ou directement de membrane à membrane. Ces modes de présentation peuvent modifier la réponse à un signal (ex : Shh) voire être nécessaires pour certaines signalisations (ex : Eph) (Holland *et al.*, 1998; Kolpak, Zhang and Bao, 2005). Ainsi, la structure des cellules de PP pourrait contrôler la navigation aux niveaux chimique (*via* la présentation des molécules de guidage) et physique (*via* la morphologie des pieds) contraignant les axones à avancer tout droit.

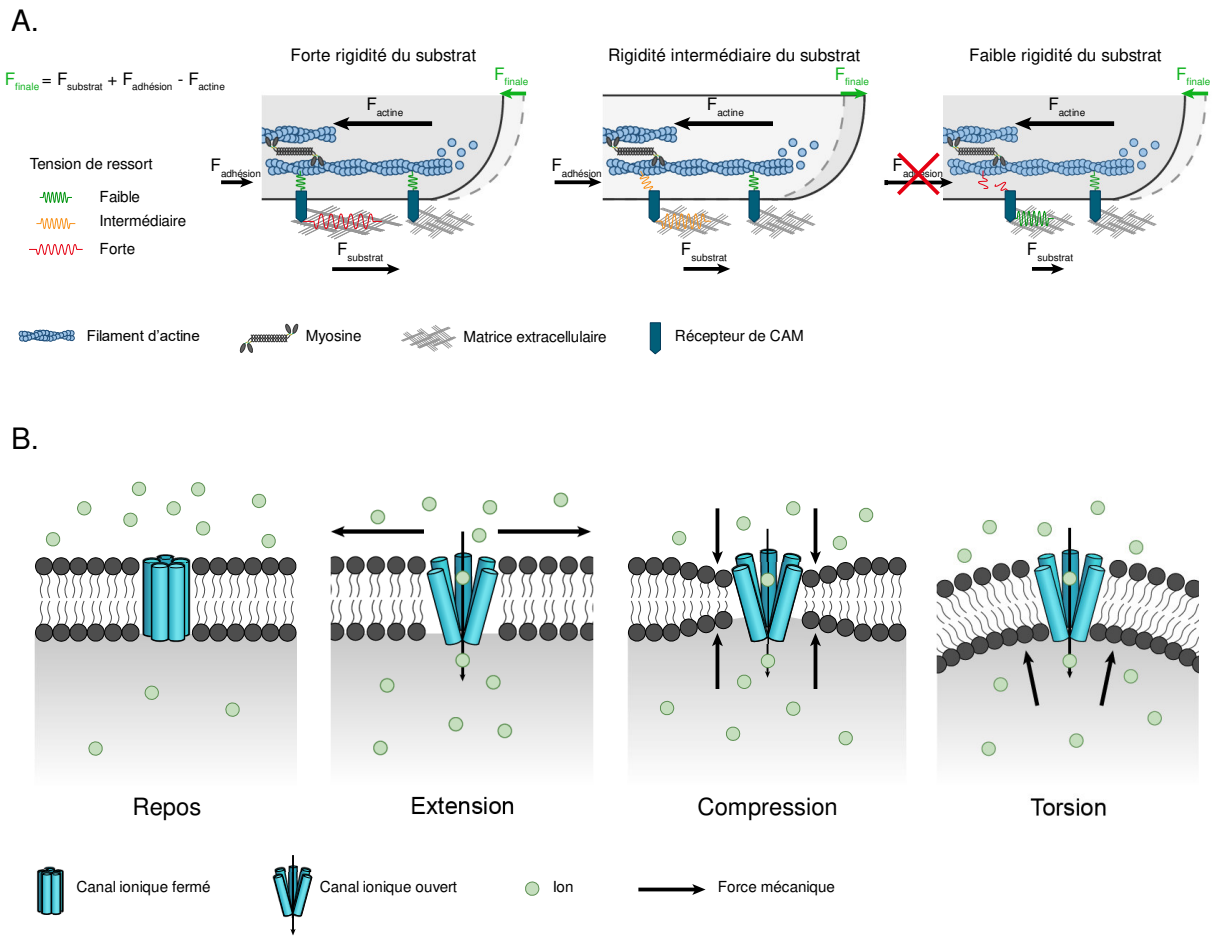

Figure 11. Contrôle du guidage axonal par les contraintes mécaniques de l'environnement

(**A**) Représentation schématique des forces de traction en fonction de la rigidité du milieu. Quand le flux rétrograde d'actine tire vers l'arrière un récepteur des CAM ancré à un substrat de faible rigidité, le substrat n'oppose que peu de résistance. Ainsi, les forces de traction sont trop faibles pour contrebalancer le flux rétrograde d'actine, et le cône de croissance (CC) ne peut se tirer vers l'avant et

reste immobile. A l'inverse, un substrat trop rigide provoque une tension trop importante sur l'adhésome qui finit par se décrocher de l'actine. Ainsi, le flux rétrograde d'actine n'est pas compensé et le CC ne peut pas se tirer vers l'avant, à nouveau. Ainsi, le CC pousse préférentiellement sur des substrats de rigidité intermédiaire. Cependant, la rigidité optimale dépend du CC et de son contenu en CAM et récepteur de CAM. Adaptée de Kerstein *et al.*, 2015. (**B**) Les déformations de la membrane par l'environnement peuvent ouvrir les canaux ioniques pour contrôler localement la concentration en ions, comme le Ca^{2+}, et influencer le remodelage du cytosquelette. Adaptée de Tyler, 2012.

La morphologie des prolongements basaux influençant physiquement la navigation axonale est une hypothèse attrayante. Un mécanisme similaire a d'ailleurs été identifié chez d'autres cellules gliales, les cellules de Schwann, dont l'alignement oriente la croissance *in vitro* des neurites de divers neurones (Thompson and Buettner, 2006; López-Fagundo *et al.*, 2013). Cependant, on ne peut pas exclure que ce sont les axones qui, en s'immisçant dans le domaine basal, vont façonner les pieds basaux. Une observation pouvant aller dans le sens de cette hypothèse est que, à des stades précoces du développement, les cellules gliales semblent ne présenter qu'un prolongement apical avec leur corps cellulaire positionné au niveau de la lame basal. Un domaine basal apparaît ensuite au stade où les axones traversent la PP. Cette observation peut suggérer que les axones s'immiscent en ventral des corps cellulaires et exercent des forces sur ces derniers pour former le domaine basal. Afin de savoir si ce sont les axones qui façonnent les pieds basaux, il serait intéressant de réaliser de l'imagerie, live en livre-ouvert, sur des axones traversant une PP marquée. Ce protocole expérimental pourrait permettre de voir les pieds se remodeler lors du passage des axones, ou bien de voir les axones emprunter un chemin déjà présent.

Un autre élément suggère que la structure physique des prolongements basaux n'est pas suffisante pour obtenir une trajectoire rectiligne des axones dans la PP. En effet, l'étude de notre modèle murin révèle que la signalisation SlitC/PlxnA1 possède un rôle clef dans le maintien de la trajectoire.

II. La signalisation SlitC/PlxnA1 possède une spécificité fonctionnelle pour la traversée de la plaque du plancher

a. La signalisation SlitC/PlxnA1 contrôle spécifiquement la polarité de traversée

L'analyse de trajectoires d'axones commissuraux traversant la PP dans une lignée murine $PlxnA1^{-/-}$ révèle deux phénotypes majeurs : la stagnation et les demi-tours (Delloye-Bourgeois *et al.*, 2015). Si l'invalidation de Sema3B phénocopie les défauts de stagnation, elle n'explique pas les demi-tours, suggérant ainsi un autre mécanisme impliquant PlxnA1 et contrôlant la traversée (Nawabi *et al.*, 2010;

Delloye-Bourgeois *et al.*, 2015). En analysant notre lignée PlxnA1^{Y1815F}, nous observons une désorganisation générale des axones traversant la PP où ils adoptent une trajectoire ondulante. De plus, cette mutation phénocopie les défauts de demi-tours, sans que l'on observe d'axones à l'arrêt. Ces résultats ont été renforcés par des expériences complémentaires réalisées par Hugo Ducuing. Ainsi, en électroporant le récepteur muté dans des axones de souris PlxnA1$^{-/-}$, il observe des trajectoires désorganisées et ondulantes, similaires à celles observées chez les mutants PlxnA1^{Y1815F}. L'ensemble de ces résultats suggèrent plusieurs choses. Premièrement, la signalisation SlitC/PlxnA1 semble jouer un rôle essentiel dans le maintien de la polarité de la trajectoire pendant la traversée de la PP. Mais ils suggèrent aussi que ce rôle est propre à SlitC/PlxnA1, puisque ces défauts ne sont pas observés chez les mutants dont les signalisations SlitN/Robo ou Sema3B/PlxnA1-Nrp2 sont invalidées. Cependant, chez ces mutants la proportion d'axones stagnant dans la PP augmente. Ainsi, nous pouvons discerner deux rôles pour les signalisations répulsives de la PP : un rôle de barrière médié par SlitC/PlxnA1, et un rôle d'expulsion médié par SlitN/Robo et Sema3B/PlxnA1-Nrp2.

Historiquement, les signalisations sont classées en tant que répulsives ou attractives, mais peu de distinctions fonctionnelles sont considérées au sein de ces deux catégories – possiblement car les tests *in vitro* permettant de classer ces signalisations exacerbent leur action et que les études *in vivo* portent sur des phénotypes sévères. En conséquence, les comportements plus fins de trajectoire individuelle, voire de remodelage du cytosquelette, ont peu été étudiés. Avec la mise en évidence de la spécificité fonctionnelle de SlitC/PlxnA1 au sein de la PP, nos résultats soulignent l'importance d'étudier plus finement le rôle des signalisations pour mieux comprendre chaque étape de la navigation.

b. Plusieurs niveaux d'études sont requis pour comprendre l'origine des spécificités fonctionnelles

Comme expliqué précédemment, les différences fonctionnelles de signalisations répulsives peuvent naître au niveau : 1) de la répartition des récepteurs ; 2) de la présentation des ligands ; 3) des acteurs en aval. De précédents travaux de l'équipe ont montré que, au cours de la traversée, PlxnA1 est adressé à la membrane du CC plus tôt que Robo1 (Pignata *et al.*, 2019). De plus PlxnA1 est essentiellement adressé à l'avant du CC, contrairement à Robo1 qui se situe à l'arrière. La présence de PlxnA1 à l'avant du cône pourrait diminuer le comportement exploratoire du CC en inhibant la formation de filopodes et lamellipodes et ainsi maintenir une trajectoire rectiligne. Cependant, PlxnA1 est également le récepteur de Sema3B, sa localisation seule ne semble donc pas pouvoir expliquer la spécificité fonctionnelle de SlitC/PlxnA1. Sema3B agissant *via* le complexe PlxnA1-Nrp2, cartographier ce complexe pourrait révéler une éventuelle compartimentation. Ces expériences pourraient être réalisée en associant BiFC et microscopie super-résolutive (Nickerson *et al.*, 2015).

En plus de la compartimentation des récepteurs, nous nous sommes intéressés aux deux autres niveaux potentiels. La recherche de partenaires en aval spécifiques de SlitC/PlxnA1 a été réalisée par Hugo Ducuing et Karine Kindbeiter au laboratoire. Dans ce but, ils ont transfecté la PlxnA1^{Y1815F} dans des cellules N2a. En collaboration avec Yoan Couté (CEA, Grenoble), ils ont réalisé des expériences de co-immunoprécipitation (co-IP) et spectrographie de masse (SM). En comparant avec les résultats obtenus pour la PlxnA1 sauvage, ils ont pu identifier différents partenaires potentiels. Sur une liste de 250 candidats, Rac1 se démarque comme potentiel partenaire en aval de SlitC/PlxnA1 pour plusieurs raisons. Premièrement, ce dernier fait partie des Rho GTPases, effecteurs impliqués dans de nombreuses signalisations de guidage axonal. Ensuite, Rac1 a été identifié en aval de différentes signalisations répulsives, et son activité est essentielle pour la traversée de la ligne médiane par les axones du corps calleux (Kassai *et al.*, 2008; Bashaw and Klein, 2010). De plus, les travaux de l'équipe ont montré que SlitC provoque une activation de Rac1 dans des cellules HEK293T exprimant PlxnA1 (Delloye-Bourgeois *et al.*, 2015). Enfin les résultats de SM montrent que la présence de Rac1 est réduite d'un facteur trois dans les co-IP PlxnA1^{Y1815F} par rapport au contrôle PlxnA1. Ces informations font de Rac1 un candidat très intéressant pour expliquer la spécificité fonctionnelle de SlitC/PlxnA1. Cependant, une première expérience de co-IP/SM sur des cellules traitées avec SlitC n'a pas fait ressortir Rac1 comme candidat potentiel. A l'inverse, d'autres candidats ont été identifiés, notamment : une ubiquitine ligase E3, impliquée dans la dégradation de protéines par le protéasome, et l'Integrin α6, connu pour son rôle de récepteur des laminines dans les cellules épithéliales. De nouvelles expériences de co-IP/SM, sur cellules et sur moelles de souris PlxnA1^{Y1815F}, seront réalisées pour confirmer l'implication des candidats potentiels.

III. Les ligands SlitN, SlitC et Sema3B sont présentés d'une manière similaire

a. La présentation de SlitC n'induit pas les spécificités fonctionnelles de la signalisation SlitC/PlxnA1

Slit2 DT nous a permis de montrer que Slit2N et Slit2C, bien que séparés dans le compartiment basal de la PP, semblent être présentés de manière similaire aux axones. Grâce à une lignée de souris GFP-Sema3B, nous avons également pu observer que les caractéristiques d'expression de Sema3B sont semblables à celles des fragments Slit2 : une majorité du signal se trouve dans le domaine apical le long des prolongements basaux ponctués. Nous avions imaginé différents cas possibles pour expliquer les spécificités fonctionnelles : des gradients médio-latéraux spécifiques des signaux, ou bien une expression restreinte à la ligne médiane ou aux extrémités de la PP. Cependant, nos résultats suggèrent

que les spécificités fonctionnelles ne proviennent pas de la présentation des ligands, mais plutôt des récepteurs et/ou de leurs effecteurs.

b. *Les mécanismes de présentation des ligands sont essentiels pour le guidage axonal*

Toutefois, nos résultats viennent confirmer ceux obtenus par Brose *et al.* : SlitC diffuse plus facilement que SlitN (Brose *et al.*, 1999). Des études, chez la souris et la drosophile, suggèrent également que SlitC possède la particularité de se lier à la matrice extracellulaire (MEC) et notamment au dystroglycan (Wright *et al.*, 2012; Bhat, 2017). Chez le poisson zèbre, Slit interagit avec le Collagen4a5 (Col4a5) qui forme la lame basale du tectum, mais que cette interaction soit due à SlitN ou SlitC n'est pas encore connu (Xiao *et al.*, 2011). Toutefois, l'étude souligne l'importance des pieds basaux des cellules gliales pour ancrer Slit à la lame basale, contrôlant ainsi la navigation des axones de la rétine. Récemment, des études ont montré que Netrin-1 est également transporté le long de prolongement de cellules, jusqu'à la surface piale, confirmant l'importance de ce type de présentation des ligands (Varadarajan *et al.*, 2017; Moreno-Bravo *et al.*, 2018). A partir de là, le parallèle avec la PP est attirant. Les pieds des cellules de la PP amèneraient donc SlitC à la lame basale, où il se lierait à la MEC pour contrôler la traversée. Notre étude montre que SlitC est en effet capable de se lier à la lame basale. De plus, l'observation de Slit2 DT suggère que l'expression de la protéine sous forme complète va permettre d'amener également SlitN à la lame basale. Bien que nous ignorions encore si l'interaction SlitC/MEC est importante pour la traversée de la PP, une étude l'implique dans la trajectoire post-traversée. A l'aide de souris présentant une invalidation du dystroglycan, Wright *et al.* observent des défauts de trajectoires post-traversée similaires à ceux des mutants Robo/Slit (Wright *et al.*, 2012). Ainsi, l'interaction Slit/MEC semble essentielle pour la signalisation SlitN/Robo. Cependant, il n'est pas encore certain qu'elle soit essentielle pour la signalisation SlitC/PlxnA1.

c. *Le clivage de Slit2 participe à la présentation des signaux*

Si nous avons pu observer que les fragments de clivage sont présentés similairement, nous avons également observé que le clivage semble essentiel pour permettre la diffusion des signaux Slit dans le domaine basal. Le clivage de Slit semble donc influencer le guidage en contrôlant la présentation des ligands. Un tel rôle a déjà été démontré, chez la drosophile, dans le processus de migration des cellules musculaires (Ordan *et al.*, 2015). Dans ce cas, le clivage de Slit permet de restreindre SlitN aux tendons pour repousser les cellules musculaires, alors que SlitC semble être dégradé. Ainsi, le clivage joue différents rôles selon les processus développementaux. Cependant, les travaux portant sur ce mécanisme restent peu nombreux. Cela s'explique entre autres par l'absence de protéase identifiée, rendant difficile l'inhibition du clivage *in vivo*. Chez la drosophile, Amontillado est impliquée, bien que

son rôle ne soit potentiellement qu'indirect (Ordan and Volk, 2016). Par conséquent, la Proprotéine convertase 2 (PC2), homologue d'Amontillado chez les vertébrés, est un candidat intéressant. De plus, l'hypothèse d'un rôle de PC2 est renforcée par son patron d'expression spécifiques des tissus neuroendocriniens et du cerveau (Smeekens and Steiner, 1991; Rouillé *et al.*, 1995; Seidah *et al.*, 1998). Enfin, nos marquages par immunofluorescence révèlent une expression spécifique à la PP et concentrée dans le domaine apical. Ce patron d'expression cohérent avec les résultats précédents consolide la position de PC2 comme candidat. Des expériences d'inhibition *in vitro*, par inhibiteur chimique, semblent confirmer son implication dans le clivage de Slit. Des expériences d'inhibition *in vivo*, par siRNA, devraient nous permettre de conclure sur le rôle de PC2, et potentiellement de renforcer les résultats obtenus avec Slit2 DT et Slit2 DTΔ.

IV. L'étude des interactions ligands-récepteurs est nécessaire pour améliorer notre compréhension de la traversée

a. L'adressage des récepteurs à la membrane ne coïncide pas forcément avec leur activation

La traversée de la PP par les axones commissuraux est intrigante puisque des axones naviguent dans un champ de signaux répulsifs. Les différents travaux de l'équipe, dont les miens, permettent d'améliorer notre compréhension de ce processus contre-intuitif. Ainsi nous comprenons mieux la régulation spatio-temporelle des récepteurs, permettant la sensibilisation aux signaux répulsifs, mais également la topographie physico-chimique du domaine que traversent les axones. Cependant, beaucoup d'inconnues subsistent. Parmi celles-ci, on retrouve la spatio-temporalité de l'activation des signalisations. En effet, différents mécanismes vont inhiber les récepteurs à la membrane. Comme présenté dans l'introduction, les récepteurs Robo possèdent une capacité d'auto-inhibition structurale, mais Robo1 va également être inhibé en formant des homodimères ou des hétérodimères avec Robo2 ou Robo3 (Long *et al.*, 2004; Evans *et al.*, 2015; Barak *et al.*, 2019). On retrouve une capacité d'auto-inhibition chez les PlxnA. Ainsi, leur domaine extracellulaire va interagir en *cis* avec un autre domaine extracellulaire de PlxnA, en « tête-à-queue », pour inhiber les deux récepteurs et cette inhibition est levée en présence de Sema3B (Kong *et al.*, 2016). Il est donc nécessaire de savoir si l'adressage des récepteurs à la membrane coïncide avec leur activation. PlxnA1 illustre bien l'importance de cette information. En effet, ce récepteur est partagé entre Sema3B et SlitC. Sachant que ces deux signalisations n'ont pas le même rôle dans la traversée, il est possible d'imaginer qu'elles

ne soient pas activées avec la même spatio-temporalité. Une autre hypothèse est que l'activation de ces signalisations, au sein du CC, soit compartimentée.

Les travaux d'Aurora Pignata ont montré que l'adressage des récepteurs à la membrane s'accompagne de changements comportementaux. Dans le cas de l'adressage de Robo1 ou Robo2, le CC va respectivement augmenter son comportement exploratoire ou tourner. L'étude de McConnell *et al.* suggère que les signalisations SlitN/Robo sont essentielles pour ces comportements (McConnell *et al.*, 2016). Pour confirmer ces observations *in vivo*, les auteurs altèrent des effecteurs des signalisations. Cependant, ces effecteurs sont partagés par de nombreuses signalisations. L'étude des interactions ligands-récepteurs est donc nécessaire pour renforcer le lien entre récepteurs et comportements.

b. L'utilisation de la BiFC dans le contexte de la traversée est prometteuse

Nous avons essayé d'aborder la question en utilisant la BiFC, technique d'analyse d'interaction protéine-protéine. Malgré des premiers résultats encourageants, le développement de cette technique aurait nécessité un sujet entier. L'un des défis à relever provient de la sécrétion des ligands de guidage. En effet, les seules études de BiFC concernant des ligands sécrétés ont été effectuées au niveau de la synapse, où la distance entre la source du ligand et récepteur est très faible (entre 20 et 40nm) (Feinberg *et al.*, 2008; Yamagata and Sanes, 2012; Macpherson *et al.*, 2015; Shearin *et al.*, 2018). Dans le cas d'un paradigme expérimental basé sur l'électroporation, le contingent de ligands disponibles est constitué à la fois de ligand BiFC et de ligand sauvage. Ainsi, à moins d'être suffisamment proche d'une source de ligand BiFC, la quantité de ce dernier sera trop faible pour induire un signal détectable. Cependant, l'étude de la morphologie révèle le contact étroit entre CC et pieds basaux. Cette information suggère que l'étude des interactions ligand-récepteur de guidage, dans la PP, devrait être possible.

Annexes

Seminars in Cell & Developmental Biology xxx (2017) xxx–xxx

Contents lists available at ScienceDirect

Seminars in Cell & Developmental Biology

journal homepage: www.elsevier.com/locate/semcdb

Review

Commissural axon navigation in the spinal cord: A repertoire of repulsive forces is in command

Hugo Ducuing, Thibault Gardette, Aurora Pignata, Servane Tauszig-Delamasure, Valérie Castellani*

University of Lyon, University of Lyon 1 Claude Bernard Lyon1, NeuroMyoGene Institute, CNRS UMR5310, INSERM U1217, 16 rue Raphael Dubois, F-69000 Lyon, France

ARTICLE INFO

Article history:
Received 4 October 2017
Received in revised form
11 December 2017
Accepted 11 December 2017
Available online xxx

Keywords:
Axon guidance
Commissural axon
Midline crossing
Guidance signaling
Repulsion
Attraction
Growth cone

ABSTRACT

The navigation of commissural axons in the developing spinal cord has attracted multiple studies over the years. Many important concepts emerged from these studies which have enlighten the general mechanisms of axon guidance. The navigation of commissural axons is regulated by a series of cellular territories which provides the diverse guidance information necessary to ensure the successive steps of their pathfinding towards, across, and away from the ventral midline. In this review, we discuss how repulsive forces, by propelling, channelling, and confining commissural axon navigation, bring key contributions to the formation of this neuronal projection.

Contents

1. Introduction

Early theories of chemotropism and chemoaffinity by Ramon Y Cajal and Sperry provided the basis for more than a century of research on axon guidance mechanisms [1,2]. These theories postulated the existence of molecules acting at long and short distances to attract the axon terminal, the growth cone. Their role was postulated to keep the axons along their proper path and to guide them towards their targets. Unanticipatedly from these theories, repulsive effects of axon guidance molecules turned out to provide major forces driving axon navigation. In 1984, Haydon and collaborators, using video-time lapse microscopy in neuronal cultures, reported that serotonin has a neuron-type specific inhibitory effect

* Corresponding author.
E-mail address: valerie.castellani@univ-lyon1.fr (V. Castellani).

https://doi.org/10.1016/j.semcdb.2017.12.010
1084-9521/

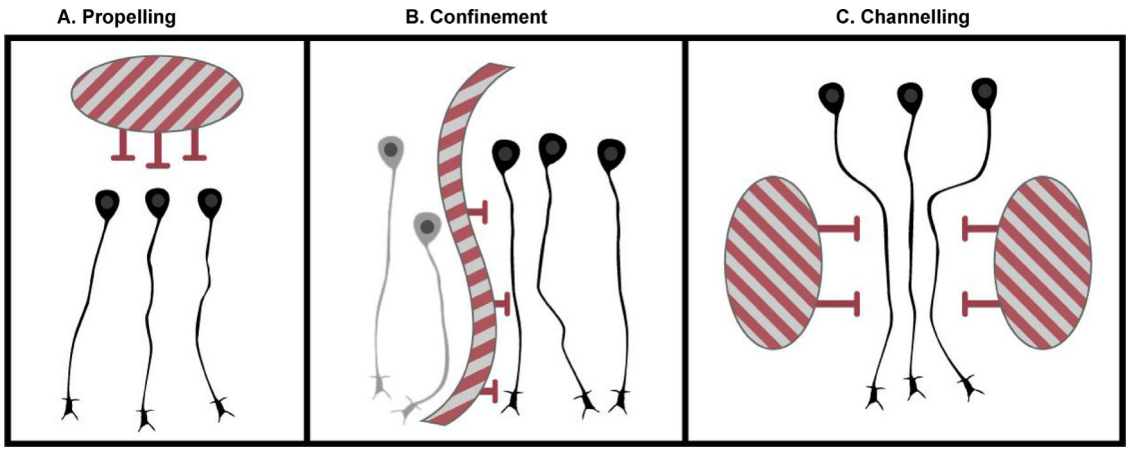

Fig. 1. Modes of action of repulsive forces in axon guidance.
As they grow, axons are oriented by a combination of attractive and repulsive forces. Among the repulsive ones, we can distinguish 3 main modes of action. A. Propelling. Axons perceive diffusible chemorepulsive cues emanating from a group of guidepost cells and turn away from this source. B. Confinement. A group of guidepost cells act as a barrier and confine the axons within a territory. They not necessarily deflect them away but prevent them from exiting it, partly by the emission of diffusible cues. C. Channeling. Several groups of physically separated guidepost cells constrain commissural axons within a narrow path, by releasing repulsive cues.

on growth cones [3]. The property of growth cone structures to retract after contact with some other axonal membrane surfaces was then discovered by Kapfhammer and Raper [4]. These observations echoed those of Verna, who wrote that dorsal root sensory neurons "interact differently with dermal than with epidermal cells. While nerve fibres readily extend over dermal cells, forming close membrane associations with some of them, they demonstrate a strong avoidance reaction with epidermal cells by changing their direction of extension" [5]. He postulated that molecules released by epidermal cells might deflect away nerve fibre growth trajectory, oppositely to those which were found to attract the axons, namely at that time, the neurotrophic factor NGF [6]. From these pioneer findings, repulsive forces have been demonstrated to play instrumental roles in a large range of developing neuronal circuits. As evidenced by numerous studies [7,8], repulsive forces can constrain axon navigation in various ways, channelling axonal bundles, deflecting away the growth cone trajectory, and creating sharp boundaries to delineate non-permissive territories (Fig. 1). As in a pinball, repulsive forces would act as launch pad, bumpers, and slingshots to propel and dynamically impact on the axon/ball trajectory. The development of commissural axons provides an appealing context to investigate how such repulsive forces can direct axon navigation. We review here the principal yet identified sources of repulsive cues, the nature of their influences and the molecular signals mediating their action during commissural axon navigation in the spinal cord.

1.1. Formation of commissural circuits

In Bilateria, commissural neurons form complex circuits that interconnect both sides of the central nervous system (CNS). They are essential for the correct processing and coordination of various sensory modalities, motor responses, and other brain functions [9]. These interneurons extend their axon across the midline at various axial levels of the CNS. For instance, the *corpus callosum* enables communication between the left and right cortical areas, the optic chiasm allows organisms with bilateral vision to correctly integrate visual cues, and spinal commissures ensure the correct coordination of various motor commands. These commissures are established during embryonic and early post-natal development in a highly specific spatial and temporal manner [10]. Defects in the correct wiring of commissural circuits have been observed in many neurodevelopmental disorders. However, if malformations of the *corpus callosum* have been well correlated with various human disorders, little is known of the consequences of spinal commissures defects. Indeed, patients having mutations in *ROBO3* gene, affecting commissures of the hindbrain and the spinal cord, have no large sensorimotor deficit. Rather, they exhibit a very specific disease referred to as horizontal gaze palsy with progressive scoliosis (HGPPS) [11]. This suggests high degree of compensation of commissural defects with developmental origin.

1.1.1. Development of the dorsal commissural tract

The spinal commissural neurons are a heterogeneous population subdivided in several pools, differing in their location and timing of birth, each of them specified by various transcription factors [12,13]. Among them, dI1 interneurons settle early in the most dorsal part of the spinal cord, close to the Roof Plate (RP). They arise from a MATH1-positive pool of progenitors, that generates both ipsilateral and commissural lineages and are specified by LHX2/LHX9 transcription factors [14,15]. dI1 commissural (dI1c) neurons trajectory is highly stereotyped and has been extensively studied in the mouse, notably by using MATH1::LacZ and MATH1::GFP transgenic mice [16]. dI1c axons first extend ventrally, turning away from the RP and laying close to the pial surface (Fig. 2). At around mid-distance of the ventral border they break away from the lateral border to re-orient medially towards the central Floor Plate (FP) by running along the motoneuron domain. Such break of trajectory is also typical of chick commissural axons, apart from the pioneer ones which course with circumferential trajectory. In contrast, in xenopus and zebrafish embryos, the axons course by following the circumference of the tube until reaching the FP [17,18]. Next, commissural axons enter the FP, cross it and turn rostrally without ever crossing the midline again to connect their final targets. Commissural neurons arise around E9.5 in the mouse and navigate towards the FP from this stage. By E10.5, some of them have already crossed the midline and by E12.5, most of them have. By E13.5, they are navigating towards their final target following longitudinal routes [19–21].

1.2. Guidepost territories instructing commissural axon navigation in the spinal cord through repulsive action

Historically, the main intermediate target and crucial signaling hub for commissural axon navigation has been found to be the FP. It heavily influences the dI1c guidance, and we can thus refer to

Please cite this article in press as: H. Ducuing, et al., Commissural axon navigation in the spinal cord: A repertoire of repulsive forces is in command, Semin Cell Dev Biol (2017), https://doi.org/10.1016/j.semcdb.2017.12.010

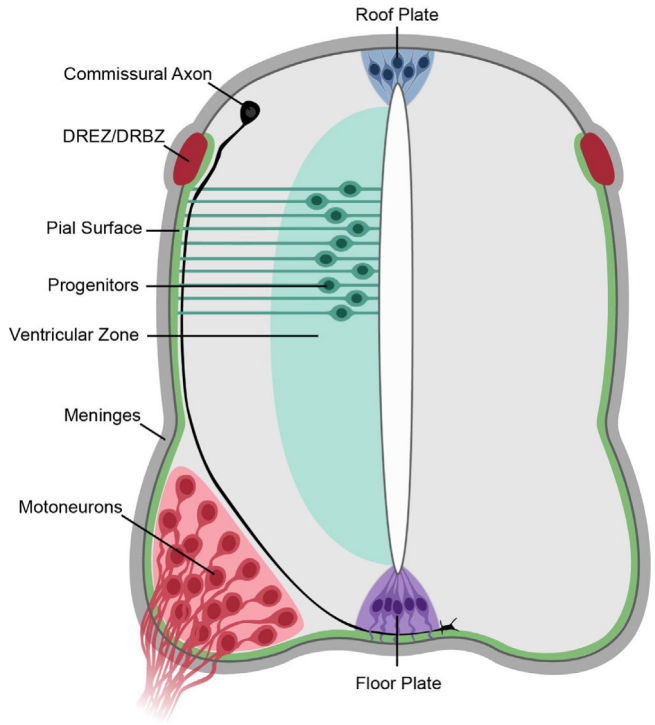

Fig. 2. Guidepost territories instructing commissural axons navigation in the spinal cord.
Spinal commissural axon trajectory is highly stereotyped. dI1c axons (in black) arise from a dorsal territory. They extend ventrally, cross the midline through the floor plate (FP), and then turn rostrally without ever crossing the midline again to connect their final target. This trajectory is influenced by various guidepost cells along the way. First, axons are pushed away by chemorepulsive cues emanating from the roof plate (RP) (in blue) and follow the pial surface (in green). Meninges (in grey) and the DREZ/DRBZ (in red) keep the axons away from the CNS/PNS boundary through diffusible cues. At around mid-distance from the ventral side, axons turn towards the FP (in purple), then run along the motoneurons domain (in red). Axons never enter the motoneuron domain nor the ventricular zone (in light green), these territories channeling the commissural tract towards the FP. As they reach the FP, axons interact with the basal lamina (in green) and navigate through the FP glial cells radial processes. Upon crossing, they gain sensitivity to repulsive cues emanating from the FP, that they did not perceive before and thus exit the FP, accomplish a sharp turning in the rostral direction and navigate longitudinally in bundles, guided by various gradients of guidance cues, including repulsive ones.

FP cells as guidepost cells. The FP has been extensively studied and many of its molecular mechanisms have been unveiled. However, a variety of other cells within the spinal cord bring contributions to the navigation of commissural axons, including glial cells, neurons and progenitors. These different cell-types contribute together to sharply delineate the path of commissural neurons.

1.2.1. Kick off repulsive forces to orient commissural axon navigation

1.2.1.1. The roof plate. The RP is probably the second most studied group of guidepost cells after the FP. It is composed of glial cells that lay on the dorsal midline of the spinal cord. These cells come from progenitors that are induced in the most lateral regions of the neural folds [22]. This induction relies heavily on BMP signalling, mediated by the transcription factors LMX1A/B [23]. Upon neural tube closure, they are not easily distinguishable from other cells, in particular neural crest cells, but as they differentiate they start to express specific markers, notably BMPs and WNTs [22]. The RP is the first dorsal structure to differentiate and then impacts all other dorsal populations differentiation. Electro-microscopy studies revealed that, when differentiated, RP cells have two small processes extending radially towards the pial surface and the central canal [24,25]. The RP acts as a barrier that no axon can cross before E16.5, when a dorsal commissure is established [26]. Interestingly, the RP itself undergoes rather important morphological changes between E11.5 and E16.5, from an arch structure to a thin wall-like structure [25]. The RP is a crucial organizing centre of the different dorsal lineages. Notably through BMPs and WNTs, it specifies several classes of adjacent dorsal interneurons and regulates their proliferation, migration, and guidance [27].

Beyond this patterning function, RP cells provide the driving force which propels dl1c axons emerging from their soma away from the dorsal side. This effect was shown to be mediated by the morphogens BMPs, namely by GDF7:BMP7 heterodimers acting *via* the BMPRIB receptor [28,29] (Fig. 3). Not only their direction but their growth rate also appears regulated by BMPs [30]. An additional repellent protein was found produced by the RP, a secreted factor named Draxin. Draxin mutant mice display commissural axonal migration and fasciculation defects consistent with a repulsive mode of action [31]. Draxin shares UNC5, DCC, and Neogenin receptors with Netrin-1, a secreted molecule initially discovered to act as a chemoattractant [32,33]. Although Draxin has been shown to bind UNC5 and Neogenin *in vitro* [34], its repellent role *in vivo* was reported to be triggered *via* its binding to DCC [35] (Fig. 3). It can also be noted that the repulsive factor Slit2 is highly expressed at the RP at E13 [36]. Most dorsal commissural axons are already on their way in the contralateral side at this stage, whether this source contributes to the kick off of commissural axons is therefore questionable.

1.2.2. Repulsive forces to confine commissural axon navigation in the central nervous system

Commissural axons are destined to connect neurons of the central nervous system (CNS) and must be consequently strictly confined within the spinal cord. This is not true for all spinal cord axons, since on the contrary, those of the motoneurons project out of the CNS through the Motor Exit Point (MET). Moreover, in this case, only the axons exit the CNS, the neuronal soma being confined within the CNS. Conversely, sensory axons of the dorsal root ganglia penetrate the spinal cord *via* the Dorsal Root Entry Zone (DREZ), while their soma remain outside. In contrast, some non-neuronal cells enter the CNS, such as endothelial cells which infiltrate the CNS tissue to build the blood vessels. Thus, cells and neurites trafficking across the CNS/PNS frontier is strictly controlled, from the onset and throughout life.

1.2.2.1. Confinement by the meninges. Meninges are a protective multi-layered structure that envelops the brain and the spinal cord. They are mainly composed of fibroelastic cells and blood vessels. Meninges originate from somatic mesoderm that covers the neural tube shortly after neural tube closure, around E9 in the mouse embryo [37,38]. They act as barriers throughout life, controlling exchanges between the central nervous system and what lays outside. In the brain, meninges have been shown to initiate a morphogenic signaling cascade that regulates the development of a major dorsal commissure, the *corpus callosum*. The meninges inhibit callosal axon outgrowth through BMP7. WNT3, expressed by pioneer callosal axons, later counters this effect. WNT3 expression is regulated by another member of the BMP family, GDF5, expressed by adjacent Cajal-Retzius neurons, which in turn is regulated by a soluble inhibitor, DAN, expressed by the meninges [37]. In the spinal cord, *in vivo* studies lack to highlight the role of the meninges on commissural neuron development. However, a recent *in vitro* study showed that the meninges are able to produce secreted cues that can either attract or repulse different neuronal populations. Consistent with *in vivo* behaviours, these experiences showed that motoneurons and sensory neurons are attracted by meninges while ipsilateral and commissural neurons are repelled by them [38].

Please cite this article in press as: H. Ducuing, et al., Commissural axon navigation in the spinal cord: A repertoire of repulsive forces is in command, Semin Cell Dev Biol (2017), https://doi.org/10.1016/j.semcdb.2017.12.010

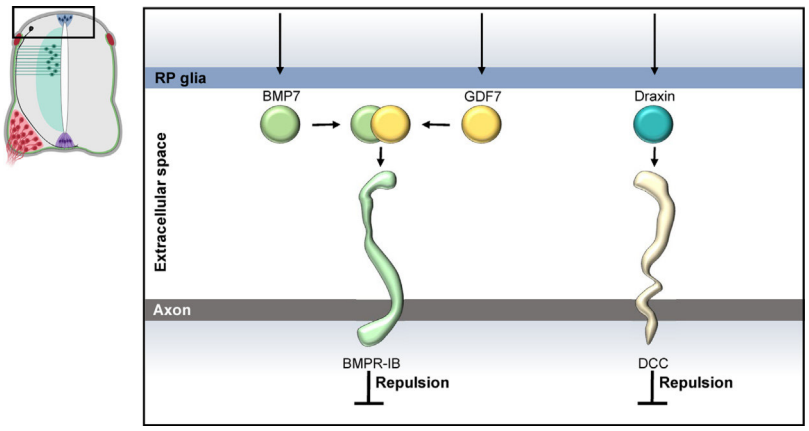

Fig. 3. Kick off repulsive forces at the roof plate.
The BMP family members GDF7 and BMP7 are secreted by roof plate glia cells and bind to the axonal BMPR-IB receptor and repel axons toward the ventral part of the spinal cord. In parallel, the secreted factor Draxin propels axons *via* axonal DCC.

1.2.2.2. Closing the CNS/PNS gate: confinement by the dorsal root entry zone (DREZ)/ dorsal root bifurcation zone (DRBZ). Commissural axons navigate at close proximity of the pia. Early studies established that their growth cones rarely, if ever, contact the basal lamina (Holley & Silver 1987, Yaginuma et al 1991). The basal lamina is punctuated by the DREZ and the MET, which ensure the circulation between the central Nervous System (CNS) and the surrounding tissues. The DREZ consists of a break in the lamina and a cluster of specialized cells arising from the neural crest, the boundary cap cells, which prevent both cell bodies and their axons from leaving the CNS, and gaps between the glial end-feet [39]. Around E11, the peripheral sensory neurons send axons towards the spinal cord through the DREZ and start to form the dorsal root bifurcation zone (DRBZ), where they project in an anterior-posterior direction within the tract [40]. Therefore, the DRBZ is in direct apposition to the DREZ.

Some cues released from these gates to confine commissural axons have been identified. Netrin-1 is expressed at the border of the DRBZ between E11.5 and E12.5 [34]. In Netrin-1 mutant embryos, commissural axons invade the DREZ and DRBZ. The presence of ectopic axons can even be detected in the dorsal root ganglia (DRG) [34]. This study thus indicates that Netrin-1 participates in forming an inhibitory boundary at the border of the DRBZ and the DREZ [34]. The nature of the Netrin receptors mediating these effects has also been investigated. Ectopic axons were detected in the DRBZ of both DCC and UNC5C mutant embryos, while only in DCC mutant was their presence observed in the DREZ, suggesting a differential contribution of these receptors [34] (Fig. 4A). Other receptors could also potentially transduce a Netrin-1 signal. Down's syndrome Cell Adhesion Molecule (DSCAM), whose expression is high in the DREZ and in commissural axons, was indeed shown to modulate Netrin-1 attractive response with or without DCC [35] (Fig. 4A). In the chick which lacks DCC [41], a candidate could be Neogenin, a Netrin-1 receptor which is expressed in some commissural axons [42] (Fig. 4A). The mode of action of Netrin-1 remains unclear. A simple view would be that it acts as a repellent in this context. Moreover, it should be noted that Netrin-1 is not detected in the dorsolateral region of the spinal cord prior to E11.5 whereas ectopic axons are already observed at E10.5 in the DRBZ of Netrin-1 and DCC mutant embryos [34]. Thus, other Netrin sources might act to confine the axons at the early stages, whose release in the mutants result in their ectopic position in the DRBZ. Additional repulsive forces might also be involved in this confinement. Draxin, transducing repulsive signals *via* axonal DCC, is namely also expressed at the dorsal pial surface and in the DREZ [27] (Fig. 4A).

Furthermore, the role of extracellular matrix (ECM) components and glycoproteins in the confinement of axons along the pial surface might be essential. Laminin is present all along the pial surface in close contact with the commissural axons during their navigation [43]. Type IV Collagen and Heparan sulfate proteoglycans are also components of the basement membrane and their deposition is spatially and temporally controlled in coordination with morphogenesis [44]. Along this line, the glycoprotein Dystroglycan, an important scaffold for ECM proteins including Laminin, has been shown to interact with Slit and this interaction is detected all along the pial surface [43]. In the visual system, Laminin has been shown to modulate the attractive response of retinal axons to Netrin-1 by turning it into a repulsive signal [45]. Thus, co-expression of Netrin-1 and Laminin could, as well, contribute to set the pia as a repulsive barrier, explaining the observed lack of contacts between the basal lamina and commissural growth cones (Fig. 4A).

1.2.3. Repulsive forces to channel commissural path

Channelling of axon tracts can be achieved by dual lateral repulsive sources constraining their growth in between. Once reaching the half ventral half of the spinal cord towards the FP, commissural axons modify their initial circumferential trajectory and re-orient medially towards the FP, navigating at the border of the ventral motoneuron domain. A triad of three territories, the ventricular zone, the basal lamina, and the motoneuron domain, might thus act in synergy to channel the pre-crossing path of commissural axons in between these different territories.

1.2.3.1. The ventricular zone. The ventricular zone (VZ) is composed of the neuronal progenitors, laying the central canal. The different populations of progenitors are specified by a combinatorial code of transcriptional factors [12]. These factors are activated by opposing gradients of BMP/WNT and SHH emanating respectively from the RP and the FP [12]. Neural progenitors of the CNS have a bipolar morphology, extending two processes, one connecting the pial surface and the other connecting the central canal [46]. During the cell cycle, their nuclei oscillate between the apical and basal pole, a process referred to as the interkinetic nuclear migration. Postmitotic neurons born from neurogenic divisions detach their apical anchor and migrate laterally to establish themselves in the mantle. Strikingly, dI1c axons navigate at the VZ/mantle interface but never enter the VZ. The mechanisms underlying this navigation choice are unclear. The Netrin-1 attractant produced by the progenitors and transported *via* their basal process for lateral deposition at the basal lamina was recently proposed to direct commissural axon growth out of the VZ and close to the pia [47]. Interestingly,

Please cite this article in press as: H. Ducuing, et al., Commissural axon navigation in the spinal cord: A repertoire of repulsive forces is in command, Semin Cell Dev Biol (2017), https://doi.org/10.1016/j.semcdb.2017.12.010

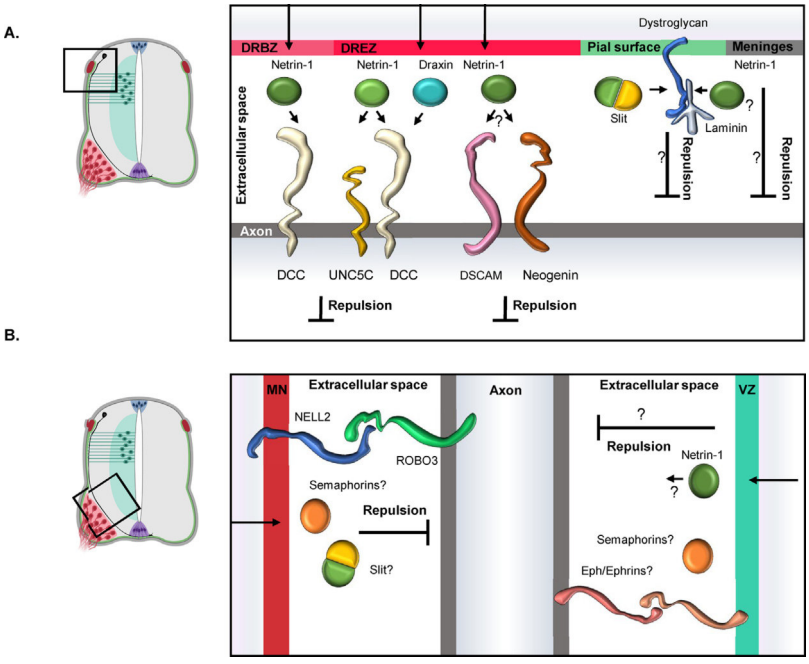

Fig. 4. Confinement and channeling of commissural axons.
A. Repulsive forces confine axons within the spinal cord.
The dorsal root entry zone (DREZ) and the dorsal root bifurcation zone (DRBZ) confine axons in the spinal cord. Netrin-1 acts *via* DCC and DCC/UNC5 heterodimer in the DRBZ and in the DREZ respectively. DSCAM may modulate Netrin-1 attractive response with or without DCC. Neogenin, whose expression was reported in chick commissural axons may also transduce the signal initiated by Netrin-1. In addition, Draxin at the pial surface and in the DREZ has a repulsive effect on axons *via* DCC. Signals originating from the meninges and the pial surface are still largely unknown but may involve the glycoprotein Dystroglycan. Dystroglycan scaffolds Laminin, which has been shown in other context to switch Netrin-1 attraction into repulsion.
B. Repulsive forces channel axons between the ventricular zone (VZ) and the motoneuron domain.
The VZ is a territory non-permissive to the entry of axons. The mechanisms mediating this barrier are still unknown but might involve Semaphorins and Eph/Ephrins. Netrin-1 is produced by progenitors. The motoneuron domain expresses Slits, Semaphorins and ROBO3 ligand, NELL2. NELL2/ROBO3 signaling mediates repulsion on commissural axons.

releasing the lateral deposition of this cue by specific deletion of Netrin-1 in progenitors induced some commissural axons, identified by their ROBO3 expression, to invade the VZ [47]. Nevertheless, some others, expressing the commissural marker TAG1, were still constrained out of the VZ [47]. A tempting model is that some repulsive forces also directly emanate from the VZ (Fig. 4B). Indeed, such a mechanism was reported to prevent cortical and thalamic axons from invading the proliferative regions of the developing brain [48]. This would be consistent with reported expressions of transcripts encoding guidance molecules bearing repulsive activity, such as the Semaphorins and the Eph/Ephrins in mouse and chick spinal cord VZ [49–53].

1.2.3.2. The motoneuron domain. Motoneurons arise at around E9.5 in the mouse embryo, from a pool of ventral progenitors. They are specified by a set of homeodomain transcription factors (notably HB9, LHX3, ISL2, and ISL3) [54]. Post-mitotic motoneurons migrate out of the VZ in streams, and cluster at various medio-lateral levels of the mantle to form distinct and adjacent pools. It is noticeable that commissural axons break their circumferential path when they reach the emerging mass of motoneurons accumulating in the ventral horn. Nevertheless, whether this reflects an instructive role of this territory in the reorientation of commissural axons is unclear. Indeed, in mouse and chick embryos in which the FP has been genetically or experimentally ablated, commissural axons no longer break their circumferential trajectory, reaching the FP through a path that resembles that of xenopus and zebrafish embryos, all along the pial surface. However, ablating the FP and/or the notochord in these experimental contexts, simultaneously prevented the specification of motoneurons, which were thus also lacking [55,56]. Interestingly, motoneurons express various guidance molecules that could define this territory as non-permissive for commissural axons, such as the Slits and the Semaphorins (Fig. 4B). A recent study features NELL2, expressed mainly in the motor columns, as mediating such a repulsive action of the motoneuron domain [57]. *In vitro*, NELL2 could repel commissural axons and this effect was found exerted *via* ROBO3. An *in vivo* contribution of signaling is suggested by the analysis of NELL2$^{-/-}$ROBO3$^{-/-}$ embryos, in which many commissural axons were observed to defasciculate and invade the motor columns [57].

The Slit/ROBO signaling pathway has been shown to be essential for the maintenance of boundaries, compartmentalizing the visual centres in the *Drosophila* brain [58]. Slits are interesting candidates to consider in this channelling. Slit1/2 mRNAs are produced by both spinal progenitors and motoneurons [36]. The Semaphorin3F (SEMA3F) is also highly detected in the motoneuron domain and its repulsive action on spinal commissural axons has been evidenced *in vitro*, although it was reported to concern post-crossing rather than pre-crossing axons [59]. Several other members of the Semaphorin family are indeed expressed both by motoneurons and progenitors. In the chick embryo, this is for example the case of SEMA3C and SEMA3A [50,51]. Specific deletion of these candidates in progenitors and motoneurons would be highly informative to address their contribution to the channelling of commissural axons.

1.2.4. Travelling a repulsive field: navigation across the midline in the floor plate

Being a prototypical example of intermediate target for long distance connections, the FP has been, by far, the most studied group of guidepost cells. The FP is composed of glial cells that lay ventrally at the midline of the embryo. Though discrepancies exist regarding its exact developmental origin and the signaling pathways involved

Please cite this article in press as: H. Ducuing, et al., Commissural axon navigation in the spinal cord: A repertoire of repulsive forces is in command, Semin Cell Dev Biol (2017), https://doi.org/10.1016/j.semcdb.2017.12.010

in its specification between species, the FP influences neuronal differentiation and axon pathfinding in the spinal cord of all vertebrates. In the mouse, SHH through GLI2 and then FOXA2 is a key factor in FP induction [60–62]. FP cells display a morphology that resembles the one of RP cells. They possess 2 processes that extend radially, the shorter one towards the central canal and the longer one towards the basal lamina [24,63]. The FP is a unique group of guidepost cells for several reasons. First, up to now, it is the only one the commissural axons go through, instead of just passing by. Indeed, commissural axons enter the FP and then navigate through a meshing of FP cells basal processes, hugging the basal lamina [64]. FP cells and commissural axons are known to establish close contacts [65]. Interestingly, it is probably the territory in which the dI1c axons form the most compact bundle during their navigation. Second, the FP is not only a group of guidepost cells but also an intermediate and not a final target. Thus, intermediate target must combine the properties of a target (a territory that the axons select to grow within) and a non-target (a territory in which the axons do not stop). Studies of FP crossing helped resolving some aspects of this apparent paradox, by bringing to the scheme the notion of temporality. Indeed, temporal regulation of axon sensitivity to the guidance cues emanating from the intermediate target is the key to endow it first, with the properties of a target and second, with those of a non-target.

Signals conferring to the FP the properties of a target tissue are the cues that are perceived first by commissural axons on their way for midline crossing. These signals are thought to combine both short-range and long range attractive/promoting effects. Cell adhesion molecules play a crucial role at a short-range level. Commissural axons and FP glial cells engage in dynamic and complex *cis* and *trans* interactions *via* various Cell Adhesion Molecules of the IgSuperfamily such as L1/NgCam, NrCam, and TAG1 [66–69]. Long range attraction by Netrins, and additionally SHH and VEGF, have been thought to provide major signals guiding commissural axons towards the FP [33,70–72]. This view has been recently revisited by studies demonstrating that Netrin-1 might indeed rather act much more locally and, as described in the above paragraphs, from spinal cord sources other than the FP, essentially neural progenitors [47,73]. Once the midline crossed, the FP must acquire the properties of non-target territory, to prevent axons to stall and terminate their navigation. This process, which has been the focus of recent reviews [74,75], appeared from several works to be achieved, not by expressing novel molecules with repulsive activity in the FP, but rather by sensitizing commissural axons to repulsive cues yet present but that had been ignored until midline crossing. The temporality of the target to non-target switch is crucial. Prematurely releasing the sensitivity to the repellents would be disastrous, as it would block commissural axons entry in the FP and midline crossing. The mechanisms controlling the switch have started to be decrypted in the recent years and turn out to be highly complex. A broad panoply of transcriptional and post-translational mechanisms is indeed deployed to first silence the perception of the repellents and second to release this silencing and set the repulsive commissural response. In parallel, the properties that made initially the FP as a target -*i.e.* attractive cues- have to be shut-down. Shirasaki and collaborators demonstrated twenty years ago that this is indeed occurring. In *ex vivo* assays, grafting an ectopic FP close to commissural axons coursing towards their endogenous FP induced their re-orientation towards the ectopic FP. In contrast, exposing commissural axons which have already crossed the endogenous FP to ectopic FP had no effect [76]. It was subsequently proposed that Slit signaling blunts Netrin-1 attraction. *cis* interaction between ROBO and DCC was reported to silence Netrin-1 attractive signaling [77]. In parallel, SHH has been proposed to be sequestered by its FP specific receptor HHIP (Hedgehog Interacting Protein) to turn off its attractive function [78].

1.2.4.1. The molecular players mediating repulsive forces. Repulsion involves several couples of ligands/receptors (Fig. 5). The secreted Semaphorin 3B (SEMA3B) mediates repulsion at the midline by activating a complex formed of NEUROPILIN 2 (NP2) and PLEXINA1 (PLEXA1) receptors [79]. In addition, the membrane-bound SEMA6B is expressed by commissural axons when they cross the FP and was reported to interact with PLEXA2 expressed by FP glial cells [80]. Slit proteins are produced by FP cells and are submitted to proteolytic processing through yet unidentified protease(s). This cleavage releases N-terminal Slit fragment (SlitN), which binds to ROBO receptors, and C-terminal Slit (SlitC) which binds to PLEXA1 [81]. B-class Ephrins can function as ligands or receptors, mediating forward or reverse signaling respectively [82]. In the FP, midline glial ephrin-B3 interacts with commissural Eph-B3 receptors [83]. Inhibitory effects of Nogo are carried out through the interaction to the Nogo receptor complex [84,85]. Nogo is expressed by radial glia at the ventral midline of the spinal cord and Nogo receptors (NogoR) are detected in commissural axons extending through the FP [86]. Recently, blocking NogoR was found to result in axon stalling at the FP and therefore in a reduction of the number of commissural fibers properly reaching the contralateral side of the spinal cord. Furthermore, it has been reported that the ligand interacting with NogoR is a truncated form of Nogo released by glial cells [87].

1.2.4.2. Temporal regulation of commissural axon sensitivity to the repellents. Pioneer studies performed in *Drosophila* revealed that ROBO protein is degraded in pre-crossing commissural axons by the endosomal protein COMM [88,89]. Yet, ROBO mutant phenotype is rescued by a mutated version of ROBO that cannot be sorted by COMM. COMM thus probably regulates Slit/ROBO interaction through an additional, sorting-independent mechanism [90]. ROBO2 is also expressed by midline glial cells and has been shown to interact with ROBO1 in *trans*. This interaction would occur upon crossing, when ROBO1 receptors reach the cell surface consequently of COMM suppression and it would repress Slit repulsion until the crossing is completed [91].

How are ROBO distribution and activity regulated in time are therefore key questions to further understand the navigation of the midline. COMM expression was shown to be controlled at least in part by Frazzled/DCC in pre-crossing [92], while it remains unknown how it is repressed after midline crossing. The nature of mechanisms silencing Slit repulsion before the crossing has been thought to totally differ in vertebrates since no COMM homolog was found in their genomes. Nevertheless, vesicular trafficking also appears as an important process in vertebrates. Indeed, vesicles containing ROBO1 were observed in commissural axons. Calsyntenin1 and RabGDI were found to regulate their trafficking and to allow the pulse exposure of ROBO1 at the growth cone surface [93,94]. Interestingly too, a recent study identified PRRG4, a protein which displays structural similarities with COMM, as capable of re-localizing ROBO1 at the cell surface *in vitro* [95]. Another reported regulator of Slit/ROBO signaling is an isoform of ROBO3, a divergent member of the ROBO family, ROBO3.1. Its distribution is restricted to the pre-crossing commissural axons and it is thought to facilitate midline crossing by antagonizing Slit/ROBO1/2 mediated repulsion [21]. The underlying mechanism is not yet known. It might not involve ROBO3 as a Slit receptor since ROBO3 was shown to have lost its affinity to bind Slit ligands with evolution, instead rather acting as a DCC co-receptor for NETRIN-1 [96]. Thus, progress as yet to be accomplished to better understand how the regulators of ROBO receptors are temporally controlled and their activity synchronized with midline crossing.

Please cite this article in press as: H. Ducuing, et al., Commissural axon navigation in the spinal cord: A repertoire of repulsive forces is in command, Semin Cell Dev Biol (2017), https://doi.org/10.1016/j.semcdb.2017.12.010

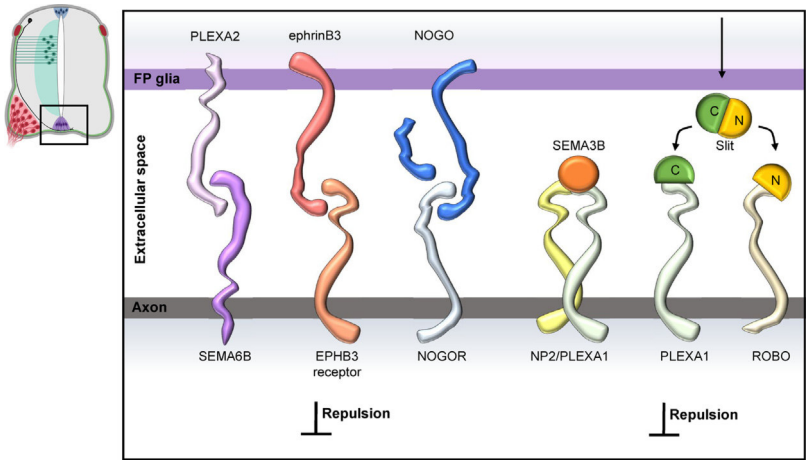

Fig. 5. Repulsive forces in the floor plate.
While crossing the floor plate (FP), axons gain sensitivity to repulsive cues they did not perceive at the pre-crossing stage. PlexinA2 (PLEXA2), EphrinB3 (EphrinB3) and NOGO, expressed at the membrane of FP glial cells, interact respectively with Semaphorin6B (SEMA6B), EphB3 receptor and NOGO receptor (NOGOR) expressed by commissural axons. In parallel, the FP glial cells also secrete repulsive cues. A truncated, diffusible version of Nogo can also bind to the axonal Nogo receptor. Sema3B binds to a heterodimer of Neuropilin2 (NP2) and PlexinA1 (PLEXA1) axonal receptors. Slit produced by FP glia is cleaved into a C-terminal (SLITC) and an N-terminal fragments (SLITN). SLITC binds to PLEXA1, while SLITN interacts with ROBO.

Similarly, axon sensitivity to Semaphorin repulsive signaling is tightly controlled and PLEXA1 sorting at the axon surface in the FP is thought to be a key event switching on the sensitivity of commissural axons to SEMA3B. We indeed found that PLEXA1 is processed by Calpains in pre-crossing axons. This processing prevents PLEXINA1 cell surface sorting, and thus the association with NP2 co-receptor needed to transduce SEMA3B signaling [79]. We also found that this silencing of SEMA3B responsiveness is released by local FP cues, GDNF and NrCAM, which trigger PLEXINA1 cell surface sorting by inhibiting Calpain activity [97]. In addition, SEMA6B and PLEXA2 were also shown to interact in *cis* at the growth cone surface and to silence the sensitivity of pre-crossing axons to midline-associated SEMA6B [80]. Thus, as it is the case for the ROBO/Slit pathway, post-translational mechanisms appear to be instrumental in regulating the timing of activity of the Semaphorin repellents.

1.3. *After FP crossing: a new pinball game starts*

A second pinball game starts when FP repulsive signals propel commissural axons out of the FP. Concomitantly, a drastic change of direction is accomplished by the dl1c axons which turn in the rostral direction to navigate longitudinally to the FP. Two opposite chemotropic gradients control this guidance choice: a caudal high to rostral low repulsive one shaped by SHH, and a caudal low to rostral high attractive one shaped by WNT. Thus, as during the pre-crossing navigation game, repulsive forces play an important role in propelling the axons and imprinting the direction of their longitudinal growth. A temporal control of these forces is also needed. SHH has a reported pre-crossing attractive activity, shown to be mediated by SMO and one of its receptors, BOC (Brother of CDO) [71,98,99]. Upon crossing, SHH attraction must be switched into repulsion, a process proposed in the chick to be achieved *via* the implication of another SHH receptor, HHIP (Hedgehog Interacting Protein), in addition to SMO in the mouse [78,100] (Fig. 6). The cytoplasmic adaptor protein, 14-3-3, increases in amount during the pre-crossing navigation to culminate at the post-crossing stage, during which it is required for SHH-dependent repulsion [100]. In parallel, the sensitivity of the complementary rostro-caudal chemoattractive gradient of WNT is also switched on upon the crossing. A mechanism was recently reported implicating a molecular cascade during which SHH/SMO downregulates transcript levels of Shisa2 in commissural neurons. Down-regulation of Shisa2 allowed the WNT receptor Frizzled3 to be glycosylated and translocated to the surface of the commissural axon growth cones [101].

Once the rostrocaudal direction is given, commissural axons segregate in several tracts. Reorganizations of post-crossing commissural axons during this step likely implicate selective fasciculation. In xenopus, live monitoring of commissural axons in the spinal cord revealed striking changes in the behaviors of the growth cones during crossing process. In fact, during pre-crossing navigation, growth cones were observed to avoid each others whereas in the post-crossing stage (after their longitudinal turning), they accomplished a series of fasciculation choices which suggest a process of bundle selection [102]. Several cell adhesion molecules are up-regulated in post-crossing commissural axons, such as the IgSFCAM L1 in the mouse [69], which could contribute to this recognition process.

In *Drosophila*, commissural axons form three longitudinal tracts [103]. Their sorting and their position relative to the midline was shown to be controlled by a combination of ROBO receptors, differing between the tracts and thought to confer them different levels of sensitivity to midline Slit repellent [104]. A theoretical model predicts that a ROBO code based on quantitative differences of ROBO proteins could be on its own sufficient to generate different lateral tract position [105].

In vertebrates, post-crossing commissural axons are sorted into two main tracts, navigating the ventral and lateral funiculi. The mechanisms underlying this sorting are still elusive. An implication of the Slit-ROBO signaling was reported from the analysis of Slit and ROBO null embryos, in which this sorting is defective [106]. An interplay of Robo and N-cadherin was also found to contribute to the lateral sorting of post-crossing commissural axons [107]. The Ephrin signaling is also involved in the mediolateral positioning of the longitudinal tracts. Blocking EphB3/EphB signaling was reported to result in a lateral shift of commissural axons [83,108].

Even though the topography of post-crossing axons differs from that of pre-crossing ones, the longitudinal navigation after midline crossing also appears constrained and channeled by the FP, the lateral basal lamina and the motoneuron domain. Whether the underlying mechanisms and signaling pathways are similar to those operating at the pre-crossing stage remains to be determined.

Please cite this article in press as: H. Ducuing, et al., Commissural axon navigation in the spinal cord: A repertoire of repulsive forces is in command, Semin Cell Dev Biol (2017), https://doi.org/10.1016/j.semcdb.2017.12.010

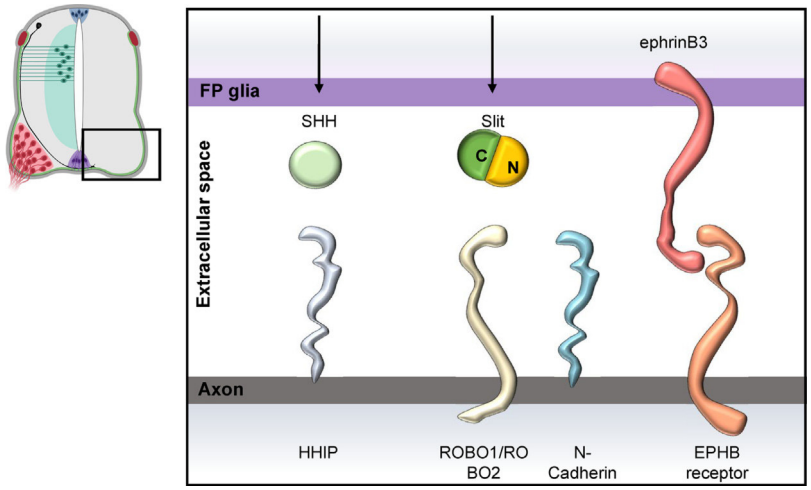

Fig. 6. Repulsive forces in command of post-crossing axon navigation.
After crossing the floor plate (FP), commissural axons turn rostrally in response to gradients of attractive and repulsive cues. Diffusible Shh from the FP glial cells interacts with the axonal receptor HHIP. In vertebrates, post-crossing commissural axons form two main tracts, the first turns in the ventral funiculus, while the second turns in the lateral funiculus. Slit contributes to this sorting through interaction with axonal ROBO1 and ROBO2. An interplay of ROBO and N-cadherin was also found to contribute to the lateral sorting of post-crossing commissural axons. Trans-interactions also occur between glial Ephrin-B3 (Eph-B3) and axonal Eph-B receptor to assign the medio-lateral position of post-crossing tracts.

1.4. Conclusion and perspectives

Important progress has been made over the years to identify components of the molecular machinery controlling axon pathfinding. The versatility of growth cone responsiveness to guidance cues endows the axon with multiple possibilities to interpret in a highly specific manner the topographic signals and the physical elements encountered in the environment during its navigation. Recent tissue-specific deletions of guidance molecules have revealed unexpected contributions of territories surrounding axonal pathways. This provides a better integrated picture, which would require to be further extended, on how axon guidance proceeds in an environment that is also subjected to continuous developmental constraints. In addition, a series of molecular mechanisms has been discovered, which brings to light the importance of spatial and temporal controls of growth cone sensitivity to guidance cues. Altogether, this raises the need of better understanding at protein levels how topographic cues are distributed and deposited in the tissues and how the activity of guidance receptors and downstream effectors in the growth cones is focused and fine-tuned.

In the context of commissural axon guidance, many types of repulsive forces which remain underestimated are likely to play key contributions in the robustness of commissural axon pathfinding. While it is rather straightforward to conceive how a repulsive cue repel away a growth cone, it is much less simple to conceive how commissural growth cone can navigate a field expressing repellents to which it progressively acquires sensitivity. Several theoretical models of axon guidance have been elaborated to explain the building of topographic maps. A recent one was based on the principle that growth cones undergo concentration-dependent alternated choices of repulsive and attractive response to guidance cues [109]. Interesting insights would come from such models of FP navigation that would integrate the different forces at play in time and space.

Acknowledgments

VC is supported by the LABEX CORTEX and DEVWECAN of the “Université de Lyon”, within the programme ‘Investissements d’Avenir’ (ANR-11-IDEX-0007) operated by the French National Research Agency (ANR), ANR-16-CE16-0023-01, and French Muscular Dystrophy Association (AFM).

References

[1] M. Tessier-Lavigne, M. Placzek, Target attraction: are developing axons guided by chemotropism? Trends Neurosci. 14 (1991) 303–310, 0166-2236(91)90142-H [pii].
[2] M. Tessier-Lavigne, C.S. Goodman, The molecular biology of axon guidance, Science 274 (Nov (5290)) (1996) 1123–1133.
[3] P. Haydon, D. McCobb, S. Kater, Serotonin selectively inhibits growth cone motility and synaptogenesis of specific identified neurons, Science 226 (1984) 561–564, http://dx.doi.org/10.1126/science.6093252 (80-.).
[4] J.P. Kapfhammer, J.A. Raper, Collapse of growth cone structure on contact with specific neurites in culture, J. Neurosci. 7 (1987) 201–212.
[5] J.M. Verna, In vitro analysis of interactions between sensory neurons and skin: evidence for selective innervation of dermis and epidermis, J. Embryol. Exp. Morphol. 86 (1985) 53–70 http://www.ncbi.nlm.nih.gov/pubmed/4031747.
[6] R. Levi-Montalcini, V. Hamburger, A diffusible agent of mouse sarcoma, producing hyperplasia of sympathetic ganglia and hyperneurotization of viscera in the chick embryo, J. Exp. Zool. 123 (1953) 233–287, http://dx.doi.org/10.1002/jez.1401230203.
[7] D. Bonanomi, S.L. Pfaff, Motor axon pathfinding, Cold Spring Harb. Perspect. Biol. 2 (1992) 28–30, http://dx.doi.org/10.1101/cshperspect.a001735.
[8] P. Suetterlin, K.M. Marler, U. Drescher, Axonal ephrinA/EphA interactions, and the emergence of order in topographic projections, Semin. Cell. Dev. Biol. 23 (2012) 1–6, http://dx.doi.org/10.1016/j.semcdb.2011.10.015.
[9] S. Vulliemoz, O. Raineteau, D. Jabaudon, Reaching beyond the midline: why are human brains cross wired? Lancet Neurol. 4 (2005) 87–99, http://dx.doi.org/10.1016/S1474-4422(05)00990-7.
[10] V. Castellani, Building spinal and brain commissures: axon guidance at the midline, ISRN Cell Biol. 2013 (2013) 1–21, http://dx.doi.org/10.1155/2013/315387.
[11] A. Chedotal, The Robo3 Receptor, a Key Player in the Development, Evolution, and Function of Commissural Systems, 2016, http://dx.doi.org/10.1002/dneu.22478.
[12] J.L. Gómez-Skarmeta, S. Campuzano, J. Modolell, Half a century of neural prepatterning: the story of a few bristles and many genes, Nat. Rev. Neurosci. 4 (2003) 587–598, http://dx.doi.org/10.1038/nrn1142.
[13] S.J. Butler, M.E. Bronner, From classical to current: analyzing peripheral nervous system and spinal cord lineage and fate, Dev. Biol. 398 (2015) 135–146, http://dx.doi.org/10.1016/j.ydbio.2014.09.033.
[14] K.J. Lee, M. Mendelsohn, T.M. Jessell, Neuronal patterning by BMPs: a requirement for GDF7 in the generation of a discrete class of commissural interneurons in the mouse spinal cord, Genes Dev. 12 (1998) 3394–3407, http://dx.doi.org/10.1101/gad.12.21.3394.
[15] N.A. Bermingham, B.A. Hassan, V.Y. Wang, M. Fernandez, S. Banfi, H.J. Bellen, B. Fritzsch, H.Y. Zoghbi, Proprioceptor pathway development is dependent on MATH1, Neuron 30 (2001) 411–422, http://dx.doi.org/10.1016/S0896-6273(01)00305-1.
[16] A.W. Helms, J.E. Johnson, Progenitors of dorsal commissural interneurons are defined by MATH1 expression, Development 125 (1998) 919–928, http://dx.doi.org/10.1074/jbc.270.15.8730.
[17] R.W. Oppenheim, A. Shneiderman, I. Shimizu, H. Yaginuma, Onset and development of intersegmental projections in the chick embryo spinal cord,

Please cite this article in press as: H. Ducuing, et al., Commissural axon navigation in the spinal cord: A repertoire of repulsive forces is in command, Semin Cell Dev Biol (2017), https://doi.org/10.1016/j.semcdb.2017.12.010

J. Comp. Neurol. 275 (1988) 159–180, http://dx.doi.org/10.1002/cne.902750202.
[18] S.A. Colamarino, M. Tessier-Lavigne, The Role of the Floor Plate in Axon Guidance, 1995, pp. 497–529.
[19] S.R. Kadison, Z. Kaprielian, Diversity of contralateral commissural projections in the embryonic rodent spinal cord, J. Comp. Neurol. 472 (2004) 411–422, http://dx.doi.org/10.1002/cne.20086.
[20] R. Imondi, A.R. Jevince, A.W. Helms, J.E. Johnson, Z. Kaprielian, Mis-expression of L1 on pre-crossing spinal commissural axons disrupts pathfinding at the ventral midline, Mol. Cell. Neurosci. 36 (2007) 462–471, http://dx.doi.org/10.1016/j.mcn.2007.08.003.
[21] Z. Chen, B.B. Gore, H. Long, L. Ma, M. Tessier-Lavigne, Alternative splicing of the Robo3 axon guidance receptor governs the midline switch from attraction to repulsion, Neuron 58 (2008) 325–332, http://dx.doi.org/10.1016/j.neuron.2008.02.016.
[22] V.V. Chizhikov, K.J. Millen, Mechanisms of roof plate formation in the vertebrate CNS, Nat. Rev. Neurosci. 5 (2004) 808–812, http://dx.doi.org/10.1038/nrn1520.
[23] J.H. Millonig, K.J. Millen, M.E. Hatten, The mouse Dreher gene Lmx1a controls formation of the roof plate in the vertebrate CNS, Nature 403 (2000) 764–769, http://dx.doi.org/10.1038/35001573.
[24] R.R. Sturrock, An electron microscopic study of the development of the ependyma of the central canal of the mouse spinal cord, J. Anat. 132 (1981) 119–136 http://www.pubmedcentral.nih.gov/articlerender.fcgi?artid=1233400&tool=pmcentrez&rendertype=abstract.
[25] D.M. Snow, D.A. Steindler, J. Silver, Molecular and cellular characterization of the glial roof plate of the spinal cord and optic tectum: a possible role for a proteoglycan in the development of an axon barrier, Dev. Biol. 138 (1990) 359–376, http://dx.doi.org/10.1016/0012-1606(90)90203-U.
[26] J.D. Comer, F.C. Pan, S.G. Willet, P. Haldipur, K.J. Millen, C.V.E. Wright, J.A. Kaltschmidt, Sensory and spinal inhibitory dorsal midline crossing is independent of Robo3, Front. Neural Circuits 9 (2015) 36, http://dx.doi.org/10.3389/fncir.2015.00036.
[27] G. Le Dréau, E. Martí, Dorsal-ventral patterning of the neural tube: A tale of three signals, Dev. Neurobiol. 72 (2012) 1471–1481, http://dx.doi.org/10.1002/dneu.22015.
[28] A. Augsburger, A. Schuchardt, S. Hoskins, J. Dodd, S. Butler, BMPs as Mediators of Roof Plate Repulsion of Commissural Neurons, 24, 1999, pp. 127–141.
[29] S.J. Butler, J. Dodd, A role for BMP heterodimers in roof plate-mediated repulsion of commissural axons, Neuron 38 (2003) 389–401, http://dx.doi.org/10.1016/S0896-6273(03)00254-X.
[30] K.D. Phan, V.M. Hazen, M. Frendo, Z. Jia, S.J. Butler, The bone morphogenetic protein roof plate chemorepellent regulates the rate of commissural axonal growth, J. Neurosci. 30 (2010) 15430–15440, http://dx.doi.org/10.1523/JNEUROSCI.4117-10.2010.
[31] S.M. Islam, Y. Shinmyo, T. Okafuji, Y. Su, I.B. Naser, G. Ahmed, S. Zhang, S. Chen, K. Ohta, H. Kiyonari, T. Abe, S. Tanaka, R. Nishinakamura, T. Terashima, T. Kitamura, H. Tanaka, Draxin, a repulsive guidance protein for spinal cord and forebrain commissures, Science 323 (2009) 388–393, http://dx.doi.org/10.1126/science.1165187 (80-.).
[32] T. Serafini, T.E. Kennedy, M.J. Gaiko, C. Mirzayan, T.M. Jessell, M. Tessier-Lavigne, The netrins define a family of axon outgrowth-promoting proteins homologous to C. elegans UNC-6, Cell 78 (1994) 409–424, http://dx.doi.org/10.1016/0092-8674(94)90420-0.
[33] T.E. Kennedy, T. Serafini, J.R. de la Torre, M. Tessier-Lavigne, Netrins are diffusible chemotropic factors for commissural axons in the embryonic spinal cord, Cell 78 (1994) 425–435, http://dx.doi.org/10.1016/0092-8674(94)90421-9.
[34] X. Gao, U. Metzger, P. Panza, P. Mahalwar, S. Alsheimer, H. Geiger, H.M. Maischein, M.P. Levesque, M. Templin, C. Söllner, A floor-plate extracellular protein-protein interaction screen identifies Draxin as a secreted Netrin-1 antagonist, Cell Rep. 12 (2015) 694–708, http://dx.doi.org/10.1016/j.celrep.2015.06.047.
[35] G. Ahmed, Y. Shinmyo, K. Ohta, S.M. Islam, M. Hossain, I.B. Naser, M.A. Riyadh, Y. Su, S. Zhang, M. Tessier-Lavigne, H. Tanaka, Draxin inhibits axonal outgrowth through the netrin receptor DCC, J. Neurosci. 31 (2011) 14018–14023, http://dx.doi.org/10.1523/JNEUROSCI.0943-11.2011.
[36] K. Brose, K.S. Bland, K.H. Wang, D. Arnott, W. Henzel, C.S. Goodman, M. Tessier-Lavigne, T. Kidd, Slit proteins bind robo receptors and have an evolutionarily conserved role in repulsive axon guidance, Cell 96 (1999) 795–806, http://dx.doi.org/10.1016/S0092-8674(00)80590-5.
[37] Y. Choe, J.A. Siegenthaler, S.J. Pleasure, A cascade of morphogenic signaling initiated by the meninges controls corpus callosum formation, Neuron 73 (2013) 698–712, http://dx.doi.org/10.1016/j.neuron.2011.11.036.A.
[38] T.A.C.S. Suter, Z.J. Deloughery, A. Jaworski, Meninges-derived cues control axon guidance, Dev. Biol. (2017) 1–10, http://dx.doi.org/10.1016/j.ydbio.2017.08.005.
[39] M. Vermeren, G.S. Maro, R. Bron, I.M. McGonnell, P. Charnay, P. Topilko, J. Cohen, Integrity of developing spinal motor columns is regulated by neural crest derivatives at motor exit points, Neuron 37 (2003) 403–415, http://dx.doi.org/10.1016/S0896-6273(02)01188-1.
[40] J. Altman, S.A. Bayer, The development of the rat spinal cord, Adv. Anat. Embryol. Cell Biol. 85 (1984) 1–164 (Accessed September 28, 2017) http://www.ncbi.nlm.nih.gov/pubmed/6741688.
[41] F. Friocourt, A.-G. Lafont, C. Kress, B. Pain, M. Manceau, S. Dufour, A. Chédotal, Recurrent DCC gene losses during bird evolution, Sci. Rep. 7 (2017) 37569, http://dx.doi.org/10.1038/srep37569.
[42] K.D. Phan, L.P. Croteau, J.W.K. Kam, A. Kania, J.F. Cloutier, S.J. Butler, Neogenin may functionally substitute for Dcc in chicken, PLoS One 6 (2011) 1–10, http://dx.doi.org/10.1371/journal.pone.0022072.
[43] K.M. Wright, K.A. Lyon, H. Leung, D.J. Leahy, L. Ma, D.D. Ginty, Dystroglycan organizes axon guidance cue localization and axonal pathfinding, Neuron 76 (2012) 931–944, http://dx.doi.org/10.1016/j.neuron.2012.10.009.
[44] K.S. O'Shea, Differential deposition of basement membrane components during formation of the caudal neural tube in the mouse embryo, Development 99 (1987) 509–519 http://www.ncbi.nlm.nih.gov/pubmed/3665768.
[45] V.H. Hopker, D. Shewan, M. Tessier-Lavigne, M. Poo, C. Holt, Growth-cone attraction to netrin-1 is converted to repulsion by laminin-1, Nature 401 (1999) 69–73, http://dx.doi.org/10.1038/43441.
[46] E. Taverna, M. Götz, W.B. Huttner, The cell biology of neurogenesis: toward an understanding of the development and evolution of the neocortex, Annu. Rev. Cell Dev. Biol. (2014), http://dx.doi.org/10.1146/annurev-cellbio-101011-155801.
[47] S. Cord, J.H. Kong, K.D. Phan, A. Kania, B.G. Novitch, S.J. Butler, S.G. Varadarajan, J.H. Kong, K.D. Phan, T. Kao, S.C. Panaitof, J. Cardin, Netrin1 produced by neural progenitors, not floor plate cells, is required for axon guidance in the report Netrin1 produced by neural progenitors, not floor plate cells, is required for axon guidance in the spinal cord, Neuron (2017) 1–10, http://dx.doi.org/10.1016/j.neuron.2017.03.007.
[48] E. Leyva-Díaz, G. López-Bendito, In and out from the cortex: development of major forebrain connections, Neuroscience 254 (2013) 26–44, http://dx.doi.org/10.1016/j.neuroscience.2013.08.070.
[49] A.W. Püschel, R.H. Adams, H. Betz, The sensory innervation of the mouse spinal, Mol. Cell. Neurosci. 431 (1996) 419–431.
[50] F. Moret, C. Renaudot, M. Bozon, V. Castellani, Semaphorin and neuropilin co-expression in motoneurons sets axon sensitivity to environmental semaphorin sources during motor axon pathfinding, Development 134 (2007) 4491–4501, http://dx.doi.org/10.1242/dev.011452.
[51] I. Sanyas, M. Bozon, F. Moret, V. Castellani, Motoneuronal Sema3C is essential for setting stereotyped motor tract positioning in limb-derived chemotropic semaphorins, Development 139 (2012) 3633–3643, http://dx.doi.org/10.1242/dev.080051.
[52] E. Arbeille, F. Reynaud, I. Sanyas, M. Bozon, K. Kindbeiter, F. Causeret, A. Pierani, J. Falk, F. Moret, V. Castellani, Cerebrospinal fluid-derived Semaphorin3B orients neuroepithelial cell divisions in the apicobasal axis, Nat. Commun. 6 (2015) 6366, http://dx.doi.org/10.1038/ncomms7366.
[53] J. Laussu, C. Audouard, A. Kischel, P. Assis-Nascimento, N. Escalas, D.J. Liebl, C. Soula, A. Davy, Eph/ephrin signaling controls progenitor identities in the ventral spinal cord, Neural Dev. 12 (2017) 10, http://dx.doi.org/10.1186/s13064-017-0087-0.
[54] J.S. Dasen, T.M. Jessell, Hox Networks and the Origins of Motor Neuron Diversity, 1st ed., Elsevier Inc., 2009, http://dx.doi.org/10.1016/S0070-2153(09)88006-X.
[55] P. Bovolenta, J. Dodd, Perturbation of neuronal differentiation and axon guidance in the spinal cord of mouse embryos lacking a floor plate: analysis of Danforth's short-tail mutation, Development 113 (1991) 625–639.
[56] T. Yamada, M. Placzek, H. Tanaka, J. Dodd, T.M. Jessell, Control of cell pattern in the developing nervous system: polarizing activity of the floor plate and notochord, Cell 64 (1991) 635–647, http://dx.doi.org/10.1016/0092-8674(91)90247-V.
[57] A. Jaworski, I. Tom, R.K. Tong, H.K. Gildea, A.W. Koch, L.C. Gonzalez, M. Tessier-Lavigne, Operational redundancy in axon guidance through the multifunctional receptor Robo3 and its ligand NELL2, Science 350 (2015) 961–965.
[58] T.D. Tayler, M.B. Robichaux, P.A. Garrity, Compartmentalization of visual centers in the Drosophila brain requires Slit and Robo proteins, Development 131 (2004) 5935–5945, http://dx.doi.org/10.1242/dev.01465.
[59] Y. Zou, E. Stoeckli, H. Chen, M. Tessier-Lavigne, Squeezing axons out of the gray matter: a role for Slit and semaphorin proteins from midline and ventral spinal cord, Cell. 102 (2000) 363–375.
[60] U. Strähle, C.S. Lam, R. Ertzer, S. Rastegar, Vertebrate floor-plate specification: variations on common themes, Trends Genet. 20 (2004) 155–162, http://dx.doi.org/10.1016/j.tig.2004.01.002.
[61] M. Placzek, J. Briscoe, The floor plate: multiple cells, multiple signals, Nat. Rev. Neurosci. 6 (2005) 230–240, http://dx.doi.org/10.1038/nrn1628.
[62] V. Ribes, N. Balaskas, N. Sasai, C. Cruz, E. Dessaud, J. Cayuso, S. Tozer, L.L. Yang, B. Novitch, E. Marti, J. Briscoe, Distinct sonic hedgehog signaling dynamics specify floor plate and ventral neuronal progenitors in the vertebrate neural tube, Genes Dev. 24 (2010) 1186–1200, http://dx.doi.org/10.1101/gad.559910.
[63] R.M. Campbell, A.C. Peterson, Expression of a lacZ transgene reveals floor plate cell morphology and macromolecular transfer to commissural axons, Development 119 (1993) 1217–1228 http://www.ncbi.nlm.nih.gov/pubmed/8306884.
[64] H. Yaginuma, S. Homma, R. Künzi, R.W. Oppenheim, Pathfinding by growth cones of commissural interneurons in the chick embryo spinal cord: a light and electron microscopic study, J. Comp. Neurol. 304 (1991) 78–102, http://dx.doi.org/10.1002/cne.903040107.

Please cite this article in press as: H. Ducuing, et al., Commissural axon navigation in the spinal cord: A repertoire of repulsive forces is in command, Semin Cell Dev Biol (2017), https://doi.org/10.1016/j.semcdb.2017.12.010

[65] N. Okabe, K. Shimizu, K. Ozaki-Kuroda, H. Nakanishi, K. Morimoto, M. Takeuchi, H. Katsumaru, F. Murakami, Y. Takai, Contacts between the commissural axons and the floor plate cells are mediated by nectins, Dev. Biol. (2004) 244–256, http://dx.doi.org/10.1016/j.ydbio.2004.05.034.
[66] E.T. Stoeckli, L.T. Landmesser, Axonin-1, Nr-CAM, and Ng-CAM play different roles in the in vivo guidance of chick commissural neurons, Neuron 14 (1995) 1165–1179, http://dx.doi.org/10.1016/0896-6273(95)90264-3.
[67] E.T. Stoeckli, L.T. Landmesser, Axon guidance at choice points, Curr. Opin. Neurobiol. 8 (1998) 73–79, http://dx.doi.org/10.1016/S0959-4388(98)80010-X.
[68] S. Kunz, M. Spirig, C. Ginsburg, A. Buchstaller, P. Berger, R. Lanz, C. Rader, L. Vogt, B. Kunz, P. Sonderegger, Neurite fasciculation mediated by complexes of axonin-1 and Ng cell adhesion molecule, J. Cell Biol. 143 (1998) 1673–1690, http://dx.doi.org/10.1083/jcb.143.6.1673.
[69] R. Imondi, A.R. Jevince, A.W. Helms, J.E. Johnson, Z. Kaprielian, Mis-expression of L1 on pre-crossing spinal commissural axons disrupts pathfinding at the ventral midline, Mol. Cell. Neurosci. 36 (2007) 462–471, http://dx.doi.org/10.1016/j.mcn.2007.08.003.
[70] T. Serafini, S.A. Colamarino, E.D. Leonardo, H. Wang, R. Beddington, W.C. Skarnes, M. Tessier-Lavigne, Netrin-1 is required for commissural axon guidance in the developing vertebrate nervous system, Cell 87 (1996) 1001–1014, http://dx.doi.org/10.1016/S0092-8674(00)81795-X.
[71] F. Charron, E. Stein, J. Jeong, A.P. McMahon, M. Tessier-Lavigne, The morphogen sonic hedgehog is an axonal chemoattractant that collaborates with netrin-1 in midline axon guidance, Cell 113 (2003) 11–23, http://dx.doi.org/10.1016/S0092-8674(03)00199-5.
[72] C.R. De Almodovar, P.J. Fabre, E. Knevels, C. Coulon, I. Segura, P.C.G. Haddick, L. Aerts, N. Delattin, G. Strasser, W. Oh, C. Lange, S. Vinckier, J. Haigh, C. Fouquet, C. Gu, K. Alitalo, V. Castellani, M. Tessier-lavigne, A. Chedotal, F. Charron, P. Carmeliet, VEGF mediates commissural axon chemoattraction through its receptor Flk1, Neuron 70 (2005) 966–978, http://dx.doi.org/10.1016/j.neuron.2011.04.014.
[73] C. Dominici, J.A. Moreno-bravo, S.R. Puiggros, Q. Rappeneau, N. Rama, P. Vieugue, A. Bernet, P. Mehlen, A. Chédotal, Floor-plate-derived netrin-1 is dispensable for commissural axon guidance, Nature (2017), http://dx.doi.org/10.1038/nature22331.
[74] A. Pignata, H. Ducuing, V. Castellani, Commissural axon navigation: control of midline crossing in the vertebrate spinal cord by the semaphorin 3B signaling, Cell Adh. Migr. 10 (2016) 604–617, http://dx.doi.org/10.1080/19336918.2016.1212804.
[75] A. Neuhaus-Follini, G.J. Bashaw, Crossing the embryonic midline: molecular mechanisms regulating axon responsiveness at an intermediate target, Wiley Interdiscip. Rev. Dev. Biol. 4 (2015) 377–389, http://dx.doi.org/10.1002/wdev.185.
[76] R. Shirasaki, Change in chemoattractant responsiveness of developing axons at an intermediate target, Science 279 (1998) 105–107, http://dx.doi.org/10.1126/science.279.5347.105 (80-.).
[77] E. Stein, M. Tessier-Lavigne, Hierarchical organization of guidance receptors: silencing of netrin attraction by slit through a Robo/DCC receptor complex, Science 291 (2001) 1928–1938, http://dx.doi.org/10.1126/science.1058445 (80-.).
[78] D. Bourikas, V. Pekarik, T. Baeriswyl, A. Grunditz, R. Sadhu, M. Nardó, E.T. Stoeckli, Sonic hedgehog guides commissural axons along the longitudinal axis of the spinal cord, Nat. Neurosci. 8 (2005) 297–304, http://dx.doi.org/10.1038/nn1396.
[79] H. Nawabi, A. Briançon-Marjollet, C. Clark, I. Sanyas, H. Takamatsu, T. Okuno, A. Kumanogoh, M. Bozon, K. Takeshima, Y. Yoshida, F. Moret, K. Abouzid, V. Castellani, A midline switch of receptor processing regulates commissural axon guidance in vertebrates, Genes Dev. 24 (2010) 396–410, http://dx.doi.org/10.1101/gad.542510.
[80] I. Andermatt, N.H. Wilson, T. Bergmann, O. Mauti, M. Gesemann, S. Sockanathan, E.T. Stoeckli, Semaphorin 6B acts as a receptor in post-crossing commissural axon guidance, Development (2014) 3709–3720, http://dx.doi.org/10.1242/dev.112185.
[81] C. Delloye-bourgeois, A. Jacquier, C. Charoy, F. Reynaud, H. Nawabi, K. Thoinet, K. Kindbeiter, Y. Yoshida, Y. Zagar, Y. Kong, Y.E. Jones, J. Falk, A. Chédotal, V. Castellani, PlexinA1 is a new Slit receptor and mediates axon guidance function of Slit C-terminal fragments, Nat. Publ. Gr. 18 (2014) 36–45, http://dx.doi.org/10.1038/nn.3893.
[82] C.A. Cowan, M. Henkemeyer, Ephrins in reverse, park and drive, Trends Cell Biol. 12 (2002) 339–346, http://dx.doi.org/10.1016/S0962-8924(02)02317-6.
[83] S.R. Kadison, T. Mäkinen, R. Klein, M. Henkemeyer, Z. Kaprielian, EphB receptors and ephrin-B3 regulate axon guidance at the ventral midline of the embryonic mouse spinal cord, J. Neurosci. 26 (2006) 8909–8914, http://dx.doi.org/10.1523/JNEUROSCI.1569-06.2006.
[84] M. Domeniconi, Z. Cao, T. Spencer, R. Sivasankaran, K.C. Wang, E. Nikulina, N. Kimura, H. Cai, K. Deng, Y. Gao, Z. He, M.T. Filbin, Myelin-associated glycoprotein interacts with the Nogo66 receptor to inhibit neurite outgrowth, Neuron 35 (2002) 283–290, http://dx.doi.org/10.1016/S0896-6273(02)00770-5.
[85] K.C. Wang, J.A. Kim, R. Sivasankaran, R. Segal, Z. He, p75 interacts with the Nogo receptor as a co-receptor for Nogo, MAG and OMgp, Nature 420 (2002) 74–78, http://dx.doi.org/10.1038/nature01176.
[86] J. Wang, L. Wang, H. Zhao, S.O. Chan, Localization of an axon growth inhibitory molecule Nogo and its receptor in the spinal cord of mouse embryos, Brain Res. 1306 (2010) 8–17, http://dx.doi.org/10.1016/j.brainres.2009.10.018.
[87] L. Wang, C. Yu, J. Wang, P. Leung, D. Ma, H. Zhao, J.S.H. Taylor, S.-O. Chan, Nogo-B is the major form of Nogo at the floor plate and likely mediates crossing of commissural axons in the mouse spinal cord, J. Comp. Neurol. 525 (2017) 2915–2928, http://dx.doi.org/10.1002/cne.24246.
[88] K. Keleman, S. Rajagopalan, D. Cleppien, D. Teis, K. Paiha, L.A. Huber, G.M. Technau, B.J. Dickson, Comm sorts Robo to control axon guidance at the Drosophila midline, Cell 110 (2002) 415–427, http://dx.doi.org/10.1016/S0092-8674(02)00901-7.
[89] K. Keleman, C. Ribeiro, B.J. Dickson, Comm function in commissural axon guidance: cell-autonomous sorting of Robo in vivo, Nat. Neurosci. 8 (2005) 156–163, http://dx.doi.org/10.1038/nn1388.
[90] G.F. Gilestro, Redundant mechanisms for regulation of midline crossing in Drosophila, PLoS One 3 (2008), http://dx.doi.org/10.1371/journal.pone.0003798.
[91] T.A. Evans, C. Santiago, E. Arbeille, G.J. Bashaw, Robo2 acts in trans to inhibit Slit-Robo1 repulsion in pre-crossing commissural axons, Elife 4 (2015) e08407, http://dx.doi.org/10.7554/eLife.08407.
[92] L. Yang, D.S. Garbe, G.J. Bashaw, A frazzled/DCC-dependent transcriptional switch regulates midline axon guidance, Science 324 (2009) 944–947, http://dx.doi.org/10.1126/science.1171320.
[93] T.A. Alther, E. Domanitskaya, E.T. Stoeckli, Calsyntenin 1-mediated trafficking of axon guidance receptors regulates the switch in axonal responsiveness at a choice point, Development 143 (2016) 994–1004, http://dx.doi.org/10.1242/dev.127449.
[94] M. Philipp, V. Niederkofler, M. Debrunner, T. Alther, B. Kunz, E.T. Stoeckli, RabGDI controls axonal midline crossing by regulating Robo1 surface expression, Neural Dev. 7 (2012) 36, http://dx.doi.org/10.1186/1749-8104-7-36.
[95] E.D. Justice, S.J. Barnum, T. Kidd, The WAGR syndrome gene PRRG4 is a functional homologue of the commissureless axon guidance gene, PLoS Genet. (2017) 1–21.
[96] P. Zelina, H. Blockus, Y. Zagar, A. Péres, F. Friocourt, Z. Wu, N. Rama, C. Fouquet, E. Hohenester, M. Tessier-Lavigne, J. Schweitzer, H.R. Crollius, A. Chédotal, Signaling switch of the axon guidance receptor Robo3 during vertebrate evolution, Neuron 84 (2014) 1258–1272, http://dx.doi.org/10.1016/j.neuron.2014.11.004.
[97] C. Charoy, H. Nawabi, F. Reynaud, E. Derrington, M. Bozon, K. Wright, J. Falk, F. Helmbacher, K. Kindbeiter, V. Castellani, Gdnf activates midline repulsion by Semaphorin3B via NCAM during commissural axon guidance, Neuron 75 (2012) 1051–1066, http://dx.doi.org/10.1016/j.neuron.2012.08.021.
[98] A. Okada, F. Charron, S. Morin, D.S. Shin, K. Wong, P.J. Fabre, M. Tessier-Lavigne, S.K. McConnell, Boc is a receptor for sonic hedgehog in the guidance of commissural axons, Nature 444 (2006) 369–373, http://dx.doi.org/10.1038/nature05246.
[99] T.F.W. Sloan, M.A. Qasaimeh, D. Juncker, P.T. Yam, F. Charron, Integration of shallow gradients of Shh and netrin-1 guides commissural axons, PLoS Biol. 13 (2015) 1–24, http://dx.doi.org/10.1371/journal.pbio.1002119.
[100] P.T. Yam, C.B. Kent, S. Morin, W.T. Farmer, R. Alchini, L. Lepelletier, D.R. Colman, M. Tessier-Lavigne, A.E. Fournier, F. Charron, 14-3-3 proteins regulate a cell-intrinsic switch from sonic hedgehog-mediated commissural axon attraction to repulsion after midline crossing, Neuron 76 (2012) 735–749, http://dx.doi.org/10.1016/j.neuron.2012.09.017.
[101] K. Onishi, Y. Zou, Sonic hedgehog switches on Wnt/planar cell polarity signaling in commissural axon growth cones by reducing levels of Shisa2, Elife 6 (2017) 1–20, http://dx.doi.org/10.7554/eLife.25269.
[102] M.S. Moon, T.M. Gomez, Adjacent pioneer commissural interneuron growth cones switch from contact avoidance to axon fasciculation after midline crossing, Dev. Biol. 288 (2005) 474–486, http://dx.doi.org/10.1016/j.ydbio.2005.09.049.
[103] T.A. Evans, G.J. Bashaw, Axon guidance at the midline: of mice and flies, Curr. Opin. Neurobiol. 20 (2010) 79–85, http://dx.doi.org/10.1016/j.conb.2009.12.006.
[104] H. Long, C. Sabatier, L. Ma, A. Plump, W. Yuan, D.M. Ornitz, A. Tamada, F. Murakami, C.S. Goodman, M. Tessier-Lavigne, Conserved roles for Slit and Robo proteins in midline commissural axon guidance, Neuron 42 (2004) 213–223, http://dx.doi.org/10.1016/S0896-6273(04)00179-5.
[105] G.J. Goodhill, A theoretical model of axon guidance by the Robo code, Neural Comput. 15 (2003) 549–564, http://dx.doi.org/10.1162/089976603321192077.
[106] A. Jaworski, M. Tessier-Lavigne, Autocrine/juxtaparacrine regulation of axon fasciculation by Slit-Robo signaling, Nat. Neurosci. 15 (2012) 367–369, http://dx.doi.org/10.1038/nn.3037.
[107] N. Sakai, R. Insolera, R.V. Sillitoe, S.-H. Shi, Z. Kaprielian, Axon sorting within the spinal cord marginal zone via Robo- mediated inhibition of N-cadherin controls spinocerebellar tract formation, J. Neurosci. 42 (2012) 115–125, http://dx.doi.org/10.1086/498510.Parasitic.
[108] R. Imondi, Z. Kaprielian, Commissural axon pathfinding on the contralateral side of the floor plate: a role for B-class ephrins in specifying the dorsoventral position of longitudinally projecting commissural axons, Development 128 (2001) 4859–4871.
[109] H. Naoki, Revisiting chemoaffinity theory: chemotactic implementation of topographic axonal projection, PLOS Comput. Biol. 13 (2017) e1005702, http://dx.doi.org/10.1371/journal.pcbi.1005702.

Please cite this article in press as: H. Ducuing, et al., Commissural axon navigation in the spinal cord: A repertoire of repulsive forces is in command, Semin Cell Dev Biol (2017), https://doi.org/10.1016/j.semcdb.2017.12.010

Thibault GARDETTE

26 ans

FORMATION

2011-2014

Licence de Biochimie
Université Claude Bernard Lyon 1
9ème sur 114

2014-2015

M1 Biochimie
Université Claude Bernard Lyon 1
3ème sur 64

2015-2016

M2 Recherche en Cancérologie
Université Claude Bernard Lyon 1

PARCOURS PROFESSIONNEL

2015-2016

Stagiaire Laboratoire "Récepteurs à dépendance, Cancer et Développement", Dr. P. MEHLEN, CNRS UMR 5286 - INSERM U1052, Centre Léon Bérard, Lyon
Importance of cancer-associated fibroblasts in promoting cancer stemness via Netrin-1 and its receptors, in colorectal cancer

Depuis octobre 2016

Doctorant Laboratoire "Neuro-développement, Cancer et Signalisation", Dr. V. CASTELLANI, CNRS UMR 5310 - INSERM U1217, Institut NeuroMyoGène, Lyon
Cartographie et fonctions des fragments issus du facteur de guidage axonal Slit
Sous la direction de Servane Tauszig-Delamasure

CONGRÈS ET PRÉSENTATIONS

International Meeting on Optical Biosensors, Gand, Belgique - 2018

Communication orale YRIN day, 1ère édition, Lyon, France - 2019

Poster Mechanobiology and Physics of Life, 4th edition, Lyon, France - 2019

Poster Axon, 3rd edition, Alicante, Espagne - 2019

PUBLICATIONS

Ducuing H, **Gardette T**, Pignata A, Tauszig-Delamasure S, Castellani V. Commissural axon navigation in the spinal cord: A repertoire of repulsive forces is in command. **Semin Cell Dev Biol.** 2019 Jan;85:3-12.
doi: 10.1016/j.semcdb.2017.12.010. **Revue**

Pignata A, Ducuing H, Boubakar L, **Gardette T**, Kindbeiter K, Bozon M, Tauszig-Delamasure S, Falk J, Thoumine O, and Castellani V. Spatial and temporal profiling of receptor membrane insertion controls commissural axon responses to midline repellents. **Cell Rep.** 2019 Oct 8;29(2):347-362.e5. **Article de recherche**

Conception de vidéos

Pour l'association Les Cellules Déambulent qui fait des actions de sensibilisation aux enjeux de la recherche en biologie cellulaire - 2018

Pour le collectif citoyen Lyon Climat, organisateur des marches pour le climat lyonnaises, afin de sensibiliser aux enjeux de solidarité climatique actuels et à venir – 2019

Présentations orales

Dans le cadre du Téléthon, Ecole Centrale de Lyon, France - 2018

Dans le cadre de l'opération Espoir en tête du Rotary Club, Cinéma Pathé Vaise, Lyon, France - 2020

Références

Ahmed, G. *et al.* (2011) “Draxin inhibits axonal outgrowth through the netrin receptor DCC.,” *The Journal of neuroscience : the official journal of the Society for Neuroscience*, 31(39), pp. 14018–23. doi: 10.1523/JNEUROSCI.0943-11.2011.

Andermatt, I. *et al.* (2014) “Semaphorin 6B acts as a receptor in post-crossing commissural axon guidance,” *Development (Cambridge)*. Company of Biologists Ltd, 141(19), pp. 3709–3720. doi: 10.1242/dev.112185.

Anderson, C. and Stern, C. D. (2016) “Organizers in Development,” in *Current Topics in Developmental Biology*. Academic Press Inc., pp. 435–454. doi: 10.1016/bs.ctdb.2015.11.023.

Augsburger, A. *et al.* (1999) “Bmps as mediators of roof plate repulsion of commissural neurons,” *Neuron*. Cell Press, 24(1), pp. 127–141. doi: 10.1016/S0896-6273(00)80827-2.

Ba-Charvet, K. T. N. *et al.* (2001) “Diversity and Specificity of Actions of Slit2 Proteolytic Fragments in Axon Guidance,” *Journal of Neuroscience*, 21(12). Available at: http://www.jneurosci.org/content/21/12/4281.long (Accessed: June 5, 2018).

Barak, R. *et al.* (2014) “Crystal structure of the extracellular juxtamembrane region of Robo1,” *Journal of Structural Biology*. Academic Press Inc., 186(2), pp. 283–291. doi: 10.1016/j.jsb.2014.02.019.

Barak, R. *et al.* (2019) “Structural Principles in Robo Activation and Auto-inhibition.,” *Cell*, 177(2), pp. 272-285.e16. doi: 10.1016/j.cell.2019.02.004.

Bashaw, G. J. *et al.* (2000) “Repulsive axon guidance: Abelson and enabled play opposing roles downstream of the roundabout receptor,” *Cell*. Cell Press, 101(7), pp. 703–715. doi: 10.1016/S0092-8674(00)80883-1.

Bashaw, G. J. and Klein, R. (2010) “Signaling from axon guidance receptors.,” *Cold Spring Harbor perspectives in biology*. doi: 10.1101/cshperspect.a001941.

Belle, M. *et al.* (2014) “A simple method for 3D analysis of immunolabeled axonal tracts in a transparent nervous system.,” *Cell reports*. Elsevier, 9(4), pp. 1191–201. doi: 10.1016/j.celrep.2014.10.037.

Bhat, K. M. (2017) “Post-guidance signaling by extracellular matrix-associated Slit/Slit-N maintains fasciculation and position of axon tracts in the nerve cord.” doi: 10.1371/journal.pgen.1007094.

Blockus, H. and Chédotal, A. (2016) “Slit-robo signaling,” *Development (Cambridge)*. Company of Biologists Ltd, 143(17), pp. 3037–3044. doi: 10.1242/dev.132829.

Bourikas, D. *et al.* (2005) “Sonic hedgehod guides commissural axons along the longitudinal axis of the spinal cord,” *Nature Neuroscience*, 8(3), pp. 297–304. doi: 10.1038/nn1396.

Bovolenta, P. and Dodd, J. (1990) “Guidance of commissural growth cones at the floor plate in embryonic rat spinal cord.,” *Development (Cambridge, England)*, 109(2), pp. 435–47. Available at: http://www.ncbi.nlm.nih.gov/pubmed/2205466 (Accessed: November 8, 2019).

Briscoe, J. and Ericson, J. (1999) “The specification of neuronal identity by graded sonic hedgehog signalling,” *Seminars in Cell and Developmental Biology*. Elsevier Ltd, 10(3), pp. 353–362. doi: 10.1006/scdb.1999.0295.

Brose, K. *et al.* (1999) “Slit proteins bind robo receptors and have an evolutionarily conserved role in repulsive axon guidance,” *Cell*. Cell Press, 96(6), pp. 795–806. doi: 10.1016/S0092-8674(00)80590-5.

Browne, E. N. (1909) “The production of new hydranths in Hydra by the insertion of small grafts,” *Journal of Experimental Zoology*. John Wiley & Sons, Ltd, 7(1), pp. 1–23. doi: 10.1002/jez.1400070102.

Butler, S. J. and Dodd, J. (2003) “A role for BMP heterodimers in roof plate-mediated repulsion of commissural axons,” *Neuron*. Cell Press, 38(3), pp. 389–401. doi: 10.1016/S0896-6273(03)00254-X.

Campbell, R. M. and Peterson, A. C. (1993) “Expression of a lacZ transgene reveals floor plate cell morphology and macromolecular transfer to commissural axons.,” *Development (Cambridge, England)*, 119(4), pp. 1217–28. Available at: http://www.ncbi.nlm.nih.gov/pubmed/8306884 (Accessed: November 8, 2019).

Catala, M. *et al.* (1996) “A spinal cord fate map in the avian embryo: While regressing, Hensen’s node lays down the notochord and floor plate thus joining the spinal cord lateral walls,” *Development*, 122(9), pp. 2599–2610.

Catala, M., Teillet, M. A. and le Douarin, N. M. (1995) “Organization and development of the tail bud analyzed with the quail-chick chimaera system,” *Mechanisms of Development*, 51(1), pp. 51–65. doi: 10.1016/0925-4773(95)00350-A.

Chan, C. E. and Odde, D. J. (2008) “Traction dynamics of filopodia on compliant substrates,” *Science*, 322(5908), pp. 1687–1691. doi: 10.1126/science.1163595.

Chance, R. K. and Bashaw, G. J. (2015) “Slit-Dependent Endocytic Trafficking of the Robo Receptor Is Required for Son of Sevenless Recruitment and Midline Axon Repulsion,” *PLoS Genetics*. Public Library of Science, 11(9). doi: 10.1371/journal.pgen.1005402.

Charoy, C. *et al.* (2012) “gdnf activates midline repulsion by Semaphorin3B via NCAM during commissural axon guidance.,” *Neuron*, 75(6), pp. 1051–66. doi: 10.1016/j.neuron.2012.08.021.

Charrier, J. B. *et al.* (2002) “Dual origin of the floor plate in the avian embryo,” *Development*, 129(20), pp. 4785–4796.

Charron, F. *et al.* (2003) “The morphogen sonic hedgehog is an axonal chemoattractant that collaborates with Netrin-1 in midline axon guidance,” *Cell*. Cell Press, 113(1), pp. 11–23. doi: 10.1016/S0092-8674(03)00199-5.

Chédotal, A. (2007) “Slits and their receptors,” *Advances in Experimental Medicine and Biology*, pp. 65–80. doi: 10.1007/978-0-387-76715-4_5.

Chizhikov, V. v. and Millen, K. J. (2005) “Roof plate-dependent patterning of the vertebrate dorsal central nervous system,” *Developmental Biology*. doi: 10.1016/j.ydbio.2004.10.011.

Chuang, W. and Lagenaur, C. F. (1990) “Central nervous system antigen P84 can serve as a substrate for neurite outgrowth,” *Developmental Biology*, 137(2), pp. 219–232. doi: 10.1016/0012-1606(90)90249-I.

Coleman, H. A. *et al.* (2010) “The Adam family metalloprotease Kuzbanian regulates the cleavage of the roundabout receptor to control axon repulsion at the midline,” *Development*, 137(14), pp. 2417–2426. doi: 10.1242/dev.047993.

Delloye-Bourgeois, C. *et al.* (2015) “PlexinA1 is a new Slit receptor and mediates axon guidance function of Slit C-terminal fragments,” *Nature Neuroscience*. Nature Publishing Group, 18(1), pp. 36–45. doi: 10.1038/nn.3893.

Dent, E. W., Gupton, S. L. and Gertler, F. B. (2011) “The growth cone cytoskeleton in Axon outgrowth and guidance,” *Cold Spring Harbor Perspectives in Biology*, 3(3), pp. 1–39. doi: 10.1101/cshperspect.a001800.

Dominici, C. *et al.* (2017) “Floor-plate-derived netrin-1 is dispensable for commissural axon guidance.,” *Nature*. doi: 10.1038/nature22331.

Ducuing, H. *et al.* (2017) “Commissural axon navigation in the spinal cord: A repertoire of repulsive forces is in command,” *Seminars in Cell and Developmental Biology*. Elsevier Ltd, pp. 3–12. doi: 10.1016/j.semcdb.2017.12.010.

Ericson, J. *et al.* (1997) “Graded sonic hedgehog signaling and the specification of cell fate in the ventral neural tube,” in *Cold Spring Harbor Symposia on Quantitative Biology*, pp. 451–466.

Evans, T. A. *et al.* (2015) “Robo2 acts in trans to inhibit slit-robo1 repulsion in pre-crossing commissural axons,” *eLife*. eLife Sciences Publications Ltd, 4(JULY 2015), pp. 1–26. doi: 10.7554/eLife.08407.

Fame, R. M., MacDonald, J. L. and Macklis, J. D. (2011) “Development, specification, and diversity of callosal projection neurons.,” *Trends in neurosciences*, 34(1), pp. 41–50. doi: 10.1016/j.tins.2010.10.002.

Feinberg, E. H. *et al.* (2008) “GFP Reconstitution Across Synaptic Partners (GRASP) Defines Cell Contacts and Synapses in Living Nervous Systems,” *Neuron*, 57(3), pp. 353–363. doi: 10.1016/j.neuron.2007.11.030.

Fitsiori, A. *et al.* (2011) “The corpus callosum: white matter or terra incognita.,” *The British journal of radiology*, 84(997), pp. 5–18. doi: 10.1259/bjr/21946513.

Francisco, H. *et al.* (2007) “Regulation of axon guidance and extension by three-dimensional constraints,” *Biomaterials*, 28(23), pp. 3398–3407. doi: 10.1016/j.biomaterials.2007.04.015.

Franze, K. (2013) “The mechanical control of nervous system development,” *Development (Cambridge)*, 140(15), pp. 3069–3077. doi: 10.1242/dev.079145.

Gallo, G. and Letourneau, P. C. (2004) “Regulation of Growth Cone Actin Filaments by Guidance Cues,” *Journal of Neurobiology*, pp. 92–102. doi: 10.1002/neu.10282.

Gara, R. K. *et al.* (2015) “Slit/Robo pathway: a promising therapeutic target for cancer.,” *Drug discovery today*. Elsevier Ltd, 20(1), pp. 156–64. doi: 10.1016/j.drudis.2014.09.008.

Glees, P. and LeVay, S. (1964) “SOME ELECTRON MICROSCOPICAL OBSERVATIONS ON THE EPENDYMAL CELLS OF THE CHICK EMBRYO SPINAL CORD.,” *Journal fur Hirnforschung*, 7, pp. 355–60. Available at: http://www.ncbi.nlm.nih.gov/pubmed/14252296 (Accessed: February 20, 2020).

Glenn C. Rosenquist (1966) *A radioautographic study of labeled grafts in the chick blastoderm*. Available at: https://search.library.wisc.edu/catalog/999745925302121 (Accessed: December 26, 2019).

Gomez, T. M. and Zheng, J. Q. (2006) "The molecular basis for calcium-dependent axon pathfinding," *Nature Reviews Neuroscience*, pp. 115–125. doi: 10.1038/nrn1844.

Gorla, M. *et al.* (2019) "Ndfip Proteins Target Robo Receptors for Degradation and Allow Commissural Axons to Cross the Midline in the Developing Spinal Cord.," *Cell reports*, 26(12), pp. 3298-3312.e4. doi: 10.1016/j.celrep.2019.02.080.

Grabowski, C. T. (1956) "The effects of the excision of Hensen's node on the early development of the chick embryo," *Journal of Experimental Zoology*. John Wiley & Sons, Ltd, 133(2), pp. 301–343. doi: 10.1002/jez.1401330207.

Griffith, C. M. and Wiley, M. J. (1991) "N-CAM, polysialic acid and chick tail bud development.," *Anatomy and embryology*, 183(2), pp. 205–12. doi: 10.1007/bf00174400.

Heidemann, S. R. and Buxbaum, R. E. (1990) "Tension as a regulator and integrator of axonal growth," *Cell Motility and the Cytoskeleton*, pp. 6–10. doi: 10.1002/cm.970170103.

Holland, S. J. *et al.* (1998) "Cell-contact-dependent signalling in axon growth and guidance: Eph receptor tyrosine kinases and receptor protein tyrosine phosphatase beta.," *Current opinion in neurobiology*, 8(1), pp. 117–27. doi: 10.1016/s0959-4388(98)80015-9.

Hwang, D. Y. *et al.* (2015) "Mutations of the SLIT2–ROBO2 pathway genes SLIT2 and SRGAP1 confer risk for congenital anomalies of the kidney and urinary tract," *Human Genetics*. Springer Verlag, 134(8), pp. 905–916. doi: 10.1007/s00439-015-1570-5.

Illman, S. A. *et al.* (2003) "The mouse matrix metalloproteinase, epilysin (MMP-28), is alternatively spliced and processed by a furin-like proprotein convertase," *Biochemical Journal*, 375(1), pp. 191–197. doi: 10.1042/BJ20030497.

Imondi, R. and Kaprielian, Z. (2001) "Commissural axon pathfinding on the contralateral side of the floor plate: A role of B-class ephrins in specifying the dorsoventral position of longitudinally projecting commissural axons," *Development*, 128(23), pp. 4859–4871.

Islam, S. M. *et al.* (2009) "Draxin, a repulsive guidance protein for spinal cord and forebrain commissures," *Science*, 323(5912), pp. 388–393. doi: 10.1126/science.1165187.

Jacobson, A. G. and Gordon, R. (1976) “Changes in the shape of the developing vertebrate nervous system analyzed experimentally, mathematically and by computer simulation.,” *The Journal of experimental zoology*, 197(2), pp. 191–246. doi: 10.1002/jez.1401970205.

Jaworski, A. *et al.* (2015) “Operational redundancy in axon guidance through the multifunctional receptor Robo3 and its ligand NELL2,” *Science*. American Association for the Advancement of Science, 350(6263), pp. 961–965. doi: 10.1126/science.aad2615.

Jaworski, A. and Tessier-Lavigne, M. (2012) “Autocrine/juxtaparacrine regulation of axon fasciculation by Slit-Robo signaling.,” *Nature neuroscience*, 15(3), pp. 367–9. doi: 10.1038/nn.3037.

Jay, D. G. (2000) “The clutch hypothesis revisited: Ascribing the roles of actin-associated proteins in filopodial protrusion in the nerve growth cone,” *Journal of Neurobiology*, 44(2), pp. 114–125. doi: 10.1002/1097-4695(200008)44:2<114::AID-NEU3>3.0.CO;2-8.

Jessell, T. M. *et al.* (1989) “Polarity and patterning in the neural tube: the origin and function of the floor plate.,” *Ciba Foundation symposium*. doi: 10.1002/9780470513798.ch15.

Justice, E. D., Barnum, S. J. and Kidd, T. (2017) “The WAGR syndrome gene PRRG4 is a functional homologue of the commissureless axon guidance gene,” *PLoS Genetics*. Public Library of Science, 13(8), p. e1006865. doi: 10.1371/journal.pgen.1006865.

Kadison, S. R. *et al.* (2006) “EphB receptors and ephrin-B3 regulate axon guidance at the ventral midline of the embryonic mouse spinal cord,” *Journal of Neuroscience*, 26(35), pp. 8909–8914. doi: 10.1523/JNEUROSCI.1569-06.2006.

Kamiguchi, H. (2007) “The role of cell adhesion molecules in axon growth and guidance,” *Advances in Experimental Medicine and Biology*, pp. 95–103. doi: 10.1007/978-0-387-76715-4_7.

Kamnasaran, D. (2005) “Agenesis of the corpus callosum: Lessons from humans and mice,” *Clinical and Investigative Medicine*, 28(5), pp. 267–282.

Kassai, H. *et al.* (2008) “Rac1 in cortical projection neurons is selectively required for midline crossing of commissural axonal formation.,” *The European journal of neuroscience*, 28(2), pp. 257–67. doi: 10.1111/j.1460-9568.2008.06343.x.

Keleman, K. *et al.* (2002) “Comm sorts Robo to control axon guidance at the Drosophila midline,” *Cell*. Cell Press, 110(4), pp. 415–427. doi: 10.1016/S0092-8674(02)00901-7.

Keleman, K., Ribeiro, C. and Dickson, B. J. (2005) “Comm function in commissural axon guidance: cell-autonomous sorting of Robo in vivo,” *NATURE NEUROSCIENCE*, 8(2). doi: 10.1038/nn1388.

Kerstein, P. C., Nichol, R. H. and Gomez, T. M. (2015) “Mechanochemical regulation of growth cone motility,” *Frontiers in Cellular Neuroscience*. Frontiers Research Foundation. doi: 10.3389/fncel.2015.00244.

Kidd, T., Bland, K. S. and Goodman, C. S. (1999) “Slit is the midline repellent for the Robo receptor in Drosophila,” *Cell*. Cell Press, 96(6), pp. 785–794. doi: 10.1016/S0092-8674(00)80589-9.

Kingsbury, B. F. (1920) “The extent of the floor-plate of His and its significance,” *The Journal of Comparative Neurology*, 32(1), pp. 113–135. doi: 10.1002/cne.900320106.

Kitchin, I. C. (1949) “The effects of notochordectomy in Amblystoma mexicanum,” *Journal of Experimental Zoology*. John Wiley & Sons, Ltd, 112(3), pp. 393–415. doi: 10.1002/jez.1401120303.

Klar, A., Baldassare, M. and Jessell, T. M. (1992) “F-spondin: A gene expressed at high levels in the floor plate encodes a secreted protein that promotes neural cell adhesion and neurite extension,” *Cell*, 69(1), pp. 95–110. doi: 10.1016/0092-8674(92)90121-R.

Kolpak, A., Zhang, J. and Bao, Z. Z. (2005) “Sonic hedgehog has a dual effect on the growth of retinal ganglion axons depending on its concentration,” *Journal of Neuroscience*, 25(13), pp. 3432–3441. doi: 10.1523/JNEUROSCI.4938-04.2005.

Kong, Y. *et al.* (2016) “Structural Basis for Plexin Activation and Regulation,” *Neuron*. Cell Press, 91(3), pp. 548–560. doi: 10.1016/j.neuron.2016.06.018.

Koohini, Zahra, Koohini, Zohreh and Teimourian, S. (2019) “Slit/Robo Signaling Pathway in Cancer; a New Stand Point for Cancer Treatment,” *Pathology and Oncology Research*. Springer Netherlands, pp. 1285–1293. doi: 10.1007/s12253-018-00568-y.

Koser, D. E. *et al.* (2016) “Mechanosensing is critical for axon growth in the developing brain,” *Nature Neuroscience*. Nature Publishing Group, 19(12), pp. 1592–1598. doi: 10.1038/nn.4394.

Lai, H. C., Seal, R. P. and Johnson, J. E. (2016) “Making sense out of spinal cord somatosensory development,” *Development (Cambridge)*. Company of Biologists Ltd, pp. 3434–3448. doi: 10.1242/dev.139592.

Lavrador, J. P. *et al.* (2019) “White-matter commissures: a clinically focused anatomical review,” *Surgical and Radiologic Anatomy*. Springer-Verlag France, pp. 613–624. doi: 10.1007/s00276-019-02218-7.

Liu, J. *et al.* (2003) “Congenital diaphragmatic hernia, kidney agenesis and cardiac defects associated with Slit3-deficiency in mice.,” *Mechanisms of development*, 120(9), pp. 1059–70. doi: 10.1016/s0925-4773(03)00161-8.

Long, H. *et al.* (2004) “Conserved roles for Slit and Robo proteins in midline commissural axon guidance,” *Neuron*, 42(2), pp. 213–223. doi: 10.1016/S0896-6273(04)00179-5.

López-Fagundo, C. *et al.* (2013) “Navigating neurites utilize cellular topography of Schwann cell somas and processes for optimal guidance,” *Acta Biomaterialia*, 9(7), pp. 7158–7168. doi: 10.1016/j.actbio.2013.03.032.

Lu, W. *et al.* (2007) “Disruption of ROBO2 is associated with urinary tract anomalies and confers risk of vesicoureteral reflux,” *American Journal of Human Genetics*. University of Chicago Press, 80(4), pp. 616–632. doi: 10.1086/512735.

Lyuksyutova, A. I. *et al.* (2003) “Anterior-posterior guidance of commissural axons by Wnt-frizzled signaling.,” *Science (New York, N.Y.)*, 302(5652), pp. 1984–8. doi: 10.1126/science.1089610.

Macpherson, L. J. *et al.* (2015) “Dynamic labelling of neural connections in multiple colours by trans-synaptic fluorescence complementation,” *Nature Communications*. Nature Publishing Group, 6. doi: 10.1038/ncomms10024.

Malacinski, G. M. and Youn, B. W. (1982) “The structure of the anuran amphibian Notochord and a re-evaluation of its presumed role in early embryogenesis.,” *Differentiation; research in biological diversity*, 21(1), pp. 13–21. doi: 10.1111/j.1432-0436.1982.tb01188.x.

McConnell, R. E. *et al.* (2016) “A requirement for filopodia extension toward Slit during Robo-mediated axon repulsion,” *Journal of Cell Biology*. Rockefeller University Press, 213(2), pp. 261–274. doi: 10.1083/jcb.201509062.

Mitchison, T. and Kirschner, M. (1988) “Cytoskeletal dynamics and nerve growth,” *Neuron*, pp. 761–772. doi: 10.1016/0896-6273(88)90124-9.

Moreno-Bravo, J. A. *et al.* (2018) “Commissural neurons transgress the CNS/PNS boundary in absence of ventricular zone-derived netrin 1,” *Development*, 145(2). Available at: http://dev.biologists.org.gate2.inist.fr/content/145/2/dev159400.long (Accessed: January 25, 2018).

Moret, F. *et al.* (2007) “Semaphorin and neuropilin co-expression in motoneurons sets axon sensitivity to environmental semaphorin sources during motor axon pathfinding,” *Development*. Company of Biologists Ltd, 134(24), pp. 4491–4501. doi: 10.1242/dev.011452.

Morlot, C. *et al.* (2007) “Structural insights into the Slit-Robo complex,” *Proceedings of the National Academy of Sciences of the United States of America*, 104(38), pp. 14923–14928. doi: 10.1073/pnas.0705310104.

Moss, D. J. and White, C. A. (1989) “A Ca2(+)-sensitive glycoprotein, GP90, associated with the cytoskeleton from brain and gizzard.,” *Journal of cell science*, 93 (Pt 1), pp. 85–94. Available at: http://www.ncbi.nlm.nih.gov/pubmed/2613760 (Accessed: February 20, 2020).

Nawabi, H. *et al.* (2010) “A midline switch of receptor processing regulates commissural axon guidance in vertebrates,” *Genes and Development*, 24(4), pp. 396–410. doi: 10.1101/gad.542510.

Nickerson, A. *et al.* (2015) “Photoactivated localization microscopy with bimolecular fluorescence complementation (Bifc-palm),” *Journal of Visualized Experiments*. Journal of Visualized Experiments, 2015(106), p. e53154. doi: 10.3791/53154.

Nicolet, P. G. (1970) “Analyse autoradiographique de la localisation des différentes ébauches présomptives dans la ligne primitive de l’embryon de Poulet,” *Development*, 23(1).

Niftullayev, S. and Lamarche-Vane, N. (2019) “Regulators of rho GTPases in the nervous system: Molecular implication in axon guidance and neurological disorders,” *International Journal of Molecular Sciences*. MDPI AG. doi: 10.3390/ijms20061497.

Nishiyama, M. *et al.* (2003) “Cyclic AMP/GMP-dependent modulation of Ca2+ channels sets the polarity of nerve growth-cone turning,” *Nature*, 423(6943), pp. 990–995. doi: 10.1038/nature01751.

Nugent, A. A., Kolpak, A. L. and Engle, E. C. (2012) “Human disorders of axon guidance,” *Current Opinion in Neurobiology*, pp. 837–843. doi: 10.1016/j.conb.2012.02.006.

Nüsslein-Volhard, C., Wieschaus, E. and Kluding, H. (1984) “Mutations affecting the pattern of the larval cuticle in Drosophila melanogaster - I. Zygotic loci on the second chromosome,” *Wilhelm Roux’s Archives of Developmental Biology*. Springer-Verlag, 193(5), pp. 267–282. doi: 10.1007/BF00848156.

O'Donnell, M. P. and Bashaw, G. J. (2013) "Distinct functional domains of the Abelson tyrosine kinase control axon guidance responses to Netrin and slit to regulate the assembly of neural circuits," *Development (Cambridge)*, 140(13), pp. 2724–2733. doi: 10.1242/dev.093831.

Okabe, N. *et al.* (2004) "Contacts between the commissural axons and the floor plate cells are mediated by nectins," *Developmental Biology*. Academic Press, 273(2), pp. 244–256. doi: 10.1016/J.YDBIO.2004.05.034.

Ordan, E. *et al.* (2015) "Slit cleavage is essential for producing an active, stable, non-diffusible short-range signal that guides muscle migration," *Development (Cambridge)*. Company of Biologists Ltd, 142(8), pp. 1431–1436. doi: 10.1242/dev.119131.

Ordan, E. and Volk, T. (2016) "Amontillado is required for Drosophila Slit processing and for tendon-mediated muscle patterning," *Biology Open*. Company of Biologists Ltd, 5(10), pp. 1530–1534. doi: 10.1242/bio.020636.

Palka, J., Whitlock, K. E. and Murray, M. A. (1992) "Guidepost cells," *Current Opinion in Neurobiology*, 2(1), pp. 48–54. doi: 10.1016/0959-4388(92)90161-D.

Parra, L. M. and Zou, Y. (2010) "Sonic hedgehog induces response of commissural axons to Semaphorin repulsion during midline crossing," *Nature Neuroscience*, 13(1), pp. 29–35. doi: 10.1038/nn.2457.

Pei, D. and Weiss, S. J. (1995) "Furin-dependent intracellular activation of the human stromelysin-3 zymogen," *Nature*, pp. 244–247. doi: 10.1038/375244a0.

Pérez, C., Sawmiller, D. and Tan, J. (2016) "The role of heparan sulfate deficiency in autistic phenotype: potential involvement of Slit/Robo/srGAPs-mediated dendritic spine formation.," *Neural development*, 11, p. 11. doi: 10.1186/s13064-016-0066-x.

Philipp, M. *et al.* (2012) "RabGDI controls axonal midline crossing by regulating Robo1 surface expression.," *Neural development*, 7, p. 36. doi: 10.1186/1749-8104-7-36.

Pignata, A. *et al.* (2019) "A Spatiotemporal Sequence of Sensitization to Slits and Semaphorins Orchestrates Commissural Axon Navigation," *Cell Reports*. Elsevier B.V., 29(2), pp. 347-362.e5. doi: 10.1016/j.celrep.2019.08.098.

Placzek, M. *et al.* (1991) "Control of dorsoventral pattern in vertebrate neural development: induction and polarizing properties of the floor plate.," *Development (Cambridge, England).*

Supplement, Suppl 2, pp. 105–22. Available at: http://www.ncbi.nlm.nih.gov/pubmed/1842349 (Accessed: November 8, 2019).

Placzek, M. and Briscoe, J. (2005) "The floor plate: Multiple cells, multiple signals," *Nature Reviews Neuroscience*, pp. 230–240. doi: 10.1038/nrn1628.

Placzek, M., Jessell, T. M. and Dodd, J. (1993) "Induction of floor plate differentiation by contact-dependent, homeogenetic signals," *Development*, 117(1).

Ren, Y. *et al.* (2018) "A low-cost microwell device for high-resolution imaging of neurite outgrowth in 3D," *Journal of Neural Engineering*. Institute of Physics Publishing, 15(3). doi: 10.1088/1741-2552/aaaa32.

Robles, E., Huttenlocher, A. and Gomez, T. M. (2003) "Filopodial calcium transients regulate growth cone motility and guidance through local activation of calpain.," *Neuron*, 38(4), pp. 597–609. doi: 10.1016/s0896-6273(03)00260-5.

Ros, O. *et al.* (2015) "Regulation of patterned dynamics of local exocytosis in growth cones by Netrin-1," *Journal of Neuroscience*. Society for Neuroscience, 35(13), pp. 5156–5170. doi: 10.1523/JNEUROSCI.0124-14.2015.

Rothberg, J. M. *et al.* (1988) "slit: An EGF-homologous locus of D. melanogaster involved in the development of the embryonic central nervous system," *Cell*, 55(6), pp. 1047–1059. doi: 10.1016/0092-8674(88)90249-8.

Rothberg, J. M. *et al.* (1990) "slit: An extracellular protein necessary for development of midline glia and commissural axon pathways contains both EGF and LRR domains," *Genes and Development*, 4(12 A), pp. 2169–2187. doi: 10.1101/gad.4.12a.2169.

Rouillé, Y. *et al.* (1995) "Proteolytic processing mechanisms in the biosynthesis of neuroendocrine peptides: the subtilisin-like proprotein convertases.," *Frontiers in neuroendocrinology*, 16(4), pp. 322–61. doi: 10.1006/frne.1995.1012.

Ruiz de Almodovar, C. *et al.* (2011) "VEGF mediates commissural axon chemoattraction through its receptor Flk1.," *Neuron*, 70(5), pp. 966–78. doi: 10.1016/j.neuron.2011.04.014.

Sabatier, C. *et al.* (2004) "The divergent Robo family protein rig-1/Robo3 is a negative regulator of slit responsiveness required for midline crossing by commissural axons.," *Cell*, 117(2), pp. 157–69. doi: 10.1016/s0092-8674(04)00303-4.

Sakai, N. *et al.* (2012) “Axon sorting within the spinal cord marginal zone via Robo-mediated inhibition of N-cadherin controls spinocerebellar tract formation,” *Journal of Neuroscience*, 32(44), pp. 15377–15387. doi: 10.1523/JNEUROSCI.2225-12.2012.

Sanyas, I. *et al.* (2012) “Motoneuronal Sema3C is essential for setting stereotyped motor tract positioning in limb-derived chemotropic semaphorins.,” *Development (Cambridge, England)*, 139(19), pp. 3633–43. doi: 10.1242/dev.080051.

Sato, H. *et al.* (1996) “Activation of a recombinant membrane type 1-matrix metalloproteinase (MT1-MMP) by furin and its interaction with tissue inhibitor of metalloproteinases (TIMP)-2,” *FEBS Letters*. Elsevier B.V., 393(1), pp. 101–104. doi: 10.1016/0014-5793(96)00861-7.

Schoenwolf, G. C. and Smith, J. L. (1990) “Mechanisms of neurulation: traditional viewpoint and recent advances,” *Development*, 109(2).

Seeger, M. *et al.* (1993) “Mutations affecting growth cone guidance in drosophila: Genes necessary for guidance toward or away from the midline,” *Neuron*, 10(3), pp. 409–426. doi: 10.1016/0896-6273(93)90330-T.

Seidah, N. G. *et al.* (1998) “Precursor convertases: An evolutionary ancient, cell-specific, combinatorial mechanism yielding diverse bioactive peptides and proteins,” in *Annals of the New York Academy of Sciences*. Blackwell Publishing Inc., pp. 9–24. doi: 10.1111/j.1749-6632.1998.tb10727.x.

Seki, M. *et al.* (2010) “Human ROBO1 is cleaved by metalloproteinases and gamma-secretase and migrates to the nucleus in cancer cells.,” *FEBS letters*, 584(13), pp. 2909–15. doi: 10.1016/j.febslet.2010.05.009.

Selleck, M. A. J. and Stern, C. D. (1991) “Fate mapping and cell lineage analysis of Hensen’s node in the chick embryo,” *Development*, 112(2), pp. 615–626.

Shearin, H. K. *et al.* (2018) “t-GRASP, a targeted GRASP for assessing neuronal connectivity,” *Journal of Neuroscience Methods*. Elsevier B.V., 306, pp. 94–102. doi: 10.1016/j.jneumeth.2018.05.014.

Smeekens, S. P. and Steiner, D. F. (1991) “Processing of peptide precursors. Identification of a new family of mammalian proteases.,” *Cell biophysics*, 19(1–3), pp. 45–55. doi: 10.1007/bf02989878.

Smith, J. L. and Schoenwolf, G. C. (1989) “Notochordal induction of cell wedging in the chick neural plate and its role in neural tube formation.,” *The Journal of experimental zoology*, 250(1), pp. 49–62. doi: 10.1002/jez.1402500107.

Song, H. J. *et al.* (1998) “Conversion of neuronal growth cone responses from repulsion to attraction by cyclic nucleotides,” *Science*. American Association for the Advancement of Science, 281(5382), pp. 1515–1518. doi: 10.1126/science.281.5382.1515.

Stawowy, P. *et al.* (2005) “Furin-like proprotein convertases are central regulators of the membrane type matrix metalloproteinase-pro-matrix metalloproteinase-2 proteolytic cascade in atherosclerosis.,” *Circulation*, 111(21), pp. 2820–7. doi: 10.1161/CIRCULATIONAHA.104.502617.

van Straaten, H. W. M. *et al.* (1988) “Effect of the notochord on the differentiation of a floor plate area in the neural tube of the chick embryo,” *Anatomy and Embryology*. Springer-Verlag, 177(4), pp. 317–324. doi: 10.1007/BF00315839.

van Straaten, H. W. M. and Drukker, J. (1987) “Influence of the Notochord on the Morphogenesis of the Neural Tube,” in *Mesenchymal-Epithelial Interactions in Neural Development*. Springer Berlin Heidelberg, pp. 153–162. doi: 10.1007/978-3-642-71837-3_13.

van Straaten, H. W. *et al.* (1985) “Induction of an additional floor plate in the neural tube.,” *Acta morphologica Neerlando-Scandinavica*, 23(2), pp. 91–7. Available at: http://www.ncbi.nlm.nih.gov/pubmed/3834777 (Accessed: January 3, 2020).

Strupp, M. *et al.* (2014) “Central ocular motor disorders, including gaze palsy and nystagmus,” *Journal of Neurology*. Dr. Dietrich Steinkopff Verlag GmbH and Co. KG, pp. 542–558. doi: 10.1007/s00415-014-7385-9.

Suter, T. A. C. S., DeLoughery, Z. J. and Jaworski, A. (2017) “Meninges-derived cues control axon guidance,” *Developmental Biology*. Elsevier Inc., 430(1), pp. 1–10. doi: 10.1016/j.ydbio.2017.08.005.

Thompson, A. J. *et al.* (2019) “Rapid changes in tissue mechanics regulate cell behaviour in the developing embryonic brain.,” *eLife*. NLM (Medline), 8. doi: 10.7554/eLife.39356.

Thompson, D. M. and Buettner, H. M. (2006) “Neurite outgrowth is directed by Schwann cell alignment in the absence of other guidance cues,” *Annals of Biomedical Engineering*, 34(1), pp. 161–168. doi: 10.1007/s10439-005-9013-4.

Tyler, W. J. (2012) “The mechanobiology of brain function,” *Nature Reviews Neuroscience*. Nature Publishing Group, pp. 867–878. doi: 10.1038/nrn3383.

Varadarajan, S. G. *et al.* (2017) “Netrin1 Produced by Neural Progenitors, Not Floor Plate Cells, Is Required for Axon Guidance in the Spinal Cord.,” *Neuron*. Elsevier, 94(4), pp. 790-799.e3. doi: 10.1016/j.neuron.2017.03.007.

Vitriol, E. A. and Zheng, J. Q. (2012) “Growth cone travel in space and time: the cellular ensemble of cytoskeleton, adhesion, and membrane.,” *Neuron*. NIH Public Access, 73(6), pp. 1068–81. doi: 10.1016/j.neuron.2012.03.005.

Vogler, G. and Bodmer, R. (2015) “Cellular Mechanisms of Drosophila Heart Morphogenesis.,” *Journal of cardiovascular development and disease*. MDPI AG, 2(1), pp. 2–16. doi: 10.3390/jcdd2010002.

Wang, K. H. *et al.* (1999) “Biochemical purification of a mammalian slit protein as a positive regulator of sensory axon elongation and branching.,” *Cell*. Elsevier, 96(6), pp. 771–84. doi: 10.1016/S0092-8674(00)80588-7.

Wang, L. *et al.* (2017) “Nogo-B is the major form of Nogo at the floor plate and likely mediates crossing of commissural axons in the mouse spinal cord,” *Journal of Comparative Neurology*. Wiley-Liss Inc., 525(13), pp. 2915–2928. doi: 10.1002/cne.24246.

Wen, J. and Liu, M. (2014) “Piezoelectric ceramic (PZT) modulates axonal guidance growth of rat cortical neurons via RhoA, Rac1, and Cdc42 pathways,” *Journal of Molecular Neuroscience*, 52(3), pp. 323–330. doi: 10.1007/s12031-013-0149-7.

Wills, Z. *et al.* (2002) “A Drosophila homolog of cyclase-associated proteins collaborates with the Abl tyrosine kinase to control midline axon pathfinding,” *Neuron*. Cell Press, 36(4), pp. 611–622. doi: 10.1016/S0896-6273(02)01022-X.

Wright, K. M. *et al.* (2012) “Dystroglycan Organizes Axon Guidance Cue Localization and Axonal Pathfinding,” *Neuron*, 76(5), pp. 931–944. doi: 10.1016/j.neuron.2012.10.009.

Wu, P., Nicholls, S. B. and Hardy, J. A. (2013) “A Tunable, modular approach to fluorescent protease-activated reporters,” *Biophysical Journal*, 104(7), pp. 1605–1614. doi: 10.1016/j.bpj.2013.01.058.

Xiao, T. *et al.* (2011) “Assembly of lamina-specific neuronal connections by slit bound to type IV collagen,” *Cell*. NIH Public Access, 146(1), pp. 164–176. doi: 10.1016/j.cell.2011.06.016.

Yaginuma, H. *et al.* (1991) “Pathfinding by growth cones of commissural interneurons in the chick embryo spinal cord: A light and electron microscopic study,” *Journal of Comparative Neurology*. Wiley-Blackwell, 304(1), pp. 78–102. doi: 10.1002/cne.903040107.

Yamada, T. *et al.* (1991) “Control of cell pattern in the developing nervous system: Polarizing activity of the floor plate and notochord,” *Cell*, 64(3), pp. 635–647. doi: 10.1016/0092-8674(91)90247-V.

Yamagata, M. and Sanes, J. R. (2012) “Transgenic strategy for identifying synaptic connections in mice by fluorescence complementation (GRASP),” *Frontiers in Molecular Neuroscience*, (FEBRUARY 2012). doi: 10.3389/fnmol.2012.00018.

Yamashita, M. (2013) “Electric axon guidance in embryonic retina: Galvanotropism revisited,” *Biochemical and Biophysical Research Communications*, 431(2), pp. 280–283. doi: 10.1016/j.bbrc.2012.12.115.

Yamashita, M. (2015) “Weak electric fields serve as guidance cues that direct retinal ganglion cell axons in vitro,” *Biochemistry and Biophysics Reports*. Elsevier B.V., 4, pp. 83–88. doi: 10.1016/j.bbrep.2015.08.022.

Yam, P. T. *et al.* (2012) “14-3-3 proteins regulate a cell-intrinsic switch from sonic hedgehog-mediated commissural axon attraction to repulsion after midline crossing.,” *Neuron*, 76(4), pp. 735–49. doi: 10.1016/j.neuron.2012.09.017.

Youn, B. W. and Malacinski, G. M. (1981) “Axial structure development in ultraviolet-irradiated (notochord-defective) amphibian embryos,” *Developmental Biology*, 83(2), pp. 339–352. doi: 10.1016/0012-1606(81)90479-6.

Zhou, A. *et al.* (1999) “Proteolytic processing in the secretory pathway,” *Journal of Biological Chemistry*, pp. 20745–20748. doi: 10.1074/jbc.274.30.20745.